The role of EB proteins in *Drosophila* mitosis

Submitted by Constantino Salomão to the University of Exeter
as a thesis for the degree of
Doctor of Philosophy in Biological Sciences
In February 2022

I certify that all material in this thesis which is not my own work has been identified and that no material has previously been submitted and approved for the award of a degree by this or any other University.

Signature: …………… …………………..

Statement

I hereby declare that the dissertation of this thesis is the result of my own work and all material which is not mine has been clearly stated in the text.

I further certify that no part of my dissertation has previously been submitted and approved for any such degree or other qualification by this or any other University.

Acknowlegement

I would like to thank my Supervisor Prof. James G. Wakefield, initially for allowing me to join his research group, then for his tireless support throughout the 4 years of my PhD. I could not achieve this great goal without his help and I am grateful for having worked with him. I have never worked with fruit flies before and found it hard initially. But thanks to his support which helped me to understand science, now I gained a passion for working with this model animal. My achievement was supported by many people and firstly I thank Dr. Karolina Jaworek who has helped me a lot and stayed close to me with her support all the time. I would also to thank Dr. Jennie Campell and Dr. Stacey Scott from Wakefield lab for giving feedback on my work. In general, I thank all Wakefield lab members, past and present for the advice and fun moments which made my past four years so pleasing.

I would also thank my boss, Dr. Cezaltina Nanduva Kahuli who is the director of Faculty of Medicine at the Universidade José Eduardos dos Santos in Huambo (Angola) for allowing me to study in the UK and for her encouraging words.

Many warm thanks to my sponsor the National Institute of Scholarship Management and the Ministry of Higher Education, Science, Technology and Innovation, without whom my PhD studies would not be a reality.

Many thanks also go to Don Angelo Falchi and my former Prof. Irene Giorgi for moral support and encouraging words.

I greatly appreciate my parents Jacinto Somaykewndje and Juliana Ngueve, my wife Rosària Nalima Salomão and all my kids for their invaluable support and patience; it was not easy to stay away from them for so long a time.

I would also thank my friends Brian and Deborah for support and friendship during my PhD studies.

Abstract

Accurate segregation of duplicated chromosomes (mitosis) relies on formation and correct dynamics of a robust mitotic spindle. This fundamental subcellular structure, present in all eukaryotic cells, is composed of microtubules (MTs), protein polymers generated from $\alpha\beta$-Tubulin dimers and organized in space and time. Although the last twenty years has resulted in a comprehensive list of proteins essential for organizing mitotic MTs, so called MT associated proteins, or MAPs, and although drugs have been developed that target some of these proteins, the complexity of spindle formation makes it difficult to know how function emerges from component parts. This is especially important given that abnormal mitosis is a hallmark of human pathogenesis, including cancer and neurodegenerative diseases.

To understand how faulty or missing gene products contribute to abnormal spindle formation, we must understand the physical properties of individual proteins, both in isolation and together with other proteins, how they are regulated in space and time and how cells activate alternative pathways to compensate for their loss. This requires a multi-scale understanding that encompasses a multi-disciplinary approach.

The *Drosophila* embryo is an excellent model system for studying mitotic spindle formation and, in this thesis, I investigate a conserved MAP, End Binding protein 1 (EB1), which binds autonomously to growing MT plus ends in order to recruit a suite of MT effectors, regulating MT dynamics. Although end binding proteins have been extensively studied, their functions in different stages of mitosis are less understood.

In this work, I aimed to investigate the roles of end binding proteins in early *Drosophila* embryos. To begin with I attempted to generate tools with which to disrupt EB protein function, focusing on interfering antibodies. Next, I used quantitative, comparative mass spectrometry and proteomics to identify proteins that interact with EB1 strongly during metaphase. A simple interpretation of my findings suggests that EB1 interacts with the Dynein/Dynactin complex, HOOK, JVL-SPNF-IK2 complex and PIGS to anchor microtubule ends to the centrosomes and to regulate invagination furrows, mitotic spindle orientation and chromosome segregation. In addition, my results suggest that EB1 interacts with the Rod-ZW10-Zwilch and spindly complex to mediate the interactions with Dynein/Dynactin to silence the spindle assembly checkpoint, leading to the onset of anaphase. Finally, I have identified novel EB1 binding proteins and generated new transgenic flies to investigate their functional relationships with EB1. This study indicates that EB1 interacts with DNApol-ε complex and with Cornetto (CORN). Although their relationships to EB1 and potential function during mitosis remain unknown, their dynamic localisation suggest both may play crucial roles in organising mitotic MTs. My work therefore suggests that EB1 plays crucial roles at the metaphase-anaphase transition, at both kinetochores and the embryo cortex, furthering our understanding of this crucial spindle-regulating protein.

Contents

List of Tables

List of Figures

List of Abbreviation

γ-TuCs	Gamma tubulin complexes
γ-TuRCs	Gamma tubulin ring complexes
γ-TuSCs	Gamma tubulin small complexes
AAs	Amino acids
APC	Adenomatous Polyposis Coli
APC/C	Anaphase promoting complex or cyclosome
AP-MS	Affinit purification-mass spectrometry
Approx.	Approximate
BDSC	Bloomingtonn Drosophila Stock Center
BSA	Bovine serum albumin
CAP-Gly	Cytoskeletal-associated protein glycine-rich
Cdks	Cyclin-dependent kinases
CDS	Coding DNA sequence
CHB	Chromosome bows
CH	Calponin homology
ch-TOG	Colonic hepatic tumor overexpressed gene
CIN	Chromsomal instability
CIP2A	Cancerous inhibitor of Protein Phosphatase 2A
Cl-AP	Cleavable affinity purification
CLASPs	CLIP-associated proteins
CLIPs	Cytoplasmic linker proteins
CM1	Centrosomin motif 1
CPVL	Carboxypeptidadase vitellogenic like
CR	Contractile actomyosin ring
CRISPR/Cas9	Clustered regularly interspaced short palindromic repeat/CRISPR-associated 9
C-ter	Carboxy-terminal
DGRC	*Drosophila* genomics resource center
DmEB1	*Drosophila melanogaster* end-binding protein 1
DmEBs	*Drosophila melanogaster* end-binding proteins

Dml	*Drosophila melanogaster*
DNA	Deoxyribonucleic acid
DSBs	Double stand breaks
EB1^{DN}	EB1 dominant negative
EBH	End-binding homology
EBs	End binding proteins
E-cad	E-cadherin
ER	Endoplasmic reticulum
E-sites	Exchangeable sites
FDR	False discovery rate
FGFR1	Fibroblast growth factor receptor1
FRAP	Fluorescence recovery after photobleaching
GAPs	GTPase activating proteins
GCDH	Glutaryl-CoA dehydrogenase
GCPs	Gamma complex proteins
GDP	Guanosine diphosphate
GEFs	Guanine nucleotide exchange factors
GFP	Green fluorescence protein
GID	Glucose degradation deficient
GO	Gene ontolgy
Grip-GCPs	Gamma complex proteins with Grip1 and Grip2 motifs
Grips	Gamma ring proteins
gRNA	guide RNA
GTP	Guanosine triphosphate
HDR	Homology-directed repair
HEPES	N-2-Hydroxyethylpiperazine-N-2-Ethane Sulfonic Acid
HsEBs	*Homo sapiens* end-binding proteins
Hs	*Homo sapiens*
HSS	High speed supernatant
IP	Immunoprecipitation
IPTG	Isopropyl β–D–1–thiogalactopyranoside
kD	Kilodalton
KMTs	Kinetochore-associtated microtubule
LB	Luria Bertani
LFQ	Label-free quantification

LxxPTPh	Leucine–any residue– any residue–proline–threonine–proline–any hydrophobic residue.
MACFs	Microtubule-actin crosslinking factors
MAPs	Microtubule associated proteins
MBP	Maltose binding protein
MCAK	Microtubule depolymerase mitotic centromere-associated kinesin
MCMs	Minichromosome maintenance protein complexes
MDa	Megadalton
MDCK	Madin-Darbay canine kidney
MSPS	Mini-spindles protein
MTOC	Microtubule organising centre
MTs	Microtubules
MTZ	Maternal-to-zygotic transition
MW	Molecular weight
MZT	MOZART
NCBI	National centre for biotechnology information
NEB	Nuclear envelope breakdown
NHEj	Nonhomologous end joining
NPCs	Nuclear pore complexes
N-sites	Non exchangeable sites
OD	Optical density
O-GlcNAc	β-linked-N-acetiylglucosmine
PBS	Phosphate buffered saline
PCM	Pericentriolar material
Pi	Inorganic phosphate
piRNAs	piwi-interacting RNAs
PP2A	Protein phosphatase 2A
PPI	Protein-protein interactions
PSB	Protein sample buffer
PTMs	Protein post-translational modifications
QC-AP-MS	Quantitative comparative affinity purification mass spectrometry
Rb	Retinoblastoma
RFP	Red fluorescence protein
RNAi	RNA interference
RNPs	Ribonucleoprotein particles
RT	Room temperature

RZZ　　　　ROD–ZW10–ZWILCH complex

SAC　　　　Spindle assembly checkpoint

SDS-PAGE　Sodium dodecyl sulphate polyacrylamide gel electrophoresis

SOC　　　　Super optimal broth with catabolite repression

ssODNs　　Single stranded oligodeoxynucleotides

Std　　　　Standard

SxIP　　　Serine-any amino acid–isoleucine–proline

TACC　　　Transforming acidic coiled-coil

TALENs　　Transcription activator-like effector nucleases

TCA　　　　Citric acid cycle

TEs　　　　Transposable elements

T.Ex　　　Total extract

-TIPs　　Minus end tracking proteins

+TIPs　　Plus end tracking proteins

TMT-MS　　Tandem mass tag mass spectometry

TOG　　　　Tumor overexpressed gene

Y2H　　　　Yeast two-hybrid

ZFNs　　　Zinc-finger nucleases

Chapter 1:   Introduction

1.1   The Cell Cycle

To continue to grow and divide, a cell performs an orderly series of events, the most fundamental of which are the duplication of its contents, including proteins, organelles and chromosomes and then their division, usually into two identical daughter cells. The process of equal segregation of duplicated chromosomes is termed mitosis. During mitosis, cells generate a structure termed the bipolar mitotic spindle – an array of organised, yet highly dynamic protein fibres that, in most animal cells, nucleate from two centrosomes and extends to the chromosomes (Berrueta et al. 1998; McIntosh 2016). These fibres, polymers of two related conserved proteins, α- and β-tubulins, generate a mitotic spindle capable of accurate chromosome segregation. These MTs gradually align the sister chromatids at the centre of the spindle through specially stabilised MT bundles, termed kinetochore MTs. Once all chromosomes are aligned, the cohesion between the sisters is lost and the MT cytoskeleton dramatically changes its dynamics, including the depolymerisation of kinetochore MTs. In this way, the individual chromosomes are segregated to the spindle poles. Subsequent coordinated cytokinesis then generates two daughter cells (Figure 1.1).

Cells rely on the spatial and temporal regulation of MT dynamics through the activity of a variety of MT associated proteins (MAPs) (Walczak and Heald 2008). Errors in spindle assembly can lead to chromosome missegregation and hence result in aneuploidy, a hallmark of cancer cells and the cause of some birth defects (Holland and Cleveland 2012; Vitre and Cleveland 2012). Therefore, a bet-

ter understanding of spindle assembly pathways is essential, particularly in developing novel anti-mitotic drugs.
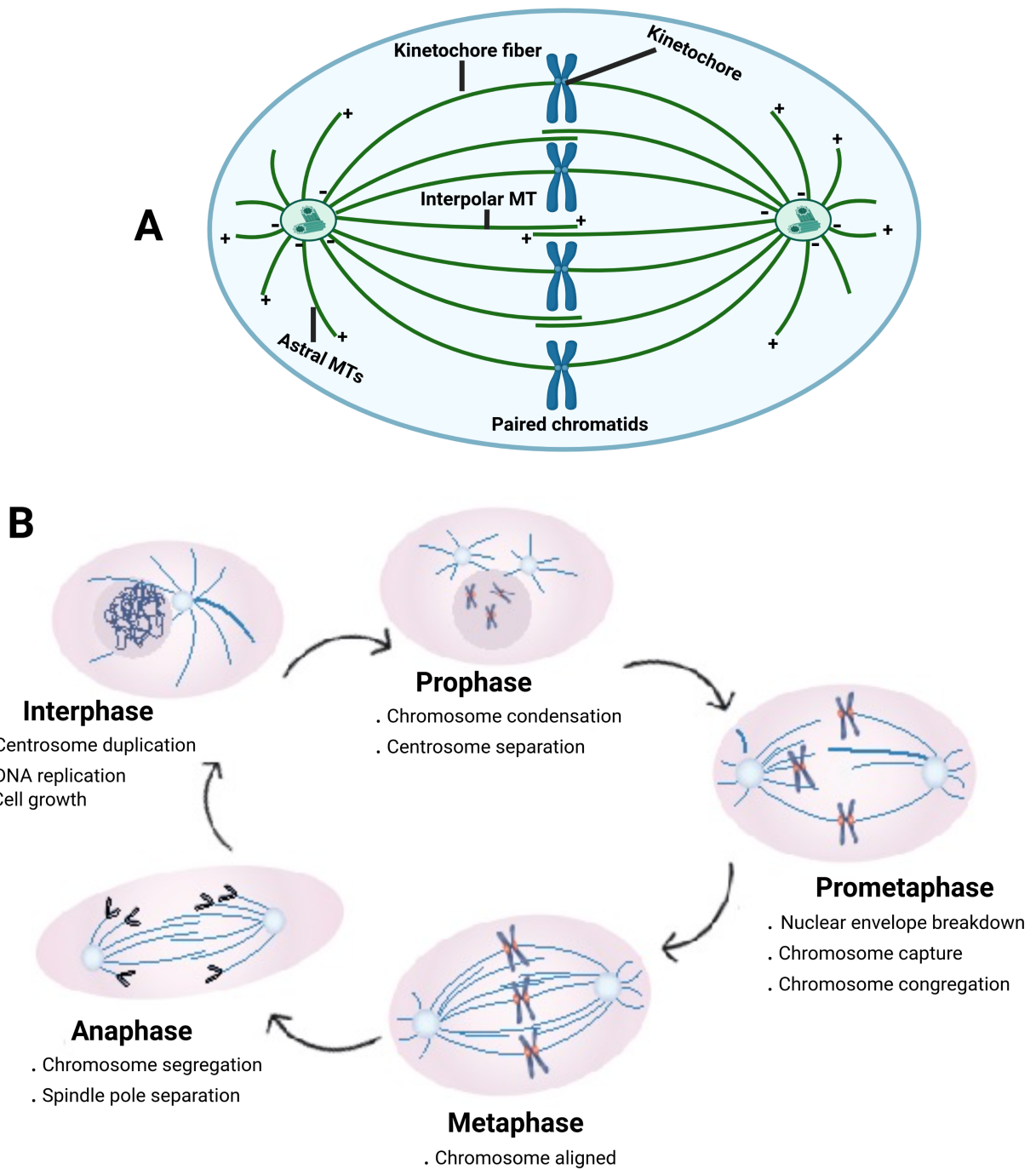
Figure 1.1: **Overview of the mitotic spindle and the cell cycle.** **(A)** Anatomy of the metaphase mitotic spindle. The minus ends of MTs are focused at the spindle poles (each spindle pole is formed by a centrosome). The dynamic plus ends of MTs radiate out from the centrosomes towards the metaphase/equatorial plate, where MT from each centrosome overlap, resulting in an antiparallel array. This spindle midzone, where interpolar MTs overlap, plays an essential role in elongation of the anaphase spindle. MTs that bind to chromosomes and mediate their movement are called kinetochore fibers (also called k-fibers). A typi-

cal k-fiber is composed of a bundle of MTs (≈18 in human cells; McEwn et al. 2001). Astral MTs emanate from the centrosomes towards the cell cortex, and they are important for cleavage furrow induction and spindle positioning. **(B)** Schematic representation of the major stages of mitosis, showing MT reorganisation and chromosome translocation. Mitosis begins with prophase, during which the replicated chromosomes condense (become visible as sister chromatids) and the mitotic spindle begins to form by the movement of centrosomes to opposite sides of the cell. At prometaphase, the nuclear envelope breaks down (in those organisms performing 'open' mitoses), chromosomes are captured by k-fibers and maneuvered to the spindle equator. Metaphase is marked by the alignment of chromosomes at the equatorial plate, the sister chromatids of each duplicated chromosome are attached to opposite centrosomes (referred to as amphitelic or bi-oriented attachment). The transition to anaphase is triggered only after all sister chromatids are correctly bi-oriented on the spindle. During anaphase the cohesion between sister chromatids is lost and they are pulled apart to opposite spindle poles. Chromosome separation is driven by k-fiber shortening and spindle elongation. Finally, at telophase (not shown), the spindle disassembles, the nuclear envelope reforms around each new set of daughter chromosomes, the chromosomes decondense, and the cell begins to assemble the machinery to divide the daughter cells. Reproduced with permission, Ammarah Tariq.

1.2   Overview of Microtubules

Microtubules (MTs) (Figure 1.2(e)) form a large part of the cytoskeletal structure in all eukaryotic cells (Chaaban and Brouhard 2017; Hevia and Fanarraga 2020; Oakley 2000). They are composed of polymers of two related proteins – α and β-tubulins, which are incorporated into MTs as heterodimers (Figure 1.2(c)). Longitudinal interactions between heterodimers generate protofilaments (Figure 1.2(d)), which then associate laterally, forming hollow cylinders with an approximate outer diameter of 25 nm and an inner diameter of 17 nm. They can be many μm in length (Akhmanova and Steinmetz 2008; Desai and Mitchison 1997). MTs with different numbers of protofilaments have been found in a large variety of species, from as few as 4 protofilaments, in *Prosthecobacter,* to as many as 40 protofilaments, in mantidfly sperm (Akhmanova and Steinmetz 2008; Chaaban and Brouhard 2017). Nevertheless, the protofilament number of MTs found in cells is generally uniform, with 13 protofilaments per MT. Accord-

ing to the straight-protofilament hypothesis (Amos and Schlieper 2005; Kollman et al. 2010), MTs in cells are formed predominantly with 13 protofilaments, because only this number allows them to generate a straight axis along the MT, which is important for motor protein processivity and for the periodic recruitment of MT Associated Proteins (MAPs). In contrast, MTs formed by different numbers of protofilaments are supertwisted (Chaaban and Brouhard 2017).

| (a) α-tubulin | (b) β-tubulin | (c) Heterodimer | (d) Protofilament | (e) Microtubule | (f) Lateral view |
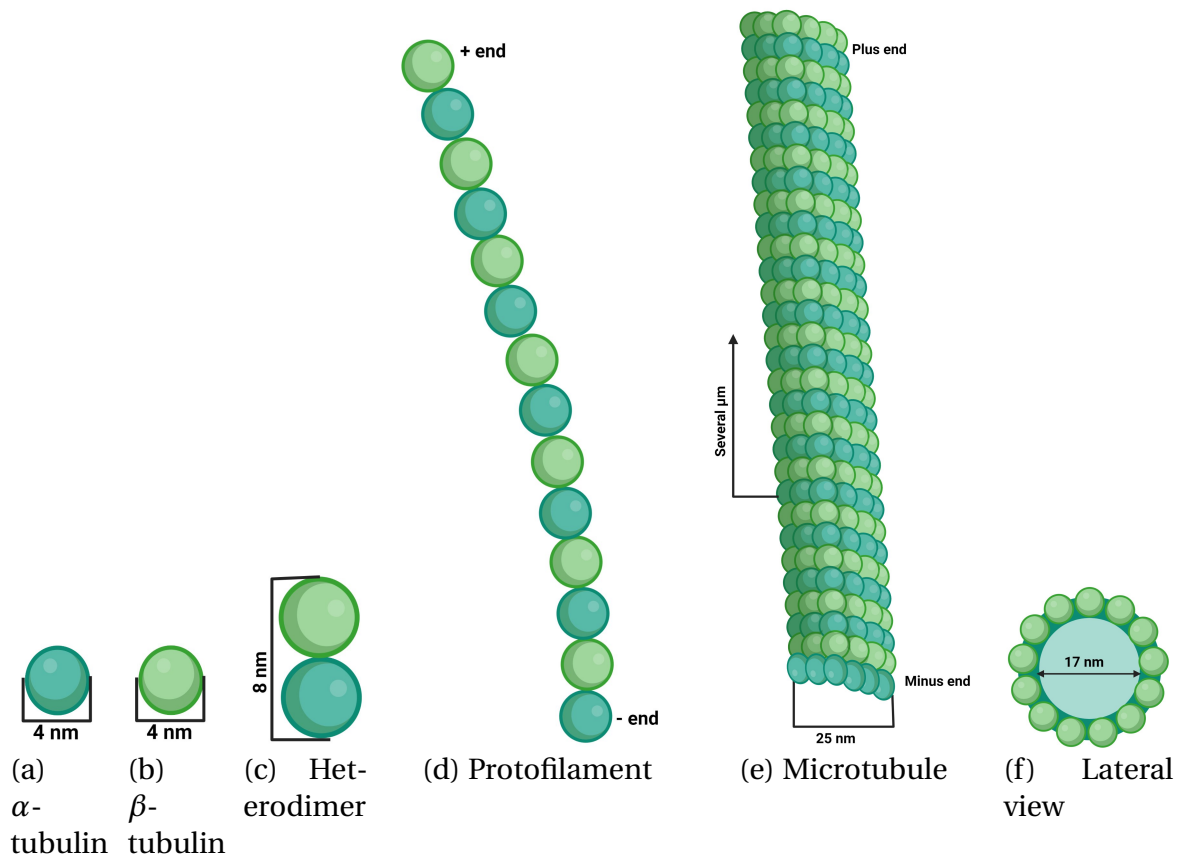
Figure 1.2: **A general structure of a MT and its building blocks.** α-tubulin (Figure 1.2(a)) and β-tubulin (Figure 1.2(b)) are globular proteins with a diameter of approximately 4 nm. These two proteins in eukaryotes exist as a heterodimer (Figure 1.2(c)) with a length of about 8 nm. In this dimer, the head of α-tublin is non covalently bonded to the tail of β-tubulin. The heterodimer polymerises to form a protofilament (Figure 1.2(d)) in which the head of β-tubulin of one dimer interacts with the tail of α-tubulin of an adjacent heterodimer by non-covalent bonds. α and β-tubulins of one protofilament non covalently bind to respective α and β proteins of adjacent protofilaments to form a MT (Figure 1.2(e)) which has an approximate outer diameter of 25 nm, several μm in length and an inner diameter of approximately 17 nm (Figure 1.2(f)).

Due to the nature of the dynamic incorporation of the tubulin dimers into MTs, MTs themselves are polar, with α subunit exposed at the minus end and β-tubulin at the plus end (Figure 1.2(e)). Thus a MT has what is termed a "plus" end and a "minus" end. In cells, the minus end is less dynamic because it is anchored at the MT organising centre (MTOC) which is usually located next to the nucleus of a cell. In contrast, the plus end of MTs are usually highly dynamic, emanating away from the nucleus. As such, the MT network in cells is used to provide positional information, moving and relating subcellular organelles and materials between the centre of the cell and the cell periphery, or cortex (Akhmanova and Steinmetz 2008).

1.3 Tubulin superfamily

The term *"tubulin"* was originally used to describe the main protein for MTs of sperm flagella (For review see Oakley 2000) and was initially isolated by affinity for colchicine – a drug which had been shown to disrupt mitosis (For review see Desai and Mitchison 1997). Further studies revealed that flagellar MTs and those from other sources were composed of two major proteins designated as α-tubulin (Figure 1.2(a)) and β-tubulin (Figure 1.2(b)). These two globular proteins are 50% similar at the amino acid sequence (For review see Bigman and Levy 2020; Desai and Mitchison 1997). Each tubulin is made of 444–450 amino acids with molecular weight of approximately 55 kD as determined by sodium dodecyl sulfate polyacrylamide gel electrophoresis (SDS-PAGE) (Oakley 2000) and they are firmly bound together by non-covalent bonds to form the heterodimers.

As a common criterion, two protein sequences are considered homologous if they share more than 30% identical alignments over their full lengths (Pearson 2013). Biochemical studies have revealed six distinct proteins within the tubulin superfamily: α-, β, γ-, δ-, ε- and ζ-tubulins (McKean et al. 2001; Oakley

2000). α-, β- and γ-tubulins are ubiquitous in all eukaryotic cells. As mentioned, α- and β-tubulins form major building blocks of MTs (Figure 1.2), whereas γ-tubulins are more concentrated at the MTOC, where they are involved in the nucleation of MT assembly. δ- and ε-tubulins are not ubiquitous but widely spread in *Clamydomonas* in which δ-tubulin plays an important function in flagellar assembly. The function of δ- and ε-tubulins in other organisms is poorly understood, while ζ-tubulin has been discovered so far exclusively in *Kinetoplastid protozoa* (Oakley 2000).

1.3.1 Microtubules are polymers of α- and β-tubulin heterodimers

Both α- and β-tubulins are asymmetrical and can be thought of as having a head and a tail. The head of an α subunit binds closely with non-covalent bonds to a tail of β-tubulin, thus, in nature, tubulin is found as $\alpha\beta$ heterodimers. *In vitro,* purified $\alpha\beta$-tubulin heterodimers polymerise spontaneously to form MTs of between 9–16 protofilaments, with the majority containing 14 protofilaments (Pierson et al. 1978). However, *in vivo* MTs are generally composed of 13 protofilaments aligned in parallel due to their templated nucleation by the γ-TuRC (Subsection 1.3.2) (Akhmanova and Steinmetz 2008; Kwiatkowska et al. 2006). Within this structure, there are two types of protein-protein interactions; in the same protofilament of a MT, the head of β-tubulin interacts via non-covalent bond with a tail of an adjacent α-tubulin and perpendicularly to these interactions, α-tubulin and β-tubulin of one protofilament form a non-covalent bond with respective α-tubulin and β-tubulin of an adjacent protofilaments. These two longitudinal and lateral types of contacts result in a helical structure and stabilises the MT lattice, which is firm and not easily bent. Consequently, the addition or removal of a heterodimer appears entirely at the MT ends.

1.3.2 Microtubule nucleation

In the MT lattice the longitudinal interactions are stronger than the lateral interactions and during MT depolymerisation, the lateral tubulin bonds disassemble prior to the longitudinal ones (Kononova et al. 2014). Stable nucleation of a MT therefore requires many interactions between subunits to occur simultaneously. As such, spontaneous nucleation of MTs *in vivo* is relatively rare. Instead, additional proteins are required that either bind to stabilise lateral and longitudinal interactions, to generate a MT seed, or provide a 13-protofilament template, upon which tubulin dimers can attach. The latter is termed "templated MT nucleation" and is orchestrated by γ-Tubulin containing protein complexes (Corinne and Paul 2011; Neuner et al. 2020).

γ-TuCs

γ-*tubulin* is present in cells at a much lower concentration than α- and β-tubulins. In association with accessory proteins, many of which contain a specific domain termed a "Grip" motif, γ-tubulin provides a stable platform on to which $\alpha\beta$-tubulin dimers can associate, increasing the favourability of generating lateral $\alpha\beta$-tubulin interactions. The localisation of γ-tubulin therefore determines the major sites of MT nucleation termed MT organising centres (MTOCs) (Andreas and Sawin 2011; Teixidó-Travesa et al. 2012). There are two kinds of γ-tubulin complexes (γ-TuCs) in animal cells; the γ-tubulin small complex (γ-TuSC, Figure 1.3(a)) and the larger complex known as the γ-tubulin ring complex (γ-TuRC, Figure 1.3(b)) . The smaller complex is formed of 4 proteins in a Y shape with a molecular weight (MW) of around 300 kD. It is composed of two molecules of γ-Tubulin, one bound to a molecule of Grip Containing Protein 2 (GCP2) and one bound to a molecule of Grip containing Protein 3 (GCP3) (Kollman et al. 2010; Oakley 2000). γ-TuSCs are able to nucleate MTs, albeit at low efficiency. γ-TuRCs have an approximate MW of 2.2 MDa and are composed

of multiple copies of 6 proteins: γ-Tubulin, GCP3, GCP4, GCP5 and GCP6 (Table 1.1). It can be thought of as a series of 7 γ-TuSCs with the additional proteins providing a platform that organises the γ-TuSCs into a stable open ring-like conformation, with a left-handed spiral. This ring, with a diameter of about 32 nm and an approximate height of 25 nm, is therefore a template for a 13 protofilament MT (Kollman et al. 2010; Neuner et al. 2020; Sulimenko et al. 2017).

(a) γ-TuSC   (b) γ-TuRC   (c) Centrosome
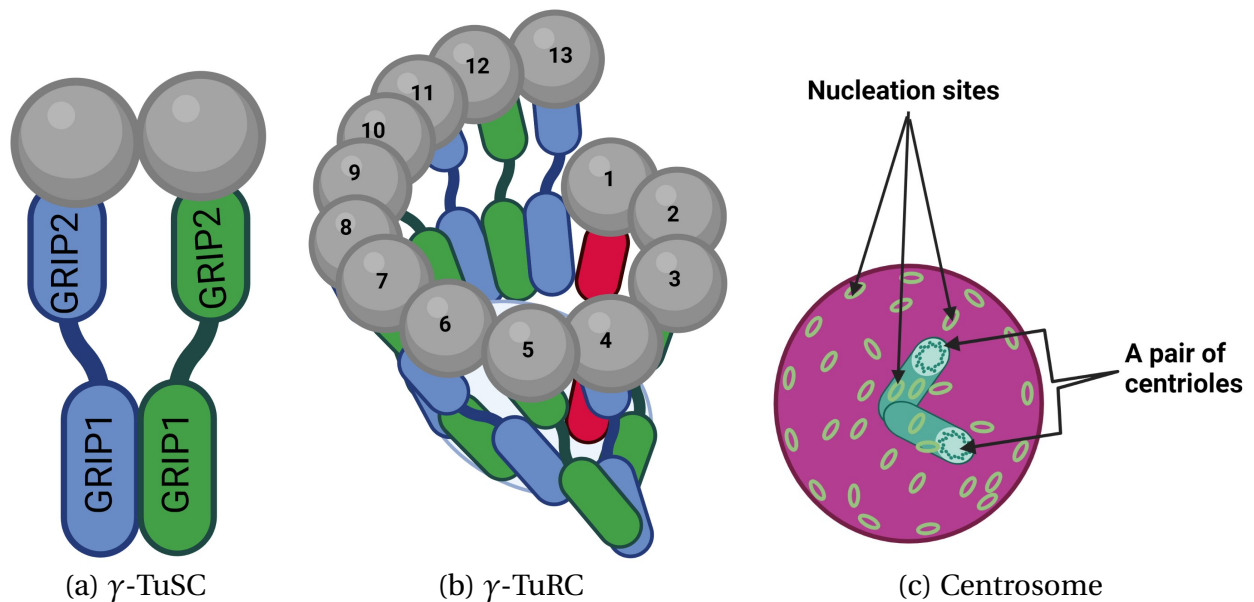
Figure 1.3: **γ-tubulin complexes and their constituents.** A γ-tubulin binding protein contains two conserved motifs; **GRIP1** which interacts lateraly with other GCPs in humans or Dgrips in *Drosophila* and **GRIP2** that binds to the γ-tubulin to form the γ-TuSC (Figure 1.3(a)) in a 1:1:2 stoichiometry. 7 γ-TuSCs associate themselves in a lateral manner via their N-terminal domains. The last half of one γ-TuSC lies beneath the first to form a left-handed spiral shaped γ-TuRC (Figure 1.3(b)) with 13 spokes used as a template to form a 13 protofilament. These γ-TuRCs are recruited to MTOCs where their GRIP1 regions interact with some fibrous proteins to create nucleation sites (Figure 1.3(c)).

Recently the ultrastructure of the human γ-TuRC has been determined by cryo-electron microscopy and the purified γ-TuRC was analysed by label-free quantification (LFQ) mass spectrometry (Neuner et al. 2020). In these studies, the authors found that the complex, in addition to γ-tubulin, contains five copies of GCP2 and GCP3, two or three copies of GCP4 and one copy of GCP5 and GCP6 (Table 1.1), giving a ratio of 5:5:2/3:1:1. GCP4-6 subunits are positioned together at the extremities of the helix in order to regulate initiation and termination of γ-TuRC assembly and stabilisation of the structure (Jauneau et al.

2016). Although these proteins are not essential for spindle formation, they may be involved in targeting γ-TuRCs to specific intracellular structures (Sulimenko et al. 2017).

Table 1.1: γ-**tubulin complexes in two model systems.** *Homo sapiens* and *Drosophila melanogaster.* γ-TuSC is a tetramer protein formed by two γ-tubulins, each one associated with GCP2 or GCP3 (Figure 1.3(a)). γ-TuRC (Figure 1.3(b)) is a complex constituted of γ-TuSCs, γ-tuSC-like structures and other factors (Table 1.2).

	Homo sapiens		*Drosophila melanogaster*	
γ-**Tubulin complexes**	**Gene name**	**Protein name**	**Gene name**	**Protein name**
	TUBG1	γ-tubulin 1	γ-*Tub23C*	γ-tubulin 1
	TUBG2	γ-tubulin 2	γ-*Tub37C*	γ-tubulin 2
γ-TuSC	*TUBGCP2*	GCP2	*Grip84*	Dgrip84
	TUBGCP3	GCP3	*Grip91*	Dgrip91
	TUBG1	γ-tubulin 1	γ-*Tub23C*	γ-tubulin 1
	TUBG2	γ-tubulin 2	γ-*Tub37C*	γ-tubulin 2
	TUBGCP2	GCP2	*Grip84*	Dgrip84
γ-TuRC	*TUBGCP3*	GCP3	*Grip91*	Dgrip91
	TUBGCP4	GCP4	*Grip75*	Dgrip75
	TUBGCP5	GCP5	*Grip128*	Dgrip128
	TUBGCP6	GCP6	*Grip163*	Dgrip163

Targetting the γ-TuRC

MT nucleation (Figure 1.4) can occur spontaneously in the cytoplasm, but occurs mainly at sites that target and concentrate the γ-TuRC. Such MT organising centres (MTOCs) include centrosomes of animal cells (Andreas and Sawin 2011; Teixidó-Travesa et al. 2012), the Golgi apparatus, the nuclear envelope, chromatin and at kinetochores (Sulimenko et al. 2017). The centrosome (Figure 1.3(c)) is a small spherical-like organelle composed of a pair of specialised MT structures (centrioles) arranged in an L-shaped configuration surrounded by an amorphous electron-dense proteinaceous matrix, termed the pericentriolar material (PCM) (Brüning-Richardson et al. 2011). In centrosomes, γ-TuRCs, through their N-terminal domains (Grip regions) and γ-TuSC binding factors, are anchored to the PCM, whilst γ-tubulin spokes are exposed in the correct geometry to serve as a template for MT polymerisation (Figure 1.3 and Figure 1.4). α-tubulin has a site for GTP and the energy from its hydrolysis drives the asso-

ciation of an α-tubulin tail with γ-tubulin. Thus the minus end is anchored to these γ-TuRCs in MTOCs and is less dynamic than the plus end which exposes β-tubulin towards the cell periphery.
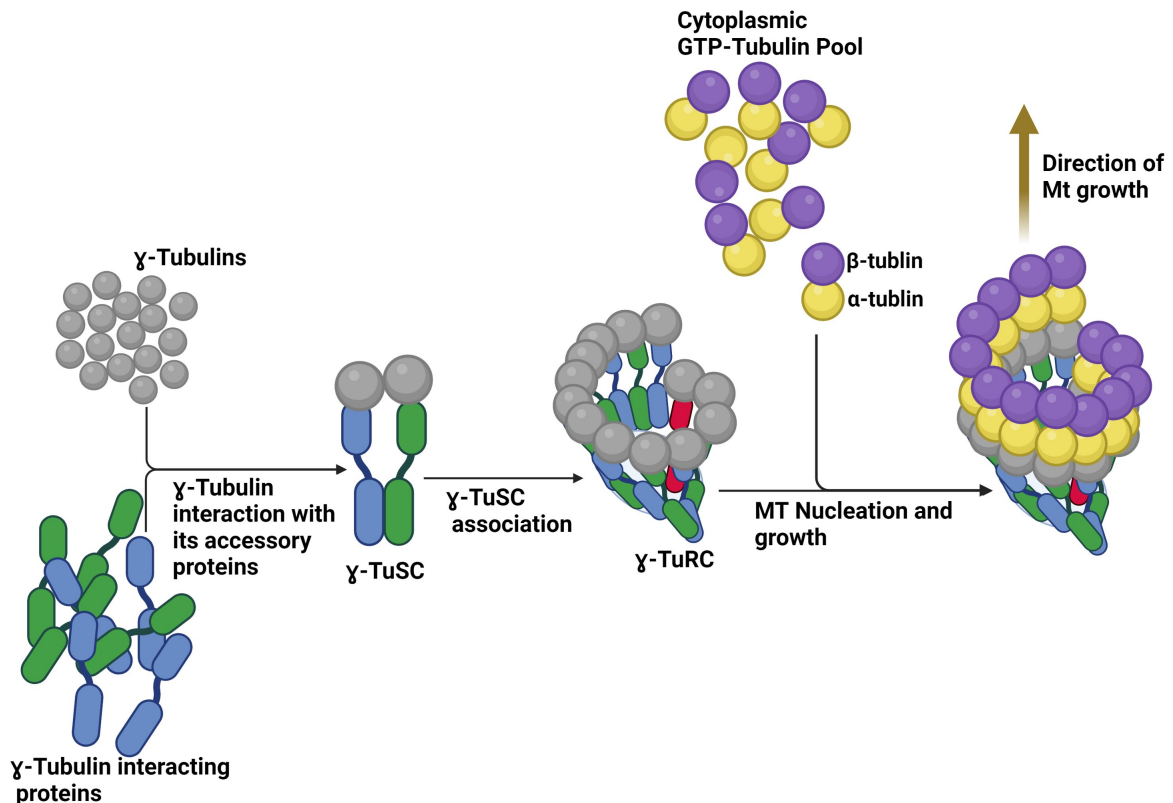
Figure 1.4: γ-**TuRC assembly and MT nucleation by γ-tubulin complexes.** γ-tubulins are ubiquitous proteins, but are highly concentrated in MTOCs where they associate with GCPs in humans (Dgrips in *Drosophila*) to form γ-TuSCs. Association of 7 small complexes (the previous γ-TuSC overlaps with the next one) and other factors creates an open conical and left-handed spiral shaped γ-TuRCs which is recruited to centrosomes to form a nucleation site (Figure 1.3(c)). These ring complexes via their N-terminal domains are anchored to some proteins within these spherical structures and 13 γ-tubulins exposed for interaction with tails of α-tubulins within $\alpha\beta$-heterodimers for MT nucleation, then other $\alpha\beta$-heterodimers are loaded for polymerisation.

The organisation of a particular MT array in a cell therefore depends on dimension, configuration and localisation of a particular type of MTOC (Andreas and Sawin 2011; Teixidó-Travesa et al. 2012). Furthermore, the nucleation site (Figure 1.3(c)) assembly and activation is regulated temporally during the cell cycle (Sulimenko et al. 2017; Teixidó-Travesa et al. 2012). For example, larger and more active centrosomes are generated at the G_2/M transition by increased targeting and activation of the γ-TuRC at centrosomes, whereas centrosome

inactivation occurs during cell differentiation by transferring nucleation sites to other cellular structures (Teixidó-Travesa et al. 2012). Nucleation sites are also involved in modulating the properties of MTs, such as constraining the MT structure or adding MAPs onto this lattice.

γ-TuRC targeting factors include GCP-WD and GCP8 (Tale 1.2) which are not important for γ-TuRC assembly (Corinne and Paul 2011; Teixidó-Travesa et al. 2012). In initial γ-TuRC pull down experiments, GCP9 and GCP8 (GCP8A and GCP8B, Table 1.2) were overlooked due to their small size, but recently have been co-immunoprecipitated with other γ-TuRC components (Merdes et al. 2011). These studies, suggest that the list of γ-TuRC interacting proteins is unfinished (Kollman et al. 2010). In contrast, MOZART2 is exclusively located in the deuterostome lineage[1] and its role of recruitment to centrosomes is only during interphase (Teixidó-Travesa et al. 2012). These activators recruit these complexes to these regions for regulation of γ-TuRC activation (Farache et al. 2018).

Table 1.2: γ-**TUSC-like structures and other factors in two model systems.** *Homo sapiens* and *Drosophila melanogaster.* GCP2 and GCP3 are the major γ-tubulin interacting proteins that form the core of γ-TuRCs. However, in these ring complexes have been found also in low concentration γ-TuSC-like subcomplex.

	Homo sapiens	*Drosophila melanogaster*
γ-TuSC-like	**Protein name**	**Protein name**
Hibrid γ-TuSC	γ-tubulin 1 γ-tubulin 2 GCP2 or GCP3 plus one of GCP4-6	γ-tubulin 1 γ-tubulin 2 Dgrip84 Dgrip91
Novel γ-TuSC	γ-tubulin 1 γ-tubulin 2 Two of GCP4-6	γ-tubulin 1 γ-tubulin 2 Two of Dgrip75, Dgrip128 or Dgrip167
Half γ-TuSC	γ-tubulin 1 γ-tubulin2 One of GCP4-6	γ-tubulin 1 γ-tubulin 2 One of Dgrip75, Dgrip128 or Dgrip167
γ-TuRC interacting factors	GCP-WD *(NEDD1)* GCP8A and GCP8B *(MZT2A and MZT2B)* GCP9 *(MZT1)* LGALS3BP NME7	Grip71 – Mozart1 ? Nmdyn-D7

---

[1]Such as, echinoderms, chordates, hemichordates and xenoturbellida.

A further γ-TuRC recruitment factor is Augmin. Augmin is a hetero-octomeric protein complex first identified in *Drosophila*, but has since been shown to be conserved in humans, *Xenopus* and plants. Augmin is a MAP that also possesses a binding site for NEDD1/DGp71WD, an accessory γ-TuRC subunit (Table 1.2). As such, Augmin is responsible for "branched MT nucleation", localising the γ-TuRC to a pre-existing "mother" MT and allowing new nucleation of a "daughter".

1.3.3 Microtubule dynamics

MT ends, especially the plus end, are dynamic and experience continuous cycles of polymerisation (growth) and depolymerisation (shrinkage) (Figure 1.5). These two phases are separated by a paused microtubule (Nehlig et al. 2017). These three phases are known as dynamic instability and are vital for chromosome segregation and intracellular organisation (Brouhard and Rice 2018; Moriwaki and Goshima 2016; Nehlig et al. 2017). The transition between MT depolymerisation and polymerisation is stochastic and is known as catastrophe and rescue respectively, which is the change from a shrinkage state to MT growth (Desai and Mitchison 1997; Howard and Hyman 2003).

Catastrophe

Rescue

Paused microtubule   **Shrinking microtubule**

Growing microtubule
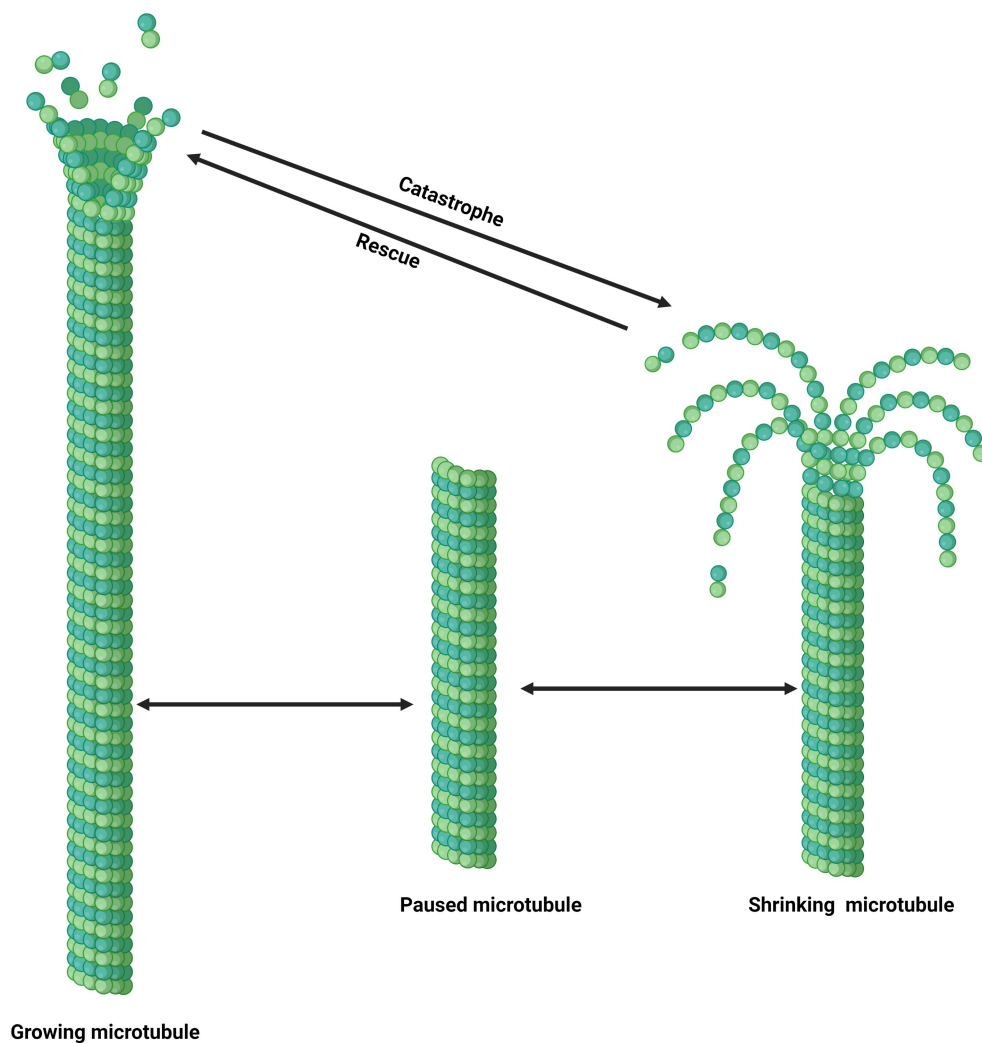
Figure 1.5: **General description of MT dynamics.** Dynamic instability is a process, which MT ends undergo stochastically three continuous periods: **polymerisation (growth)** and **depolymerisation (shrinkage)** which are seperated by a **pause** phase (paused microtubule). The transition from polymerisation to depolymerisation is known as catastrophe, whereas from the shrinkage to growth is known as rescue.

Each α- or β-tubulin has a binding site for one molecule of GTP. The GTP-binding site in the α-tubulin is known as the non-exchangeable site (N-site) and the site in β-tubulin is the exchangeable site (E-site) (Alushin et al. 2014; Nehlig et al. 2017; Nogales et al. 1998). The GTP at the N-site is trapped at the heterodimer interface and can not be exchanged or hydrolyzed, whereas the GTP bound to the E-site can be hydrolysed (GTP $\longleftrightarrow$ GDP +Pi) or exchanged with GTP from a soluble tubulin heterodimer. The binding and hydrolysis of GTP at the β subunit influences the MT dynamics (Gudimchuk et al. 2020; Nehlig et al. 2017). The GTP hydrolysis in free soluble heterodimers is very slow, but after their incorporation into MTs this hydrolysis occurs much quicker. This hydrol-

ysis releases an inorganic phosphate group (Pi) and the GDP remains attached to β-tubulin in the MT lattice. Consequently, the MT plus end can exist in T and D forms. The T form is when the GTP is bound to the β-tubulin and in the D form this GTP has been hydrolysed with release of the phosphate group (Gudimchuk et al. 2020; Nehlig et al. 2017). The GTP hydrolysis occurs with a delay at the end of the MTs after the incorporation of α- and β-tubulin dimer into the sheet-like structure of growing MT ends (Akhmanova and Steinmetz 2008). As a consequence of the delay in GTP hydrolysis, a cap of GTP-tubulin (GTP-cap) is formed at the end of growing MTs and protects the MT from catastrophe, which occurs with disappearance of GTP-cap leading to an exposure of GDP-Tubulin at the end of the MTs (Mitchson and Kirschner 1984). MT polymerisation occurs with the addition of GTP-tubulin heterodimers at MT plus end (Brouhard and Rice 2018; Desai and Mitchison 1997; Nehlig et al. 2017). Thus, the rate of GTP hydrolysis at the E-Site is essential for the regulation of MT dynamic instability (Alushin et al. 2014; Nehlig et al. 2017).

As MT polymerisation and depolymerisation is important for the life of a cell, it is strictly regulated. This function is performed by a large number of MT associated proteins (MAPs) – proteins that bind the lattice or the ends of MTs.

1.3.4 Microtubule associated proteins

MT associated proteins (MAPs) target specific $\alpha\beta$-tubulin conformations and were initially discovered in the early 1970s (Bodakuntla et al. 2019; Brouhard and Rice 2018). There are various MAPs which have classified upon their actions (Bodakuntla et al. 2019; Böhler et al. 2021; Brouhard and Rice 2018) – **Motile MAPs:** these are motor proteins that move along MTs using energy from GTP hydrolysis to transport cargos, such as, vesicles and organelles, and perform different functions in a cell. The two important classes are Kinesins which generally move toward the plus end, and the large, multiprotein Dynein/Dynactin complex, which walks towards the minus end of MTs. If tethered, for example at the

cell cortex, these kinesins/dynein are able to exert force on the MT, resulting in movement. Classical MAPs: these are generally expressed in neuronal cells and bind along the length of MTs, stabilising them and protecting them against the activity of MT severing enzymes, such a katanin (Bodakuntla et al. 2019). They include the proteins Tau, MAP2 and MAP4. Due to the involvement of classical MAPs in the brain, their loss causes defects that can be related to different pathological conditions. For example, mice missing tau may have neurodegeneration problems and those which overxpress *Map2* or *Map1b* have shown neurodevelopmental disorders, and *Map6* knockout developed schizophrenia (Bodakuntla et al. 2019; Hirokawa et al. 1985). **MT nucleators:** as already specified, these include the γ-TuSC and γ-TuRC. They also include proteins that stabilise the lateral and longitudinal interactions between $\alpha\beta$ heterodimers, increasing the likelihood of generating a MT seed, such as TPX2 and HURP. **End-binding proteins:** these proteins specifically bind at MT plus or minus ends. By far the most studied are the plus end binding proteins, or +TIPs. A large number of +TIPs regulate growth, shrinkage, pause or transition between catastrophe and rescue states (Kline-Smith and Walczak 2004; van der Vaart et al. 2011). For example, cytoplasmic linker proteins (CLIPs) and CLIP-associated proteins (CLASPs) trigger rescue, whilst end binding proteins (EBs) stimulate MT dynamicity and polymerisation, and prevent catastrophes. Among these +TIPs, end-binding protein 1 (EB1) plays an essential role in recruiting interacting +TIPs to regulate dynamic instability. Due to this importance, EB1 is subject to extensive investigation (Nehlig et al. 2017). Finally, MT depolymerase mitotic centromere-associated kinesin (MCAK) stimulates catastrophes (van der Vaart et al. 2011). **Structural MAPs:** these MAPs connect MTs to cytoskeletal components and are otherwise known as cytoskeletal crosslinkers. Two principal classes are MT-actin crosslinking factors 1 and 2 (MACF1 and MACF2). These two proteins have an N-terminal actin-binding domain and C-terminal MT-binding motif. Due to

their ability to interact with different cytoskeletal components, MACFs participate in different cellular functions. For instance, MACF1 is important for cell migration, thus they regulate wound healing, migration of neurons during brain development and axon growth (Bodakuntla et al. 2019; Hu et al. 2017).

1.3.5 Regulation of the cell cycle

The cell cycle is firmly regulated by various checkpoints (Figure 1.6) to ensure complete and precise chromosome replication and segregation (Tan et al. 2017; Vermeulen et al. 2003). The cell division regulatory system is composed of checkpoints that arrest cell cycle progression during phase transition to check if cellular conditions are satisfactory for growth and separation (Satyanarayana and Kaldis 2009; Tan et al. 2017).
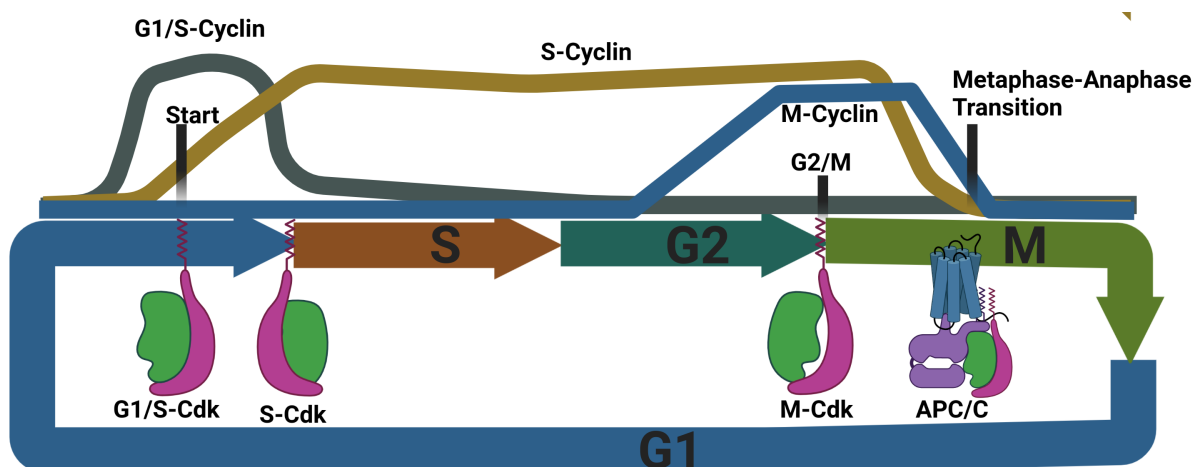
Figure 1.6: **Cyclin-Cdk complexes of cell cycle regulation.** In eukaryoteic cells, three classes of cyclin proteins are involved in regulation of cell division: G_1/S cyclins, which concentration increases at the first checkpoint found at the end of G_1 phase and decreases in S phase, S-cyclins increase their levels in late G_1 and remain constant until metaphase-anaphase transition. M-cyclins increase their concentration at the G_2/M transition,where stimulate Cdks and fall in metaphase.

Cyclin-dependent kinases (Cdks, Table 1.3) are major proteins involved in cell division regulation and their activities increase and decrease as the cell moves forward through the cell cycle (Malumbres and Barbacid 2005). The activity of Cdks is regulated by a large number of enzymes and other proteins, and the most eminent are cyclin proteins (Figure 1.6 and Table 1.3) discovered by Tim Hunt in 1982 (reviewed by Peters 2002) and termed as cyclin by Evans et al. (1983). In each cell cycle, cyclin proteins are subjected to a cycle of synthesis and degradation, whilst the concentration of Cdks is constant. These cyclical changes in cyclin protein concentration lead to cyclic binding and stimulation of cyclin-Cdk complexes at specific points of the cell division cycle (Peters 2002; Satyanarayana and Kaldis 2009). Four classes of cyclins are implicated in the activation of Cdks. Of particular relevance to the work in this thesis are the Mitotic, or M-cyclins.

G_1-cyclins help the function of G_1/S-cylins to regulate the checkpoint in the late G_1 phase.

G_1/S-cyclins stimulate Cdks in late G_1 and therefore activate progression through checkpoint.

S-cyclins activate Cdks involded in DNA replication.

M-cyclins at the G_2/M transition, stimulate Cdks that trigger entry into mitosis.

Table 1.3: **Principle cyclins and Cdks of vertebrates.**

Cyclin-Cdk complex	Cyclin	Cdk partner
G_1-Cdk	Cyclin D (D1, D2 and D3)	Cdk4 and Cdk6
G_1/S-Cdk	Cyclin E (E1 and E2)	Cdk2
S-Cdk	Cyclin A (A1 and A2)	Cdk2 and Cdk1
M-Cdk	Cyclin B (B1, B2 and B3)	Cdk1

Cyclin B is synthesized during the G_2 phase, associating with Cdk1 (Malumbres and Barbacid 2005; Schafer 1998). In mammalian cells, Cdk1-CyclinB complexes phosphorylate more than 70 proteins implicated in different stages during G_2/M checkpoint and mitotic progression (Malumbres and Barbacid 2005). Cdk1-CyclinB complexes are implicated in activating proteins that regulate chromosome condensation, such as Histones (HMG-I and RIIa), fragmentation of the Golgi apparatus, which includes Nir2, p47, GM130 and GRASP65, and phosphorylaltion of complexes involved in nuclear envelope breakdown, such as different lamins, which include lamin B receptor and the nuclear pore complex (Malumbres and Barbacid 2005; Schafer 1998). Additionally, Cdk1-CyclinB proteins also phosphorylate MAPs, for instance, motor proteins, such as Eg5 which promotes centrosome separation (Khodjakov and Rieder 2001; Malumbres and Barbacid 2005) and many other mitotic kinases, such as Polo, Aurora A and Mps1 (Barbosa et al. 2020; Conde et al. 2013; Tipton et al. 2013). The inhibition of Cdk1, triggered by the degradation of CyclinB by the anaphase promoting complex (APC/C), leads to the dephosphorylation of the Cdk1 targets; therefore triggering the changes in MT organisation required for chromosome segregation and cytokinesis.

1.3.6 Regulation of mitotic MT dynamics

The depolymerisation of the interphase array of MTs that occurs just prior to mitosis results in an increased pool of soluble tubulin dimers. At the same time, there is a large recruitment and activation of the γ-TuRC at the duplicated, but closely paired centrosomes. Together these things result in a dramatic increase in MT nucleation, predominantly from the centrosome, resulting in MT asters. Activation of MT motor proteins, such as the kinesin-like protein Eg5, drive the separation of the two centrosomes away from each other, pushing them around the nuclear envelope. This is also helped by pulling forces generated by the minus-end directed motor protein, Dynein/Dynactin, which is

immobilised both at the nuclear envelope and at the cell cortex. As the nuclear envelope breaks down, the MTs nucleated by centrosomes can enter the nuclear space and begin to attach to the sister chromatids. In addition, the increase in soluble tubulin in the nuclear space results in Ran-dependent MT nucleation around chromosomes, increasing the number of short MTs and MTs that can be directly nucleated by kinetochores.

Kinetochores are specialised structures present on the chromosomes, composed of various proteins, about 100 in human cells. They include structural proteins, signaling proteins, proteins involved in monitoring chromosome attachment to kinetochore MTs, such as the ROD-ZWILCH-ZW10 (RZZ) complex, Ndc80, KNL1, CLASP1, CENP-F and motor proteins that bind to MTs to create forces to regulate chromosome position and MT dynamic instability (Kline-Smith and Walczak 2004; McIntosh 2016; Mosalaganti et al. 2017). In animal cells, Dynein/Dynactin also associates with kinetochores. Here, it facilitates the removal of the RZZ complex from kinetochores towards the spindle poles. The removal of RZZ from kinetochores is a key part of the Spindle Assembly Checkpoint (SAC), which ensures that sister chromatid segregation does not occur until all chromosomes are aligned at the metaphase plate. At this point, inhibition of an E3 Ubiquitin ligase, the Anaphase Promoting Complex/Cyclosome (APC/C) is relieved, triggering protein polyubiquitination and consequently proteolysis of two key proteins (Figure 1.7). Cyclin B and securin which is a repressor of separase involved in hydrolysis of cohesin complex that hold sister chromatids together (Hornig et al. 2002).
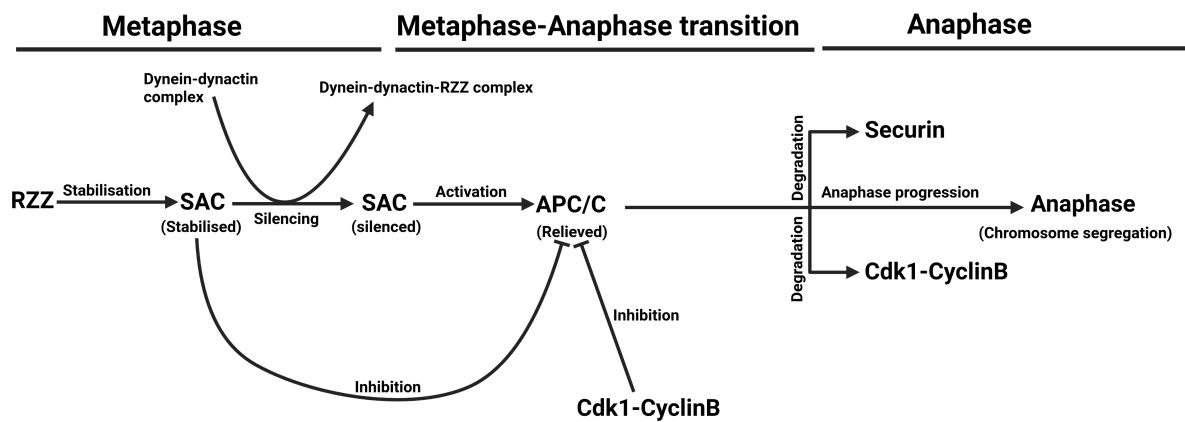
Figure 1.7: **Illustration of the anaphase promoting complex/cyclosome (APC/C) signalling pathway in cell cycle control.** ROD-ZWILCH-ZW10 (RZZ) complex is a component of kinetochore involved in stabilising the Spindle Assembly Checkpoint (SAC) to allow correct attachment of all spindle MTs to chromosome kinetochores. The mitotic checkpoint proteins directly inhibit APC/C and sequester Cdc20. In addition, Cdk1-CyclinB also contributes to this inhibition via Cdc20 phosphorylation. Upon proper attachment of all kinetochore fibers to chromosome kinetochores, rapidly RZZ complex is removed from the kinetochore to MT minus ends via Dynein/Dynactin complex. This results in silencing SAC, consequently the inhibition of APC/C is relieved, promoting the degradation of securin and Cdk1-CyclinB, which leads to anaphase progression.

As previously mentioned, the inactivation of Cdk1 through cyclin B destruction leads to dephosphorylation of all proteins responsible for the onset of mitosis, including regulators of MT dynamics. This leads to the three MT-dependent movements that characterise chromosome segregation: the distance between the chromosome and the pole it faces decreases as kinetochore MTs depolymerise, from both their plus end and minus end; the distance of separation between two spindle poles increases as motor proteins present on the interpolar MTs slide the anti-parallel MT bundles (McIntosh 2016); and the astral MTs dramatically increase in length, increasing their contacts with the cell cortex and pulling the spindle poles further apart. Finally, in telophase, the MTs nucleated by centrosomes begin to re-organise into interphase-like arrays, while the interpolar MTs bundle and stabilise to form, first, a central spindle which is important in the placement of the acto-myosin contractile ring and, second, a midbody which is important in the terminal stages of cytokinesis (Chircop 2014;

Leite et al. 2019; McIntosh 2016).

1.3.7   End binding proteins (EBs)

As many MTs are nucleated and anchored at the centrosome by their minus ends, much of the cell-cycle dependent changes in MT organisation are as a result of changing the dynamics of the MT plus ends, or their association with key structures, such as kinetochores, the nuclear envelope or the cell cortex. The role of MT plus end proteins (+TIPs) therefore should not be underestimated. Among +TIPs proteins, one of the most well studied and most important is end-binding protein 1 (EB1). This was identified in 1995 as an Adenomatous Polyposis Coli (APC)-interacting partner (Baek et al. 2013; Nehlig et al. 2017) although subsequently other related proteins were identified. The EB family each share a common molecular structure (Komarova et al. 2009; Nehlig et al. 2017); an N-terminal calponin homology (CH) domain which is responsible for MT binding, a flexible linker, and a C-terminal coiled-coil domain which is involved in dimerisation (Figure 1.8 and 1.9). The coiled-coil domain overlaps with an end-binding homology (EBH) domain which is involved in auto-inhibition and interaction with +TIPs in humans, whereas in *Drosophila* this coiled-coil motif does not overlap with EBH (Figure 1.8). This domain ends with a tail that contains the C-terminal sequence EEY/F (Akhmanova and Steinmetz 2008; Komarova et al. 2009; Nehlig et al. 2017). The sequence EEY/F undergoes contintuous detyrosination and tyrosination cycles for modulating the interactions between EB and MTs. The detyrosination of this sequence leads to an increase of EB decoration time at MT plus ends, thereby decreasing the MT catastrophe (Zhang et al. 2013).
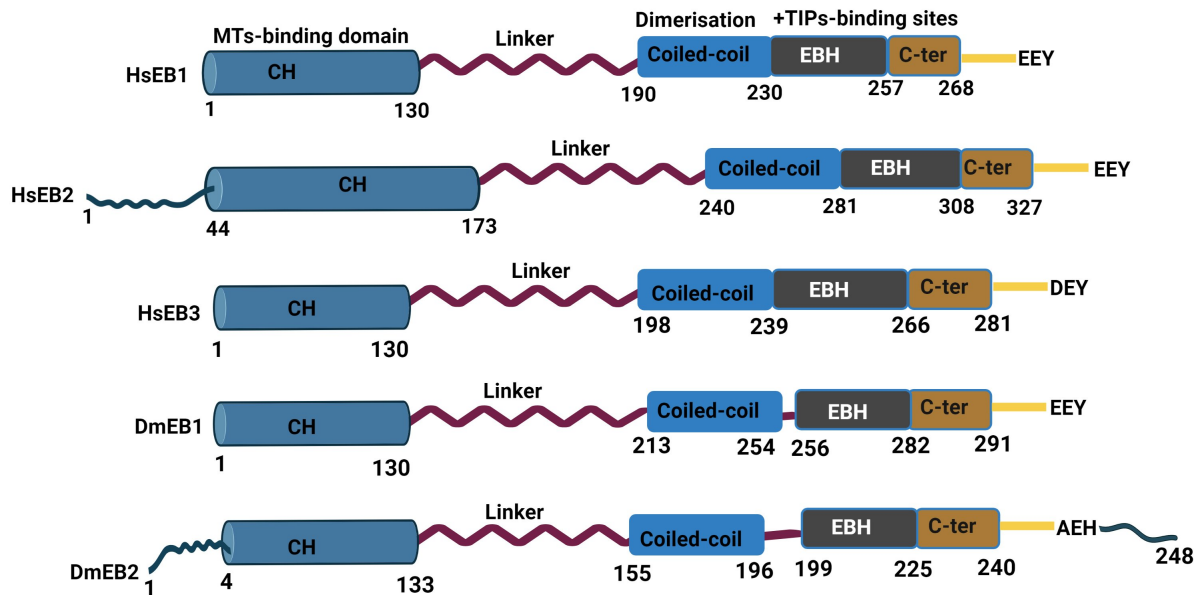
Figure 1.8: **Schematic depiction of homodimeric end-binding proteins.** The figure shows a general structure of EBs with a plus end-binding homology (EBH) domain implicated in +TIP interaction and MT binding calponin homology (CH) involved in MT binding. These two motifs are separated by a flexible linker. Hs = human and Dm = *Drosophila*. HsEB coiled-coils overlap with EBH while DmEB coiled-coils do not.
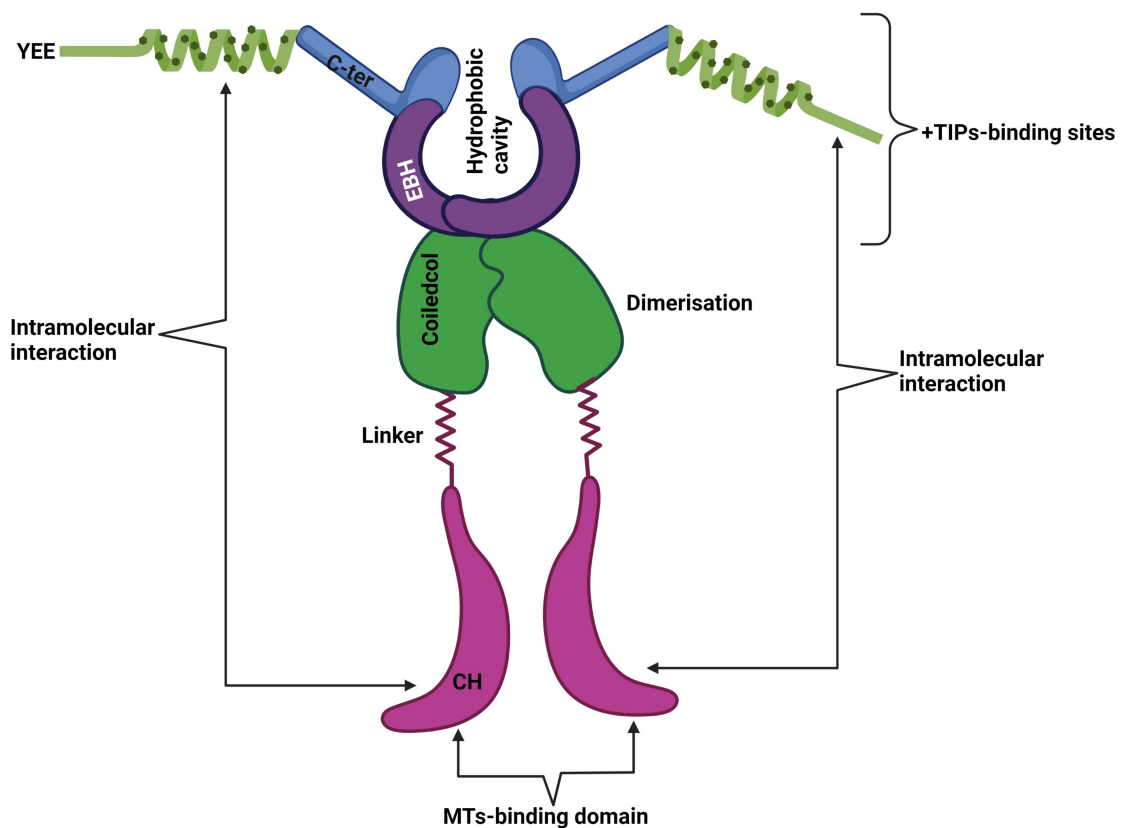
Figure 1.9: **General EB dimer representation.** The coiled coil region is responsible for dimerisation, the CH domain for MT binding and the EBH cavity for +TIP interactions. The C-terminus can also intramolecularly interact with CH for self-regulation.

EB proteins are thought to function by recruiting a wide variety of effector proteins to the plus ends of MTs. Currently, there are three major classes of EB1 interacting proteins (Akhmanova and Steinmetz 2008; Kumar et al. 2017; Nehlig et al. 2017); those that contain a cytoskeletal-associated protein glycine-rich (CAP-Gly) motif, those with a Ser/Thr-x-Ile-Pro (SxIP) motif and Leu-x-x-Pro-Thr-h (LxxPTPh) containing proteins. A small group of proteins, such as CLIP-115, CLIP-170 and dynactin complex p150^{Glued} possess CAP-Gly which mediates their interaction between MTs and EB1, whereas the proteins containing SxIP form a large family of EB1 interactors (For EB1-SxIP interactions, see EBH-S/TxIP interactions and regulations, Page 24) (Hayashi et al. 2005; Nehlig et al. 2017). These SxIP containing proteins are structurally heterogeneous and are involved in several aspects of MT dynamics and functions, such as the regulation of rescues and catastrophes, as well as providing a link between MT plus ends and cellular components (Kumar et al. 2017; Nehlig et al. 2017). A more recently described category of EB1 interacting proteins contain an Lxx PTPh motif. Their interaction with EB1 does not rely on the C-terminal tail of EBs, which is in contrast to the interaction of EB1 with CAP-Gly and SxIP-containing proteins (Jain and Tran 2017; Kumar et al. 2017).

1.3.8 *Drosophila* EB proteins

Sequence homology searching is one of the most informative steps in analysis used by molecular biologists to identify homologous proteins or genes, which reflect similar functions and common ancestry (Davison 1985; Pearson 2013). There is a large number of homology searching programs including BLAST, FASTA and HMMER3 (Pearson 2013).

The genome of the fruit fly, *Drosophila melanogaster,* contains two EB-like homologues, *Drosophila melanogaster* EB1 (DmEB1) and a relatively uncharacterised protein, CG18190, which we refer to as DmEB2. To identify the identical amino acid sequences in end-binding homology regions (EBH) of HsEBs

and DmEBs, I aligned these domains (Table 1.4).

Table 1.4: **Sequence identity searching in EBH domain.** The identitical sequence alignment in EBH regions of DmEB1 and DmEB2 is 40.0%, DmEB1 and HsEB1 is 51.9% and DmEB2 and HsEB2 is 28.6%. This suggests that EBs play similar functions in living beings. Indeed, serine or threonine of S/TxIP-containing proteins may form a network of hydrogen bonds with arginine (R)/lysine (K), tyrosine (Y), glutamine (Q) and glutamic acid (E)/aspartic acid (D) in EBH region of EB proteins.

```
40.0% identity in 15 residues overlap; Score:
31.0; Gap frequency: 0.0%
DmEB1        8 IIQKILDILYATEDG
DmEB2        8 LCKRIQAVLYKTIDG
               *    ** * **

51.9% identity in 27 residues overlap; Score:
85.0; Gap frequency: 0.0%
DmEB1        1 DDAEAHPIIQKILDILYATEDGFAPPD
HsEB1        2 NEGENDPVLQRIVDILYATDEGFVIPD
               *   *   * * ****** **   **

28.6% identity in 21 residues overlap; Score:
28.0; Gap frequency: 0.0%
DmEB2        7 ELCKRIQAVLYKTIDGEINEE
HsEB2        8 DLVQRLMDILYASEEHEGHTE
               *   *    **    *    *
```

1.3.9   EBH-S/TxIP interactions and regulations

S/TxIP-containg proteins interact at the end of end-binding domain via an extensive hydrogen bonds with arginine (R)/lysine (K), tyrosine (Y), glutamine (Q) and glutamic acid (E)/aspartic acid (D) in the EBH region and these interactions are coordinated by water (Almeida et al. 2017; Nehlig et al. 2017). The regulation of these interactions is coordinated by post-translational modifications, including phosophorylation and dephosphorylation, acetylation and deacetylation of arginine (R) or lysine (K), and tyrosination and detyrosination of tyrosine (Y) (Nehlig et al. 2017; Zhang et al. 2013). Sequences flanking S/TxIP motifs have a net postitive charge and via electrostatic attractions interact with negative groups within the EBH, these include glutamic acid (E), aspartic acd

(D), phosphorylated tyrosine (Y) and threonine (T)/serine (S) (Honnappa et al. 2009; Nehlig et al. 2017). Thus, serine or threonine phosphorylation of S/TxIP motif, impairs the interactions of S/TxIP-containing proteins with EBH, due to electrostatic repulsions (Zhang et al. 2016).

1.3.10 EB1 functions in interphase and in mitosis

In interphase, Human EB1 colocalises to cytoplasmic MTs and recruits +TIP partners, such as, SLAIN2, cytoplasmic linker proteins (CLIPs) and CLIP-associated proteins (Berrueta et al. 1998; Elliott et al. 2005; van der Vaart et al. 2011). During interphase SLAIN is dephosphorylated to form a complex with colonic hepatic tumor overexpressed gene (ch-TOG) which interacts with EB1 to stimulate MT polymerisation (Nakamura et al. 2012; van der Vaart et al. 2011). In addition, studies using *Drosophila* S2 cells treated with EB1RNAi have shown a decrease in MT dynamics due to reduction of catastrophe and rescue frequencies, demonstrating that MTs spent most of their lifetime in a period of pause (Rogers et al. 2002). Furthermore, EB1 interacts with APC and p150^{Glued} to anchor MT minus end at centrosomes in interphase and maintains a radial MT array (Askham et al. 2002; Brüning-Richardson et al. 2011; Green et al. 2005). These MTs, which radiate from the centrosome during interphase, supply tracks for MT motors carrying cargos, such as, membrane, RNA and protein complexes away and toward the cell centre (Rogers et al. 2002). EB1 has also been suggested to interact with constituents of the cytoplasmic Dynein/Dynactin complex during interphase, however, the role of this interaction remains unknown (Askham et al. 2002; Berrueta et al. 1998).

Through its C-terminus (C-ter) EB1 interacts with numerous +TIP partners and recruits them at the MT plus ends to create +TIP molecular networks that help the management of MT dynamic instability (Nehlig et al. 2017). This dynamic instability is important for chromosome alignment and segregation and spindle orientation (Gudimchuk et al. 2020; Hevia and Fanarraga 2020; Rogers

et al. 2002; Sulimenko et al. 2017; Teixidó-Travesa et al. 2012).

In mitosis EB1 interacts with ACP to regulate MT dynamic instability, chromosome alignment and segregation, and is implicated in spindle orientation (Brüning-Richardson et al. 2011; Green et al. 2005). In addition, EB1 is also involved in interaction with fibroblast growth factor receptor 1 (FGFR1) oncogene partner (FOP) in association with CAP350 to create an important complex for MT plus end anchorage at the centrosome (Brüning-Richardson et al. 2011). EB1 knockdown increases defects in chromosome segregation and errors in spindle orientation, but the mechanism of this process is not clear (Brüning-Richardson et al. 2011; Green et al. 2005).

1.3.11   EB1 in human pathology

Overexpression of EB1 has been found in numerous cancer types including, hepatocellular carcinoma, glioblastoma, breast, colon and oral cancers (Nehlig et al. 2017). In addition, EB1 may be a predictive biomarker, where high level of expression is related to poor survival rates. As such, EB1 represents a potential target against various cancers (Brüning-Richardson et al. 2011; Nehlig et al. 2017). This has been demonstrated in principle through siRNA studies. siRNA depletion of EB1 resulted in inhibition of cancer cell proliferation while its overexpression caused proliferation of cancer cells (Brüning-Richardson et al. 2011). Due to the importance of EB1 involvement in a large number of cancers, a deeper understanding of EB1 regulation at MT plus ends and the identification of +TIP molecular networks, will be a vital step for the design of novel +TIP-targeted drug therapies (Nehlig et al. 2017). For instance, the potent MT-associated protein ATIP3, negatively regulates EB1 at MT plus end in colon, breast, liver and oral cancers (Brüning-Richardson et al. 2011; Haykal et al. 2021; Nehlig et al. 2017). Interestingly, EB1 may play a role as an oncogene by activating the WNT[2] signalling pathaway in cancer cells (Brüning-Richardson et al.

---

[2]Wnts are secreted glycoproteins and constitue a large family of nineteen proteins in human. The Wnt signalling pathway is an ancient and concerved pathaway involved in crucial

2011).

1.4   Early *Drosophila* embryo as a model organism for mitosis

Drosophila melanogaster, originally from sub-Saharan Africa, migrated out of Africa to America, Europe, Asia and Australia about 12,000-19,000 years ago (Fabian et al. 2015; Flatt 2020). This organism was first proposed as model to study genetics in 1900 by Charles W. W., an American entomologist (Ugur et al. 2016). It has high fertility and a short life cycle (2 weeks), thus allowing for the rapid raising and expansion of populations for genetic, biochemical and molecular investigations. It is easy to grow, to manipulate genetically, to breed in the laboratory and they are low cost. There are many available genetic tools, such as balancer chromosomes, classical mutants, transgenic line and lines that allow *in vivo* RNA interference (RNAi), whilst well-characterised physiology and cell biology development make them amenable to high spatio-temporal live microscopy (Flatt 2020; Garcia et al. 2007). Furthermore, about 60% of genes in this species have homologues in humans while around 75% of genes involved in human pathology have homologues in *Drosophila* (Ugur et al. 2016, reviewed by Mirzoyan et al. 2019). Despite the fact that humans and flies differ greatly in terms of dimension and cellular features, their various molecular mechanisms implicated in developmental control, cellular and physiological processes are conserved in both organisms (Ugur et al. 2016). All these features have made *Drosophila melanogaster* one of the most powerful and experimentally versatile model organisms (Flatt 2020; Mirzoyan et al. 2019).

---

regulation of cell migration, cell polarity and organogenesis in embryonic development process (Komiya and Habasi 2008).

Despite the advantages of using *Drosophila* as model organism to study human diseases, there are potential disadvantages of using them. Fruit flies lack cells implicated in regulating the adaptive immune system, such as B and T cells. Additionally, these organisms do not have some important key branches of immune signalling, such as interferon responses (Harnish et al. 2021). The genome of *Drosophila melanogaster* is much smaller than the human genome (Wolf and Rockman 2008) and have four pairs of chromosomes (X, 2, 3 and 4) compared to 23 pairs of chromosomes in human. Consequently, some important factors involved in human diseases may be ignored or mssing in *Drosophila*, such as factors implicated in immunological diseases, brain infarcts and hemorrhage (Jeibmann and Paulus 2009) or to investigate human diseases related to hemoglobin, as fruit flies do not have hemoglobin (Prüβing et al. 2013). Therefore, before using *Drosophila* as a model for diseases, it is important to take into account all factors and to make sure that the mechanism of action for a disease of interest occurs on a well conserved pathway.

Drosophila have been, and continue to be used widely as a model to study mitosis, as the components implicated in the cell cycle control system in *Drosophila* are functionally and structurally similar to humans (Garcia et al. 2007; Jones et al. 2000; Tang 2016). Thus, this investigation contributes to our comprehension of the cell cycle mechanisms and gives solutions to several human pathologies, such as, cancers, neurodegenerative disease and male infertility. Following fertilisation of the *Drosophila* egg, the early cell cycles of *Drosophila* embryos have principally two phases: S and M phases. Each S/M cycle lasts approximately 10 minutes. In contrast, gap phases (G_1 and G_2) are short or undetectable (Edgar and O'Farrell 1989; Garcia et al. 2007). *Drosophila* S/M cycles corresponding to the 1–13 cycles occur synchronously without cytokinesis in a common cytoplasmic embryo, which is called a syncytium (Garcia et al. 2007). This syncytium can be exploited for mitosis research; for example, it can

withstand a single injection of antibodies, dominant negative proteins, drugs or dsRNA to study the effect simultaneously on numerous nuclei by live imaging microscopy. Nuclei in cycles 1–3 remain grouped at the anterior third of the egg (Figure 1.10), close to the site of male and female pronuclei fusion. During cycles 4–6 the nuclei become distributed along the length of the embryo in a process known as axial expansion (Figure 1.10) (Albertson et al. 2008; Tram et al. 2002). From cycle 8, nuclei start migrating from the centre towards the periphery of the embryo, and by cycle 10 some nuclei reach the actin-rich cortex just beneath the plasma membrane of the embryos where the 10-13 syncytial divisions occur (Figure 1.10) (Garcia et al. 2007; Tram et al. 2002). Nuclei that arrive at the posterior end of the cortex are germline precursors (9–13, Figure 1.10) (Tang 2016; Tram et al. 2002). Ultimately by cycle 13, the embryo has formed about 6000 nuclei which cease their synchronous divisions and from nuclear cycle 14, undergoes a process of cellularisation (Garcia et al. 2007; Tram et al. 2002).
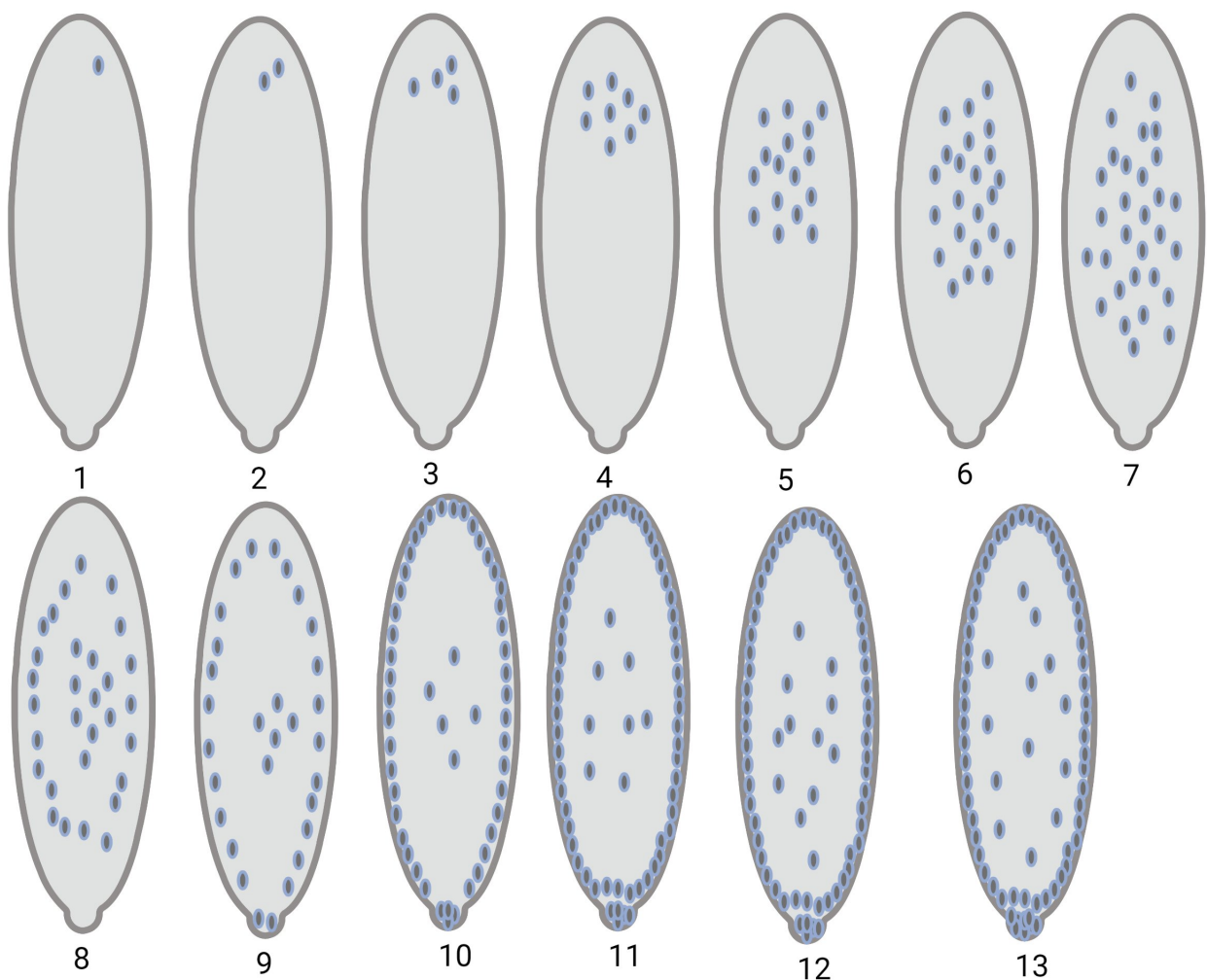
Figure 1.10: ***Drosophila melanogaster* embryo cell cycles 1–13.** The first 13 nuclear divisions happen synchronously and without cytokinesis in the same cytoplasm known as a syncytium. Cycles 1-7 ocurr in the centre of the cytoplasm and from cycle 8 nuclei start migrating to the cortex of the embryo where some of the nuclei reach at cycle 10. Syncytial cycles 10-13 occur just behind the cortex of the embryos. From cycle 14 the embryo starts the cellularisation process and gap 2 (G_2) phase can be detectable.

During the syncytial divisions, centrosomes play a crucial role in generating astral MTs that drive and avoid the collision of neighbouring syncytial nuclei. Thus as the number of nuclei increases, astral MTs act as barriers that impede collisions. Furthermore, astral MTs are important in establishing general orientation and distribution of syncytial nuclei, and contributing to cortical nuclei migration (Albertson et al. 2008; Tram et al. 2002). The arrival of nuclei (cycles 10-13) at the embryo cortex induces the redistribution of the actin beneath the plasma membrane, which will become concentrated into apical caps centred above each cortical nucleus. As centrosomes migrate toward the opposite poles during prophase, the actin caps experience dramatic changes to form a

ring that outlines each nucleus with its pair of centrosomes (Tram et al. 2002). These rings are similar in components to cytokinesis contractile rings and contain actin, myosin II, anillin, spectrins, formins and septins (Sobral et al. 2021; Tram et al. 2002). During metaphase, the furrows invaginate to form a half shell that encompasses each mitotic spindle. During late anaphase and telophase, the metaphase furrows regress rapidly to their initial state. Centrosomes duplicate during late anaphase and in the following interphase, the newly formed pairs of centrosomes are again localised apically and the actin caps reform for a subsequent cycle (Tram et al. 2002). These transitions between metaphase furrow formation and interphase actin caps occurs during interphase of the cell cycle 14. After this cycle, the cortical nuclei remain in interphase and the embryo cellularises.

In this thesis, I focussed on investigating EB protein functions in *Drosophila* embryos during metaphase between cycles 10–13, as these nuclei undergo synchronous divisions, which allows observation and manipulation of multiple cell cycles in a short period of time (9–20 min/cycle). End binding protein 1 and 2 (EB1 and EB2) are the only EB family proteins in *Drosophila*. Although EB1 is more extensively studied than EB2, its functions during mitosis remains poorly understood (Nehlig et al. 2017; Rogers et al. 2002). In this work, I expressed and purified these proteins from bacteria to assess their capacity to associate with MTs *in vitro* using MT-cosedimentation. Additionally, I microinjected anti-EB1, anti-EB2 or the combination of anti-EB1 and anti-EB2 antibodies into these embryos to interfere with EB functions. Finally, I identified several EB1 binding proteins, including novel interactors to construct the protein-protein interaction (PPI) network asscociated with EB1 during metaphase. The analysis of this PPI network combined with antibody microinjection and relevant biological knowledge of these interactors provided new information about EB biological functions in the early *Drosophila* embryo mitosis.

Chapter 2:   Materials and Methods

2.1   Fly husbandry

2.1.1   *Drosophila* Stocks

Table 2.1: ***Genotype.*** The table shows the fly lines that have been used in experiments of the project.

Drosophila Stock	Fly phenotypes and functions	Source
$w; \dfrac{+}{+}; \dfrac{mat\alpha t-GAL4}{mat\alpha t-GAL4}$	Flies carry the GAL4 transcription factor, under the control of the maternal-α-tubulin promoter, driving GAL4 expression only in the developing oocyte and early embryos.	Bloomington Stock Center
$w; \dfrac{pUASp(EB1-GFP)}{Cyo}; \dfrac{mat\alpha t-GAL4}{mat\alpha t-GAL4}$	Females express EB1-GFP in developing oocytes and laid early embryos due to the expression of GAL4 driven by maternal-α-tubulin promoter, and the presence of the UASp-EB1-GFP transgene.	Ohkura Lab
$w; \dfrac{pNcd(EB1-GFP)}{Cyo}; \dfrac{+}{+}$	Females express EB1-GFP in developing oocytes and laid early embryos due to the expression of the EB1-GFP transgene driven by the maternal *non-claret disjunction (ncd)* promoter. Cyo is a floating second chromosome balancer.	Endow Lab
$w; \dfrac{HisRFP*pUAS(EB1-GFP)}{Cyo}; \dfrac{mat\alpha t-GAL4}{mat\alpha t-GAL4}$	Females express EB1-GFP in developing oocytes and laid early embryos due to the expression of GAL4 driven by maternal-α-tubulin promoter, and the presence of the UASp-EB1-GFP transgene. They also express Histone-RFP in all tissues. Cyo is a floating second chromosome balancer.	Wakefield Lab

Continuation of the Table 2.1

Drosophila Stock	Fly phenotypes and functions	Source
$w;\dfrac{pUB(\alpha Tub-GFP)(HisRFP)}{Cyo};\dfrac{MKRS}{TM6B}$	Flies (and embryos laid by mothers of this embryos) express Histone-RFP, and α-Tubulin-GFP, in all tissues, due to the transgenes being under the control of the polyubiquitin promoter. Cyo is a floating second chromosome balancer. MKRS and TM6B are 3rd chromosome balancers.	Wakefield Lab
$w;\dfrac{HisRFP}{Cyo};\dfrac{mat\alpha t-GAL4}{mat\alpha t-GAL4}$	Flies expressing Histone-RFP in all tissues, under control of the polyubiquitin promoter. The presence of the maternal-α-tubulin-GAL4 transgene means that, when they are crossed to lines carrying UASp-GFP fusion genes, resultant embryos will co-express both the Histone-RFP and the GFP-fusion in the early embryo. Cyo is a floating second chromosome balancer.	Bloomington Stock Center
$w;\dfrac{pUASp(mCh-JVL)}{Cyo};\dfrac{Pri}{TM6B}$	Flies carrying the gene encoding Javelin (JVL), fused to the gene encoding the fluorescent protein, mCherry, under the control of the UASp promoter. When crossed to flies expressing maternal-α-tubulin-GAL4, resultant embryos will express mCh-JVL fusion protein. Cyo is a floating second chromosome balancer. Pri is a dominant 3rd chromosomer marker. TM6B is a third chromosome balancer.	Abdu Lab
$w;\dfrac{+}{Cyo};\dfrac{pUASp(GFP-SPN-F)}{TM3}$	Flies carrying the gene encoding SPN-F, fused to the gene encoding GFP, under the control of the UASp promoter. When crossed to flies expressing maternal-α-tubulin-GAL4, resultant embryos will express the GFP-SPN-F fusion protein. Cyo is a floating second chromosome balancer. TM3 is a third chromosome balancer.	Abdu Lab
$w;\dfrac{pUAp(IK2-GFP)}{Cyo};\dfrac{Pri}{TM6B}$	Flies carrying the gene encoding IK2, fused to the gene encoding GFP, under the control of the UASp promoter. When crossed to flies expressing maternal-α-tubulin-GAL4, resultant embryos will express the IK2-GFP fusion protein. Cyo is a floating second chromosome balancer. Pri is a dominant 3rd chromosome marker. TM6B is a third chromosome balancer.	Abdu Lab

Continuation of the Table 2.1

Drosophila Stock	Fly phenotypes and functions	Source
$w; \dfrac{SP}{Cyo}; \dfrac{pUASp(SLAM-GFP)}{SLAM-GFP}$	Flies carrying the gene encoding slow as molasses (SLAM), fused to the gene encoding GFP, under the control of the UASp promoter. When crossed to flies expressing maternal-α-tubulin GAL4, resultant embryos will express the SLAM-GFP fusion protein. SP is a dominant second chromosome marker. Cyo is a floating second chromosome balancer.	Grosshans Lab
$w; \dfrac{pUB(SLAM-GFP)}{SLAM-GFP}; \dfrac{+}{+}$	Flies expressing SLAM-GFP in all tissues, under the control of the polyubiquitin promoter.	Grosshans Lab
$w; \dfrac{pUASp(HOOK-GFP)}{HOOK-GFP}; \dfrac{+}{+}$	Flies carrying the gene encoding HOOK, fused to the gene encoding GFP, under the control of the UASp promoter. When crossed to flies expressing maternal-α-tubulin-GAL4, resultant embryos will express the HOOK-GFP fusion protein.	Bloomington Stock Center
$w; \dfrac{+}{+}; \dfrac{pUASp(GFP-DNApol-epsilon58)}{GFP-DNApol-epsilon58}$	Flies carrying the gene encoding DNA Polymerase epsilon 58, fused to the gene encoding GFP, under the control of the UASp promoter. When crossed to flies expressing maternal-α-tubulin-GAL4, resultant embryos will express the DNApol-epsilon58-GFP fusion protein.	Wakefield Lab
$w; \dfrac{pUASp(GFP-PIGS)}{GFP-PIGS}; \dfrac{+}{+}$	Flies carrying the gene encoding Pickled Eggs (PIGS), fused to the gene encoding GFP, under the control of the UASp promoter. When crossed to flies expressing maternal-α-tubulin-GAL4, resultant embryos will express the GFP-PIGS fusion protein.	Roeper Lab
$w; \dfrac{+}{+}; \dfrac{pUASp(GFP-CORN)}{GFP-CORN}$	Flies carrying the gene encoding Cornetto (CORN), fused to the gene encoding GFP, under the control of the UASp promoter. When crossed to flies expressing maternal-α-tubulin-GAL4, resultant embryos will express the GFP-CORN fusion protein.	Wakefield Lab

Continuation of the Table 2.1

Drosophila Stock	Fly phenotypes and functions	Source
$w; \dfrac{pUASp(GFP-CG12702)}{GFP-CG12702}; \dfrac{+}{+}$	Flies carrying the gene encoding CG12702, fused to the gene encoding GFP, under the control of the UASp promoter. When crossed to flies expressing maternal-α-tubulin-GAL4, resultant embryos will express the CG12702-GFP fusion protein.	Wakefield Lab
$w; \dfrac{pUASp(EB1-RNAi)}{EB1-RNAi}; \dfrac{+}{+}$ (36680)	Flies carrying a shRNA corresponding to a region of the EB1 gene, under the control of the UASp promoter. When crossed to flies expressing maternal-α-tubulin-GAL4, resultant embryos will express the shRNA, driving RNA interference of expressed EB1.	Bloomington Stock Center
$w; \dfrac{pUASp(EB1^{DN}-mCh)}{EB1^{DN}-mCh}; \dfrac{+}{+}$	Flies carrying the gene encoding a putative dominant negative version of EB1 (EB1^{DN}), fused to mCherry, under the control of the UASp promoter. When crossed to flies expressing maternal-α-tubulin-GAL4, resultant embryos will express the EB1 mutant protein-mCh fusion protein.	Bloomington Stock Center

2.1.2 *Drosophila* stock maintenance

Fly stocks were maintained at room temperature and knocked over fortnightly in 25×95 mm fly food vials (500 g yeast, 350 g flour, 75 g agar, 60 ml propionic acid, 15.5 g nipigen and 1 L H_2O) or at 18 °C and knocked over every three weeks.

2.1.3 Fly collection for crosses

Flies were kept in food vials and bottles were maintained at 25 °C, 60% relative humidity and knocked over each day or every two days, depending on laying. After 9–10 days, female virgins were collected under CO_2 anaesthesia conditions and crossed to adult males. Subsequently, crossed flies were expanded under the same conditions and after 10 days offspring from crosses were collected for further early embryo collections. All the crosses done in this thesis are presented from Table 2.2 to Table 2.13.

Table 2.2: **Cross.** GFP-SPN-F x matαt-GAL4

$$\female\female \; w; \frac{K2}{Cyo}; \frac{GFP-SPN-F}{TM3} \qquad \times \qquad \male\male \; w; \frac{+}{+}; \frac{mat\alpha t-GAL4}{mat\alpha t-GAL4}$$

$$w; \frac{K2}{+}; \frac{GFP-SPN-F}{mat\alpha t-GAL4} \qquad\qquad w; \frac{+}{Cyo}; \frac{GFP-SPN-F}{mat\alpha t-GAL4}$$
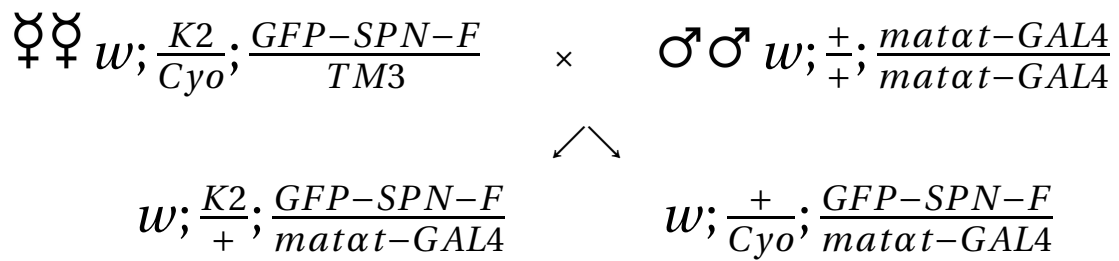
Table 2.3: **Cross.** IKK-epsilon-GFP x matαt-GAL4

$$\female\female \; w; \frac{IK2-GFP}{Cyo}; \frac{Pri}{TM6B} \qquad \times \qquad \male\male \; w; \frac{+}{+}; \frac{mat\alpha t-GAL4}{mat\alpha t-GAL4}$$

$$w; \frac{IK2-GFP}{+}; \frac{Pri}{mat\alpha t-GAL4} \qquad\qquad w; \frac{IK2-GFP}{+}; \frac{mat\alpha t-GAL4}{TM6B}$$
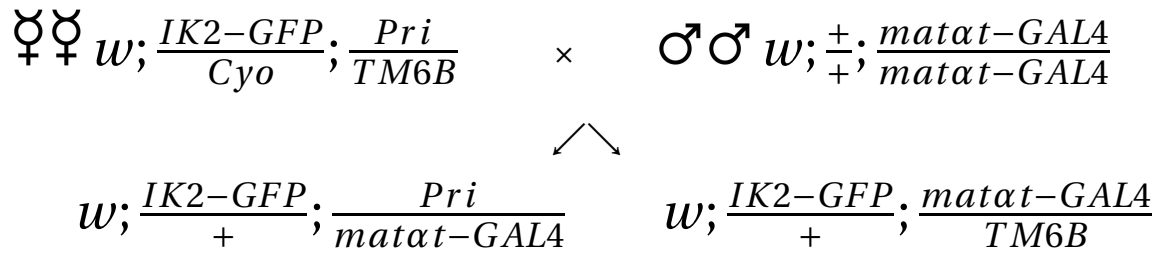
Table 2.4: **Cross.** mCh-JVL x matαt-GAL4

$$\female\female \; w; \frac{mCh-JVL}{Cyo}; \frac{Pri}{TM6B} \qquad \times \qquad \male\male \; w; \frac{+}{+}; \frac{mat\alpha t-GAL4}{mat\alpha t-GAL4}$$

$$w; \frac{mCh-JVL}{+}; \frac{Pri}{mat\alpha t-GAL4} \qquad\qquad w; \frac{mCh-JVL}{+}; \frac{mat\alpha t-GAL4}{TM6B}$$
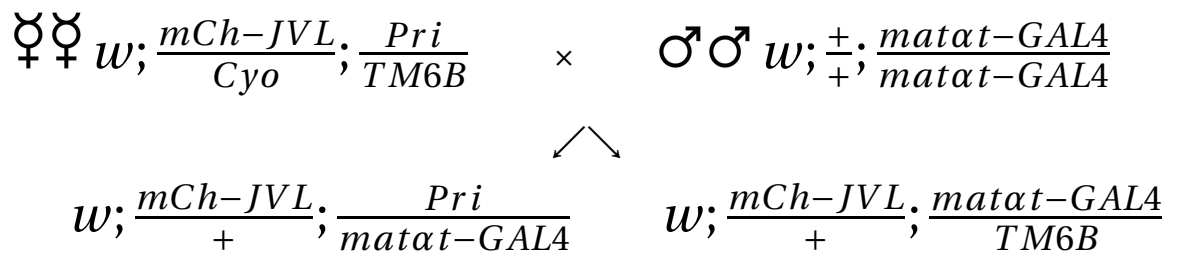
Table 2.5: **Cross.** GFP-PIGS x matαt-GAL4

$$\female\female \; w; \frac{+}{+}; \frac{GFP-PIGS}{GFP-PIGS} \qquad \times \qquad \male\male \; w; \frac{+}{+}; \frac{mat\alpha t-GAL4}{mat\alpha t-GAL4}$$

$$\Downarrow$$
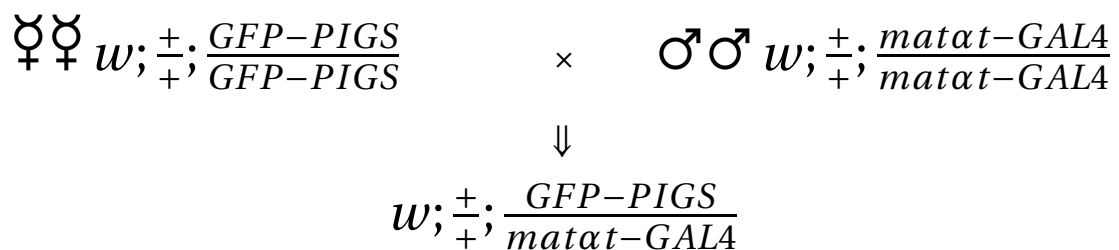
$$w; \frac{+}{+}; \frac{GFP-PIGS}{mat\alpha t-GAL4}$$

Table 2.6: **Cross.** GFP-PIGS x HisRFP;matαt-GAL4

$$\female\female \; w; \frac{+}{+}; \frac{GFP-PIGS}{GFP-PIGS} \qquad \times \qquad \male\male \; w; \frac{HisRFP}{Cyo}; \frac{mat\alpha t-GAL4}{mat\alpha t-GAL4}$$

$$\Downarrow$$

$$w; \frac{HisRFP}{+}; \frac{GFP-PIGS}{mat\alpha t-GAL4}$$

Table 2.7: **Cross.** HOOK-GFP x matαt-GAL4

$$\female\female \; w; \frac{HOOK-GFP}{HOOK-GFP}; \frac{+}{+} \qquad \times \qquad \male\male \; w; \frac{+}{+}; \frac{mat\alpha t-GAL4}{mat\alpha t-GAL4}$$

$$\Downarrow$$

$$w; \frac{HOOK-GFP}{+}; \frac{+}{mat\alpha t-GAL4}$$

Table 2.8: **Cross.** SLAM-GFP x matαt-GAL4

$$\female\female \; w; \frac{SP}{Cyo}; \frac{SLAM-GFP}{SLAM-GFP} \qquad \times \qquad \male\male \; w; \frac{+}{+}; \frac{mat\alpha t-GAL4}{mat\alpha t-GAL4}$$

$$\diagdown\diagup$$

$$w; \frac{+}{Cyo}; \frac{SLAM-GFP}{mat\alpha t-GAL4} \qquad\qquad w; \frac{SP}{+}; \frac{SLAM-GFP}{mat\alpha t-GAL4}$$

Table 2.9: **Cross.** SLAM-GFP x HisRFP; matαt-GAL4

$$\female\female \; w; \frac{SP}{Cyo}; \frac{SLAM-GFP}{SLAM-GFP} \qquad \times \qquad \male\male \; w; \frac{HisRFP}{Cyo}; \frac{mat\alpha t-GAL4}{mat\alpha t-GAL4}$$

$$\diagdown\diagup$$

$$w; \frac{HisRFP}{Cyo}; \frac{SLAM-GFP}{mat\alpha t-GAL4} \qquad\qquad w; \frac{HisRFP}{SP}; \frac{SLAM-GFP}{mat\alpha t-GAL4}$$

Table 2.10: **Cross.** GFP-CG12702 x matαt-GAL4

$$\female\female \; w; \frac{GFP-CG12702}{GFP-CG12702}; \frac{+}{+} \qquad \times \qquad \male\male \; w; \frac{+}{+}; \frac{mat\alpha t-GAL4}{mat\alpha t-GAL4}$$

$$\Downarrow$$

$$w; \frac{GFP-CG12702}{+}; \frac{+}{mat\alpha t-GAL4}$$

Table 2.11: **Cross.** GFP-DNApol-ε58 x matαt-GAL4

$$\female\female \; w; \frac{+}{+}; \frac{GFP-DNApol-\epsilon58}{GFP-DNApol-\epsilon58} \qquad \times \qquad \male\male \; w; \frac{+}{+}; \frac{mat\alpha t-GAL4}{mat\alpha t-GAL4}$$

$$\Downarrow$$

$$w; \frac{+}{+}; \frac{GFP-DNApol-\epsilon58}{mat\alpha t-GAL4}$$

Table 2.12: **Cross.** GFP-DNApol-ε58 x HisRFP;matαt-GAL4

$$\female\female \; w; \frac{+}{+}; \frac{GFP-DNApol-\epsilon58}{GFP-DNApol-\epsilon58} \qquad \times \qquad \male\male \; w; \frac{HisRFP}{Cyo}; \frac{mat\alpha t-GAL4}{mat\alpha t-GAL4}$$

$$\Downarrow$$

$$w; \frac{HisRFP}{+}; \frac{GFP-DNApol-\epsilon58}{mat\alpha t-GAL4}$$

Table 2.13: **Cross.** GFP-CORN x HisRFP;matαt-GAL4

$$\female\female \; w; \frac{+}{+}; \frac{GFP-CORN}{GFP-CORN} \qquad \times \qquad \male\male \; w; \frac{HisRFP}{Cyo}; \frac{mat\alpha t-GAL4}{mat\alpha t-GAL4}$$

$$\Downarrow$$

$$w; \frac{HisRFP}{+}; \frac{GFP-CORN}{mat\alpha t-GAL4}$$

2.1.4 Collection of embryos (cycling and MG132 treatment)

Flies were placed in *Drosophila* embryo collection cages, which were capped with apple juice agar plates (25 g agar, 300 ml apple juice concentrate and 700 ml H_2O) containing yeast paste for feeding (5 g baker's yeast in 6.43 ml H_2O). 8 batches (≈ 0.4 g each) of their embryos aged 1-3 hours were collected with paint-brush from apple juice agar plates. After dechorionation with bleach (100%) for 1–2 minutes, 4 of these batches were treated with MG132 for 20 minutes with shaking to arrest them in methaphase, whereas the other remaining 4 batches were treated as a control and allowed to progress with development. Successively embryos were filtrated into a filtration apparatus and washed three times with embryo washing buffer (0.05% Triton X-100 into H_2O). Finally, washed embryos were placed into weighed 1.5 ml eppendorf tubes, weighed again for getting the weight of embryos (weight of a 1.5 ml eppendorf tube of embryos minus the weight of the same tube without embryos) , labelled, flash-frozen in liquid nitrogen and then stored at -80 °C.

2.2 Biochemistry and Molecular Cell Biology

2.2.1 Expression and purification of bacterially-expressed MBP-EB1, MBP-EB2 and MBP

For bacterial transformation, 1 μl of pMAL-MBP-EB1, pMAL-MBP-EB2 and pMAL-MBP vectors (Okhura lab) in respective 1.5 ml Eppendorf tubes were incubated with 25 μl of BL21 (DE3) Competent *Escherichia coli* cells (ThermoFisher; `https://www.thermofisher.com/uk/en/home.html`) for 30 minutes on ice. Then the heat shock was conducted in a water bath at 42 °C for 35 seconds. After a further incubation on ice for 1–2 minutes, 400 μl of super optimal broth with catabolite repression (SOC) medium (ThermoFisher) was added to each sample and a subsequent incubation at 37 °C for 60 minutes with shaking. Afterwards, 200 μl of each sample were spread on LB-amp plates (Lauria broth and Lauria agar media and 100 μg/ml of ampicillin) and incubated at 37 °C overnight. 15 ml

tubes that contain 2 ml of fresh LB-Amp broth with one colony of each sample, were incubated at 37 °C overnight with shaking. 200 μl of each suspension and 2 ml of fresh LB-Amp broth in respective 15 ml tubes were incubated for further 4 hours, then isopropyl β-D-1-thiogalactopyranoside (IPTG, 1:1000. BIO-37036; `https://www.bioline.com/iptg.html`) was added to each sample and let grow up to 0.6-0.8 optical density (OD) at 37 °C with rotation. Then suspensions were centrifuged at 8000 rpm for one minute and pellets of samples were re-suspended into 10 ml of phosphate buffered saline (PBS) by vortex and cells disrupted by sonification for 5 minutes on ice, then extracts were centrifuged at 10,000 rpm for 20 minutes. After incubation of supernatant with amylose resin slurry (ThermoFisher SCIENTIFIC. #E8021S; `https://www.thermofisher.com/uk/en/home.html`) for 1 hour at 4 °C, suspensions were loaded into respective columns and proteins were eluted with maltose 10 mM in C buffer (50 mM HEPES pH 7.4, 1 mM EGTA, 1 mM $MgCl_2$, in 10 ml dH_2O) and then stored at -20 °C.

2.3   Affinity purification of anti-EB1, anti-EB2 and anti-MBP antibodies

Purified proteins, as described in Subsection 2.2.1, were subsequently dialysed with 100 mM of 3-(N-morpholino) propanesulfonic acid (MOPS) buffer, pH 7.5, according to the ThermoFisher Scientific protocol (`https://www.ther\mofisher.com/uk/en/home/references/protocols.html`) to remove unwanted small molecules from purified proteins in solution. Then dialysed proteins were chemically coupled to Affi-Gel 15 gel (BIO-RAD. Cat # 1536051; `https://www.bio-rad.com/en-uk`) in respective columns. Sera of polyclonal anti-EB1 and anti-EB2 antibodies (Okhura lab) were run 3 times through respective Affi-Gel 15 columns containing MBP as antigen. Successivly, the run through of antibodies was passed 3 times in respective Affi-Gel 15 columns with MBP-EB1 and MBP-EB2 proteins. Finally, the respective antibodies were eluted with

100 mM glycine HCl pH 2.4/150 mM NaCl buffer. Solutions of antibodies were neutralised with 1 M Tris.HCl pH 8 and stored at -20 °C.

2.3.1 Cleavage of MBP-EB1 and MBP-EB2 proteins

To remove MBP tag from purified protein, MBP-EB1 and MBP-EB2 proteins were incubated with Factor Xa (1:50) (BioLabs, Cat # P8010S; `https://www.neb.uk.com`) at room temperature for 2 hours, 4 hours, 8 hours and overnight, and the yield of cleavage was assessed by an SDS-PAGE (Nagai and Thiϕgerson 1984, 1987).

2.3.2 MT Cosedimentation assay

To assess the ability of purified proteins binding to microtubules, dialysed proteins were diluted to 1 mg/ml with C buffer (50 mM HEPES pH = 7.4, 1 mM EGTA, 1 mM $MgCl_2$, 9.470 ml dH_2) and ultra-centrifuged at 48,000 rpm for 5 minutes at 4 °C. 10 μl of proteins were incubated with 2.5 μl of GTP (10 mM) (Tubulin Polymerisation Assay Kit, Cat # BK011P; `https://www.cytoskeleton.com/bk011p`) and 10 μl of Tubulins (5 mg/ml) at 37 °C for 15 minutes. Then 2.5 μl of taxol (2 mM) was added to the mixture of reaction and incubated for further 10 minutes at the same temperature. Subsequently, the solution was added on the top of 40 % glycerol in respective ultracentrifuge tubes and spun down at 48,000 rpm for 45 minutes at 4 °C. Afterwards, the affinity of binding to MTs was assessed by Western blot.

2.3.3 Immunoprecipitation

To isolate a protein of interest and its interactors from *Drosophila* embryos, these embryos aged 1–3 hours expressing GFP fused to a protein of interest were homogenised by use of a drill in immunoprecipitation (IP) buffer (50 mM HEPES pH = 7.4, 1 mM EGTA, 1 mM $MgCl_2$, 100 μl Lysozyme 100 ×, 1 PhosSTOP tablet Roche, Cat # 4906837001"Merck; `https://www.sigmaaldrich.com/GB/en/product/roche/phossro`", 1 Complete MINI protease inhibitor tablet Roche

" Cat # 11836170001 Merck" " and 9.370 ml dH_2O) at 4 °C, subsequently ultracentrifuged at 48,000 rpm for 45 minutes and the high speed supernatant (HSS) was added to a fresh 1.5 ml Eppendorf tube containing 30 μl of GFP-TRAP Agarose (Chromotek; `https://www.chromotek.com`) previously washed three times with IP buffer (10 minutes for each wash), then incubated overnight with rotation at 4 °C. After washing for three times with IP buffer and centrifuged at 2,000 rpm for 30 seconds, pellets were kept at -80 °C.

2.3.4   Sodium dodecyl sulphate polyacrylamide gel electrophoresis (SDS-PAGE)

Resolving gel (9.58 ml dH_2O, 5 ml acrylamide/bis-acrylamide 40%, 5 ml 1.5 M Tris pH = 8.8, 200 μl SDS 10% and 20 μl Temed) and stacking gel (3.4 ml dH_2O, 0.5 ml acrylamide/bis-acrylamide 40% 1 ml 0.5 M Tris pH = 6.8, 80 μl SDS 10%, 50 μl APS and 5 μl Temed). Proteins were boiled with 2 × protein sample buffer (2 × PSB) which contains 100 mM Tris-HCl pH = 6.8, 4% SDS, 20% glycerol, 0.2% bromophenol blue and 100 mM dithiothreitol (DTT) at 85–95 °C for 5 minutes. Successively, 10 μl of samples (1 mg/ml) and 2.5 μl of PageRuler^{TM} Plus, Cat # 26619 (ThermoFisher SCIENTIFIC; https://www.thermofisher.com/uk/en/home.html), as a molecular weight control, were loaded into gel and then run at 250 V and 50 mA for 1 hour in Bio-Rad Mini-PROTEAn Tetra Verical electrophoresis Cell (BIO-RAD), which contains running buffer (14.4 g glycin, 3.02 g Tris, 1.0 g SDS in 1 L of H_2O). After washing with dH_2O, gels were stained for 1 hour with GelCode^{TM} Blue Stain Reagent or overnight with Coomassie Brilliant Blue R-250 Staining solution (0.1% Coomassie R-250, 40% methanol, 10% acetic acid) (ThermoFisher SCIENTIFIC; `https://www.thermofisher.com/uk/en/home.html`) and destain with a solution of 50% methanol and 1% acetic acid for 1–2 hours and repeated 2–3 times for protein visualisation.

2.3.5 Western blot

Proteins were transferred from polyacrylamide gel onto nitrocellulose membranes using Mini Trans-Blot^R Cell (BIO-RAD) containing transferring buffer (14.4 g glycin, 3.02 g Tris in 1 L of dH$_2$O). After transferring at 300 V and 150 mA for 1 hour using Techne DRI-Block DB-2A heater (TECHNE), membranes were blocked with 5% dried milk (Tesco) in 1 × Phosphate buffered saline and 0.1% Tween^R 20 Detergent (PBS/T) at room temperature for 1 hour with rotation. Then membranes were washed 3 times (5 minutes each) with PBS/T with rotation at room temperature and successively incubated with primary antibodies (Table 2.14) in PBS/T overnight at 4 °C.

Table 2.14: **Antibodies used in this project.**

Antibodies	Dilution	Source
Monoclonal Anti-GFP mouse	1:1000	Merck, Cat # SAB4200681
Monoclonal Anti-RFP rabbit	1:1000	Merck, Cat # SAB5701259
Polyclonal anti-EB1 rabbit	1:1000	Okhura lab (Elliott et al. 2005)
Polyclonal anti-EB2 rabbit	1:1000	Okhura lab (Elliott et al. 2005)
Polyclonal anti-MBP rabbit	1:1000	Okhura lab (Elliott et al. 2005)
Monoclonal DM1A anti-α-tubulin mouse	1:1000	Sigma, Cat # T6199
Polyclonal Donkey anti-Rabbit antibody	1:1000	ThermoFisher, Cat # A-21206
Polyclonal Goat anti-mouse antibody	1:1000	ThermoFisher, Cat # A32731

Several primary antibodies have been used in my experiments, these include rabbit polyclonal anti-EB1, anti-EB2 and anti-MBP antibodies that I have previously purified in the lab, as described in Materials and Methods 2, in section 2.3 and in section 3.5. These antibodies were used at 1:1000 dilution, monoclonal anti-RFP and anti-α-tubulin (DM1A) antibodies (ThermoFisher SCIENTIFIC) used at 1:1000 (Table 2.14). After overnight incubation, 3 times washes were carried out at room temperature with rotation in PBS/T, and then incubated with secondary antibodies (1:1000 in PBS/T) at room temperature. Polyclonal Goat anti-Mouse and Donkey anti-Rabbit antibodies were used as secondary at 1:1000 dilution (Table 2.14) (ThermoFisher SCIENTIFIC; `https://www.thermofisher.com/uk/en/home.html`). Finally, after 3 washes, membranes were imaged for protein visualtisation using LI-COR ODYSSEY^R XF (LI-COR; `https://www.licor.com/bio/odyssey-xf/`).

2.3.6 Tandem mass tag mass spectrometry (TMT-MS/MS)

To identify and quantify isolated proteins from *Drosophila* embryos via immunoprecipitation (IP), IP pellets (Subsection 2.3.3) were sent to the University of Bristol (Proteomics Facility), where they were subjected to Trypsin digestion and then labelled with Tandem Mass Tags (TMT) prior to Mass Spectrometry (MS/MS) for fragmentation. Taken together, the mass-to-charge (m/z) data of fragments and full peptides are subjected to computational search in large databases of the organism of interest to identify and quantify predicted proteins. Afterwards, results were shipped back in spreadsheet excel and data were analysed as below (Section 2.3.7) using Wakefield lab internal controls to identify proteins that are enriched in the MG132-treated samples (Subsection 2.3.7).

2.3.7 Bioinformatics

MS results were filtered by removing protein IDs (Accession: the unique iden-
tifer given to a particular *Drosophila* polypeptide; Name: the corresponding
protein name as given by Flybase (`www.Flybase.org`)) with; I) < 3 unique pep-
tide hits, II) < 10% coverage (the percentage coverage of a polypeptide sequence
represented in the peptides matched to that polypeptide) and III) overall MS
score of < 30 (score: the logarithmic summed score for the individual peptides
identified). This is the standard filter applied to all MS results in the Wakefield
Lab. Filtered results were then run through our false-positive database, accu-
mulated from eight independent control GFP-TRAP-A experiments (Palumbo et
al. 2015).

2.3.8 Generating transgenic flies

CG12702, DNApol-ε 58, CORN and GFP gene sequences were determined
using FlyBase (`https://flybase.org/`) and National Center for Biotechnol-
ogy Information (NCBI; `https://www.ncbi.nlm.nih.gov/`), and then veri-
fied with Expasy Translate program (`https://web.expasy.org/translate/`).
Subsequently, each gene sequence was fused upstream with GFP gene sequence
and then sent to GeneART for respective gene synthesis. Synthetic genes were
cloned into pDONR vector as Gateway and recombined into a pPGW (DGRC;
`https://dgrc.bio.indiana.edu/Home`) as destination plasmid in an *in vitro*
recombinase reaction. Finally, about 200 μl of each pPGW vector (1μg/μl) with
respective genes of interest were shipped back. 50 μl of pPGW-GFP-CG12702,
pPGW-GFP-DNApol-ε 58 and pPGW-GFP-CORN from GeneArt were sent to Best-
Gene for *Drosophila* embryo microinjection. Plasmid constructs were microin-
jected by BestGene into the germline of syncytial *Drosophila* embryo w^{118} mu-
tants as control. The individual transgenic flies with red eyes (those that had
stably incorporated GFP-CORN, GFP-CG12702 and GFP-DNApol-ε 58 under the

pUASP promoter) were collected and balanced by BestGene, then sent back to the lab.

2.3.9 Embryo preparation and antibody microinjections

Prior to *Drosophila* embryo collection, flies were incubated overnight at 25 °C in a lay cage covered with an apple juice plate which contains a yeast paste. This plate was replaced with a fresh one and changed every 1 hour of incubation. Changed plates were incubated for further 30 minutes from which embryos were collected using a paintbrush and placed on double sticky tape on coverslip (#1.5, 22 × 22 mm). Using a pair of tweezers, embryos were dechorionated manually and aligned in parallel on the embryo-glue line (20 cm of double-side tape and 250 μl of heptane in a 50 ml bottle) on coverslip under microscopy (Nikon SMZ645) conditions and successively covered with oil 27/700 (1:1). After embryo localisation under a 60× objective immersion oil using olympus spinning disc confocal microscopy, microinjection buffer (100 mM HEPES pH = 7.4 and 50 mM KCl in dH$_2$O), anti-EB1, anti-EB2 or the combination of anti-EB1 and anti-EB2 antibodies (2–4 mg/ml) were injected using eppendorf Femtotips^R II needles into embryos under 10× objective lens. A variable volume of antibody solution was injected, corresponding to an area of clearing within the embryo interior, without causing damage (Conduit et al. 2015).

2.3.10 Live imaging of *Drosophila* embryos

Embryos were imaged using a spinning disk confocal microscope equipped with an Olympus IX81 inverted microscope, a CSO-X1 spinning disk unit, CoolSNAP HQ2 CCD camera (Photometrics), and a UPlanSAPO x60, NA 1.35 oil objective. Image acquisition was done using VisiView software (Visitron Systems, Germany). Images were acquired at 5 second intervals, with a z stack consisting of 5 planes with a 1 μm step size. Exposure time was set to 200 ms. Lasers (power = 10–30%) at the wavelength of 488 and 561 nm were used to excite rescpective

GFP and RFP.

2.3.11 Image analysis (FIJI/Image J)

FIJI/ImageJ (ImageJ; `https://imagej.net/`) was used to analyse all obtained images from time lapse spinning disc confocal microscopy (Subsection 2.3.10). Sets of images (5 z images, multiple time points) were uploaded onto Image-JWindow. Initially, the Z project tool was applied, with maximum projection intensity, in order to generate a single image per timepoint. This was followed by the Bleach Correction tool, in order to maintain similar overall intensity throughout the time points. Next, image sets were subjected to the HiLo Look Up Table (LUT). This scales image intensities between blue (greyscale value 0 – minimum/black) and red (greyscale value 256 – maximum/white). Image sets at timepoint 0 were set so that only a few pixels were blue and red (i.e. maximising the image intensity between all 256 shades of grey). Following this optimisation, Greyscale LUT was reapplied. For image sets with more than 1 channel (e.g. GFP and RFP), channels were merged and pseudocoloured blue for DNA and green for different proteins.

2.3.12 Cytoscape analyses

To build the protein-protein interaction (PPI) map, enriched proteins in metaphase (Subsection 2.3.3) and identified through TMT-MS (Subsection 2.3.6) were visualised using Cytoscape Software 3.8.2 (https://cytoscape.org/). An empty network was created on which nodes and edges were added manually. A bait protein node was added in centre and surrounded by its interactors which are connected by edges. Moreover, different colours, sizes and shapes were applied onto nodes and edges and then the PPI network was exported to image as PNG.

Chapter 3: Dynamic localisation and depletion of EB1 in the early *Drosophila* embryo

3.1 Introduction

The first aim of my work was to document and understand the dynamic localisation of EB1 in the early embryo. For that purpose, I obtained two available *Drosophila* lines, one expressing EB1 fused to GFP, driven by the *ncd* (non-claret disjunction) promoter, driving expression of the transgene in the maternal germline and therefore early embryo (Flybase; FBrf0206773; `https://flybase.org/reports/FBrf0225681.html`). A second one was EB1 fused to GFP, driven by the UASp promoter. When crossed to flies expressing GAL4, driven by the maternal-α-tubulin promoter ($w; \frac{+}{+}; \frac{mat\alpha t - GAL4}{mat\alpha t - GAL4}$ flies), again, expression of EB1-GFP was driven in the maternal germline and early embryo.

The second aim in this Chapter was to identify a tool with which EB1 or EB2 could be specifically compromised in the early *Drosophila* embryo. For that goal, I initially started with attempts of depleting the levels of EB1 via EB1RNAi and EB1^{DN}, and finally to disrupt EB1 and EB2 functions via antibody microinjection.

There are three main approaches towards understanding the function of a gene product or protein in the cell. A biochemical approach relies on the isolation of the protein, either on its own or in association with interacting proteins, and measurement of its physical properties under a variety of conditions. The second approach investigates the protein *in situ.* The fusion of proteins with a genetically encoded fluorescent tag, such as GFP or mCherry, allows its dy-

namic localisation to be recorded and analysed over time, providing clues as to the protein's function. Alternatively, the function of the protein can be compromised and the consequences of removing or perturbing the protein on cell function can be studied. There are many different ways in which protein function can be perturbed. The main ones are genetic mutation, RNA interference, and interference of protein function through drugs, aptamers or interfering antibodies.

3.1.1   Disrupting gene product function in *Drosophila*

There are many different ways in which the function of a particular gene product can be perturbed – acting at the level of the gene, the messenger RNA (mRNA) or the protein.

Classical genetic approaches in *Drosophila* rely on the generation and study of organisms carrying mutations in a gene of interest (e.g. substitutions, insertions, deletions, rearrangements). These have relied on large scale screens, often using chemical mutagens which randomly cause mutations or transposon-mediated mutagenesis (González and Petrov 2009; Gratz et al. 2014; Levi et al. 2020). In recent years, different tools have emerged for precisely editing a locus in the genome; these include zinc-finger nucleases (ZFNs), transcription activator-like effector nucleases (TALENs) and the now widely-used clustered regularly interspaced short palindromic repeat associated 9 (CRISPR/Cas9) system (reviewed by Prykhozhij et al. (2018) and Ran et al. (2013)). Until recently, these approaches resulted in the loss of gene function in all cell types of an organism at all stages of development. However, recent developments, reported after the initiation of this PhD, allow for tissue-specific gene knockout (Meltzer et al. 2019; Port et al. 2020).

An alternative genetic approach has been the development of *in vivo* RNA interference (RNAi). RNAi was initially discovered in *Caenorhabditis elegans* (Fire et al. 1998). It is reliant on a cellular pathway that recognises double-stranded

RNA, cleaves it to 21 bp fragments, and uses one strand as a template to recognise and cleave the complementary endogenous mRNA in an autocatalytic cycle. In *Drosophila,* this has been adapted to generate a library of flies, each possessing an integrated short hairpin RNA (shRNA) construct, corresponding to a different gene, under the control of an inducible (pUAS) promoter (Bernards et al. 2006; Lu et al. 2007; Nishikawa and Sugiyama 2010; Shirane et al. 2004). While flies carrying these constructs will possess wild type levels of corresponding mRNA transcript, crossing them to flies expressing the DNA binding domain of the yeast GAL4 transcription factor will result in the GAL4 binding to the pUAS promoter, therefore driving shRNA expression (Figure 3.1 for an overview of the GAL4-UAS system). As there are many hundreds of fly lines each expressing GAL4 in a different tissue and/or developmental timepoint, the degradation of a specific mRNA, and therefore knock-down of a specific gene, can be targeted in space and time (Heigwer et al. 2018).
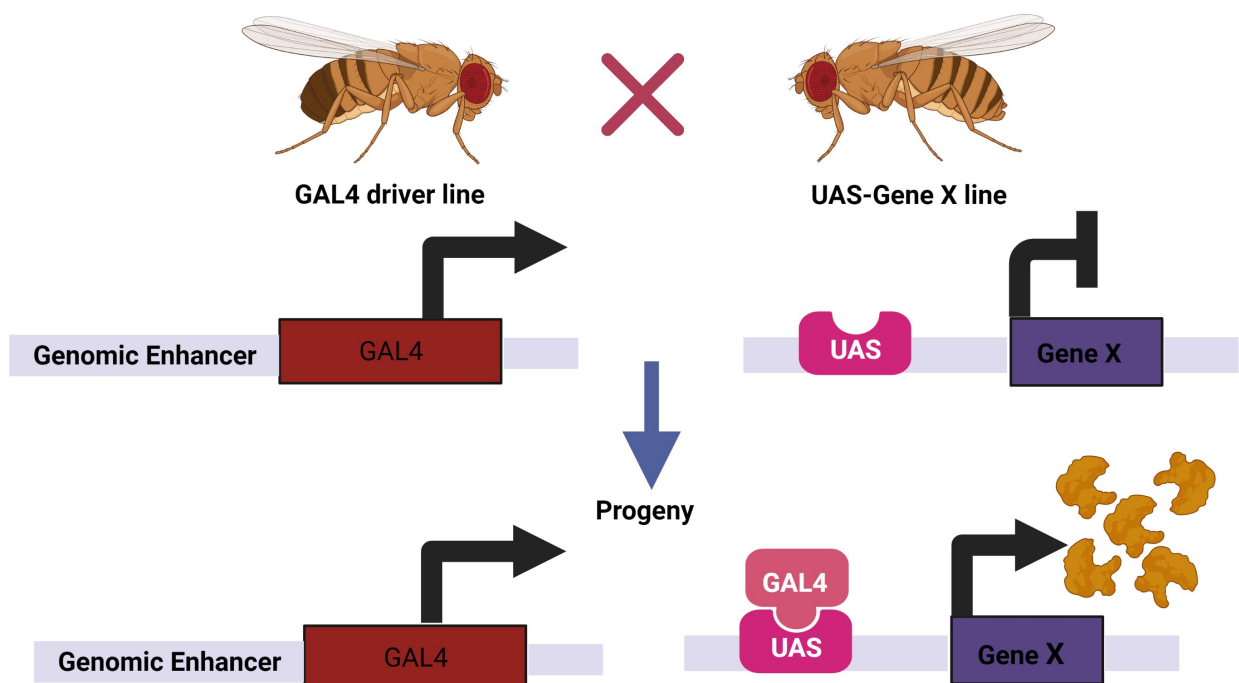
Figure 3.1: **General description of UASp-GAL4 system.** The GAL4-UAS system was developed in 1993 by Brand and Perrimon (Brand and Perrimon 1993). Both GAL4 driver and UASp-gene X lines are generated and maintained in separate stocks. The target gene X is not expressed in the absence of GAL4, but after cross of both lines, offspring will carry GAL4 driver which will result in driving the targeted gene X expression in a tissue specific manner. The GAL4-UAS system is widely used for driving the expression of fluorescently tagged proteins and for gene silencing by RNA interference (RNAi) in numerous model organisms.

Although a powerful technique, RNAi still faces a time lag between the initiation of mRNA degradation and the loss of protein function, since the level of knockdown is not always reliable. Moreover, RNAi techniques interfere with global level of a target protein. It is therefore sometimes not straightforward to understand the precise function of a protein using such approach. This limitation is overcome by the direct disruption of protein function. This can be attempted through either direct or indirect approaches. Indirect approaches rely on the expression of modified gene products that can be controlled externally, such as optogenetics (Krueger et al. 2019), or dominant negatives, where mutated versions of genes retain one functional element (e.g. the binding to one interacting partner), but lose another (e.g. enzymatic activity, localisation to a specific cellular component etc) (Bulgakova et al. 2013; Plochocka et al. 2021). Direct approaches include the treatment of cells or tissues with small molecule inhibitors, peptide aptamers or interfering antibodies. The latter has been used extensively in early *Drosophila* embryos as its syncytial nature means that injected material will diffuse throughout the embryo, affecting different nuclei to different extents, depending on whether close to or distant from the site of injection, where the effect of antibody is more pronounced than far away (Palumbo et al. 2020, 2015; Rogala et al. 2017; Tariq et al. 2020; Wakefield and Hayward 2014).

In this chapter I describe cell biological approaches to disrupt the function of the main EB proteins in *Drosophila,* EB1 and CG18190 (hereafter termed EB2). The aim was to acutely disrupt EB protein function in the syncytial blastoderm, without affecting earlier stages of development, such as oogenesis or the embryonic mitoses that occur deep inside the embryo (cycles 1-8). For this reason, I initially chose approaches expressing either an shRNA construct or a dominant negative version of EB1, using UAS-GAL4, under the control of the maternal-α-Tubulin promoter. It was hoped that, as the RNAi took effect or the pool of

endogenous maternal EB1 became sequestered as the number of mitotic spindles increases, the effects of interfering with EB1 would become apparent. No effect was seen, though it remains unclear whether this was due to lack of expression of the shRNA and/or dominant negative EB1 (see Results). I therefore switched approaches, purifying antibodies generated against either EB1 or EB2, and conducting a series of microinjections to interfere with EB1 activities during mitosis (Figure 3.11 – 3.16). I show that anti-EB1 and anti-EB2 antibodies can be used as tools to disrupt function, leading to disruption of chromosome segregation and spindle elongation in anaphase, presumably through intereferring with EB function. This paves the way for analysing the effect of disrupting EB function on the localisation of EB1 interacting partners (Chapter 5).

3.2   The dynamic localisation of EB1-GFP in the early embryo

To determine the EB1-GFP localisation in the early *Drosophila* embryos during mitosis, 30 embryos expressing EB1-GFP were manually dechorionated and imaged using spinning disc confocal microscopy (Figure 3.2).

During interphase, EB1-GFP is located at centrosomes and astral MTs, and is seen as speckles/comets that have been shown to correspond to the plus ends of growing MTs (Hayward et al. 2014). After nuclear envelope breakdown, EB1 decreases from astral MTs and increases at the mitotic spindle, labelling the entire spindle by metaphase (Figure 3.2(a) and 3.2(h)). During anaphase elongation, EB1 retracts from mitotic spindles and increases at the astral MTs (Figure 3.2(b) – 3.2(d)) to drive the chromosome segregation and anaphase elongation. This dynamic localisation is repeated through recurring mitotic cycles. These results are in agreement with works previously reported by Liang et al. (2009) and Rogers et al. (2002).

(a) **Metaphase.** (b) **Met-Anaphase.** (c) **Mid-Anaphase.** (d) **Telophase.**

(e) **Early interphase.** (f) **Late interphase.** (g) **NEB.** (h) **Metaphase.**
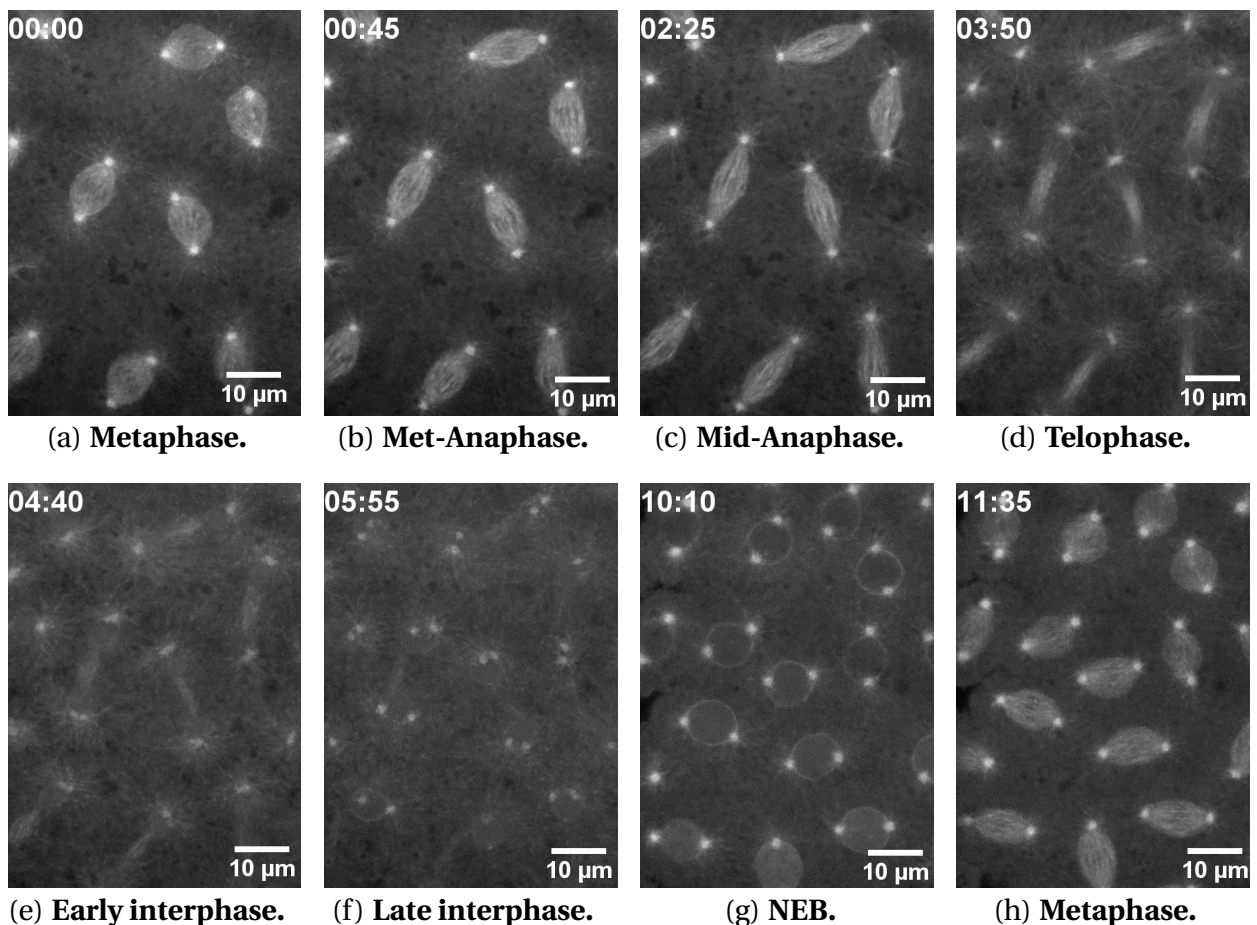
Figure 3.2: **Dynamic localisation of EB1-GFP in 1–2 hr old embryo.** During metaphase EB1 is concentrated at two dots, corresponding to the centrosomes, and the area of the mitotic spindle. This localisation is mantained until mid-anaphase, where EB1 can be seen also on astral MTs. The localisation to specific structures is weaker during interphase. As nuclei progress into the next mitosis, immediately after nuclear envelope breakdown (NEB) EB1 relocalised strongly to centrosomes and the mitotic spindles. Olympus IX2-UCB, 60X immersion oil objective. Exposure 200 ms, Z stack 5 and 1μm, interval time 5 seconds. 30 movies were taken in this experiment and all showed similar dynamic localisation.

3.3   *In vivo* RNAi of EB1 in the early embryo does not lead to a mitotic phenotype

In order to interfere with EB1 function in the early embryo, I obtained a fly line carrying an shRNA against EB1, stably incorporated into the *Drosophila* genome, driven by a UASp derivative (Ni et al. 2011). These flies were crossed to flies simultaneously expressing Histone-2AV-RFP, driven in all tissues by the polyubiquitin promoter, UASp-driven αTubulin-GFP and matαt-GAL4. The resultant embryos, which should express the EB1 hairpin RNAi in the female germline, leading to embryos with reduced EB1 protein, were imaged using spinning disc confocal microscopy (Figure 3.3). The dynamics of the chromosomes (His-2AV-RFP) and MTs (TubGFP) in these embryos, during cycles 10-13 were compared to flies lacking the shRNA (Figure 3.4). Although no quantitative analysis was undertaken, this suggests embryos expressing the shRNA progressed through multiple cycles of mitosis with similar dynamics. Given that EB1 is an essential gene and that interfering with EB1 functions through antibody injections leads to defect in mitosis (Section 3.7), this suggests that the shRNAi line did not significantly affect EB1 levels. Although a Western blot to assess levels of EB1 protein in control and shRNAi expressing embryos was attempted the results were inconclusive.

(a) **NEB.**	(b) **Metaphase.**	(c) **Met-Anaphase.**	(d) **Mid-Anaphase.**
(e) **NEB.**	(f) **Metaphase.**	(g) **Met-Anaphase.**	(h) **Mid-Anaphase.**
(i) **Telophase.**	(j) **Early interphase.**	(k) **Late interphase.**	(l) **NEB.**
(m) **Teophase.**	(n) **Early interphase.**	(o) **Late interphase.**	(p) **NEB.**
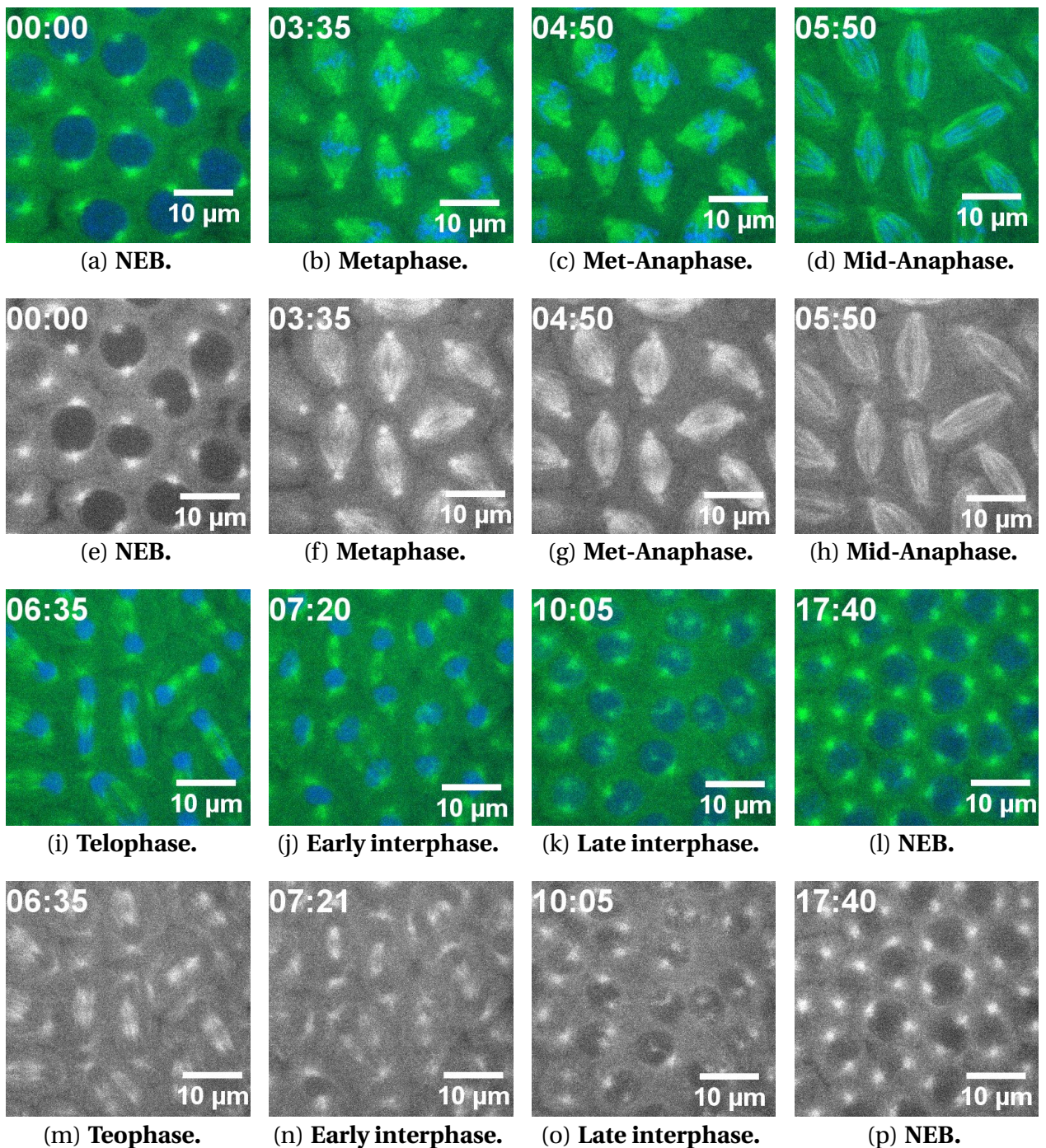
Figure 3.3: **His-RFPα-TubGFP EB1RNAi.**   To inhibit EB1 functions, virgin females of EB1RNAi line were crossed to HisRFP, αTubGFP males. 8 embryos were imaged and did not show any significant phenotypes upon imaging of the above cross and embryos show normal progression through several cell cycles similar to the control (Figure 3.4). 3.3(a) – 3.3(d) and 3.3(i) – 3.3(l) HisRFP in blue merged with αTubGFP in green. 3.3(e) – 3.3(h) and 3.3(m) – 3.3(p) αTubGFP split.
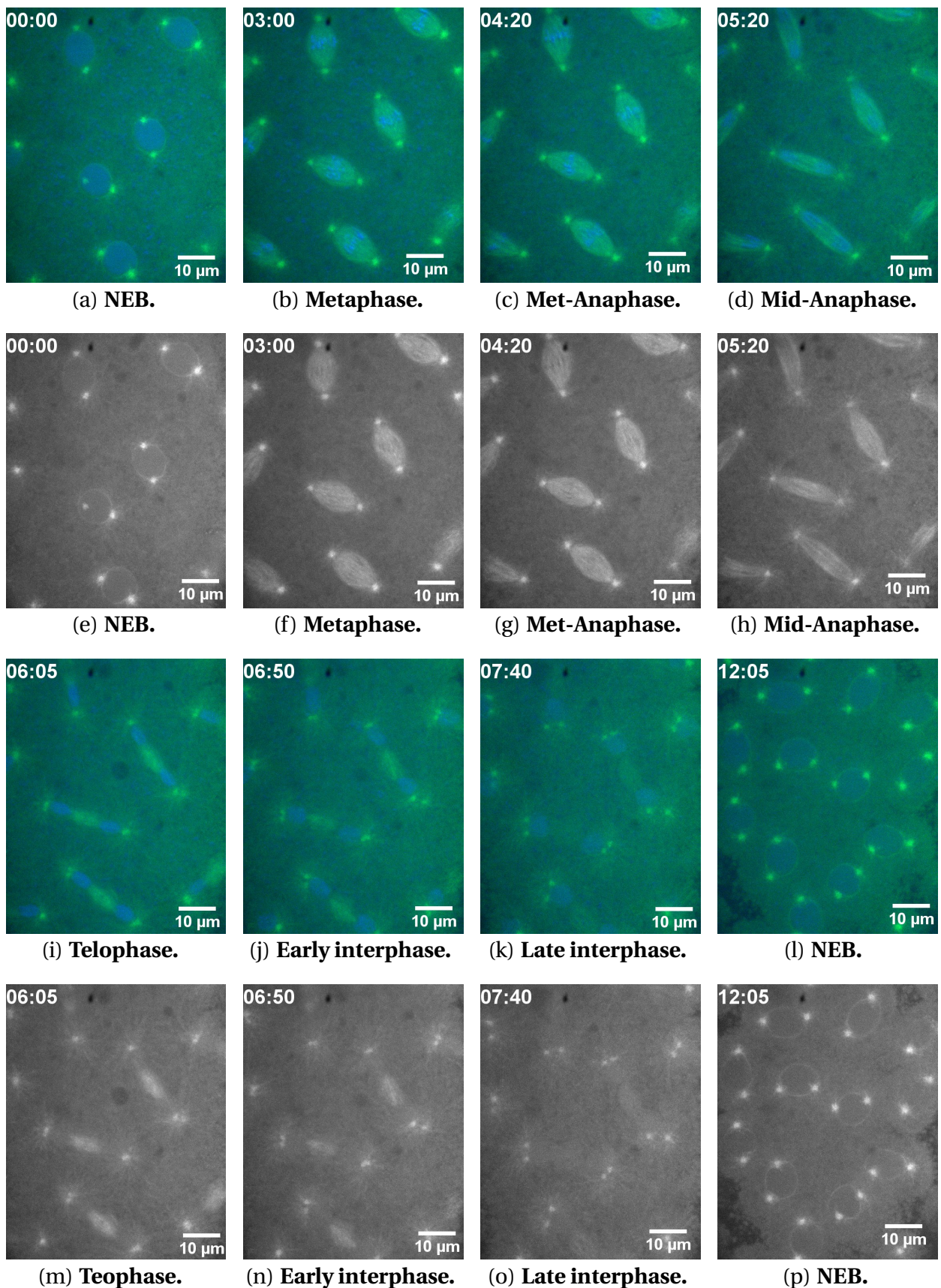
Figure 3.4: **Control for His-RFPα-TubGFP EB1RNAi.** Four embryos expressing HisRFP, αTubGFP, but lacking shRNA were taken and analysed as negative control for HisRFP, α-TubGFP EB1RNAi. 3.4(a) – 3.4(d) and 3.4(i) – 3.4(l) His-RFP in blue merged with αTubGFP in green. 3.4(e) – 3.4(h) and 3.4(m) – 3.4(p) αTubGFP split.

3.4 *In vivo* dominant negative EB1 in the early embryo does not lead to a mitotic phenotype

A further attempt to disrupt EB1 functions was carried out by crossing αTubGFP; matαt-GAL4 male flies to virgin females carrying an RFP-EB1^{DN} -MCh transgene, which was obtained from Bulgakova lab (Flybase FBtp0089741; `http://flybase.org/reports/FBtp0089741.html`). This construct does not possess N-terminal domain and C-terminal motif, but still has the coiled-coil region which allows to dimerise with full-length EB1. However, this dimer is unable to bind to MTs and interacts with its partners, which leads to reduction of EB1 levels in late *Drosophila* embryos. EB1^{DN} was used by Bulgakova et al. (2013) to investigate the role of E-cadherin (E-cad) during epithelial tissue morphogenesis and homeostasis in *Drosophila melanogaster* embryos at stage 15. According to these authors, the distribution of E-cad junctions at cell-cell borders, is tightly regulated by MT dynamics. Therefore, they have shown that EB1^{DN} modifies the MT dynamics due to EB1 depletion, consequently, the E-cad distribuition was altered in their studies. In my project, unfortunately, despite several attempts, imaging of these embryos failed to show expression of an MCherry protein, while the dynamics of the MTs through mitosis appeared normal. I therefore conclude that the flies obtained did not, in fact, carry the RFP-EB1^{DN} transgene (Figure 3.5), since mCherry was not observed using 561 laser for RFP filter. However, Western blot with anti-EB1 or anti-mchr/RFP antibodies was not carried out for further verification of EB1^{DN} expression in early embryos.
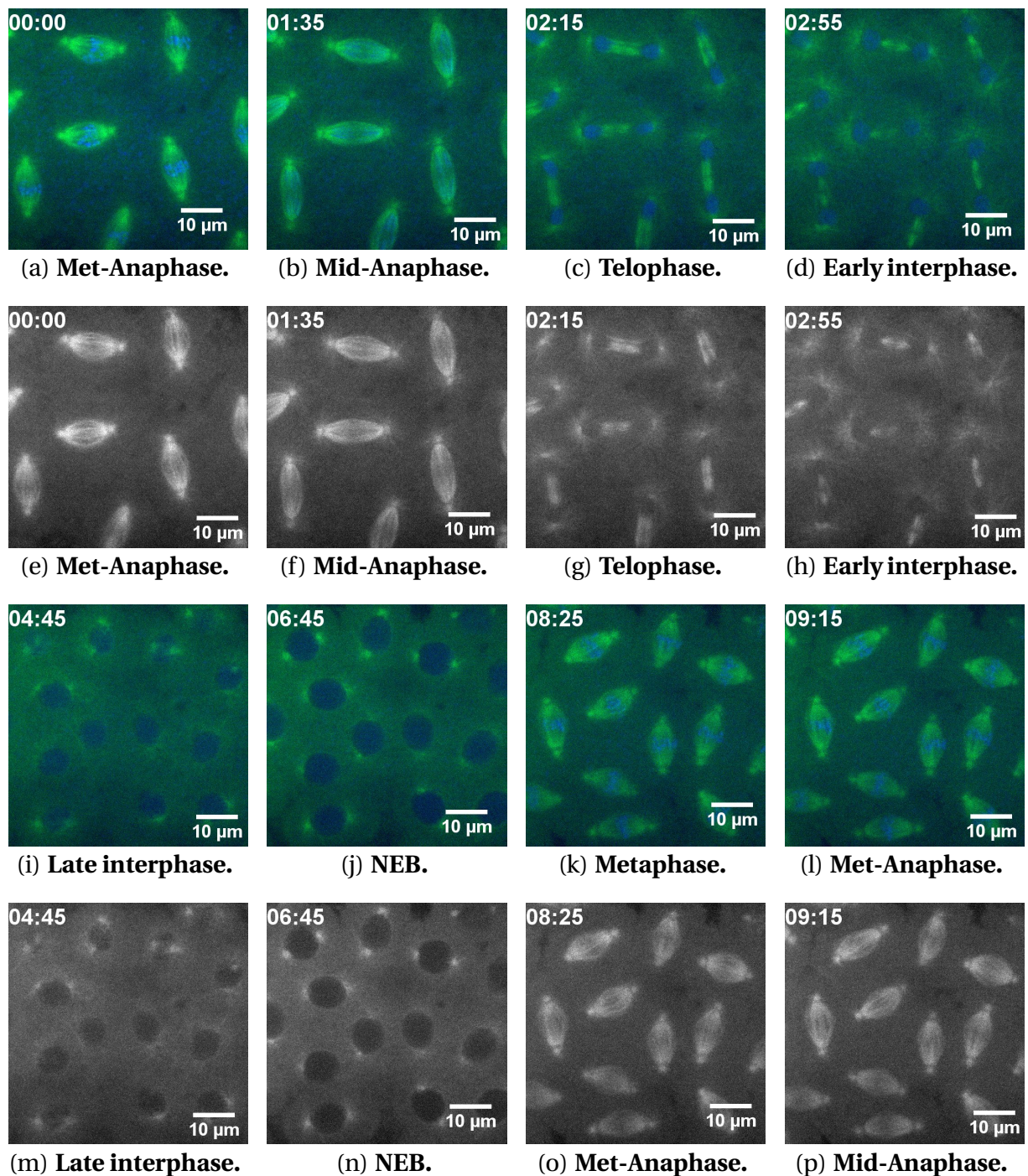
Figure 3.5: **His-RFPα-TubGFP EB1 dominant negative.** Different attempts were carried out crossing mCh-EB1^{DN} with HisRFP, αTubGFP to disrupt EB1 protein. However, five embryos analysed did not express mCh-EB1^{DN} as it was not visualised in both green and red channels in this experiment. Alternatively, in these circumstances EB1 levels were not significantly affected by these lines. As a consequence, embryos did not show any phenotype and progressed normally through several cell cycles. 3.5(a) – 3.5(d) and 3.5(i) – 3.5(l) HisRFP in blue merged with αTubGFP in green. 3.5(e) – 3.5(h) and 3.5(m) – 3.5(p) αTubGFP.

3.4.1   Expression and purification of bacterially-expressed MBP-EB1, MBP-EB2 and MBP

Having attempted to disrupt EB1 function genetically, I turned to a biochemical and physical manipulation approach – purifying antibodies generated against *Drosophila* EB1 and EB2, and injecting them into early embryos. Similar approaches were conducted by Rogers et al. (2002), Wakefield and Hayward (2014). These authors in their studies demonstrated that injecting anti-EB1 antibody into *Drosophila* embryos, leads to depletion of DmEB1 levels and consequently mitotic defects. Antibodies to both EB1 and EB2 have been generated in rabbits by the Ohkura lab (Elliott et al. 2005). We obtained the serum containing these antibodies and DNA constructs that drive expression of Maltose Binding Protein (MBP) fusions of EB1 and EB2.

The first step was to express and purify EB1 and EB2 from bacteria, in order to subsequently purify antibodies from the respective sera. Purified plasmids were transformed into BL21 (DE3) competent *E.coli* cells, resultant transformant cultures grown to exponential stage and protein expression induced by IPTG. After centrifugation, pellets were re-suspended into PBS by vortex and the disruption of cells was conducted by sonification. After centrifugation of extracts, supernatants were incubated with amylose resin slurry, and then proteins were eluted with 10 mM maltose. Finally, SDS–PAGE was used to assess the level of expression and purity of proteins.

3.4.2   Attempted cleavage of MBP tag from the purified proteins

The anti-EB1 and anti-EB2 serum was generated by injecting rabbits with pu-
rified MBP-EB1 and MBP-EB2, consequently the serum, in addition to anti-EB1
and anti-EB2 contains also anti-MBP antibodies. Then ideally, efficient purifi-
cation of the antibodies from serum would use pure EB1 and EB2 proteins with-
out the MBP tag and couple them to Affi-Gel 15 gel in respective 1 ml columns to
avoid any contamination with anti-MBP antibodies. A series of attempts were
therefore undertaken to cleave the MBP tag from purified proteins using the
protease Factor Xa at room temperature (Nagai and Thiϕgerson 1984, 1987).
SDS-PAGE was used to assess the yield of cleavage. Although the protease is
highly specific in cleaving after arginine in sequence Ile-Glu/Asp-Gly-Arg, in all
my experiments it resulted in the presence of two bands, which are fragment1
of 14 kD and fragment2 of approximately 18 kD (Figures 3.6 and 3.7). I there-
fore conclude that EB1 possesses an internal cleavage site for Factor Xa. In con-
trast, the Figure 3.7 indicates that EB2 was not internally cleaved. However, the
bond between MBP and EB2 was partially cleaved after overnight incubation,
precluding the MBP tag removal from EB2.

Factor Xa cleaves after the arginine residues in sequence Ile-Glu-Arg or Asp-
Gly-Arg. However, it can also cleaves after any basic residues, depending on the
structural conformation of the protein and the most common secondary site is
Gly-Arg. However, EB1 in my experiment was cleaved after arginine in sequence
Ala-Val-Arg[130], which is consistent with previous observations (Marlowe et al.
2000; McRae et al. 1981).
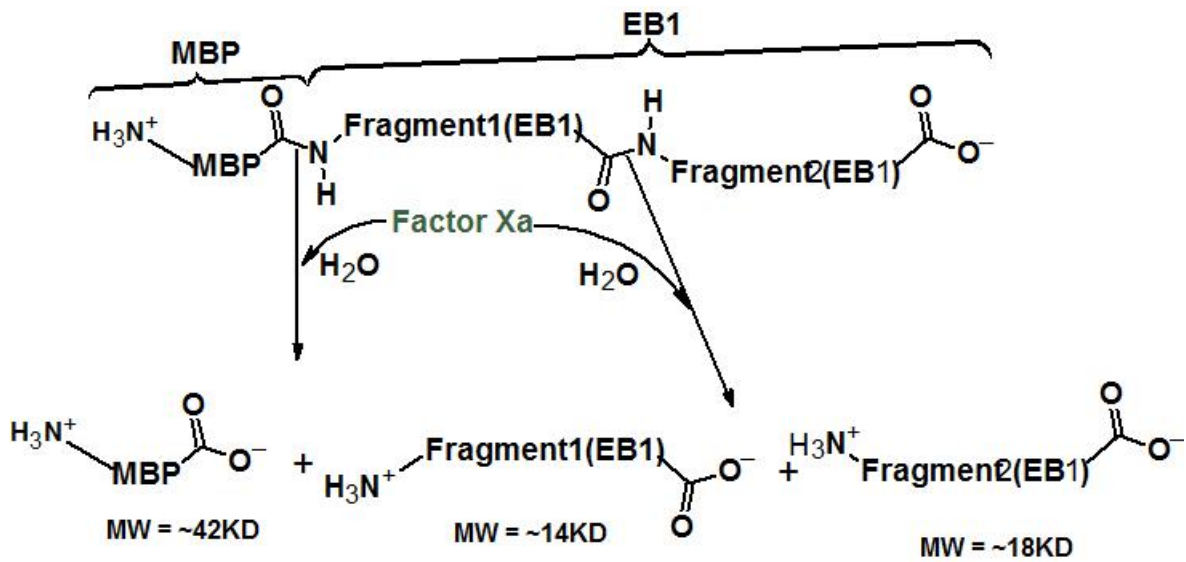
Figure 3.6: **MBP tag cleavage from MBP-EB1.** Factor Xa was incubated with respective fusion proteins for 2, 4, 8 hours and overnight at room temperature. SDS-PAGE used to assess the yield of cleavage, has shown that this protease cleaves also EB1 after arginine[130] in sequence Ala-Val-Arg[130], which has given two respective fragments of approximate 14 and 18 kD (Figure 3.7). MBP-EB1 MW ≈ 74 kD, MBP MW ≈ 42 kD.
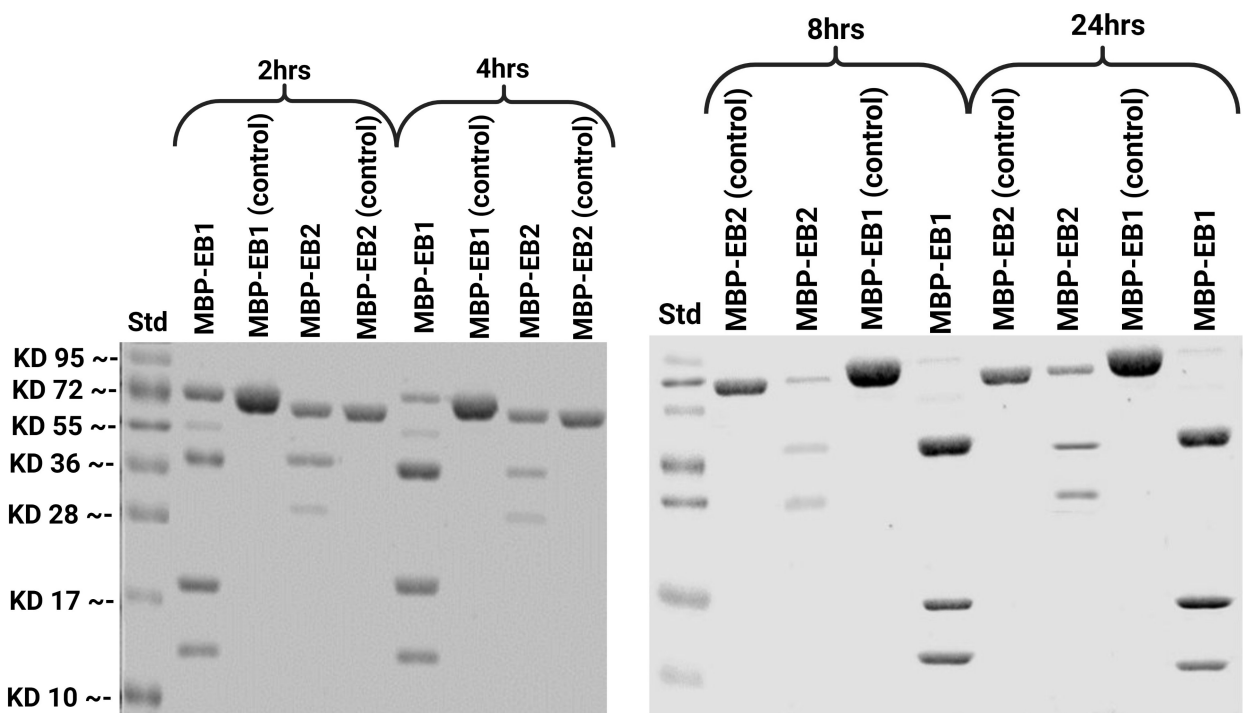
(a) **SDS-PAGE of Cleavage.** MBP-EB1 and MBP-EB2 incubated with Factor Xa for 2 and 4 hours.

(b) **SDS-PAGE of Cleavage.** MBP-EB1 and MBP-EB2 incubated with Factor Xa for 8 and 24 hours.

Figure 3.7: **SDS-PAGE to assess the yield of MBP-EB1 and MBP-EB2 cleavage.** Factor Xa was incubated with respective fusion proteins for 2, 4, 8 hours and overnight at room temperature. SDS-PAGE used to assess the yield of cleavage, has showed that this protease cleaves also EB1 in two respective fragments of approximate 14 kD and 18 kD. In the control, samples were incubated without Factor Xa. MBP MW ≈ 42 kD, MBP-EB1 MW ≈ 74 kD and MBP-EB2 MW ≈ 69, MBP MW ≈ 42 kD, EB1 MW ≈ 32 kD and EB2 MW ≈ 27 kD.

3.5 Affinity purification of anti-EB1, anti-EB2 and anti-MBP antibodies

Due to technical difficulties it was impossible to remove the MBP-tag from MBP-EB1 and MBP-EB2, I decided to purify the anti-EB1 and anti-EB2 antibodies from the sera in two steps. Firstly, incubation of serum with pure MBP, to deplete it of any MBP-specific antibodies, and then incubation of that flow through with immobilised MBP-EB1 or MBP-EB2, prior to elution of the specific antibodies.

Before affinity purification of antibodies, purified proteins were dialysed into a suitable buffer (Chapter 2) and coupled to Affi-Gel 15 gel in respective 1 ml columns. Then, sera of polyclonal anti-MBP-EB1 and anti-MBP-EB2 antibodies (donated by Okhura lab) were run 3 times in respective Affi-Gel 15 gel columns immobilised with purified MBP. Subsequently, respective flow throughs were run 3 times through respective columns containing MBP-EB1 and MBP-EB2 as antigens. Finally, respective antibodies were eluted with elution buffer and neutralised with TrisHCl. The affinity of these antibodies was tested using Western blot. Their respective proteins were used as antigens (Figure 3.8(b) – 3.8(d)).

At the time, I imaged Figures 3.8(b) – 3.8(d) using LI-COR ODYSSEY^R XF (LI-COR; `https://www.licor.com/bio/odyssey-xf/`) at 700 nm channel. This channel does not detect the third band of the ladder at kD 72 (PageRuler^{TM} Plus, Cat # 26619; ThermoFisher SCIENTIFIC; `https://www.thermofisher.com/uk/en/home.html`), this band is dectable using 600 nm channel. Whereas, the Figure 3.8(a) was imaged using both channels (600 and 700 nm).

(a) **SDS-PAGE.**

(b) **Western blot.** Anti-MBP elute

(c) **Western blot.** Anti-EB1 elute

(d) **Western blot.** Anti-EB2 elute
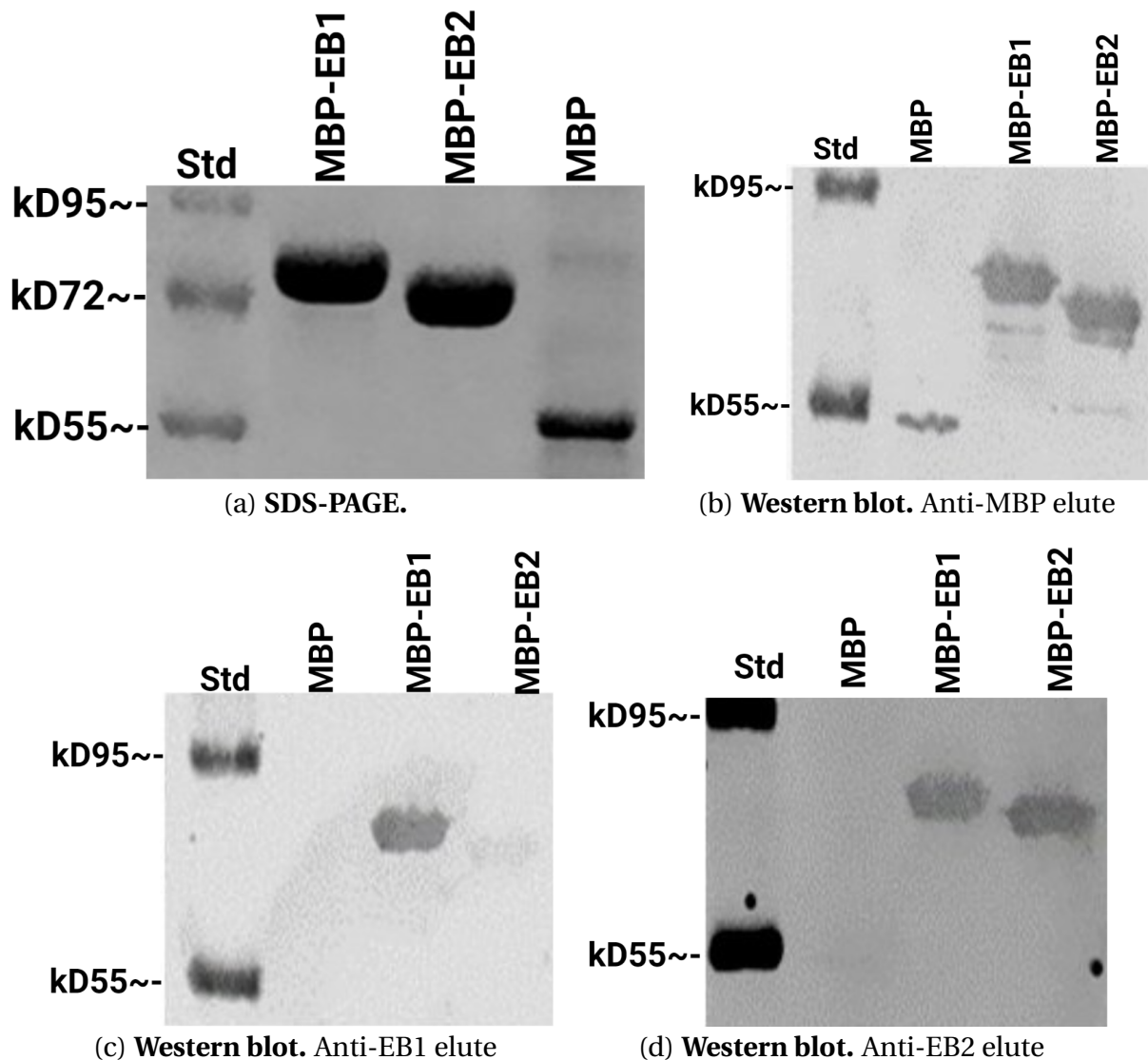
Figure 3.8: **Purified proteins were assessed through SDS-PAGE and the specificity of antibodies was determined via Western blot.** The purity of purified proteins was tested by SDS-PAGE 3.8(a). SDS-PGE was stained using Coomassie Brilliant Blue R-250. The specificity of antibodies was tested by Western blot 3.8(b) – 3.8(d). Anti-MBP antibodies have recognised all three antibodies as it was expected 3.8(b). Anti-EB1 antibody is highly specific in recognising EB1 3.8(c), whereas anti-EB2 antibodies have also recognised EB1 3.8(d). MBP MW $\approx$ 44 kD, MBP-EB1 MW $\approx$ 79 kD and MBP-EB2 MW $\approx$ 69 kD.

As shown in the Figure 3.8, and as expected, purified anti-MBP antibodies strongly recognized all three proteins. The purified anti-EB1 antibodies recognized only MBP-EB1, demonstrating its specificity and the complete depletion of anti-MBP antibodies using this technique. Finally, the purified anti-EB2 antibodies strongly recognized both MBP-EB1 and MBP-EB2, but not MBP. Therefore the antibodies have specific affinity for both *Drosophila* EB1 and EB2, suggesting a shared epitope between these proteins.

3.5.1 Microtubule cosedimentation assay

To invetigate the binding affinities between EB1 or EB2 proteins and MTs *in vitro,* I next undertook an *in vitro* MT co-sedimentation assay. To do this, I separately incubated the purified MBP-EB1 and MBP-EB2 (1 mg/ml) with purified, commercially available porcine tubulin (5 mg/ml) in the presence of 10 mM GTP and 2 mM taxol at 37 °C (Hughes et al. 2008; Tariq et al. 2020; Ti et al. 2016; Zhu et al. 2009). Taxol allows tubulins to polymerise and it is expected that MBP-EB1 and MPB-EB2 will bind to tubulin polymers in respective tubes, thus allowing the detection of these proteins in pellets. In contrast, in samples incubated without taxol (-taxol), it is not expected to have tubulin polymers. As a result of this, MBP-EB1 and MBP-EB2 will be dected in supernant. After centrifugation at 48,000 rpm for 45 minutes over a cushion of 40% sucrose, supernatant and pellets were used for Western blot analysis (Figure 3.9). Although the presence of sucrose in the pellet resulted in a "fuzzy" band, it was clear that a significant proportion of both MBP-EB1 and MBP-EB2 co-sedimented with MTs in respective tubes.
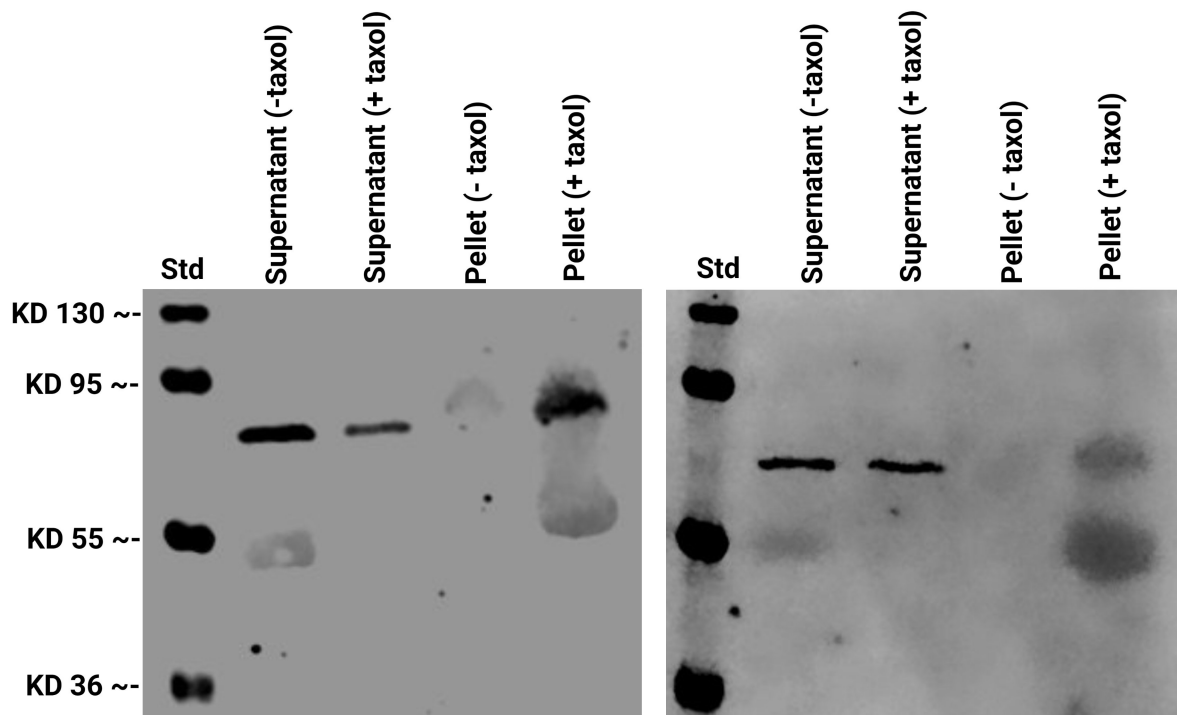
(a) **Western blot of MBP-EB1 cosedimentation assay.**

(b) **Western blot of MBP-EB2 cosedimentation assay.**

Figure 3.9: **Western blot of MT Cosedimentation Assay.** The Western blot shows that purified proteins interact with MTs (Hughes et al. 2008; Tariq et al. 2020; Ti et al. 2016; Zhu et al. 2009). Without taxol there is no MT cosedimentation, then MBP-EB1 and MBP-EB2 are expected to be found in supernatant and not in pellet samples, whereas with taxol proteins are expected to be found in pellets and non in supernatant. The Western blot shows this expectation, although the supernatant with taxol indicates also the presence of proteins due to excess used in comparison with tubulin concentration, supported by complete depletion of these proteins in pellet without taxol and their presence with taxol. The sucrose in pellet caused a fuzzy. MBP-EB1 MW ≈ 74 kD and MBP-EB2 MW ≈ 69 kD. 3.9(a) elute anti-EB1 antibodies and 3.9(b) elute anti-EB2 antibodies.

3.6   Injection of anti-EB1, anti-EB2 or the combination of anti-EB1 and anti-EB2 antibodies into EB1-GFP expressing embryos does not interfere with EB1 function in the early embryo

The purification of anti-EB1 and anti-EB1/2 (henceforth anti-EB2) antibodies from the respective sera allowed me to test their abilities to disrupt EB protein function in the early *Drosophila* embryo. As a control (Figure 3.10), I used microinjection buffer. Given the differing affinities of the anti-EB1 and anti-EB2 antibodies to their antigens, I decided to inject them alone, or in combination. Microinjection buffer was injected into 18 syncytial *Drosophila* embryos, anti-EB1 (2–4 mg/ml) into 26 embryos, anti-EB2 (2–4 mg/ml) into 14 embryos

and anti-EB1+EB2 antibodies were injected into 11 embryos, then all these embryos expressing EB1-GFP were imaged via time lapse spinning disc confocal microscopy EB1-GFP, to ascertain whether the antibodies resulted in displacement of EB1 from centrosomes, astral MTs or the mitotic spindle. The volume of microinjection buffer and antibodies injected was variable, but corresponded to an area of clearing within the embryo interior, without causing embryo damage (Conduit et al. 2015).

(a) **Telophase.**   (b) **Early interphase.**   (c) **Late interphase.**   (d) **NEB.**

(e) **Metaphase.**   (f) **Met-Anaphase.**   (g) **Mid-Anaphase.**   (h) **Telophase.**
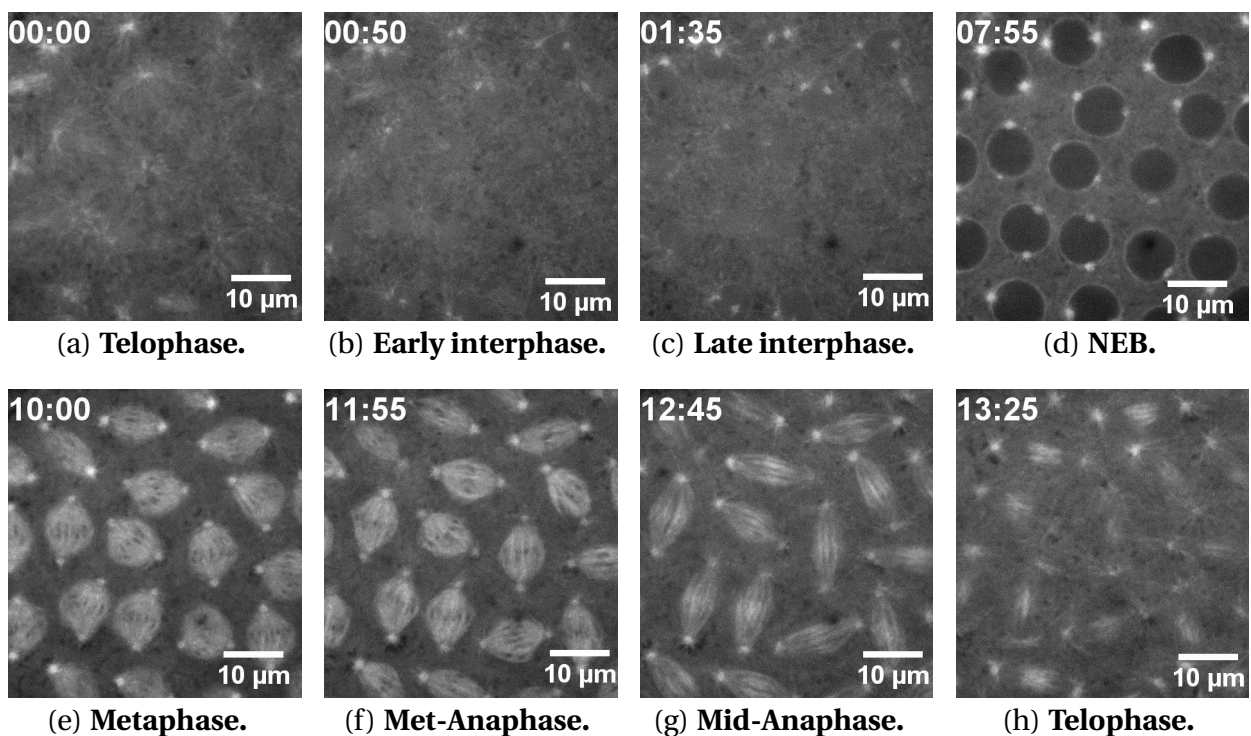
Figure 3.10: **Microinjection buffer injected into 1–2 hr old embryos expressing EB1-GFP.** A variable volume of microinjection buffer was injected into 18 early *Drosophila* embryos expressing EB1-GFP which were used as control. After injection, all these embryos indicate a normal progression through three consecutive cell cycles, and this figure shows the first cell cycle.

In these initial experiments, neither anti-EB1, anti-EB2 nor the combination of anti-EB1 + EB2 antibodies appeared to interfere either with EB1-GFP localisation, or mitotic progression (Figures 3.11 – 3.13). Given that injections of these antibodies causes defects in mitosis in embryos expressing GFP-tubulin and RFP-Histone (Section 3.7) there are two possible reasons for the lack of effect. First, it may be that the antibodies, although recognizing EB1 and EB2 on a Western blot, may not be able to bind their epitopes *in vivo,* due to protein folding. Second, it is possible that the expression of exogenous GFP-tagged EB1,

in addition to the EB1 and EB2 present in the embryo sequesters the anti-EB1 and EB2 antibodies, such that functional EB1 and EB2 are still present.
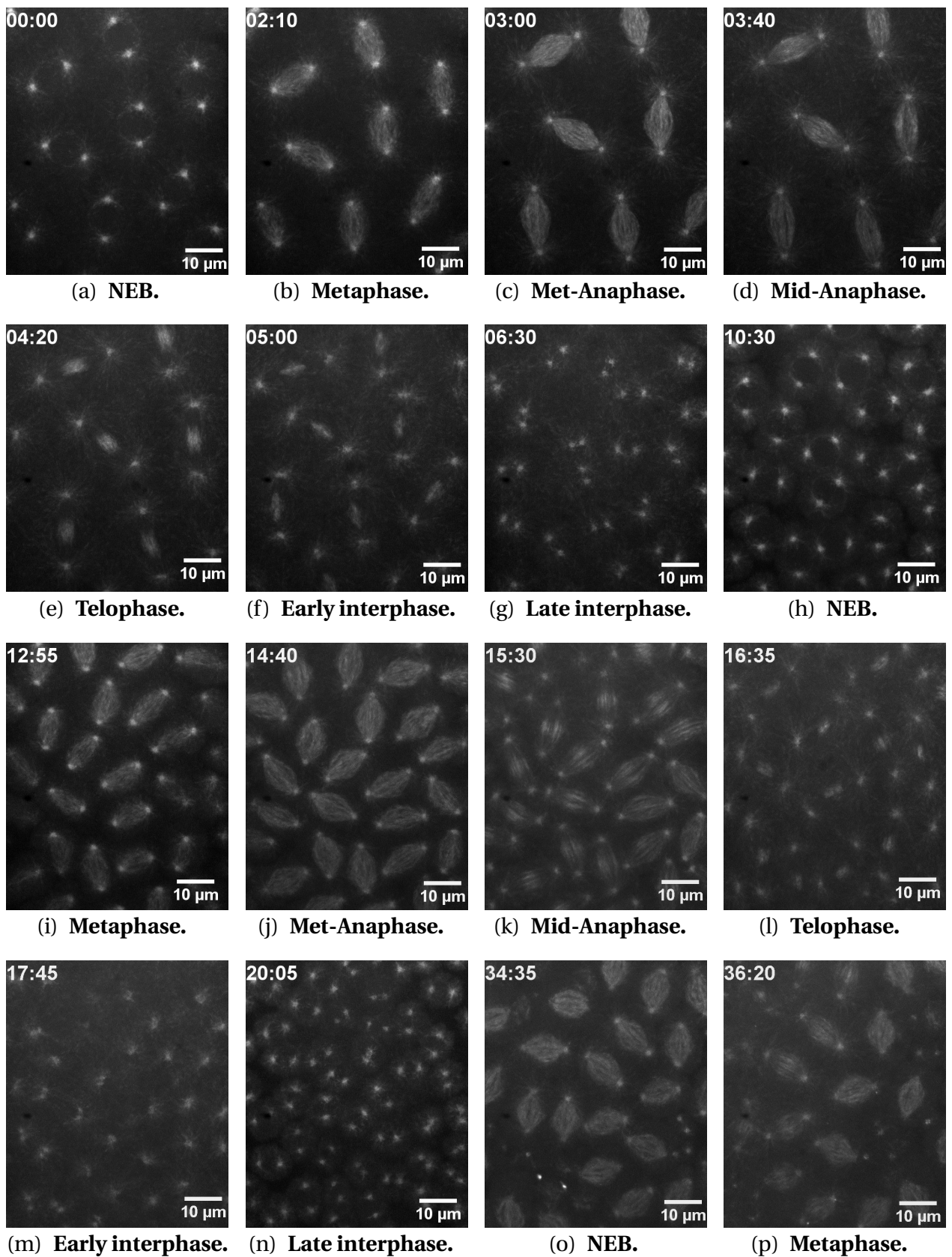
Figure 3.11: **Anti-EB1 antibody microinjection into 1–2 hr old embryos expressing EB1-GFP.** A variable volume of anti-EB1 antibody solution (2–4 mg/ml) was injected into 26 embryos that express EB1-GFP. After injection, these embryos showed a normal progression through three consecutive cell cycles and the two first cycles are shown in this figure.
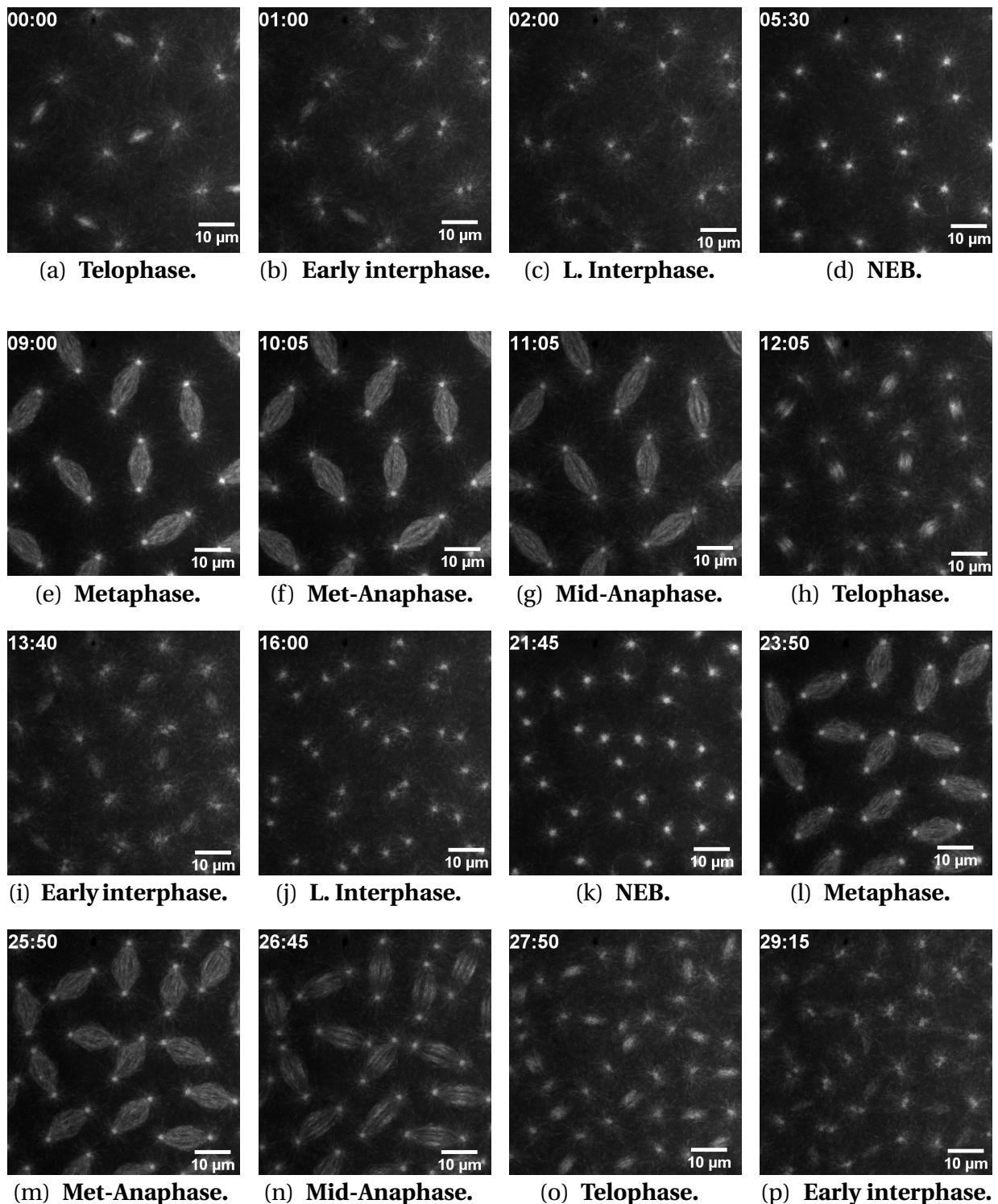
Figure 3.12: **Anti-EB2 antibody microinjection into 1–2 hr old embryos expressing EB1-GFP.** A variable volume of anti-EB2 antibody solution (2–4 mg/ml) was injected into 14 early embryos that express EB1-GFP and this antibody did not interfere with EB1 function and they showed normal progression through three consecutive cell cycles and the figure illustrates the two first cycles.

(a) **Prometaphase.** (b) **NEB.** (c) **Metaphase.**

(d) **Met-Anaphase.** (e) **Mid-Anaphase.** (f) **Telophase.**

(g) **Early interphase.**
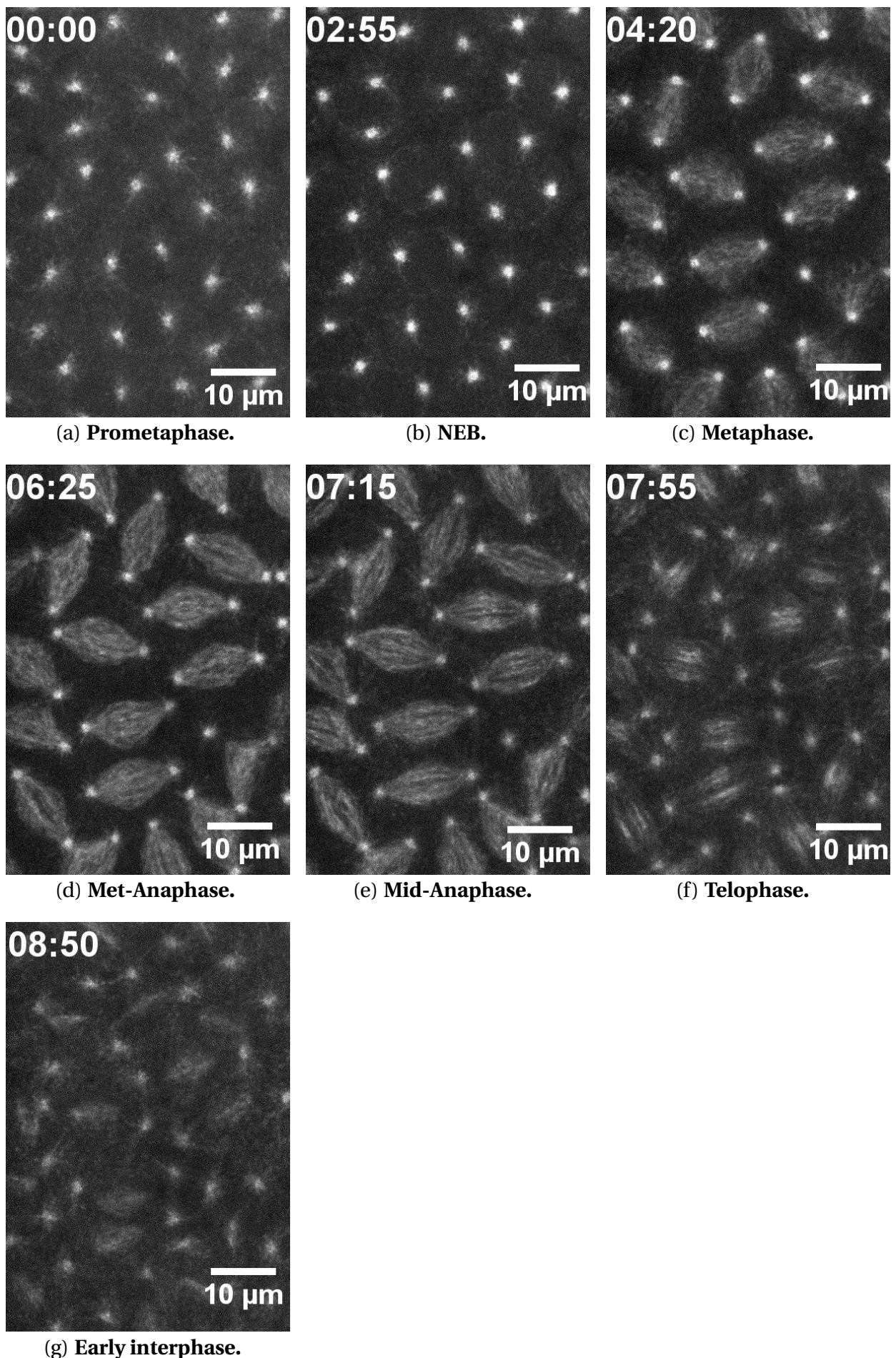
Figure 3.13: **Anti-EB1 and anti-EB2 antibody microinjection into 1–2 hr old embryos expressing EB1-GFP.** A variable volume of the combination of anti-EB1 and anti-EB2 antibodies (1:1, 2–4 mg/ml) was injected into 11 early embryos that express EB1-GFP. After injection, these embryos showed a normal progression through three consecutive cell cycles, without showning any phenotypes or disruption of EB1 functions.

3.7   Injection of anti-EB1 or anti-EB2 antibodies into HisRFP, αTubGFP embryos leads to defects in mitosis

To assess the hypothesis that anti-EB1 and anti-EB2 antibodies had no effects in interfering with EB1 functions into embryos expressing EB1-GFP due to the higher concentration of EB1, I decided to inject them into embryos that express HisRFP, αTubGFP with no expression of exogenous EB1, monitoring the effect on mitosis. As shown in Figures 3.14 – 3.16, while the injection of buffer into these embryos did not result in any observable difference in MT organisation, chromosome alignment and segregation, or mitotic progression, injection of anti-EB1, anti-EB2 or the combination of anti-EB1 and anti-EB2 antibodies caused a consistent, comparible and reproducible phenotype. In these embryos, mature mitotic spindles in metaphase close to the site of injection, visibly were shorter than those further away, and also possessed smaller astral MTs. During anaphase, chromosome segregation was often inhibited (Indicated by arrows. 8 embryos in 10 showed phenotype in the first cell cycle and the remaining 2 embryos showed it in the second cycle of division), resulting in "dumbbell-shaped" telophase chromosome complements and subsequent problems in the following mitoses.

Given the specificity of these phenotypes, I conclude that the purified EB1 and EB2 antibodies have the ability to interfere with EB protein function in the early embryo.
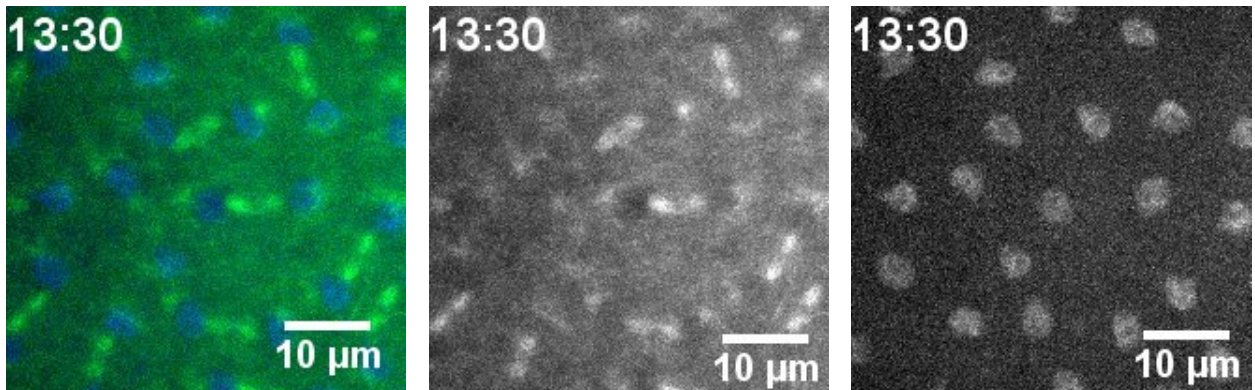
(a) **Telophase.** As a control, embryo was injected with microinjection buffer. HisRFP in blue merged with αTubGFP in green

(b) **Telophase.** As a control, embryo was injected with microinjection buffer. αTubGFP split.

(c) **Telophase.** As a control, embryo was injected with microinjection buffer. HisRFP split.
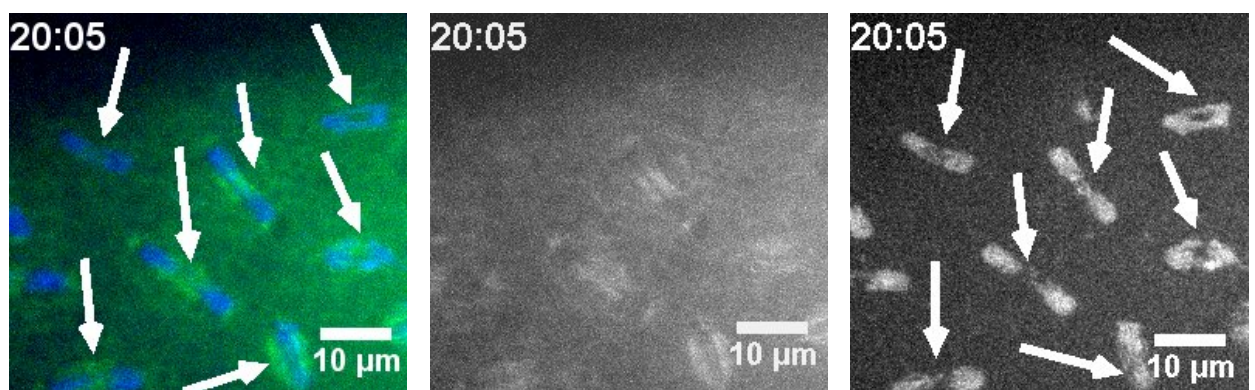
(d) **Telophase.** Embryo injected with anti-EB1 antibody. HisRFP in blue merged with αTubGFP in green.

(e) **Telophase.** Embryo injected with anti-EB1 antibody. αTubGFP split.

(f) **Telophase.** Embryo injected with anti-EB1 antibody. HisRFP split.

Figure 3.14: **Anti-EB1 antibody microinjection into 1–2 hr old embryos expressing HisRFP, αTubGFP.** As a control (Figures 3.14(a) – 3.14(c)), 9 embryos expressing HisRFP,αTubGFP were injected with a variable volume of microinjection buffer and they showed normal progression through three consecutive cell cycles. After a variable volume of Anti-EB1 antibody (2–4 mg/ml) injection into 17 embryos expressing HisRFP and αTubGFP, these embryos during anaphase showed mitotic spindles close to the site of injection shorter (not measured) than those further away, resulting in chromosome segregation defects, consequently dumbbell-shaped formation during telophase (Indicated by arrows, Figures 3.14(d) and 3.14(f)).
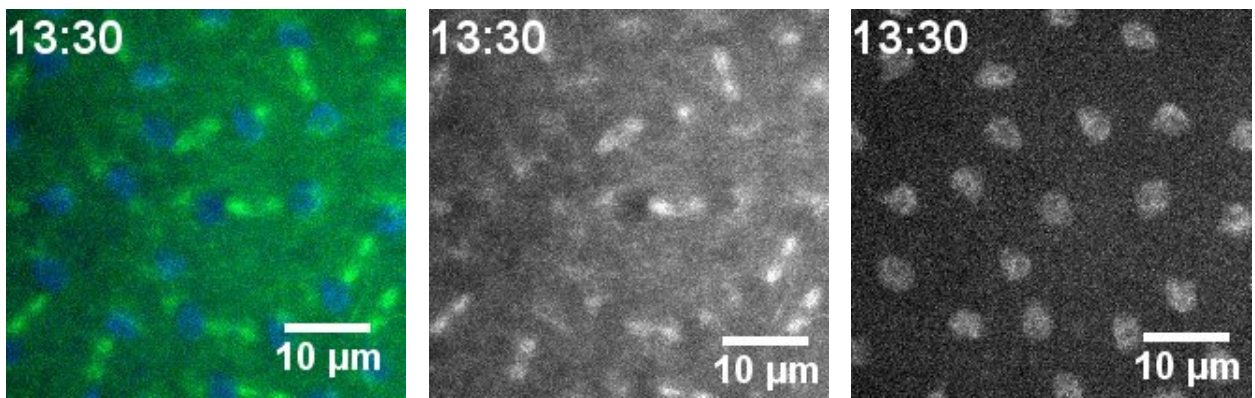
(a) **Telophase.** Embryo injected with microinjection buffer as a control. HisRFP in blue merged with αTubGFP in green.

(b) **Telophase.** Embryo injected with microinjection buffer as a control. αTubGFP split.

(c) **Telophase.** Embryo injected with microinjection buffer as a control. HisRFP split.
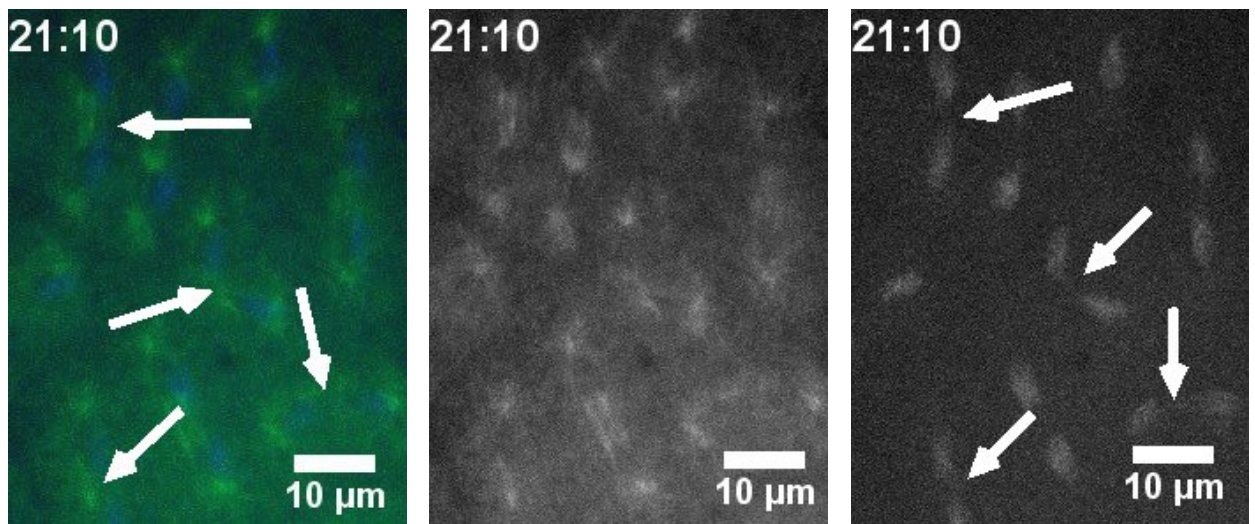
(d) **Telophase.** Embryo injected with anti-EB2 antibody. HisRFP in blue merged with αTubGFP split in green.

(e) **Telophase.** Embryo injected with anti-EB2 antibody. αTubGFP split.

(f) **Telophase.** Embryo injected with anti-EB2 antibody. HisRFP split.

Figure 3.15: **Anti-EB2 microinjection into 1–2 hr old embryos expressing His-RFP, αTubGFP.** 9 embryos expressing HisRFP,αTubGFP were injected with a variable volume of microinjection buffer as a control (Figures 3.15(a) – 3.15(c)). The injection into these embryos did not cause any phenotypes and embryos progressed normally through three consecutive cell cycles. Immediately, after a variable volume of anti-EB2 antibody (2–4 mg/ml) injection into 12 early embryos that express HisRFP and αTubGFP, they showed problems during anaphase and telophase due to chromosome segregation defects (Indicated by arrows, Figures 3.15(d) and 3.15(f)), leading to embryos death in the following cell cycle.
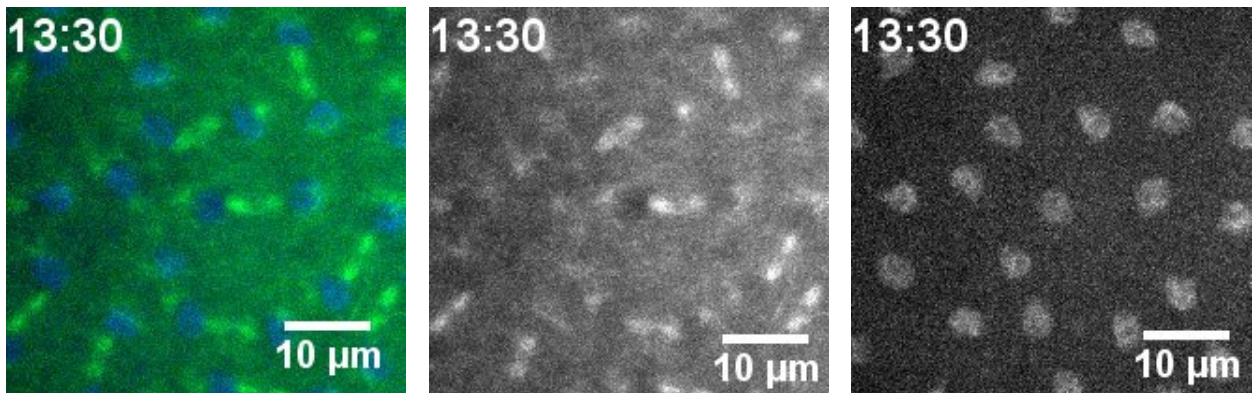
(a) **Telophase.** As a control, embryo was injected with microinjection buffer. HisRFP in blue merged with αTubGFP in green.

(b) **Telophase.** As a control, embryo was injected with microinjection buffer. αTubGFP split.

(c) **Telophase.** As a control, embryo was injected with microinjection buffer. HisRFP split.
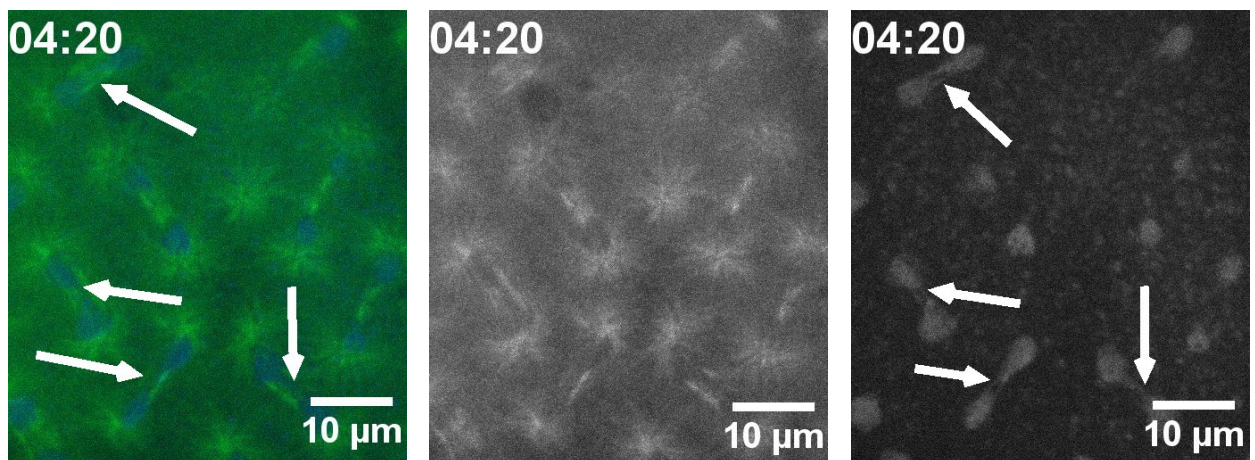
(d) **Telophase.** The combination of anti-EB1 and anti-EB2 antibodies was injected into embryo. HisRFP in blue merged with αTubGFP in green.

(e) **Telophase.** The combination of anti-EB1 and anti-EB2 antibodies was injected into embryo. HisRFP split.

(f) **Telophase.** The combination of anti-EB1 and anti-EB2 antibodies was injected into embryo. αTubGFP split.

Figure 3.16: **Combination of anti-EB1 and anti-EB2 antibodies microinjection into early embryos expressing HisRFP, αTubGFP.** As a control (Figures 3.16(a) – 3.16(c)), 9 embryos were injected with a variable volume of microinjection buffer and this injection did not cause a visible phenotype through three consecutive cell cycles. As expected, a variable volume of the combination of anti-EB1 and anti-EB2 antibodies (1:1, 2–4 mg/ml) injection into 8 embryos expressing both HisRFP and αTub-GFP disrupts EB1 and/or EB2 functions, which results in chromosome segregation defects with formation of dumbbel-shaped chromosomes during anaphase and telophase (Indicated by arrows, Figures3.16(d) and 3.16(f)). Consequently, this leads to embryo death in the following mitosis.

3.8 Discussion

In this chapter, I was initially aimed to determine the localisation of EB1 in wild-type *Drosophila* embryos during cell division using time-lapse confocal disc microscopy and to identify a tool with which EB1 or EB2 function could be specifically compromised in the early embryo. Results shown in Figure 3.2 indicate that EB1 dynamically colocalises with MTs during mitosis. In interphase, EB1-GFP is present on centrosomes and weakly on astral MTs. Upon entry into mitosis through to metaphase, its localisation mimics that of MTs themselves. In anaphase, there is a dramatic shift of EB1 to the astral MTs, although EB1 remains on the spindle as it disassembles through to telophase. This observation is consistent with studies previously reported by Berrueta et al. (1998), Brüning-Richardson et al. (2011), and Rogers et al. (2002).

To further assess the ability of MBP-EB1 and MBPP-EB2 binding to MTs *in vitro*, I carried out the MT cosedimentation assay. As shown in Figure 3.9, MBP-EB1 and MBP-EB2 are able to bind to MTs *in vitro*. These observations are consistent with investigations conducted by Zhu et al. (2009) using untagged EB1 via MT cosedimentation assay, by Hayashi et al. (2005) and Slep and Ronald (2007) using tubulin polymerisation and light scattering assay.

Experiments conducted by authors (Komarova et al. 2009; Kumar et al. 2017; Nehlig et al. 2017; Rogers et al. 2002) indicate that EB1 is the structural and evolutionary core of MAPs involved in regulating the MT dynamic instability. However, its functions and mechanisms of actions are still poorly understood (Zhu et al. 2009).

Therefore, my second aim was to investigate EB1 functions in early *Drosophila* embryos. For that objective, I initially attempted to deplete EB1 function via transgenic expression of a shRNA construct in the female germline. Virgin females of this line were crossed to HisRFP, αTubGFP; matαt-GAL4 males to drive

the expression of EB1RNAi using the UASp-GAL4 system. Image analysis upon confocal microscopy, did not show any phenotype resulting from this cross (Figure 3.3). These my studies are inconsistent with investigations carried out by Rogers et al. (2002). These authors showed that RNAi depletion of DmEB1 affects MT dynamics, which leads to defects in mitotic spindle formation in *Drosophila* S2 cells. There are three major possibilities why my approach was not successful. Firstly, it may be that this RNAi construct did not express well in the female germline and therefore did not suppress the levels of EB1 mRNA sufficiently to inhibit the protein function. Secondly, it may be that the RNAi construct does not actually function under these circumstances of crosses, considering that I used early *Drosophila* embryos and previous authors have used *Drosophila* S2 cells, instead. Finally, it could be that EB1 is not required for mitosis in this system. To assess these possibilities, the levels of EB1 mRNA and protein could be determined in these embryos – undertaking qPCR and Western blot respectively and comparing with siblings that do not carry the matαt-GAL4 transgene.

A further attempt to genetically disrupt EB1 function was explored, through expressing a previously characterised dominant-negative form of EB1 (EB1^{DN}) in the early embryo. EB1^{DN} lacks the N-terminus and C-terminus of EB1, but still possesses the coiled-coil region which should allow dimerisation with endogenous EB1. However, this dimer should be unable to bind to MTs and +TIP partners, leading to loss of EB1 functions (Bulgakova et al. 2013; Plochocka et al. 2021). Previous work has been undertaken in late *Drosophila* embryos (stage 15) by the same authors and showed that E-cad junctions are involved in cell-cell adhesion in epithelial tissues, and the distribuition of E-cad at the cell periphery is regulated by MT dynamics. Next work disrupted EB1 using EB1^{DN} and has led to a misdistribution of E-cad around the cell periphery in the late *Drosophila* embryos (Bulgakova et al. 2013). In addition, cells elongate in late

embryo periphery during cell differentiation and MTs align along the apical-basal axis and disruption of EB1 functions via EB1^{DN}, lead to a decrease number of MTs aligned in cells (Plochocka et al. 2021).

In my experiment set up, the embryos laid by offspring of mch-EB1^{DN} flies crossed to HisRFP, αTubGFP;matαt-GAL4 males did not show any abnormalities in MT organisation or chromosome alignment or segregation (Figure 3.5). As shown in this Figure, mCh-EB1^{DN} was not expressed and the image was taken using both 488 nm (20%) and 561 nm (20%) lasers for green and red filters, respectively. Then, I did not verify the levels of its expression in the flies undertaking a Western blot with anti-EB1 or anti-mCh/RFP antibodies, which would have confirmed that these embryos really were not expressing the reported dominant negative version of EB1. Lack of time due to COVID precluded me from investigating this further.

Due to the difficulties with the above genetic approaches, I instead sought to disrupt EB1 function using microinjection. Microinjection is an important and useful technique to investigate protein functions via introduction of different molecules and reagents in early *Drosophila* embryos (Brüning-Richardson et al. 2011; Rogers et al. 2002) . I was fortunate that there already exist sera generated by injection into rabbits of MBP-EB1 and MBP-EB2 (Elliott et al. 2005). Full-length DmEB1 and DmEB2 fused with MBP were expressed and purified in bacteria. These proteins were injected into a rabibit and after a period of time, the animal's immune system produced antibodies specific for these antigens and the sera is harvested. This sera, and the bacterial expression vectors for the antigens (MBP-EB1 and MBP-EB2) were kindly gifted to me by the Okhura lab. First, I was able to express and purify these antigens, and MBP on its own, using amylose resin. After biochemical characterisation, I then used these purified proteins to affinity purify their respective antibodies from the rabbit sera. I originally planned to remove the MBP tag from MBP-EB1 and MBP-EB2 to eas-

ily purify the antibodies. However, I found that the protease Factor Xa not only cleaved the MBP-EB1 link, but also cleaved EB1 internally, generating two EB1 fragments by Western blot (Figure 3.7). In contrast, I could not remove MBP tag from EB2 either, because the link between these two proteins was partially cleaved after overnight incubation, although the protease did not cleave EB2 internally, as shown in Figure 3.7. I therefore switched to a two-step approach of first removing MBP antibodies, prior to purifying the specific EB1 or EB2 antibodies. Although successful, this approach demonstrated that the affinity purified anti-EB2 antibodies also recognised an epitope on purified EB1.

Initially, affinity purified anti-EB1, anti-EB2 and anti-EB1+EB2 (1:1) antibodies in a concentration 2–4 mg/ml were injected into embryos expressing EB1-GFP. This did not result any different phenotype when compared with control in which only microinjection buffer was injected (Figure 3.10 – 3.13). This maybe due to the high concentration of EB1 in these embryos, as they express both endogenous and exogenous EB1.

To investigate this hypothesis, these antibodies were injected into embryos that do not express additional EB1, but instead expressed both Histone 2AV-RFP and αTubulin-GFP. Although interphase MT dynamics and organisation were not affected by injection of anti-EB1, anti-EB2 and anti-EB1+EB2 antibodies into embryos, mitotic spindles close to the site of injection were shorter (not measured), astral MTs in anaphase were less apparent and chromosome segregation was perturbed, leading to polyploidy an accumulation of embryonic defects and, ultimately, embryo death. The fact that the same antibodies did not cause mitotic defects in embryos overexpressing GFP-EB1 suggests the phenotypes observed are specific for EB1 and not non-specific.

Future work to further attempt to disrupt EB1 functions in early *Drosophila* embryos, should involve the use of peptide aptamers. Leśniewska et al. (2014) have synthesised aptamers and tested their interactions with EB1 *in vitro* using

Drosophila S2 cells and by isothermal titration calorimetry. The large majority of EB1 proteins contain SxIP motifs and according to these authors, the SxIP alone is insufficient for the interaction with EB1. These EB1 aptamers are peptide with SxIP domain preceded and followed by seven random residues and are able to interact with EB1, which results in replacing its endogenous interactors, as stated by the same authors.

I had hoped to be able to investigate the similarities and potential differences in EB1 and EB2 function by specifically inhibiting each protein. In Chapter 4 I will demonstrate that, when EB1-GFP is purified from *Drosophila* embryos, EB2 (CG18190) is co-purified at similar levels, suggesting the presence of a functional EB1-EB2 dimer in the early *Drosophila* embryo. However, given that the anti-EB2 antibodies that were purified recognized both EB1 and EB2 via Western blot, the effect on MT organisation and chromosome segregation after injection of anti-EB2 antibodies cannot be interpreted as the specific result of inhibiting EB2. As such, it remains unclear whether EB2 functions specifically in the early embryo. Nonethless, the results presented in this Chapter strongly suggest that purified anti-EB1 and EB2 antibodies can be used to disrupt EB protein function in the early *Drosophila* embryo.

Chapter 4:   Identification and characterisation of the metaphase EB1 interactome

4.1   Introduction

Proteins are involved in control of all biological processes in a cell. Many proteins function independently, but a large number of them interact with others to perform different biological activities. The biochemical purification of a protein and its interacting partners from its endogenous environment allows an opportunity to infer its function. However, it is usually limited by the low abundance of the protein of interest, the amount of tissue required for biochemical purification of the target, and subsequent identification of its interactors via Mass Spectrometry. These issues can be overcome in the *Drosophila* embryo. Following oogenesis and fertilisation, the *Drosophila* embryo undergoes 13 rounds of DNA replication and chromosome segregation in the absence of any major zygotic transcription or translation. Accordingly, the mother lays down enough mitotic proteins to be able to generate $\approx$ 6–8000 mitotic spindles. As such, relatively small amounts of embryos ($\approx$ 0.2–0.4 g) expressing endogenous or tagged genes are sufficient to undertake protein affinity purification followed by mass spectrometry.

The Wakefield lab has extensive experience in optimising affinity purification-mass spectrometry (AP-MS) to isolate and identify interacting partners of key mitotic proteins from syncytial *Drosophila* embryos. This approach uses GFP as a tag with which to purify the protein of interest in combination with the commercially available GFP-TRAP-A reagent from Chromotek – a camelid nanobody

covalently attached to agarose beads. Following incubation of the beads with a high speed extract generated from embryos expressing the relevant GFP-fusion protein, and extensive washing, Mass Spectrometry and cross-referencing to the *Drosophila* genome/proteome provides a list of interacting proteins. Further cross-referencing to an abundance list of *Drosophila* proteins consistently present in every GFP-TRAP-A affinity purification in embryos allows the removal of "false positives". This pipeline has been used to robustly identify the interactomes of over 30 different proteins involved in mitosis (Wakefield lab, unpublished) including Misato (Palumbo et al. 2015), Morgana (Palumbo et al. 2020), and the Augmin and γ-TuRC protein complexes (Rogala et al. 2017; Tariq et al. 2020). Such an AP-MS approach can also be extended to investigate the changes in protein interaction networks that occur as a result of cell cycle changes.

Collection of 0–3 hr *Drosophila* embryos results in a mixed cycling population, where approximately 80% of embryos will be in interphase. However, if 0–3 hr embryos are dechorionated and incubated with the proteasomal inhibitor MG132 for 20 mins, $\approx$ 80% of embryos accumulate at the metaphase-anaphase transition, with mature mitotic spindles and aligned chromosomes. Immediate washing and flash freezing in liquid nitrogen therefore provides a source of late-metaphase/early anaphase tissue in contrast to a predominantly cycling population. The differences in interactomes between these two tissues can then be quantified using trypsin digestion followed by TMT (Tandem Mass Tag) labelling MS. A TMT is formed by three functional groups: a reporter, a balancer and a reactive group. During TMT labelling, the reactive group is replaced by a peptide present in the tryptic mix. A reporter combined with a balancer of different TMTs has the same mass, but each reporter or balancer has different mass, such that, during LC-MS/MS peptides are ionised and separated by their mass-to-charge ratio (m/z) and molecules with lower mass appear first and the height of a peak is related to their abundance. Up to 12 different TMT reactions

can be run simultaneously through one LC-MS/MS run. As such, replicates of individual affinity purifications, or affinity purifications from different tissues (such as the cycling and MG-132/mitotic embryos) can be simultaneously analysed, and differences in the interactomes quantified.

In this chapter, I have taken this Quantitative Comparative Affinity Purification Mass Spectrometry (QC-AP-MS) approach to identify and compare the EB1-GFP interactomes between cycling and MG-132 treated embryos. After validation, this identified a number of proteins whose interaction with EB1 significantly changed between cell cycle stage. I then focussed on five of these proteins – SPN-F, JVL, IKK, HK, PIGS – which have previously been suggested to have a functional link to EB1, MTs or the interaction between MTs and the embryonic cortex in interphase. In each case, I investigated the cell-cycle dependent localisation of these proteins, fused to GFP, in the syncytial embryo before using standard AP-MS of MG-132 treated embryos expressing these proteins to identify their mitotic interactomes. The results strongly suggest that four of these proteins, SPN-F, JVL, IKK and HK, functionally and physically interact during metaphase and anaphase in the early embryo, consistent with a role at the plus ends of MTs.

4.2 Quantitative comparative proteomics identifies proteins that interact with EB1 differentially in mitosis compared to interphase

4.2.1 Affinity purification of EB1 interacting partners and their identification

To identify EB1 interactors in metaphase from *Drosophila melanogaster*, 4 batches of ≈ 0.4 g of embryos expressing EB1-GFP, under the control of the UASp promoter and driven by GAL4 under the control of the maternal-α-tubulin promoter, of age 0–3 hours were collected both for cycling populations (i.e. predominantly interphase embryos) and for those treated with MG132 for 20 minutes prior to flash freezing (i.e. mitotic embryos). High Speed Supernatants

(HSS – 100,000 g) from each of these 8 batches of embryos were incubated with GFP-TRAP-A overnight with rotation (Figure 4.1 a) and after incubation, a series of washes were carried out in order to eliminated unbound proteins from protein complexes which are bound to beads (Figure. 4.1 b). Western blot was conducted to confirm the efficiency of affinity purification (Figure 4.2, for an example). After confirmation, each of the 8 batches of EB1-GFP beads were subjected to trypsin digestion, Tandem Mass Tag (TMT) labelling and LC-MS/Ms by the Bristol Proteomics Service.
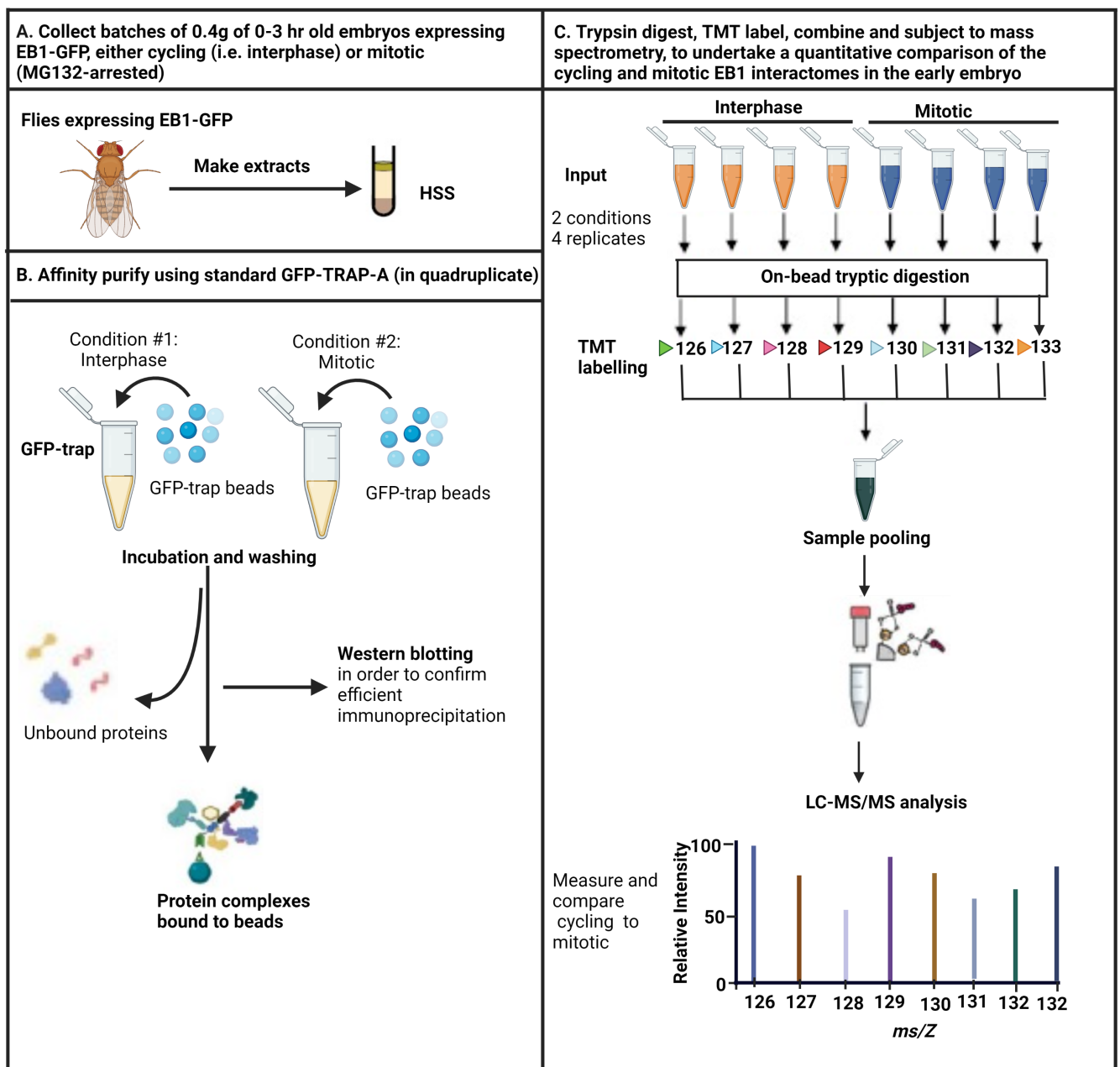
Figure 4.1: **General illustration of immunoprecipitation and TMT-MS workflow.** The table illustrates immunoprecipitation and tandem mass tag based on mass spectrometry to identify EB1 interactors in metaphase. Reproduced with permission, Ammarah Tariq

Following TMT-MS, the list of predicted proteins and their relative abundance in each sample was produced. As expected, the bait protein EB1 was present in all samples at very high abundance. The mean value for EB1 in the 4 cycling purifications (35694) and the 4 mitotic purifications (33217) allowed the calculation of a normalising factor, to take into account the slightly different amounts of EB1. This normalising factor was then applied to the mean values for each of the interacting proteins to allow the direct comparison of amounts of EB1 interacting proteins in cycling or mitotic embryos.
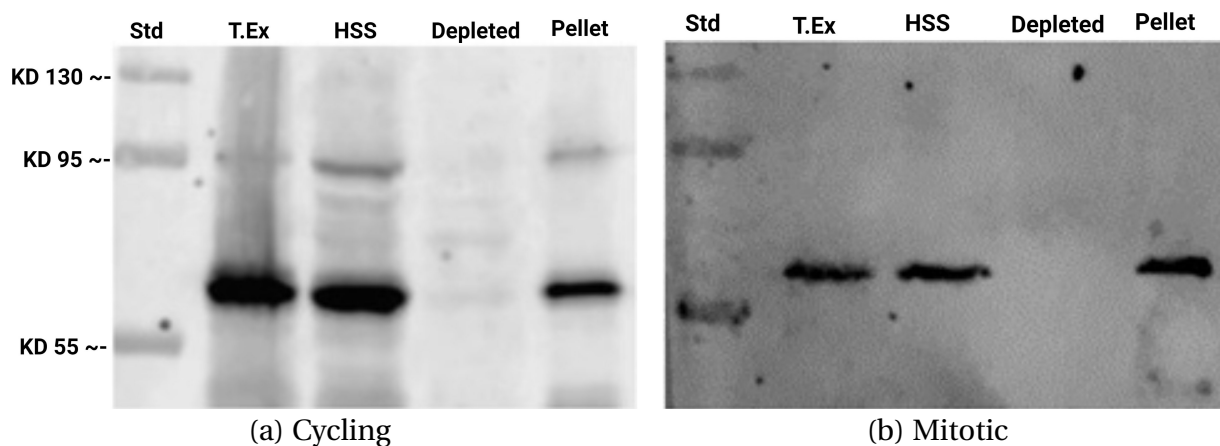
(a) Cycling   (b) Mitotic

Figure 4.2: **Western blot of EB1 IP.** In both EB1 cycling and mitotic, the results show the presence of a GFP-positive band at the expected molecular weight in the total extracts (T.Ex), high speed supernatant (HSS) and in the GFP-TRAP-A pellet (Pellet), thereby, the GFP-positive band completely depleted in the total extracts (Depleted). The depleted condition is the HSS after incubation with GFP-TRAP-A beads. EB1-GFP MW $\approx$ 59 kD. The variation in intensity between 4.2(a) and 4.2(b) is due to loading and exposure differences. The additional low intensity band seen at $\approx$ 90 kD in cycling Western blot may correspond to undenatured heterodimer of GFP-EB1 ($\approx$ 60 kD) and GFP (30 kD) which may be present in the embryo. This is not apparent in the lower intensity and exposure mitotic Western blot

4.3   General description of the Top 100 EB1 interactors in mitosis

Following TMT-MS/MS, the list of EB1 binding proteins in each replacate was produced. I therefore generated the mean value for the list of predicted proteins in 4 cycling samples and in 4 mitoic samples. The mean value 35694 for EB1 in cycling was similar to the mean value 33217 for EB1 in mitotic. Consequently, I caluclated the normalising factor $0.9306 = \frac{33217}{35694}$, which was applied to the mean values for each of EB1 binding proteins in cycling and in mitosis to correct the slightly different amounts of EB1. Before focusing on the comparison between EB1 interacting proteins in cycling and mitotic extracts, I first explored the mitotic EB1 interactome, concentrating on the 100 most abundant proteins present in the MG-132 treated EB1-GFP affinity purifications (Table 4.1). EB1 would be expected to be the most abundant protein purified from embryos, given the use of the GFP tag. Small amounts of EB1 are present in the WakefieldLab false positive list (Score 32.9), while the mean score for EB1 in the mitotic IPs was 2964.8 – the protein ID with the highest score and a fold increase of 81.9. The Score itself is a composite value, taking into account the peptide percentage coverage and size of the protein, in addition to the peptide abundance. When protein IDs were ranked according to the peptide abundance alone, EB1 was the second most abundant protein, with dynein heavy chain (DHC64C) being present at similar, but slightly higher, abundance. The Top 100 mitotic EB1 interactome also identified CG18190, otherwise known as EB2 (Chapter 3). The very high levels of EB2 co-purified with EB1 strongly suggest the presence of a substantial population of EB1-EB2 heterodimers in the early embryo.

Table 4.1: **Top 100 Mean Abundance (Mitotic).** The table indicates top 100 EB1 interactors with their respective mean values of all four replicates in metaphase with higher Mean Abundance (Mitotic) and 2.0 or more fold increase in mitotic if present in false positive (FP) list. Colours of protein Names reflect those used throughout this Chapter to group particular complex (e.g. Dynein/Dynactin = yellow). See Table 4.6 for further explanation

Name	ID	% Coverage	# Unique Peptides	# AAs	MW [kDa]	Score Sequest HT	Mean Abundance (Mitotic)	Present in FP list	FP Score	Mitotic Score minus Score in FP	Fold Increase in Mitotic
DHC64C	FBpp0304991	68.4	290	4661	532.3	1692.3	36836.7	NO	0.0	1692.3	
EB1 (PE)	FBpp0089088	96.2	1	290	32.5	2694.8	33216.6	YES	32.9	2662.0	81.9
CLIP-190	FBpp0304729	77.5	141	1690	189	1014.5	16669.5	NO	0.0	1014.5	
CG18190	FBpp0271746	82.3	21	248	28.7	678.7	12790.4	YES	55.6	623.1	12.2
HSC70-4	FBpp0082518	84.0	44	651	71.1	720.2	11106.3	NO	0.0	720.2	
APOLPP	FBpp0088252	49.1	161	3351	372.4	662.5	9550.7	YES	321.2	341.3	2.1
DNAPOL-EPSILON255	FBpp0083800	63.1	120	2236	256.5	474.8	9352.6	NO	0.0	474.8	
SHOT	FBpp0086743	41.9	5	5385	614.9	626.1	8417.1	NO	0.0	626.1	
DCTN1-P150	FBpp0075498	67.7	87	1265	141.1	365.9	8059.6	YES	57.7	308.1	6.3
EEF1ALPHA1	FBpp0304260	77.3	30	463	50.3	486.6	7905.9	NO	0.0	486.6	
ROD	FBpp0085156	48.4	88	2089	239.5	445.0	7779.7	NO	0.0	445.0	
POE	FBpp0305301	44.5	205	5322	590.3	744.1	7012.5	NO	0.0	744.1	
R	FBpp0088675	63.8	113	2224	246.5	581.4	6690.7	YES	175.2	406.2	3.3
CHB	FBpp0088469	51.5	70	1491	165.5	325.9	6661.4	NO	0.0	325.9	
MSPS	FBpp0293341	60.1	116	2082	230.3	498.1	5920.1	NO	0.0	498.1	
CG17514	FBpp0112471	57.6	132	2630	293.7	549.5	5598.6	NO	0.0	549.5	
FAF	FBpp0085202	50.5	123	2778	310.9	566.2	5288.2	NO	0.0	566.2	
NIPPED-A	FBpp0292385	39.4	124	3790	435.1	435.0	5281	NO	0.0	435.0	
GLYS	FBpp0082496	67.7	44	709	81.7	300.0	4827.4	NO	0.0	300.0	
DCTN2-P50	FBpp0087722	76.6	31	380	42	152.3	4679.3	YES	41.3	111.1	3.7
CCT3	FBpp0082788	83.6	48	544	59.4	396.9	4465.7	NO	0.0	396.9	
DLIC	FBpp0073299	54.4	34	493	54.4	144.9	4407.9	YES	33.6	111.4	4.3
ALPHACOP	FBpp0072693	65.5	72	1234	139.2	320.4	4030.8	YES	70.7	249.7	4.5
HDAC6	FBpp0303431	44.5	39	1179	130.8	140.2	3975.4	NO	0.0	140.2	
GCC185	FBpp0112136	64.8	76	1135	130	322.3	3904	NO	0.0	322.3	
MTOR	FBpp0087140	44.4	103	2346	262.2	351.7	3860.2	NO	0.0	351.7	
NUP358	FBpp0293235	39.6	93	2718	298.7	394.5	3827.5	NO	0.0	394.5	
MTPALPHA	FBpp0079454	67.2	44	783	84	313.5	3702.5	NO	0.0	313.5	
EIF4G1	FBpp0111817	48.6	83	1919	211	443.1	3699.6	NO	0.0	443.1	
CG12702	FBpp0307136	61.8	42	870	97.1	252.1	3473.9	NO	0.0	252.1	
PLP	FBpp0297121	22.3	61	2895	327.1	211.9	3369.9	NO	0.0	211.9	
NOT1	FBpp0111584	41.5	92	2505	281	340.2	3337.8	NO	0.0	340.2	
DNAPOL-DELTA	FBpp0075277	57.1	62	1092	124.8	270.9	3337.4	YES	68.0	202.9	4.0
GLUPRORS	FBpp0083898	51.6	86	1714	189.3	301.9	3251.4	YES	141.0	160.9	2.1
JVL	FBpp0296974	40.5	41	1151	122.3	159.6	3089.9	NO	0.0	159.6	
CMET	FBpp0304511	49.9	105	2189	251.3	364.8	3088.8	NO	0.0	364.8	
SW	FBpp0088428	58.5	25	663	73.9	149.9	3012.3	NO	0.0	149.9	
DROJ2	FBpp0082221	65.0	28	403	45.2	185.1	2955.8	NO	0.0	185.1	
NURF-38	FBpp0072250	77.2	21	338	37.9	175.7	2904.4	NO	0.0	175.7	
HYD	FBpp0081568	28.2	71	2885	318.7	247.1	2836.2	NO	0.0	247.1	
CG8184	FBpp0073898	25.0	105	5146	556.5	349.2	2813.3	NO	0.0	349.2	
ILERS	FBpp0078150	61.8	70	1229	141	267.5	2809.6	YES	110.7	156.7	2.4
HOOK	FBpp0080722	59.4	39	679	76.6	166.4	2808.7	NO	0.0	166.4	
RANBP16	FBpp0292664	37.7	41	1110	126.9	151.2	2768.6	NO	0.0	151.2	
MUD	FBpp0304868	28.1	57	2501	286.3	182.2	2722.1	NO	0.0	182.2	
YL	FBpp0073715	30.9	48	1984	219.4	189.1	2710.1	NO	0.0	189.1	
ZIP	FBpp0072306	39.5	75	2056	236.5	290.0	2699.3	NO	0.0	290.0	
PRP8	FBpp0087124	38.6	81	2396	279.4	294.7	2675.6	YES	39.8	254.9	7.4
TOR	FBpp0080003	35.3	77	2470	280.9	256.0	2612.1	NO	0.0	256.0	
IKKEPSILON	FBpp0080920	49.4	35	720	81.9	139.5	2602	NO	0.0	139.5	
UBA5	FBpp0073354	67.8	17	404	44.1	158.9	2551.1	YES	31.7	127.2	5.0
PUF	FBpp0303341	26.1	89	3930	442.1	299.0	2504.6	NO	0.0	299.0	
CANA	FBpp0079795	45.7	77	1931	221.7	291.7	2473.3	NO	0.0	291.7	
NIPPED-B	FBpp0110410	34.4	66	2077	236.6	189.8	2463.7	NO	0.0	189.8	
BRUCE	FBpp0304071	14.9	65	4852	536.2	208.6	2402.5	NO	0.0	208.6	
CTR9	FBpp0072562	42.6	41	1150	130.4	178.0	2377	NO	0.0	178.0	
LIS-1	FBpp0089100	56.2	23	411	46.4	120.0	2337.3	NO	0.0	120.0	
ARP1	FBpp0082121	65.4	23	376	42.7	134.9	2287.3	YES	71.2	63.7	1.9
KST	FBpp0289294	20.8	81	4337	497.2	224.0	2287	NO	0.0	224.0	
FS(2)KET	FBpp0294035	68.0	41	884	98.6	277.8	2278.2	NO	0.0	277.8	
RPII140	FBpp0082353	51.7	55	1176	134	227.0	2271.8	YES	53.2	173.8	4.3
GCS2ALPHA	FBpp0070058	53.0	47	924	105.7	164.6	2266.6	NO	0.0	164.6	
SKAP	FBpp0112118	46.8	24	502	54.8	156.8	2235.3	NO	0.0	156.8	
RPN2	FBpp0303405	47.8	49	1029	114.1	216.6	2203.7	NO	0.0	216.6	
GAMMACOP	FBpp0303129	55.0	1	897	99.4	204.6	2194.5	NO	0.0	204.6	
LEURS	FBpp0077251	53.6	54	1182	134.8	207.0	2181.7	YES	76.9	130.1	2.7
STI	FBpp0304889	34.5	64	1858	211.6	179.1	2163.3	NO	0.0	179.1	
ZWILCH	FBpp0085138	54.0	31	641	72.4	119.7	2162.7	NO	0.0	119.7	
BETACOP	FBpp0074348	49.1	40	964	107.3	208.9	2157.1	YES	49.3	159.6	4.2
RPII215	FBpp0073387	38.8	65	1887	209	203.5	2135.9	YES	31.7	171.8	6.4
ALPHA-SPEC	FBpp0305100	39.6	84	2457	282.4	268.1	2082.4	NO	0.0	268.1	
EIF3A	FBpp0078584	47.7	56	1140	133.8	220.8	2076.4	YES	100.3	120.5	2.2
LOST	FBpp0078561	67.5	36	545	59.7	164.4	2050	NO	0.0	164.4	
DNAPOL-EPSILON58	FBpp0076789	49.5	23	525	58.7	96.9	2044.1	NO	0.0	96.9	
PDS5	FBpp0087082	45.8	52	1218	138.8	161.0	2023.9	NO	0.0	161.0	
TACC	FBpp0291770	45.4	53	1227	136.6	217.8	2010.1	NO	0.0	217.8	
MMS19	FBpp0078425	59.5	43	959	107	187.9	1998.4	NO	0.0	187.9	
LDS	FBpp0081255	39.4	41	1061	118.3	142.8	1996.3	NO	0.0	142.8	
CG32164	FBpp0303949	53.7	46	1080	120.8	239.3	1943.2	NO	0.0	239.3	
RANBP21	FBpp0074528	39.5	43	1241	139.1	177.6	1942.4	YES	38.8	138.8	4.6
ZW10	FBpp0070425	49.9	26	721	82.2	152.4	1938.3	NO	0.0	152.4	
CG7029	FBpp0083705	36.2	42	1744	192.2	200.7	1913.1	NO	0.0	200.7	
NCM	FBpp0080638	23.1	30	1330	151.5	92.3	1901.6	NO	0.0	92.3	
ASP	FBpp0084071	28.4	60	1954	230	174.2	1894	NO	0.0	174.2	
WECH	FBpp0289359	48.2	32	832	90.5	122.7	1860.7	NO	0.0	122.7	
NCD	FBpp0084900	50.1	30	700	77.4	110.4	1795.8	YES	41.7	68.7	2.6
CUL1	FBpp0087924	60.3	43	774	89.5	180.1	1768.6	NO	0.0	180.1	
METRS	FBpp0085809	64.5	55	1022	112.4	236.5	1759.4	YES	113.8	122.7	2.1
SMC2	FBpp0086591	48.7	51	1179	134.3	195.0	1755.8	NO	0.0	195.0	
MI-2	FBpp0099808	36.6	56	1983	224.2	218.6	1753.2	NO	0.0	218.6	
UFD4	FBpp0079663	24.2	55	2727	302	185.8	1744.8	NO	0.0	185.8	
TNPO	FBpp0076708	46.2	34	893	101.5	204.1	1740.2	YES	56.7	147.3	3.6
GRSM	FBpp0082198	74.4	31	558	60.1	215.9	1730.4	NO	0.0	215.9	
KIS	FBpp0289115	12.5	59	5517	593.1	192.5	1721.5	NO	0.0	192.5	
BETA'COP	FBpp0080048	61.1	45	914	102.6	206.6	1717	NO	0.0	206.6	
RM62	FBpp0078301	48.1	24	719	78.5	133.0	1708	NO	0.0	133.0	
CUL5	FBpp0084786	43.7	37	852	96.9	135.3	1681.7	NO	0.0	135.3	
HSC70-5	FBpp0086694	47.5	34	686	74	143.9	1661.2	YES	73.0	71.0	2.0
AGO3	FBpp0289158	58.0	42	867	99.1	151.6	1651.5	NO	0.0	151.6	
HYX	FBpp0081448	51.9	28	538	61.3	92.8	1626.7	NO	0.0	92.8	

Of the Top 100 EB1-GFP mitotic interacting proteins, many have known functional relationships with EB1 or functions related to mitotic MT organisation. When compared to the String database (`https://string-db.org/`) 7 of the 10 known EB1 associated proteins were present in the top 100 (DHC64C, CLIP-190, MSPS, SHOT, LIS-1, CANA, NCD). I took the Top 100 proteins and undertook a Gene Ontology (GO) enrichment analysis (Table 4.2) (`http://geneontology.org/`) to formalise the relationships between Top 100 EB1-GFP mitotic binding proteins and EB1 or mitotic MT organisation. This identified a number of classes of proteins with known functional links to MTs and EB1 Table 4.2. GO databases are incomplete as not every protein with a known, published function or localisation is present in the GO database (See Subsection 4.3.1, Table 4.3 for an example relating to the Dynein/Dynactin complexes). There are a number of other bioinformatic tools that can be used to analyse physical protein interactions. However, as my focus was only 100 proteins I individually mined Flybase to learn about each of the proteins. Together with the GO analysis, this allow me to comprehensively characterise functional and physical classes of proteins identified in the Top 100 mitotic EB1 interactors.

Table 4.2: **Top 100 EB1 interactors GO Enrichment Analysis.** The Gene Ontology (GO) enrichment analysis identified different classes of proteins within top 100 EB1 binding proteins with known functional relationship with MTs and EB1.

GO cellular component complete	Reference List (13811)	Present in EB1 IP (Top 100)	Expected	Fold Enrichment	P-value	FRD	Protein names
cytoplasmic dynein complex (GO:0005868)	27	3	0.19	16.16	1.09E-03	1.76E-02	DLIC, DHC64C, SW
dynactin complex (GO:0005869)	7	2	0.05	41.57	1.61E-03	2.47E-02	LIS-1, DCTN2-P50
microtubule plus-end (GO:0035371)	17	6	0.12	51.35	7.93E-09	3.92E-07	DCTN1-P150, CLIP-190, EB1, MSPS, SHOT, CHB
RZZ complex (GO:1990423)	3	3	0.02	>100	6.07E-06	1.80E-04	ROD,ZW10, ZWILCH
spindle microtubule (GO:0005876)	37	11	0.25	43.25	1.52E-14	2.03E-12	DCTN1-P150, NCD, TACC, ROD, CLIP-190, EB1, LIS-1, ZWIlLCH, ZW10, ASP, CHB
basal cortex (GO:0045180)	12	3	0.08	36.37	1.32E-04	2.76E-03	MUD, ZIP, CHB
spectrosome (GO:0045170)	8	2	0.05	36.37	2.00E-03	2.85E-02	CHB, ALPHA-SPEC
COPI-coated vesicle (GO:0030137)	8	3	0.05	54.56	4.89E-05	1.26E-03	ALPHACOP, GAMMACOP, BETACOP
epsilon DNA polymerase complex (GO:0008622)	4	2	0.03	72.74	6.80E-04	1.16E-02	DNAPOLe255, DNAPOLe58

Below, I describe in more detail some of the classes of proteins identified in the Top 100 mitotic EB1 interactome (Table 4.1).

4.3.1 Known mitotic MAP complexes

Dynein/Dynactin complex

Dynein/Dynactin complex (Table 4.1, yellow): As mentioned above, DHC64C was the most abundant EB1 interactor. DHC64C is part of the Dynein/Dynactin motor complex (Table 4.3), which has many functions during mitosis – as both a MT minus-end directed motor, moving cargo along MTs, and as an immobilised motor at the cell cortex and nuclear envelope, generating force to move MTs in relation to these membrane structures (J. Liu 2017).

Table 4.3: **Subunits of cytoplasmic Dynein/Dynactin complex.** The table shows subunits of cytoplasmic Dynein/Dynactin complex and adaptors identified as EB1 binding proteins. Dynein heavy chain subunit 64 (DHC64C), dynein light intermediate chain (DLIC), dynein intermediate chain (DIC), dynactin subunit 1, 2 and 4 (DCTN1, DCTN2 and DCTN4), actin-related protein 1 and 10 (ARP1 and ARP10), capping protein alpha and beta (CPA and CPB), shortwing (SW) and lissencephaly-1 (LIS-1).

Dynein subunits	Dynactin subunits	Dynein/Dynactin adaptors
DHC64C	DCTN1-p$^{150 Glued}$	SW
DLIC	DCTN2-p$^{50 Dynamitin}$	LIS-1
DIC	DCTN4-p^{62}	
	ARP1	
	ARP10	
	CPA	
	CPB	

The GO analysis of the Top 100 EB1 interacting proteins identified 3 subunits (DLIC, DHC64C and SW) of the Dynein and 2 subunits (LIS-1 and DCTN2-P^{50}) of the Dynactin (Table 4.2). However, manual attribution of known Dynein/Dynactin subunits demonstrate the presence of 7 proteins (DLIC, DHC64C, SW, LIS-1, DCTN2-P^{50}, DCTN1-P^{150} and ARP1) (Table 4.3) in the Top 100 (Table 4.1) and 5 proteins (DIC or CTP, DCTN4-P^{62}, ARP10, CPA and CPB) within the Top 56. This strongly suggests that the whole of the Dynein/Dynactin complex interacts with EB1 in mitosis.

CLIP190-CLASP

CLIP190-CLASP (Table 4.1 red): In addition, the Top 100 EB1 interactors include a number of MT associated proteins (MAPs) with roles in mitosis. CLIP-190 is the homologue of human CLIP-170 – a MT +TIP which is found associated with CLASP (CLIP-170 Associated Protein)/MAST/Orbit/CHB (Chromosome bows). In addition, chromosome bows (CHB), was also other member of CLIP190-CLASP complex identified within the top 100. CLIP190-CHB has been shown to be important in MT stabilisation and bipolar mitotic spindle organisation (Inoue et al. 2000; Lemos et al. 2000). CLIP-190 was the third most abundant EB1 interacting protein while CHB was the 14th most abundant.

RZZ complex

RZZ (Table 4.1, orange): During metaphase, the Dynein/Dynactin complex might be recruited to kinetochores by EB1 where it interacts with the ROD-ZWILCH-ZW10 (RZZ) complex via the protein Spindly. As kinetochore MTs mature, Dynein/Dynactin is able to transport the RZZ complex polewards, towards the MT minus ends, thus resulting in silencing the spindle assembly checkpoint (SAC) promoting the onset of anaphase and chromosome segregation. In addition, my work suggests that EB1 may also interact with RZZ complex via ROD, which has one SxIP domain (Table 4.4) to facilitate the interaction between the Dynein/Dynactin complex and RZZ-spindly complex (Mosalaganti et al. 2017;

Pereira et al. 2018). All four proteins – ROD, ZW10, ZWILCH and Spindly were identified within the Top 100 EB1 interacting mitotic proteins.

Table 4.4: **EB1 interacting domains.** The table shows a research of some EB1 interactor motifs. (-) the protein does not have any type of motifs. (+) the protein has at least one EB1 interacting motif and in brackets number and kind of motif.

Protein Name	EB1 binding motifs	Location
ATU	-	
CG12702	-	
CG4572	-	
CG9547	-	
CG46338	-	
CHB	+ (2 SxIP)	N- and C- terminuses
CORN	-	
DNApol-ε 58	+ (1 SxIP)	C-terminus
DNApol-ε 255	+ (1 TxIP)	N-terminus
HOOK	-	
IKK-ε	-	
JVL	+ (3 SxIP)	C-terminus
NUF	-	
NURF	-	
Dynactin P150^{glued}	+ (1 CAP-Gly)	N-terminus
PIGS	+ (2 SxIP)	C-terminus
PLP	-	
ROD	+ (1 SxIP)	N-terminus
SHOT	+ (1 SxIP)	C-terminus
SLAM	-	
SPINDLY	-	
SPN-F	-	
SW	+ (1 SxIP)	N-terminus
TORSIN	-	
TSF1	-	
ZW10	-	
ZWILCH	-	

TACC-TOG

TACC-TOG (Table 4.1, blue): Mini-spindles protein (MSPS) is the homologue of human TOG, which in association with the MAP TACC is important for MT stabilisation and normal spindle function in the early *Drosophila* embryo (Jeffers et al. 2020, for review see Peset and Vernos 2008). Both were within the Top 100 EB1 interactors in mitosis. TACC proteins are found in different organisms and only one protein (D-TACC) found *Drosophila melanogaster,* TAC-1 in *Drosophila elegans,* Alp7 also known as Mia1p in *Schizosaccharomyces pombe,* Maskin in *Xenopus laevis.* However, Three TACC (TACC1-TACC3) proteins are present in mammals (Still et al. 2004). The phosphorylation of TACC by Aurora-

A kinase allows its interactions with clathrin to bind to the MTs (For review see Gutiérrez-Cabalerro et al. 2015). A cancer-associated protein, transforming acidic coiled-coil protein 3 (TACC3) binds to ch-TOG (Prumbaum et al. 2013), therefore TACC3-chTOG-Clathrin complex is implicated in stabilising kinetochore fibers and MTs, in regulating MT behaviour (Gergely et al. 2001; Prumbaum et al. 2013; Thakur et al. 2014). In addition, D-TACC is reported to interact with MSPS to modulate the MT dynamics (Gergely et al. 2001).

4.3.2 Other known mitotic MAPs

PLP

Pericentrin-like protein (PLP)(Table 4.1): PLP does not exhibit an EB1 interacting motif (Table 4.4), is localised to centrioles and centrosomes and is implicated in organising pericentriolar material (PCM). The examination of *Drosophila* PLP function *in vivo* in tissues, has revealed that centrioles of *Plp* mutant show four principal defects (Roque et al. 2018) – I) they are short and abnormal structures. II) They dissociate prematurely and consequently they overduplicate. III) They create fewer MTs during interphase and IV) in cilia, they fail to form and maintain a correct connection to the plasma membrane.

During interphase, in fly culture cells, PLP molecules concentrate around the mother centriole, with the C-terminus connected to the centriole and the N-terminus extends outwards and coordinates the recruitment of PCM proteins, including γ-tubulin and Cnn (Baumann 2012; Mennella et al. 2012; Richens et al. 2015). In addition, PLP was shown to interact with Cnn scaffold in the outer-region of the PCM to strengthen the PCM and the depletion of PLP causes only subtle disruption of early embryo development, of centrosome behaviour and MT dynamics (Richens et al. 2015).

CMET and CANA

CENP-meta (CMET) and *CENP-ana (CANA) (Table 4.1):* CMET and CANA are essential kinesin-like proteins in *Drosophila* and both proteins are related to CENP-E in verterbates (Yucel et al. 2000). However, research of CMET depletion using RNAi in *Drosophila* S2 cell suggests that CMET is more likely to be the homogue of mammalian CENP-E than CANA (Goshima and Vale 2003). These two proteins are components of kinetochore and are involved in different functions during cell division, including MT capture, spindle assembly checkpoint, chromosome congression and alignment (Schaar et al. 1997; Weaver et al. 2003; Yu et al. 2019; Yucel et al. 2000). Between nuclear envelope breakdown and late anaphase-A, CENP-E is associated with kinetochores and at metaphase is implicated in crucial roles of capturing MTs, modulating cromosome movements (Coulson et al. 1994; Putkey et al. 2002). These observations are consistent with studies conducted by Schaar et al. (1997) in which the depletion of CENP-E by anti-CENP-E antibody microinjection was responsible for chromosome missgregation and missalignment as well as the delay of the onset of anaphase. Finally, in late G_2 CENP-E accumulates in cytoplasm of cells, from where migrated to kinetochores upon nuclear envelope breakdown and restart the cycle (Coulson et al. 1994).

MUD and NCD

Mushroom body defect (MUD) and *Non-claret dysjunctional (NCD) (Table 4.1):* The defect of chromosome segregation in NCD mutant of *Drosophila simulans* was first observed by Sturtevant in 1929 (For review see She and Yang 2017) and subsequent studies revealed that *Drosophila* NCD move from MT plus ends toward the minus ends with an approximate velocity of 42.7 ± 2.19 nm/s (Salmon et al. 1990; She and Yang 2017; Stewart et al. 1990) using chemical energy from hydrolysis of ATP.

Drosophila Mushroom body defect (MUD) is an orthologue of human Nuclear Mitotic Apparatus (NuMA) and is involved in functions of regulating spindle orientation during cell division and MT polymerisation (Bowman et al. 2006; She and Yang 2017). In addition, it has been suggested that MUD binds to NCD to facilitate the MT binding of NCD, thus to modulate its activities during mitosis (She and Yang 2017), however, functions of MUD-NCD interactions are poorly understood and need further exploration.

ASP

Abnormal spindle (ASP) (Table 4.1): ASP is a MT binding protein localised to the pole of the mitotic spindle and is required for proper spindle structure and MT organisation *in vivo* in *Drosophila* embryos and larval brain cells (Bonaccorsi et al. 2001; Saunders et al. 1997). Furthermore, studies conducted *in vitro* suggest the involvment of this protein in MT nucleation (Avides and Gover 1999). Investigations carried out by Bonaccorsi et al. (2001) in early *Drosophila* embryos and larval neuroblasts, illustrate that ASP is implicated in cross-linking of MT minus ends during mitosis and contributing to organisation of the spindle poles and the central spindle.

4.3.3   Cortical proteins with links to EB1

I also identified a number of proteins that have previously been shown to interact with EB1 or MTs that have roles in interphase.

SPNF-IK2-JVL complex

SPNF-IK2-JVL (Table 4.1 purple): Javelin-like (JVL), coiled-coil protein spindle-F (SPNF) and IKK-ε have been shown to form a complex, while EB1 has previously been shown to interact via JVL *in vitro*, which possesses three SxIP motifs (Table 4.4) (Baskar et al. 2019). However, there is no report of direct interactions between SPN-F or IKK-ε and EB1. Fathermore, SPN-F mediates the interactions between IKK-ε and the Dynein/Dynactin complex through interaction

with cut up (CTP) subunit, to promote the redistribution of JVL-SPNF-IK2 complex, which is essential for actin and MT organisation, cell polarity and bristle elongation (Amsalem et al. 2013; Bitan et al. 2010; Dubin-Bar et al. 2008; Kimpara et al. 2015). Furthermore, IK2 modulates recycling endosome dynamics by interacting with NUF, Rab11, dynein (Otani et al. 2011).

SHOT

Short stop (SHOT) (Table 4.1): SHOT is a member of the spectraplakin. Spectraplakins are cytoskeletal linker proteins that comprise three molecular families (Hahn et al. 2016; Voelzmann et al. 2017):

Plakins: In mammals, this includes – desmoplakin, plectin, bullous pemphigoid antigen-1 (BPAG1), envoplakin, periplakin, MT cross-linking factor 1 (MCF1) and epiplakin. In invertebrate organisms, plakins comprise short stop (SHOT) *Drosophila melanogaster* and *vab-10* in *Caenorhabditis elegans* (yue et al. 2017).

Spectrins: For example, $\alpha - /\beta$-spectrin, dystrophin, α-actinin and utrophin which are implicated in linking different proteins to the cell cortex and are components of contractile ring which is important for cytokinesis and invagination furrows(Albertson et al. 2008; Broderick and Winder 2005; Tram et al. 2002 and for review see Voelzmann et al. 2017). Spectrin are composed of heterotetramer made of two antiparallel heterodimers of α- and β- spectrin (Duan et al. 2018). In mammilian, there are two chains of α-spectrin (αI and αII) and five β-spectrin (βI $-$ βV), while in invertabrates only contain one α-spectrin and two β-spectrin (β and β Heavy) (Duan et al. 2018; Zhao et al. 2013). The $\alpha\beta$Heavy spectrin is also known as Karst (KST) (Duan et al. 2018; Fletcher et al. 2015), which was also identified within Top 100 EB1 interacting mitotic proteins (Table 4.1). Spectrin plays important roles, including the maintenance of the structure and stability of the cell membrane, the shape of a cell, and contribution of the cell-cell adhesion, cell

proliferation and the cell cycle (Zhao et al. 2013).

Gas2-like proteins: which comprises – Gas2, Gas2-like 1–3. These protein are involved in linking MTs, EB proteins and F–actin for regulation of cytoskeletal dynamics during cell division and development (For review see Nazgiewicz et al. 2019; Voelzmann et al. 2017; yue et al. 2017).

The *Drosophila* plakins in general have two domains at its C-terminus – C-tail and GAS2 domains (Takács et al. 2017). I have identified SHOT as an EB1 interactor, containing one EB1 binding motif within its C-terminal domain (Table 4.4). This is consistent with previous studies which have revealed that the C-tail domain at C-terminus interacts with EB1 to be localised at the MT plus ends. The GAS2 motif then binds to MT lattice and the N-terminus interacts with the actin network through two calponin homology (CH) domain. This is important for modulation of cytoskeletal rearrangement during cell divisions. (Takács et al. 2017; yue et al. 2017).

4.3.4   Other MT adaptor proteins

HOOK

HOOK (Table 4.1, green): A further interactor identified in my AP, HOOK, has a known functional interaction with Dynein/Dynactin complex, through the adaptors Rab5 and Rab11. HOOK is implicated in trafficking of vesicles (Arst et al. 2014; Krämer and Phistry 1999; J. Liu 2017; Yao et al. 2014) which are essential for invagination furrows during metaphase and cellularisation (Albertson et al. 2008; Xiang and Qiu 2020). In addition, the localisation of HOOK at the tip of the bristle is regulated by SPN-F and IK2, which suggests that the MT dynamics within the bristle is important for endocytic trafficking to the tip of the bristle (Bitan et al. 2010). However, HOOK does not appear to interact directly with MTs (Olenick et al. 2016) and there is not any report showing interactions betwen HOOK and EB1.

In summary, of the 100 most abundant EB1 interactors in mitosis, as identified from my AP-MS, over 1/3 have previously been implicated in MT or EB1 related cellular functions. The purification was performed at 4 °C and with no enrichment of tubulin, strongly suggesting that it is not co-purifying MTs and therefore this is a valid dataset that reflects the *in vivo* mitotic EB1 interactome.

Table 4.5: **Top 100 EB1 interactors in mitosis.** The table summarises EB1 binding proteins identified within top 100 in mitosis, based on manual attribution in addition to the GO enrichment. As identified from my AP-MS, over 1/3 have previously been implicated in MT or EB1 related cellular functions, strongly suggesting it is a valid dataset that reflects the *in vivo* mitotic EB1 interactome.

Known mitotic MAP proteins and complexes	Known interactors and functions
Dynein/Dynactin complex	The complex is a MT minus end directed motor, involved in transporting cargo along MTs (J. Liu 2017; Tan et al. 2018) and regulate MT network reorganisation (Tan et al. 2018).
CLIP-190-CLASP complex	CLIP-190 in *Drosophila* interacts with chromosome bows (CHB) to stibilise MT and organise mitotic spindle (Inoue et al. 2000; Lemos et al. 2000).
RZZ complex	Rod-Zw10-Zwilch (RZZ) complex is the kinetochores components which interacts with Dynein/Dynactin complex to silence the spindle assembly checkpoint during metaphase-anaphase transition (Mosalaganti et al. 2017; Pereira et al. 2018).
TACC-MAP	TACC interacts with mini-spindles protein (MSPS) to stablise MT and regulate MT dynamics (Jeffers et al. 2020, reviewed by Peset and Vernos 2008).
PLP	Pericentrin-like protein (PLP) is involved in organising pericentriolar material (PCM) and centriole maturation (Roque et al. 2018).
CMET and CANA	CENP-meta and CENP-ana (CMET and CANA) are components of kinetochores involved in MT capture, spindle assembly checkpoint, chromosome congression and alignment during cell division (Schaar et al. 1997; Weaver et al. 2003; Yu et al. 2019; Yucel et al. 2000).
MUD and NCD	Mushroom body defect (MUD) and Non-claret dysjunctional (NCD) are involved in MT orientation and polymerisation (Bowman et al. 2006; She and Yang 2017), alhough functions of the complex are poorly understood (She and Yang 2017).
ASP	Abnormal spindle (ASP) is important for proper spindle structure and organisation (Bonaccorsi et al. 2001; Saunders et al. 1997), MT nucleation (Avides and Gover 1999) and in cross-linking of MT minus ends for organisation of the spindle poles and central spindle (Bonaccorsi et al. 2001).
Cortical proteins and complexes with links to EB1	Known interactors and functions
SPNF-IK2-JVL complex	This complex interacts with EB1 through JVL subunit (Baskar et al. 2019) and Dynein/Dynactin complex to regulate cytoskeletal organisation, modulate vesicle transport, cell polarity and bristle elongation (Amsalem et al. 2013; Bitan et al. 2010; Dubin-Bar et al. 2008; Kimpara et al. 2015).
SHOT	Short stop (SHOT) is a spectraplain protein, which interacts with EB1 to be localised at the MT plus ends for modulation of cytoskeletal rearrangement during cell divisions (Takács et al. 2017; yue et al. 2017)
MT adaptor proteins	Known interactors and functions
HOOK	HOOK interacts with Dynein/Dynactin complex (Olenick et al. 2016) and does not appear to interact direcly with MTs (Olenick et al. 2016). This protein is involved in trafficking of vesicles (Arst et al. 2014; Krämer and Phistry 1999; J. Liu 2017; Yao et al. 2014). This endocytic trafficking is important for invagination furrows and cellularisation (Albertson et al. 2008; Xiang and Qiu 2020).

4.4   Proteins that increase their association with EB1 during mitosis

Having analysed the Top 100 EB1 interacting proteins in mitosis, I wanted to compare the interphase/cycling and mitotic interactomes to identify proteins and protein complexes that specifically increase their association with EB1 during mitosis. To do this, I compared the mean abundance of EB1 in the 4 cycling IPs (35693.7) with the EB1 mean abundance in the 4 mitotic/MG-132 IPs (33216.6). The closeness of these values demonstrate the reproducibility of the multiple IPs but, to ensure as accurate comparison as possible, I used the values to generate a normalising constant ($\frac{33216.6}{35693.7} = 0.9306$), then applied this to the cycling mean abundance for every protein ID. I then calculated the Abundance Ratio Mitotic:Cycling – a value that shows the increase/decrease in the amount of each protein interacting with EB1 in mitotic embryos, relative to cycling embryos.

Across all 8 proteomics data sets, I identified 1400 proteins that interacted with EB1. After normalising to Mean EB1 abundance mitotic:cycling, only 4% of interactors (56) showed an increased abundance in mitotic extracts (Table 4.6). I then applied a final cut-off of 1.2 fold increase in mitosis, to account for non-significant variation between embryo populations. This generated a final list of 30 proteins (Table 4.7). These 30 are arranged in the Table 4.7 according to known function and the presence/absence of known EB1 interacting motifs (SxIP, CAP-Gly and LxxPTPh) in their sequences (Table 4.4).

Table 4.6: **Top 56 EB1-GFP Mitotic v Interphase Network.** The table shows top 56 EB1 interactors in metaphase v interphase, then in accordance with their abundance ratio of mitotic/cycling after normalisation versus EB1 were ordered from the highest to the lowest. Proteins with highest ratio on the top of the table are more enriched in metaphase than the lowest in the bottle of the table. Colours of protein Names correspond to particular proteins and complexes (e.g. Dynein/Dynactin = yellow, RZZ complex subunits = orange). See Table 4.7 for full list of colours/complexes.

Protein Name	Coverage (%)	# Unique Peptides	# AAs	MW [kDa]	Mean Abundance Mitotic	Mean Abundance (Normalised) : Cycling	Mean Abundances: Cycling	Abundance Ratio (normalised) Mitotic/Cycling	Score Sequest HT
NUF	24.7	12	530	60.1	627.5	189.6	203.7	3.31	45.08
DCTN2-P50	76.6	31	380	42	4679.3	1771.2	1902.5	2.64	152.31
SW	58.5	25	663	73.9	3012.3	1181.2	1268.7	2.55	149.89
DLIC	54.4	34	493	54.4	4407.9	1994.4	2142.2	2.21	144.9
SPN-F	58.8	19	376	42.3	1076	511.0	548.9	2.11	79.89
LIS-1	56.2	23	411	46.4	2337.3	1131.6	1215.5	2.07	120.04
CG12702	61.8	42	870	97.1	3473.9	1717.7	1845	2.02	252.08
DNAPOL-EPSII	63.1	120	2236	256.5	9352.6	4761.8	5114.7	1.96	474.75
DHC64C	68.4	290	4661	532.3	36836.7	18988.3	20395.6	1.94	1692.33
PEO	45.5	11	244	28.1	546.5	287.4	308.7	1.90	32.01
IKKEPSILON	49.4	35	720	81.9	2602	1468.6	1577.4	1.77	139.48
ARP1	65.4	23	376	42.7	2287.3	1300.0	1396.3	1.76	134.9
DNAPOL-EPSII	49.5	23	525	58.7	2044.1	1186.6	1274.5	1.72	96.92
JVL	40.5	41	1151	122.3	3089.9	1795.9	1929	1.72	159.59
HOOK	59.4	39	679	76.6	2808.7	1705.9	1832.3	1.65	166.43
ZWILCH	54.0	31	641	72.4	2162.7	1370.2	1471.8	1.58	119.65
ROD	48.4	88	2089	239.5	7779.7	4942.1	5308.4	1.57	445.01
DCTN4-P62	56.2	21	514	57.9	1083.2	717.3	770.5	1.51	89.93
TORSIN	54.7	17	340	38.1	1597.5	1104.9	1186.8	1.45	64.29
ARP10	56.6	18	378	42.2	985.4	687.7	738.7	1.43	78.83
RPL13	43.6	11	218	24.9	620.2	434.0	466.2	1.43	32.85
CATHD	48.7	15	392	42.4	1610.5	1135.4	1219.5	1.42	70.13
DCTN1-P150	67.7	87	1265	141.1	8059.6	5724.8	6149.1	1.41	365.87
CG4572	30.1	12	482	54.4	1099.2	782.9	840.9	1.40	56.99
RPL7	39.3	10	252	29.5	688.1	498.5	535.4	1.38	31.05
ZW10	49.9	26	721	82.2	1938.3	1430.3	1536.3	1.36	152.43
CPA/MIRO	70.3	14	286	32.7	571.6	427.6	459.3	1.34	61.4
CORN	18.1	18	1107	121.9	748.9	571.4	613.7	1.31	63.67
CG9547	42.2	11	419	45.7	477.4	384.5	413	1.24	50.05
PIGS	13.6	11	977	104.4	838.1	696.2	747.8	1.20	37.52
SLAM	16.9	18	1173	130.5	886.9	742.3	797.3	1.19	56.55
PLP	22.3	61	2895	327.1	3369.9	2831.1	3040.9	1.19	211.89
CG30499	44.3	7	221	24.2	430.6	362.0	388.8	1.19	39.69
GLYCOGENIN	26.6	10	545	61.7	1289.6	1092.7	1173.7	1.18	40.93
TRX-2	79.2	7	106	11.7	1309.7	1116.7	1199.5	1.17	76.87
NURF-38	77.2	21	338	37.9	2904.4	2477.9	2661.5	1.17	175.65
GCS2BETA	48.2	19	548	61.5	956.9	843.8	906.3	1.13	91.09
RPL18A	59.3	14	177	21	1538.2	1372.9	1474.7	1.12	33.31
SPINDLY	29.7	20	781	88.6	837.6	751.8	807.5	1.11	64.98
RPL7A	41.3	12	271	30.7	747.5	676.7	726.8	1.10	33.16
CBP	50.7	11	298	34	684.5	619.7	665.6	1.10	37.62
RPL4	48.1	21	401	45	1585.6	1438.8	1545.4	1.10	58.52
CTR9	42.6	41	1150	130.4	2377	2196.2	2359	1.08	178.04
PHB2	33.1	12	338	37.3	812.4	752.9	808.7	1.08	39.41
MEN	38.7	25	763	84.6	1367.8	1277.3	1372	1.07	96.14
GCC185	64.8	76	1135	130	3904	3651.5	3922.1	1.07	322.32
APC7	28.6	18	615	70.3	828	777.6	835.2	1.06	54.3
SESB	71.2	24	312	34.2	1508.2	1441.1	1547.9	1.05	93.35
CG18190	82.3	21	248	28.7	12790.4	12423.6	13344.4	1.03	678.74
ATMS	50.2	21	538	60.8	1193.5	1164.1	1250.4	1.03	107.81
SAP-R	19.7	18	953	105.9	866	848.0	910.8	1.02	44.01
CG17333	81.5	17	243	26.7	1168.6	1147.0	1232	1.02	70.12
CHB	51.5	70	1491	165.5	6661.4	6606.8	7096.5	1.01	325.85
PXT	77.8	43	809	90.5	3670	3656.9	3927.9	1.00	271.27
SHOT	39.7	1	5434	618.9	46.5	46.4	49.8	1.00	601.83
ATU	18.6	17	725	77.4	872.5	873.0	937.7	1.00	46.26
EB1 (PE)	96.2	1	290	32.5	33216.6	33230.8	35693.7	1.00	2694.84

Table 4.7: **Mitotic v Interphase Network.** Proteins are grouped on basis of their similarity of actions or complexes that they form, thereby compared mean mitotic abundance versus mean cycling abundance after normalisation versus EB1. * indicates after normalisation versus EB1.

Protein Name	Mean Mitotic Abundance	Mean Cycling Abundance*	Abundance Ratio Mitotic/Cycling	Score Sequest HT	Summary Info	Availability of GFP-fusion flies
DHC64C	36836.7	18988.3	1.94	1692.33	Dynein–Dynactin complex	YES
DCTN2-P50	4679.3	1771.2	2.64	152.31	Dynein–Dynactin complex	YES
DIC	3012.3	1181.2	2.55	149.89	Dynein–Dynactin complex	
DLIC	4407.9	1994.4	2.21	144.9	Dynein–Dynactin complex	
LIS-1	2337.3	1300.0	2.07	120.04	Dynein–Dynactin complex	
ARP1	2287.3	717.3	1.76	134.9	Dynein–Dynactin complex	
DCTN4-P62	1083.2	687.7	1.51	89.93	Dynein–Dynactin complex	
ARP10	985.4	687.7	1.43	78.83	Dynein–Dynactin complex	
DCTN1-P150	8059.6	5724.8	1.31	365.87	Dynein–Dynactin complex	
CPA / MIRO	571.6	427.6	1.25	61.4	Dynein–Dynactin complex	
ROD	7779.7	4942.1	1.57	445.01	kinetochore-associated. Transported via Dynein-Dynactin	YES
ZW10	1938.3	1430.3	1.36	152.43	kinetochore-associated. Transported via Dynein-Dynactin	YES
ZWILCH	2162.7	1370.2	1.58	119.65	kinetochore-associated. Transported via Dynein-Dynactin	YES
SPINDLY	837.6	807.5	1.11	64.98	kinetochore-associated. Links RZZ to Dynein	
SPN-F	1076	511.0	2.11	79.89	IKK-JVL-SPNF complex	YES
IKKEPSILON	2602	1468.6	1.77	139.48	IKK-JVl-SPNF complex	YES
JVL	3089.9	1795.9	1.72	159.59	IKK-JVL-SPNF complex. Dynein cargo	YES
NUF	627.5	189.6	3.31	45.08	Dynein adaptor and Rab11 binding. Regulated by IKK. Required to localise Slam	YES
SLAM	886.9	742.3	1.19	56.55	Required for furrow ingression at cellularisation. Localises to metaphase furrows.	YES
HOOK	2808.7	1705.9	1.65	166.43	binds Rab5 and Rab11. Dynein relationship	YES
PIGS	838.1	696.2	1.20	37.52	Plus TIP	YES
CORN	748.9	571.4	1.31	63.67	Apical MT binding	NO
PLP	3369.9	2831.1	1.19	211.89	Centrosomal protein	YES
DNAPOL-EPSILON255	9352.6	4761.8	1.96	474.75	DNA Polymerase complex	NO
DNAPOL-EPSILON58	2044.1	1186.6	1.72	96.92		NO
CG12702	3473.9	1717.7	2.02	252.08	Homologue CIP2A (Cancerous inhibitor of Protein Phosphatase)	NO
TORSIN	1597.5	1104.9	1.45	64.29	AAA-ATPase implicated in export of large RNPs through nuclear membrane	
CATHD	1610.5	1135.4	1.42	70.13	involved in apoptosis and defense response to Gram-negative bacteria	
CG4572	1099.2	782.9	1.40	56.99	carboxypeptidase vitellogenic-like protein	
CG9547	477.4	384.5	1.24	50.05	Glutaryl-CoA dehydrogenase	

Many of these protins on the top 30 (Table 4.7) corresponded to proteins that were also in our Top 100 EB1 mitotic interactor list, including Dynein/Dynactin, RZZ, SPNF-JVL-IKK-ε and HOOK. However, there were a number of other proteins of lower abundance that, nonetheless, increased their association with EB1 specifically in mitotic/MG-132 treated embryo extracts. Subsequently, I briefly describe what is known of the proteins in the Table 4.7 that have not yet been considered in Section 4.3.

4.4.1 Known MT interacting proteins

NUF-SLAM complex

Nuclear fallout (NUF)-Slow as molasses (SLAM) (Table 4.7, grey): Nuclear fallout (Nuf) is a dynein adaptor that binds to Rab11. It binds to IKK-ε , which by interaction with HOOK is involved in the regulation of cytoskeletal organisation, cell elongation and endosome trafficking (Otani et al. 2011). During mitosis, the metaphase furrows (the transient invaginations of the plasma membrane) extend internally in the embryo to keep adjacent mitotic spindles separated (Acharya et al. 2014). During cell division, SLAM is localised to the metaphase furrows and interacts with NUF to form a complex involved in the regulation of furrow invagination, recycling endosomes needed for furrow invagination (Acharya et al. 2014; Otani et al. 2011).

PIGS

Pickled eggs (PIGS) (Table 4.7, pink): PIGS is sole the *Drosophila* orthologue of human Gas2-like proteins (See SHOT, Page 94). I have identified PIGS as an EB1 binding protein with two SxIP motifs at C-terminus (Table 4.4), which is consistent with its mammalian orthologues (Pines et al. 2010). Biochemical studies and live imaging analysis revealed that Gas2 family contains two SxIP motifs at their C-terminus responsible for interactions with MT plus-end binding proteins and are involved in regulating actin-MT cross-linking (Nazgiewicz

et al. 2019; Stroud et al. 2014; Wolter et al. 2012). Gas2-like proteins are involved in different functions, for example, GAS2L3 is expressed in G_2 and mitosis (Stopp et al. 2017; Wolter et al. 2012). PIGS is implicated in specific functions in cardiomyocyte proliferation and cytokinesis during heart development. These results were obtained by GAS2L3 depletion through RNAi knowkdown, which led to defects in cardiomyocyte cytokinesis (Gründl et al. 2017; Stopp et al. 2017). The same results were obtained by studies conducted in HeLa cells, which have shown that GAS2L3 is required for correct cytokinesis and the genome stability (Wolter et al. 2012). Further studies carried out by Pines et al. (2010) using *pigs* mutant flies concluded that ≈ 17% of them died before reaching adulthood, and these authors demonstrated that the remaing adults showed degeneration of flight muscles which impaired their ability to fly. Additionally, the females were sterile due to the disruption of ovarian morphology.

PIGS is also implicated in Notch signaling. Unbound Notch is a transmembrane receptor that interacts with ligands, this interaction cleaves and releases the Notch intracellular domain, which migrates to the nucleus to modulate transcription complexes that contains the DNA-binding protein (For review see Kopan 2012). This Notch pathway is implicated in cell proliferation, differentiation, cell fate and apoptosis (Grotek et al. 2013; Kopan 2012).

CORN

Cornetto (CORN) (Table 4.7, light orange): During the cell cycle, all apical proteins are localised at the cell cortex from late interphase to metaphase, but they disappear in anaphase (Bulgheresi et al. 2001). CORN is an apical MT binding protein that colocalises with MTs during metaphase and is localised apically between anaphase and telophase (Bulgheresi et al. 2001; Finan et al. 2011). Inscuteable is an apical protein that colocalises at the cell cortex and modulates mitotic spindle orientation along the apical-basal axis in mitotic neuroblasts(Kraut et al. 1996). Studies conducted by Bulgheresi et al. (2001) using yeast

two-hybrid system, have shown that CORN interacts with inscuteable. However, these two proteins were not co-immunoprecipitated by the same authors from *Drosophila* embryonic extracts, thus interactions were suggested to be transient *in vivo.* Further investigations carried out in *Drosophila* embryos have shown that CORN binds to myosin VI via its C-terminus, which is a minus end-directed actin-based motor protein involved in many processes, these include regulation of cargo transport, slide actin filament (Arden et al. 2007; Bulgheresi et al. 2001; Cramer 2000; Finan et al. 2011; Hasson 2003).

Table 4.8: **Top 30 EB1 interactors in mitosis.** The table summarises MT binding proteins or complexes with relationships with EB1 and/or MT functions within Top 30 in mitosis (Table 4.7), but not identified within Top 100 EB1 interacting proteins (Table 4.1).

Known MT interacting proteins and complexes	Known interactors and functions
NUF-SLAM	Nuclear fallout (NUF) and slow as molasses (SLAM) interact with dynein and SPNF-JVL-IK2 complex to regulate endosome trafficking (Otani et al. 2011) needed for invagination furrows and cellularisation (Acharya et al. 2014; Otani et al. 2011).
PIGS	Pickled eggs (PIGS) is a spectraplakin Gas2-like protein involved in regulating actin-MT cross-linking for modulation of cytoskeletal dynamics (Reviewed by Nazgiewicz et al. 2019; Stroud et al. 2014; Voelzmann et al. 2017) and cytokinesis (Gründl et al. 2017; Stopp et al. 2017).
CORN	Cornetto (CORN) is an apical MT binding protein (Bulgheresi et al. 2001; Finan et al. 2011) and together with inscuteable and Myosin VI is involved in regulation of cargo transport (Arden et al. 2007; Bulgheresi et al. 2001; Cramer 2000; Finan et al. 2011; Hasson 2003) and mitotic spindle orientation (Kraut et al. 1996).

4.4.2   Proteins with no known MT or EB1 relationship

DNApol-ε complex

DNA polymerase epsilon 58 and 255(Table 4.7, blue): DNA polymerase epsilon (DNApol-ε) plays a key role in DNA replication and repair in eukaryotic cells (Oshige et al. 2000; Sahashi et al. 2013). It is a heterotretameric enzyme in most species, comprising a catalytic subunit A (≈ 250 kD), a subunit B (≈ 60 kD, but in budding yeast is ≈ 80 kD) and two similar subunits (≈ 20 kD) (Sahashi et al. 2013). However, in *Drosophila* DNApol-ε complex exists in two subunits: a catalytic subunit of ≈ 255 kD and a subunit of ≈ 58 kD (Oshige et al. 2000).

CG12702

The *Drosophila CG12702 (Table 4.7, dark green):* this protein is uncharacterised and is orthologous to the human cancerous inhibitor of protein phosphatase 2A (CIP2A) which is found highly concentrated in most types of human cancer (Jeong et al. 2014). CIP2A inhibits the protein phosphatase 2A (PP2A) and causes the stabilisation of the oncogenic transcription factor c-Myc, resulting in cancer cells (Jeong et al. 2014; Kim et al. 2013). However, this role is related to its overexpression, but in normal conditions, CIP2A plays roles in regulating centrosome segregation (Jeong et al. 2014) and mitotic spindle functions in cell-cycle progression (Golsteyn et al. 1995; Kim et al. 2013).

Torsin

Torsin: Torsins are the only proteins of the AAA+ATPase family and they are localised to the ER and perinuclear space (Laudermilch and Schlieker 2016; Luithle et al. 2020). In vertebrates, these proteins are encoded by four paralogous genes – *TOR1A, TOR1B, TOR2A,* and *TOR3A;* by contrast in *Drosophila* only one gene *dtorsin* on X chromosome encodes the Dtorsin protein (Reviewed by Wakabayashi-Ito et al. 2011). Among these family members, TorsinA encoded by *TOR1A* is the most studied and its defect is responsable for hereditary dystonia (Laudermilch and Schlieker 2016; Wakabayashi-Ito et al. 2011).

The nuclear envelope is formed by a double membrane – the inner and the outer membranes (Hetzer 2010). The inner nuclear membrane contains many proteins that link to nuclear lamins and chromatin, thus they are invovled in chromatin organisation and gene regulation (Hetzer 2010; Luithle et al. 2020). During prophase, interactions between inner nuclear membrane proteins, nuclear lamins and chromatin are broken, allowing the membrane separation from chromatin and enclosing inner nuclear membrane proteins into the mitotic ER network (For review see Luithle et al. 2020). Recent studies have shown that TorsinA requires cofactors – lamina-associated polypeptide 1 (LAP1) and lumi-

nal domain like LAP1 (LULL1) (Chase et al. 2017; Laudermilch and Schlieker 2016) and *LAP1* or *Torsin1A* mutation causes cytokinesis defects, mitotic chromosome organisation and segregation defects due to the failure in membrane removal from chromatin (Luithle et al. 2020).

Currently there are no studies that report the interactions between Torsin proteins and EB1 or MTs, but I have identified it as an EB1 interactor. I have also identified several proteins of the nuclear membrane, such as nucleoporines. Considering that this protein is localised to the ER and continuous perinuclear space, and due to its crucial role in mantaining the integrity of genome and chromsome regulation, it is consistent to be identified also as an EB1 interacting protein.

CATH-D

CATH-D: the cathpsin D (CATH-D) is a lysosomal enzyme that degrades different substrates in acidic compartments, thus regulating different physiological and pathological processes (For review see Wang et al. 2021). However, CATH-D plays also important functions outside acidic compartments (lysosomes), in regulating different cellular processes. These include apoptosis, cell division, defense response against Gram-negative bacteria, cell motility and proliferation through interaction with actin-based cellular activities (Platet et al. 1996; Wang et al. 2021). Moreover, CATH-D is involved in mitosis and cytokinesis through its cofilin phosphatase activity, which plays a key role in modulating mitosis and CATH-D mutation leads to actin organisation defects and cytokinesis failure (Bach et al. 2015; Wang et al. 2021). CATH-D is overexpressed in breast cancer cells and helps tumor growth and formation of metastasis. Furthermore, in the nucleus of breast cancer cells, CATH-D associates with chromatin and interacts with TRPS1 (tricho-rhinophalangeal-syndrome 1) which is a gene involved in carcinogenesis. Consequently, the activity of TRPS1 is enhanced by interaction with CATH-D (Bach et al. 2015), thus, CATH-D has been suggested as a target

in cancer by inhibiting binding protein activity and/or proteolytic activities. Finally, CATH-D should be also considered as biomarker for diagnosis, in which high concentration is correlated with poor prognosis (Masson et al. 2010; Wang et al. 2021).

CG4572

CG4572: is orthologous to human carboxypeptidase vitellogenic like (CPVL). CPVL is a serine carboxypeptidase that cleaves one amino acid from the C-terminus of proteins or peptides (Mahoney et al. 2001; Skidgel and Erdös 1998). Carboxypeptidases are classified on the basis of their active site mechanism into three principal groups – cysteine, metallo and serine carboxypeptidases, and among them the serine carboxpeptidase is the most studied and was first discovered in human macrophages, in which is localised to the endoplasmic reticulum and membrane ruffles (Harris et al. 2006; Skidgel and Erdös 1998). Initial investigations suggested that CPVL functions are largely confined to the monocytic lineage (For review see Harris et al. 2006), however, recent studies indicated that CPVL mRNA is also highly expressed in heart and kidney, which sugggest that this protein may have additional important roles outside the immune system (Mahoney et al. 2001). In addition, CPVL may have a role in some cancers and has shown to interacts with BTK/p300 axis to inhibit STAT1 pathway which leads to promotion of glioma progression (Yang et al. 2021). Finally, there is also indication of CPVL interacting with CATH-D (Harris et al. 2006).

CG9547

CG9547: The orthologous human glutaryl-CoA dehydrogenase (GCDH) is implicated in degradation of lysine, tryptophan and hydroxylysine. GCDH mutations lead to their accumulation in body fluids and high excretion of 3-hydroxyglutaric acid and glutaric acid, which is a condition known as glutaric aciduria type 1 (GA1) (Külkens et al. 2005; McClelland et al. 2007).

I was not able to find a paper that reports a relationship between CG9547 or GCDH and mitosis, however the vast majority of EB1 interacting proteins identified with proteomics approach plays roles in mitosis, therefore I suggest also that this protein in addition to its traditional implication in metabolism, may also play a role in cell division.

Table 4.9: **Top 30 EB1 interactors in mitosis.** The table summarises proteins and complexes identified as EB1 binding proteins within top 30 in mitosis. However, they are not known previously to be as MT associated proteins or EB1 interactors.

Proteins and complexes with no known MT or EB1 relationship	Known interactors and functions
DNApol-ε 58 and 255	DNA polymerase epsilon 58 and 255 are involved in DNA replication and repair (Oshige et al. 2000; Sahashi et al. 2013). However, the complex is not known as MT or EB1 binding proteins.
CG12702	CG12702 is an uncharacterised and unexplored protein. However, its orthologous human cancerous inhibitor of protein phosphatase 2A (CIP2A) promotes different types of human cancer (Jeong et al. 2014) and regulation of centrosome segregation and mitotic spindle functions (Golsteyn et al. 1995; Jeong et al. 2014; Kim et al. 2013).
TORSIN	This protein is implicated in removing nuclear membranes from chromatin upon nuclear envelope breakdown and enclosing them into the mitotic ER network (Reviewed by Luithle et al. 2020). However, the protein is not known as MT or EB1 interactor.
CATH-D	cathpsin D (CATH-D) is a lysosomal protease (Reviewed by Wang et al. 2021). Moreover, the protein plays different other functions, including apoptosis and cell division regulation (Platet et al. 1996; Wang et al. 2021).
CG4572	CG4572 is other protein that still needs its characterisation. The human carboxypeptidase vitellogenic like (CPVL) is a protease (Mahoney et al. 2001; Skidgel and Erdös 1998) and may play also a role in cancer progression (Yang et al. 2021).
CG9547	This protein is not characterised and the orthologous human glutaryl-CoA dehydrogenase (GCDH) is implicated in degradation of some amino acids, such as, lysine, tryptophan and hydroxylysine (Külkens et al. 2005; McClelland et al. 2007).

4.4.3 The rationale for further investigation into the mitotic EB1 interactome

Based on the comprehensive Flybase data mining and analysis, I decided to focus my further studies on a subset of those proteins that are enriched > 1.2 fold in the mitotic EB1 interactome (Table 4.7). Given the well-characterised role of EB1 in interacting with Dynein/Dynactin complex (Berrueta et al. 1999; Watson and Stephens 2006) and the interaction of this complex with kinetochore-associated RZZ complex in metaphase to promote the onset of the anaphase (Gama et al. 2017; Mosalaganti et al. 2017), I decided to focus my studies first on

the proteins that constitute the SPN-F, IKK, JVL complex, as well as SLAM-NUF, and the HOOK and PIGS proteins. All had available lines that express GFP/RFP-fusions, allowing me to take both a biochemical, reciprocal IP approach and a cell biological approach (the rest of this Chapter). Concurrently, I sought to engineer flies that could express GFP-fusions to some of the 30 proteins for which there were not available lines (CG12702, DNApol-ε 58, CORN) (Chapter 5).

4.5 Dynamic localisation and protein-protein interaction network of SPN-F in early embryos

To determine the localisation and identification of SPN-F binding proteins, I crossed female virgins of flies of genotype UASp-GFP-SPN-F to matαt-GAL4 males (Table 2.2) for early embryo collection and subsequent live imaging analysis. Previous studies using GFP-SPN-F have been conducted in *Drosophila* germline and bristles, which illustrated that SPN-F localised to MT minus ends through interaction with cut up (CTP). Thus, the protein stabilises the connection between MT minus ends and actin cytoskeleton (See SPNF-JVL-IK2 complex, Page 93). To date, no physical interaction between SPN-F and EB1 has been reported.

4.5.1 Mitotic Localisation of GFP-SPN-F

To investigate the dynamic localisation of GFP-SPN-F in early embryos, I imaged 1–2 hr old embryos laid by $w; \frac{K2}{+}; \frac{GFP-SPN-F}{mat\alpha t-GAL4}$ and $w; \frac{+}{Cyo}; \frac{GFP-SPN-F}{mat\alpha t-GAL4}$ mothers using spinning disc confocal microscopy. Embryos were imaged every 5 seconds across 5 x 1 μm z planes. Image sets were analysed using ImageJ, as maximum intensity projections. 11 movies were taken and after analysis, all of them showed similar dynamic localisation. As shown in Figure 4.3, during nuclear envelope breakdown, SPN-F is found concentrated at the centrosomes and also in high-intensity spots throughout the embryo (these spots appear randomly positioned and quite immobile over the course of a movie and likely reflect in-

soluble, non-functional GFP-SPN-F aggregates). Upon nuclear envelope break-down, SPN-F becomes less intense on centrosomes, accumulating in the region of the mitotic spindle. However, the localisation does not appear to exactly re-flect the entire mitotic spindle, instead appearing more "rounded" in the region of the nuclear space. The intensity of astral MT localisation in relation to other MT populations appears to increase in anaphase, such that a "cloud" of GFP is more visible than the central spindle region. Post-telophase, as nuclei reform, SPN-F intensity increases at the centrosomes.

(a) **NEB.**   (b) **Metaphase.**   (c) **Met-Anaphase.**   (d) **Mid-Anaphase.**

(e) **Telophase.**   (f) **Early interphase.**   (g) **Late interphase.**   (h) **NEB.**
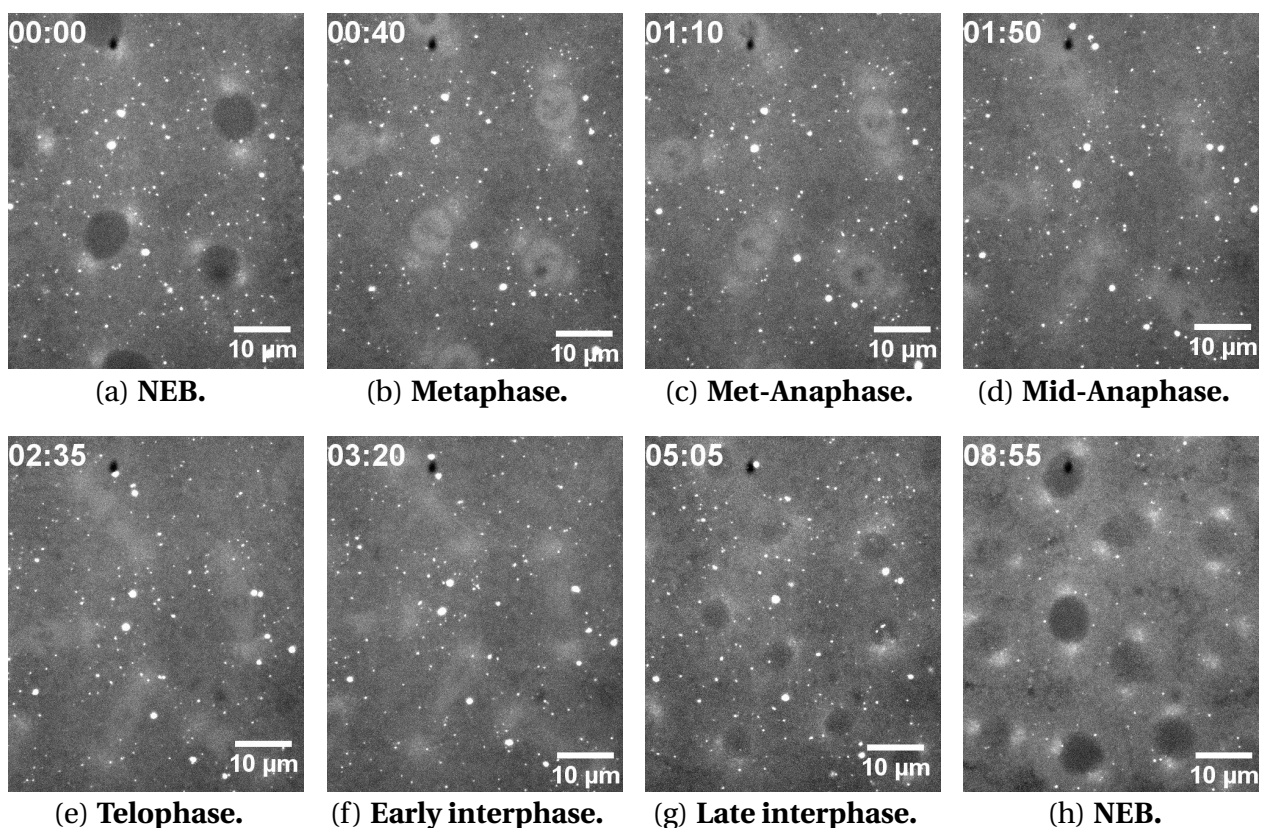
Figure 4.3: **Dynamic localisation of GFP-SPN-F in the early *Drosophila* embryo.** 11 movies were taken and analysed. All movies showed similar dynamic localisation, as shown in this Figure, during nuclear envelope break-down (NEB), SPN-F is concentrated to the centrosomes. Upon NEB, the protein is also localised in the region of the mitotic spindle, then decreases from centrosomes and mitotic spindle region between metaphase-anaphase transi-tiom (Met-Anaphase) and early interphase. During late interphase the protein restarts accumulating to the centrosomes for the following cycle.

4.5.2 Identification of the SPN-F mitotic interactome

In order to characterise the SPN-F mitotic interactome, I undertook a GFP-TRAP-A purification, using $\approx$ 0.4 g of 0–3 hr MG-132 arrested GFP-SPN-F expressing embryos followed by LC-MS/MS analysis. The associated Western blot is shown in Figure 4.4, demonstrating the presence of a GFP-positive band at the expected molecular weight, its presence in the GFP-TRAP-A pellet and its complete depletion in the extracts.
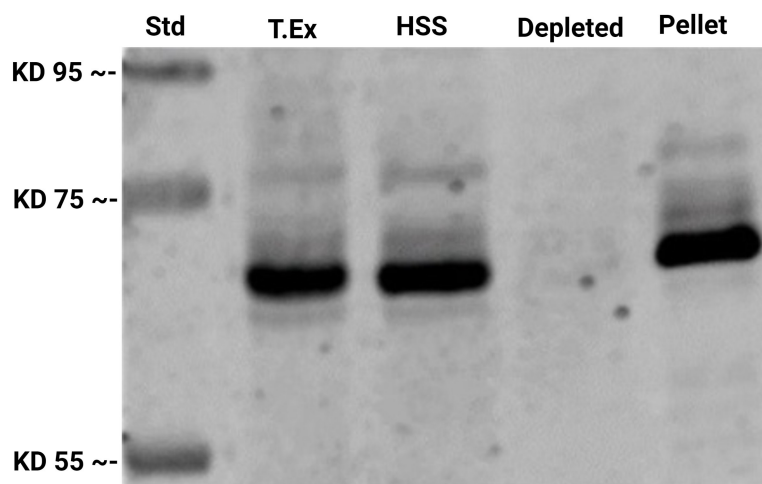
Figure 4.4: **Western blot of GFP-SPN-F IP.** The assay indicates that the GFP-SPN-F has been isolated due to the presence of GFP-positive band at the expected molecular weight (MW) $\approx$ 68 kD.

Following MS, the identified protein IDs were subjected to the WakefieldLab standard bioinformatics (Chapter 2). Briefly, any protein IDs that do not meet minimum criteria (score of > 30, ID with 3 or more associated peptides, > 10% coverage) were discarded. The remaining IDs were compared with our standard false positive database. Proteins that were < 2 fold enriched in the IP, in relation to the false positives were also discarded. All remaining protein IDs were sorted by mean abundance and those proteins with an Area/Abundance of 1.3E7 and more were retained in the list. This bioinformatics pipeline resulted in the identification of 50 proteins (Table 4.10). SPN-F has the highest area (1.78 E10), as expected, confirming the Western blot (Figure 4.4).

Table 4.10: **SPN-F interactors.** The table illustrates SPN-F interacting proteins in metaphase and ordered by area.

Name	Accession	Coverage	# Unique Peptides	# AAs	MW [kDa]	Score	Area
spn-F	FBpp0085122	90.11	44	364	40.9	4267.81	1.776E10
Ubi-p63E	FBpp0073034	88.86	12	763	85.7	488.95	8.251E9
IK2	FBpp0080919	73.70	60	711	81.0	2397.24	6.198E9
ctp*	FBpp0070672	65.17	9	89	10.4	407.78	2.268E9
CG7546	FBpp0293610	61.25	44	1298	138.0	481.84	3.347E8
Droj2	FBpp0082219	62.03	20	403	45.2	211.11	2.541E8
CG9853	FBpp0078589	59.88	19	339	38.5	190.71	2.293E8
cathD	FBpp0087972	45.15	12	392	42.4	114.88	1.692E8
Uba5	FBpp0073354	67.33	16	404	44.1	131.17	1.654E8
mtSSB	FBpp0082729	63.01	11	146	16.4	80.35	1.561E8
RanBPM	FBpp0087357	56.52	23	598	66.4	193.88	1.186E8
DnaJ-1	FBpp0076830	48.20	14	334	37.0	101.41	1.145E8
Set	FBpp0082521	33.46	5	269	31.0	62.09	1.056E8
Cp1	FBpp0086717	43.11	13	341	37.9	99.98	8.621E7
CG12264	FBpp0079874	49.78	20	462	51.0	159.71	8.083E7
CG7215	FBpp0099676	69.23	7	130	14.7	61.74	7.731E7
hook	FBpp0080722	46.98	27	679	76.6	153.52	7.485E7
jvl	FBpp0296974	32.84	25	1151	122.3	182.15	6.504E7
CG11982	FBpp0081445	36.84	11	380	40.3	89.73	6.127E7
r	FBpp0088675	45.55	71	2224	246.5	375.50	5.869E7
CG6617	FBpp0074386	60.44	10	225	26.0	64.92	5.584E7
CG8036	FBpp0081372	50.00	21	580	63.0	90.59	4.488E7
Zw10	FBpp0070425	36.06	23	721	82.2	106.58	4.479E7
muskelin	FBpp0086998	36.93	21	853	97.4	140.96	4.426E7
DNApol-delta	FBpp0075277	37.36	38	1092	124.8	140.83	4.274E7
GCS2alpha	FBpp0070057	47.84	29	924	105.7	151.26	3.906E7
Torsin	FBpp0070658	39.12	10	340	38.1	51.25	3.903E7
Smn1	FBpp0302038	37.90	26	1008	111.7	132.61	3.843E7
Klp10A	FBpp0073331	32.17	17	805	88.6	70.37	3.694E7
atms	FBpp0078508	29.74	12	538	60.8	60.16	3.354E7
Klp61F	FBpp0072616	27.20	20	1066	121.1	88.43	2.920E7
GCS2beta	FBpp0080551	22.08	12	548	61.5	64.79	2.856E10
GCC185	FBpp0112136	32.42	29	1135	130.0	107.45	2.847E7
Zwilch	FBpp0085138	33.39	17	641	72.4	74.49	2.702E7
CG31357	FBpp0084110	51.78	16	394	45.3	81.20	2.565E7
CG8184	FBpp0073898	13.00	52	5146	556.5	200.21	2.274E7
HDAC6	FBpp0298373	19.18	15	1022	113.3	69.26	2.177E7
Ranbp16	FBpp0292662	18.66	19	1077	123.1	50.95	2.089E7
CG3295	FBpp0071476	41.44	15	432	49.2	67.79	2.077E7
betaCOP	FBpp0074348	27.49	18	964	107.3	109.68	1.970E7
Sherpa	FBpp0072563	31.66	28	1058	118.9	75.64	1.797E7
hyd	FBpp0081568	16.85	35	2885	318.7	145.94	1.760E7
CG7611	FBpp0078015	36.51	15	630	69.6	72.47	1.660E7
wech	FBpp0289357	22.48	14	832	90.5	57.38	1.610E7
lok	FBpp0080861	32.46	10	459	52.3	55.75	1.592E7
lds	FBpp0081255	23.19	21	1061	118.3	52.16	1.531E7
ref(2)P	FBpp0080794	25.04	10	599	65.3	66.93	1.506E7
DNApol-epsilon255	FBpp0083800	17.44	28	2236	256.5	81.31	1.315E7
rod	FBpp0085156	12.64	23	2089	239.5	83.32	1.311E7
CG12512	FBpp0078711	33.90	14	593	65.2	63.78	1.308E7

Of the remaining 49, 38 were not in our false positive list, while the other 11 were > 2 fold enriched in comparison to our false positive database. The interactors included others already described in our EB1-GFP mitotic interactor list – for example, IK2, JVL, ZW10.

To further understand the functional relationships between SPN-F and its mitotic interactors, I took the 50 proteins and subjected them to GO enrichment analysis (Table 4.11). 4 functional cellular component terms were identified – the RZZ complex, the GID complex, mitotic spindle pole and ER membrane insertion complex. To aid visualisation, the protein-protein interaction software package, Cytoscape was again used. The network constituted the SPN-F interacting proteins within the GO-enriched cellular components terms, along with SPN-F interacting proteins already identified as enriched EB1-GFP interacting proteins, where the size of the nodes (Figure 4.5) corresponds to the abundance of the protein identified in the SPN-F IP. To visually compare my experiment with the known protein-protein interaction data, I added any interactions already present in the biological general repository for interation datasets TheBioGrid database (`https://thebiogrid.org`) (Figure 4.5).

Table 4.11: **SPN-F GO Enrichment Analysis.** This analysis shows SPN-F interactors of cellular compoenents that were identified via SPN-F immunoprecipitation with high fold enrichment. Cellular components describe intracellular structures and macromolecular complexes to annotate cellular localisations of proteins (Roncaglia et al. 2013).

GO cellular component complete	Reference List (13811)	SPN-F IP	Expected	Fold Enrichment	P-value	FDR	Proteins
RZZ complex (GO:1990423)	3	3	0.01	> 100	8.24E-07	1.84E-04	Rod, Zw10, Zwilch
GID complex (GO:0034657)	6	5	0.02	> 100	2.04E-10	2.73E-07	CG31357, RanBPM, CG3295, Muskelin, CG7611
mitotic spindle pole (GO:0097431)	3	2	0.01	> 100	1.22E-04	1.17E-02	Klp10A, Klp61F
ER membrane insertion complex (GO:0072379)	3	2	0.01	> 100	1.22E-04	1.09E-02	CG7546, CG9853
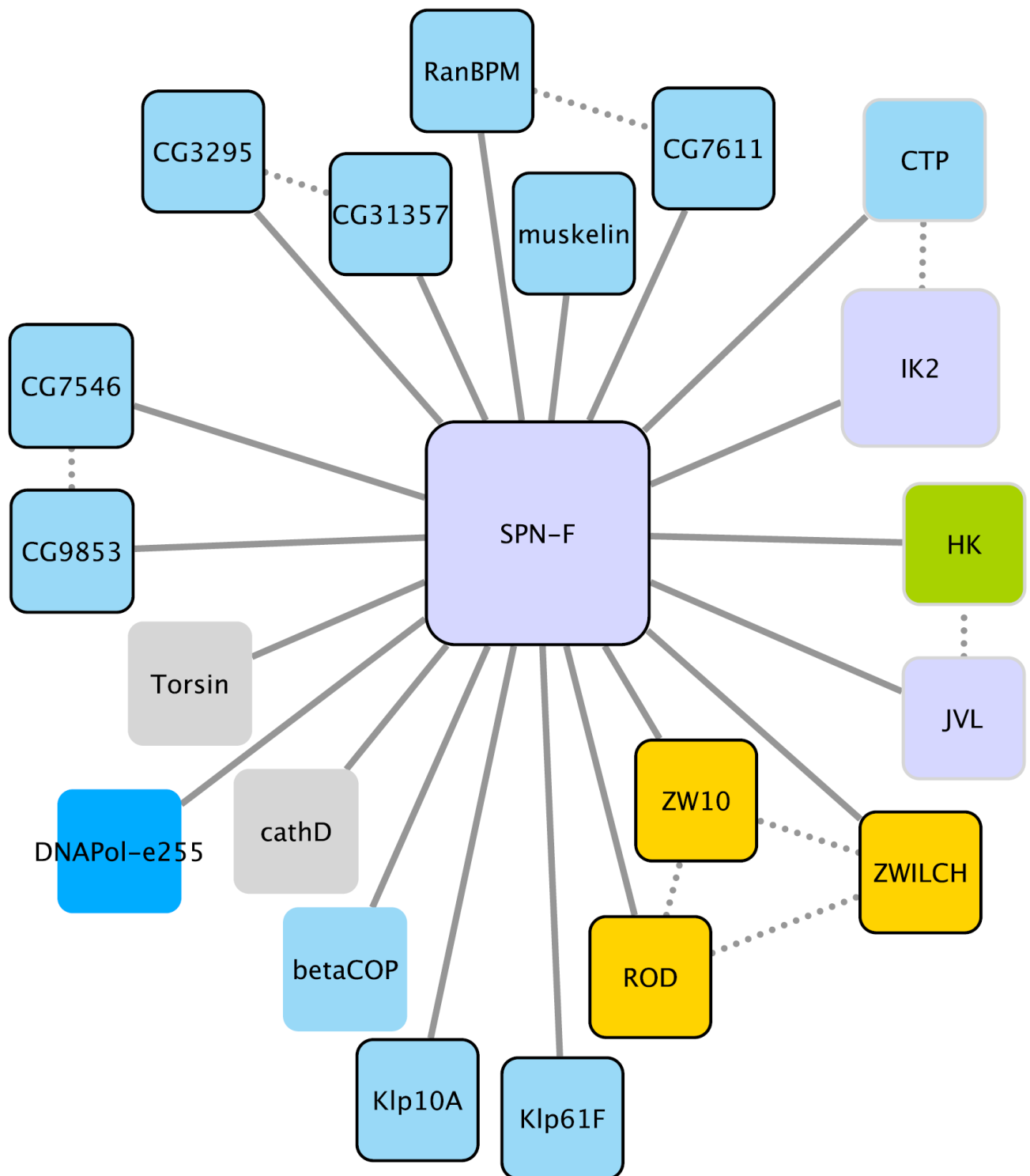
Figure 4.5: **SPN-F interactors in metaphase.** The figure shows SPN-F PPI after BioGrid Analysis for visualising interaction networks. Interactions identified in this experiment are indicated by solid lines and interactions from BioGrid database are shown with dotted lines.

4.5.3 SPN-F interacting proteins

To have the final SPN-F interacting proteins in metaphase (Figure 4.5), in addition to SPN-F binding proteins within GO-enriched cellular components terms (Table, 4.11), I manually chose SPN-F interactors in metaphase from Table 4.10 that were already identified either as EB1 interacting proteins with a final cut-off of 1.2 fold increase in mitosis (Section 4.4 and Table 4.7) or EB1 interacting proteins within GO term enrichment cellular components (Table 4.2). As shown in the Figure 4.5, this analysis demonstrates the presence of the full SPNF-JVL-IKK-ε complex in the GFP-SPN-F mitotic IP. It also shows the presence of the full RZZ complex. The GO analysis also identified a further complex – the GID complex. Glucose induced deficient (GID) complex is composed of seven subunits involved in polyubiquitination and elemination of fructose-1,6-bisphosphatase, which is a key to switch from gluconeogenesis to glycolysis (Menssen et al. 2012; Santt et al. 2008). In addition to regulation of glucose metabolism, this ubiquitin ligase complex is involved in different functions in vertebrates, which includes regulation of the cell cycle, energy homeostasis and primary cilia function (Santt et al. 2008). Other proteins of interest included the +TIP protein HOOK, and the DNAPol epsilon complex component DNApol-ε 255. The IP also possessed CTP, which is the *Drosophila* dynein light chain 8 (DLC8). DLC8 is present in the original EB1-GFP mitotic interactome, but was not within the Top 100 proteins; as such it appears in the Cytoscape network in Figure 4.5. Interestingly, EB1 was not identified as an enriched interactor of SPN-F, despite it being the protein which identified SPN-F in the original TMT analysis (See Discussion 4.13 for a full explanation of why this might be).

4.5.4 General description of some SPN-F binding proteins

CTLH E3 ligase complex

Table 4.12: **CTLH E3 ligase complex.** This table shows subunits of CTLH E ligase complex identified as SPN-F interactors in the project. This identification, strongly suggest that the whole complex interacts with SPN-F in metaphase.

Subunits of the CTLH E3 ligase complex
CG3295
CG31357
CG7611
Muskelin
RanBPM

CTLH E3 ligase complex (Table 4.12): This complex is required for degradation of ME31B, Cup and TRAL proteins during the maternal-to-zygotic transition (Cao et al. 2020; Zavortink et al. 2020). Before the onset of zygotic transcription, embryogenesis is ensured by maternally loaded proteins and mRNAs, therefore during the maternal-to-zygotic transition (MTZ), genetic regulation is transferred from these maternally deposited genes products to freshly made zygotic ones. Thus, this transfer requires the destruction of maternal transcripts and activation of zygotic transcriptions (For review see Cao et al. 2020; Zavortink et al. 2020). Recent studies have revealed that three RNA-binding proteins: ME31B, Cup and TRAL play key roles in oogenesis and embryogenesis (Zavortink et al. 2020), thus during MTZ are degradated by the ubiquitin-proteosome system. The CTLH E3 ligase complex is implicated in this biological process. The Ran-binding protein M (RanBPM, also known as RanBP9) is localised both in nucleus and cytoplasm, and in addition to its traditional role in the ubiquitin-proteosome system, may play other different functions, including regulation of apoptosis, cell adhesion, transcription, morphology and cell migration (For review see Salemi et al. 2017).

Transmembrane domain recognition complex (TRC)

Transmembrane domain recognition complex: The *Drosophila* CG7546 and CG9853 are orthologous to human Bag6 and Get4 respectively and, together with GET5, form the transmembrane domain recognition complex (TRC) in which SGT is also probably implicated (Krenciute et al. 2013; Simpson et al. 2010). The TRC complex is localised ubiquitously in the cytoplasm, the nucleus and at the membranes of the ER (Krenciute et al. 2013; Xu et al. 2013). This complex is implicated in the ubiquitin-proteosome system, in the delivery of tail-anchored proteins to the ER, in mediating DNA injury signaling and in apoptosis (Krenciute et al. 2013; Suloway et al. 2010; Tambe et al. 2020; Xu et al. 2013).

Coatomer complex

betaCOP: Coat protein (coatomer) β (βCOP) is one of seven subunits that form coat protein complex which comprises four classes – Clathrin and its adaptor proteins, the adaptor-related AP-3 complex, COPI and COPII (Kreis et al. 1995). This complex is localised at the cytoplasm and is made of seven different subunits – α-,β-, β'-, δ-, ε-, ξ- and ζ-COP (Stenbeck et al. 1993). The coatomer complex is implicated in regulation of vesicle trafficking in eukaryotes (Kreis et al. 1995; Kuge et al. 1993; Peter et al. 1993; Stenbeck et al. 1993). *AP complex:* Adaptor protein (AP) complexes are heterotetrameric protein complexes which include AP-1, AP-2 and AP-3 clathrin-associated complexes and further AP-4 and AP-5 which are not clathrin-associated protein complexes (Nakatsu and Ohno 2003; Park and Guo 2014). These complexes, which include AP-1-2beta and AP-1gamma are involved in vesicle trafficking containing different proteins, such as, receptors, adhesion proteins, and viral molecules (For review see Park and Guo 2014).

KLP10A and KLP61F

KLP10A and KLP61F: These subunits belong to kinesin superfamily proteins (KIFs) which are implicated in transporting vesicles, mRNAs and protein complexes to specific destinations using MTs as tracks and ATP as an energy source (Hirokawa 1996; Nakagawa et al. 2000; Schwimmer et al. 2004). In addition, these proteins also play roles in chromosome rearrengement and spindle assembly during mitosis and meiosis (Schwimmer et al. 2004).

The Kinesin-like protein at 10A (KLP10A) is the kinesin-13 family of MT depolymerase and shows a dynamic localisation during the cell cycle. Between interphase and prophase it is concentrated on MT plus ends, upon NEB relocalises to centrosomes and mitotic spindles where remains throughout anaphase, to promote depolymerisation, thereby chromosomes segregation, MT and centriole lengths (Delgehyr et al. 2012; Schwimmer et al. 2004). Previous studies suggested that KLP10A is carried on MT plus ends by EB1 (Goshima and Vale 2005), but my data from EB1 AP-MS do not show this protein as EB1 interactor.

Kinesin-like protein at 61F (KLP61F) is the MT polymerase of the kinesin-5 family of cytoskeletal motor proteins and is localised to spindle MTs during cell division (Chen and Hancock 2015; Ferenz et al. 2010). This protein is implicated in crosslinking and sliding apart antiparallel MTs, which is vital for mitosis. KLP61F further contributes to the establishment and maintenance of bipolar spindles (For review see Ferenz et al. 2010).

CTP

CTP: Cut up (CTP) is the smallest subunit of the dynein motor complex (See Dynein/Dynactin complex, Page 88) and also know as dynein light chain 8 (DLC8). CTP was shown to interact with SPN-F to localise SPN-F to MT minus ends in the oocyte (Abdu et al. 2006). This protein exists as homodimer which interacts with several partners in diverse biological processes and acts as a cargo adaptor in the transport of various vesicles (For review see Barve et al. 2006; Mohan and Hosur 2008).

Table 4.13: **SPN-F interacting proteins in metaphase.** The table summarises mitotic SPN-F binding proteins (Figure 4.5).

Proteins and complexes	Known interactors and functions
CTLH E3 ligase complex	This complex is formed by at least 5 subunits (Table 4.12) and mediates the proteolysis of ME31B, Cup and TRAL proteins during maternal-to-zygotic transition (MTZ) during oogenesis and embryogenesis (Cao et al. 2020; Zavortink et al. 2020).
Transmembrane domain recognition complex (TRC)	This complex is constituted by CG7546, CG9853 (GET4), GET5, CG7546 (GET6). The complex is involved in proteolitc process, delivery proteins to ER, DNA damage signalling and apoptosis (Krenciute et al. 2013; Lu et al. 2007; Simpson et al. 2010).
Coatomer complex	The complex is formed by various COPI, clathrin and adaptor proteins implicated in regulation of vesicle trafficking in all eukaryotes (Kreis et al. 1995; Kuge et al. 1993; Peter et al. 1993; Stenbeck et al. 1993).
KLP10A and KLP61F	These proteins belong to kinesin superfamily proteins (KIPs) and are motor proteins implicated in transporting various vesicles using MTs as tracks (Hirokawa 1996; Nakagawa et al. 2000; Schwimmer et al. 2004). Moreover, these proteins are involved in chromosome organisation and segregation, spindle assembly and depolymerisation during cell division (Delgehyr et al. 2012; Schwimmer et al. 2004).
Cut up (CTP)	CTP is the subunit of dynein motor protein and acts as a cargo adaptor in the transport of different vesicles (Reviewed by Barve et al. 2006; Mohan and Hosur 2008).

4.6   Dynamic localisation and protein-protein interaction network of IKK-epsilon-GFP in the early embryo

To investigate the localisation and identification of IKK-ε interactors, I crossed female virgins of flies of gentoype UASp-IK2-ε-GFP to matαt-GAL4 males (Table 2.3) for early embryo collection and subsequently live imaging analysis. To date, IKK-ε was investigated in studies involving *Drosophila* germline and bristles, where it is implicated in regulation of interactions between the MT minus ends and actin-rich cortex in the oocyte (Baskar et al. 2019) (See SPNF-JVL-IK2 complex, Page 93), and no interaction between this protein and EB1 has been reported so far.

4.6.1   Mitotic Localisation of IKK-epsilon-GFP

To study the dynamic localisation of IK2-GFP in early embryos, I imaged 1–2 hr old embryos laid by w; $\frac{IK2-GFP}{+}$; $\frac{Pri}{mat\alpha t-GAL4}$ and w; $\frac{IK2-GFP}{+}$; $\frac{TM6B}{mat\alpha t-GAL4}$ females using spinning disc confocal microscopy. Embryos were imaged every 5 seconds across 5 x 1 μm z planes. Image sets were analysed using ImageJ, as maximum intensity projections. 7 movies in total were captured and analysed. All of them have showed similarity in their dynamic localisation. As shown in Figure 4.6, during nuclear envelope breakdown (NEB), IKK-ε is highly concentrated at the centrosomes. Upon NEB, IKK-ε becomes less intense on centrosomes, accumulating in the region of the mitotic spindle. However, the localisation does not appear to be the exact reflection of the entire mitotic spindle, but rounded in the region of the nuclear space. During post-telophase, as nuclei reform, IKK-ε intensity increases at the centrosomes. The localisation of IKK-ε (Figure 4.6) is similar to that of SPN-F (Figure 4.3), reflecting their involvement in the complex .

(a) **NEB.**   (b) **Metaphase.**   (c) **Met-Anaphase.**   (d) **Mid-Anaphase.**

(e) **Telophase.**   (f) **Early interphase.**   (g) **Late interphase.**   (h) **NEB.**
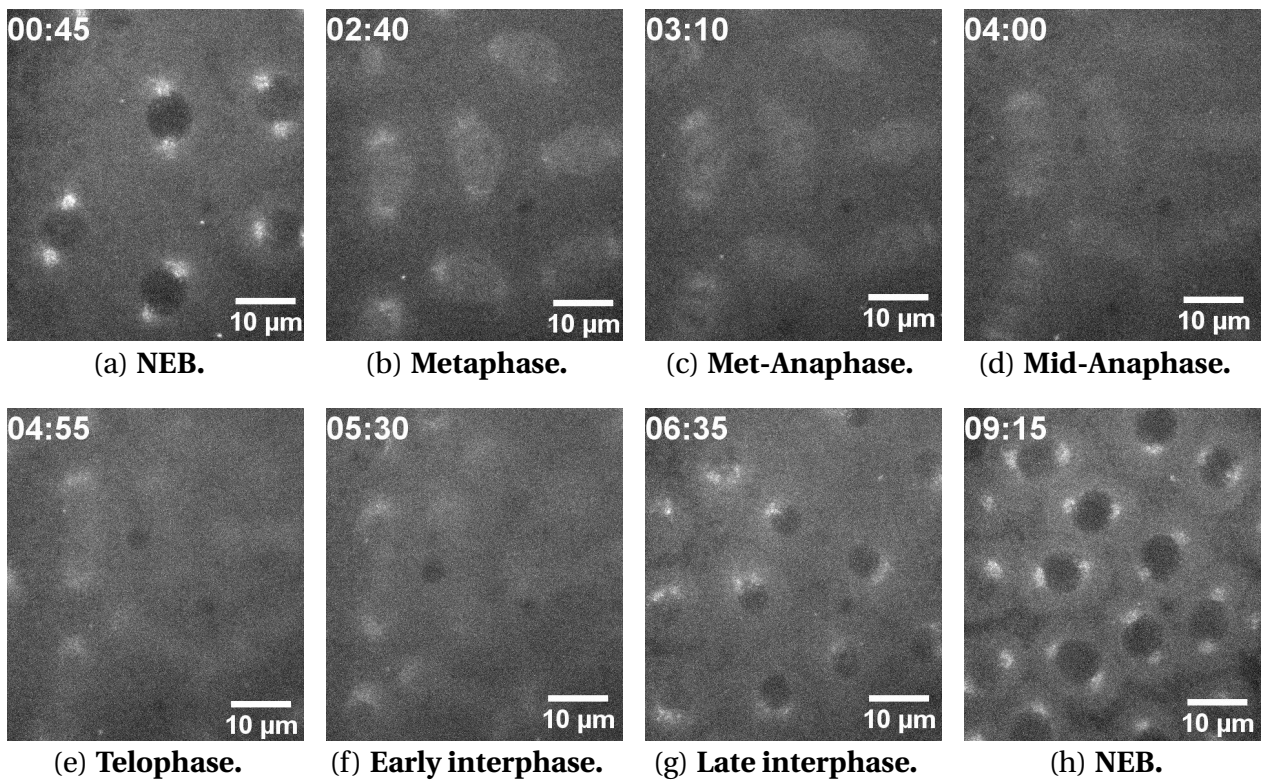
Figure 4.6: **Dynamic localisation of IKK-epsilon-GFP in the early *Drosophila* embryo.** To determine the IKK$-\varepsilon$ localisation, 7 movies were taken and analysed. The Figure illustrates that IKK-ε (Figure 4.6) and SPN-F (Figure 4.3) have similar localisation, confirming that they form a complex. During nuclear envelope breakdown (NEB), IKK-ϵ is concentrated to the centrosomes. In metaphase, the protein is also localised to the mitotic spindle region, then decreases from centrosomes and mitotic spindle region between metaphase-anaphase transitiom (Met-Anaphase) and early interphase. From late interphase the protein starts relocalising to the centrosomes to repeat the cycle.

4.6.2   Identification of the IKK-ε mitotic interactome

In order to characterise the IK2-GFP-ε mitotic interactome, I undertook a GFP-TRAP-A purification, using $\approx$ 0.4 g of 0–3 hr MG-132 arrested IK2-GFP-ε expressing embryos followed by LC-MS/MS analysis. The associated Western blot is shown in Figure 4.7, demonstrating the presence of a GFP-positive band at the expected molecular weight, its presence in the GFP-TRAP-A pellet and its complete depletion in the extracts.
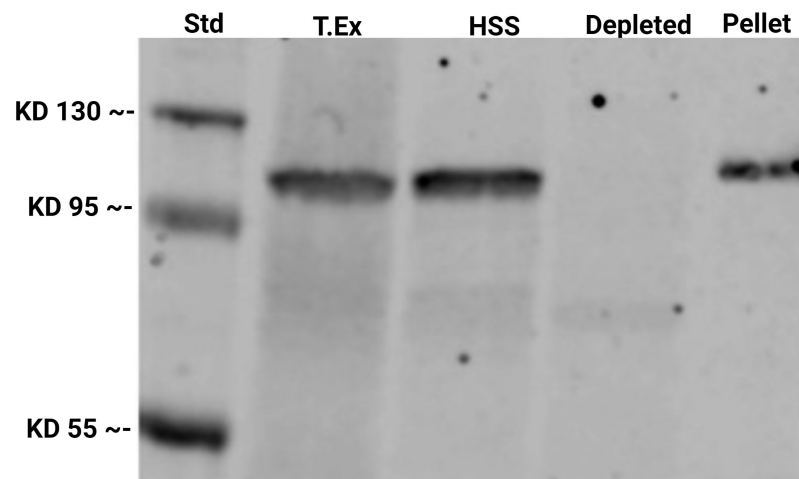
Figure 4.7: **Western blot of IK2.** This Western shows the positivity of the isolated IKK-ε-GPF band at the expected molecular weight (MW) $\approx$ 105 kD.

Following MS, the identified protein IDs were subjected to the Wakefield-Lab standard bioinformatics (Chapter 2). All remaining protein IDs were sorted by mean abundance and those proteins with an Area/Abundance of 1.3E7 and more were retained in the list. This bioinformatics pipeline resulted in the identification of 82 proteins (Table 4.14). IKK-ε has the highest area (6.538E9), as expected, confirming the Western blot (Figure 4.7).

Table 4.14: **IK2 interactors in metaphase.** IKK-epsilon interacting proteins isolated from embryos expressing IK2-GFP after MG132-treatment.

Name	Accession	Coverage	# Unique Peptides	# AAs	MW [kDa]	Score	Area
IK2	FBpp0080920	86.81	78	720	81.9	3319.64	6.538E9
Uba5	FBpp0073354	69.31	18	404	44.1	232.76	5.066E8
spn-F	FBpp0085122	73.35	29	364	40.9	256.17	3.979E8
Drp1	FBpp0077424	54.15	33	735	82.5	224.17	1.974E8
CG12702	FBpp0074578	58.74	40	870	97.1	307.67	1.947E8
Droj2	FBpp0082219	62.03	21	403	45.2	173.87	1.603E8
Idgf4	FBpp0071328	61.54	19	442	48.6	165.68	1.354E8
Idgf6	FBpp0086257	61.28	23	452	50.3	220.51	1.291E8
jvl	FBpp0296973	9.08	7	958	102.4	96.09	1.287E8
Sgt	FBpp0080535	28.10	9	331	36.2	56.10	1.260E8
Mtpbeta	FBpp0072135	46.48	16	469	50.6	151.03	1.193E8
ctp*	FBpp0070672	64.04	6	89	10.4	98.82	1.117E8
me31B	FBpp0079566	65.19	29	428	48.6	146.16	9.592E7
CG5028	FBpp0084275	61.19	17	402	44.4	151.43	8.912E7
GCC185	FBpp0112136	47.84	53	1135	130.0	337.43	8.054E7
Cdk1	FBpp0079641	72.73	18	297	34.4	96.08	7.903E7
Rab5	FBpp0077475	54.34	8	219	23.9	51.78	6.500E7
Rab1	FBpp0083503	68.29	9	205	22.7	52.44	6.325E7
CG7461	FBpp0289511	51.04	25	627	68.3	162.54	5.673E7
gammaTub37C	FBpp0080769	63.24	17	457	51.3	139.51	5.381E7
cher	FBpp0088478	52.31	85	2210	239.0	446.75	5.240E7
didum	FBpp0088685	39.80	38	1196	137.8	188.89	5.124E7
CG5174	FBpp0085863	44.62	7	186	20.5	34.80	4.785E7
fax	FBpp0075170	42.11	15	418	47.1	77.53	4.772E7
nuf	FBpp0075476	33.44	10	305	36.1	40.86	4.705E7
Hsp23	FBpp0076181	60.75	8	186	20.6	64.10	4.675E7
betaCOP	FBpp0074348	36.93	27	964	107.3	141.96	4.161E7
CG10237	FBpp0080748	43.52	13	301	35.1	49.45	4.089E7
HDAC6	FBpp0290988	38.05	25	883	98.2	104.58	4.076E7
AP-1-2beta	FBpp0074558	27.58	22	921	101.1	92.62	3.929E7
Nfs1	FBpp0079874	46.32	19	462	51.0	121.51	3.582E7
qua	FBpp0080549	35.74	28	887	100.9	118.71	3.514E7
Rho1	FBpp0086354	59.38	9	192	21.7	47.58	3.373E7
gammaCOP	FBpp0290505	26.42	1	878	97.1	87.75	3.257E7
CG11899	FBpp0084759	32.97	11	364	39.5	43.69	3.038E7
Ge-1	FBpp0079818	17.21	22	1354	149.2	75.52	3.035E7
AP-1mu	FBpp0081592	43.43	13	426	48.9	54.23	2.921E7
GILT1	FBpp0082228	57.60	9	250	27.7	68.88	2.898E7
sn	FBpp0071057	32.81	12	512	57.2	60.22	2.884E7
sesB	FBpp0073277	47.83	14	299	32.9	34.88	2.704E7
porin	FBpp0079771	44.68	11	282	30.5	53.74	2.638E7
Actn*	FBpp0070330	52.29	39	895	103.7	160.43	2.602E7
CG9281	FBpp0073872	32.41	17	611	69.5	76.77	2.474E7
Srp68	FBpp0076244	36.26	18	604	69.0	65.24	2.438E7
His2B:CG33882	FBpp0091127	36.59	5	123	13.7	35.47	2.430E7
yl	FBpp0073714	10.43	14	1937	214.8	52.33	2.418E7
alphaCOP	FBpp0072693	29.98	28	1234	139.2	118.69	2.416E7
Srp72	FBpp0083319	37.23	18	650	72.8	81.06	2.398E7
smid	FBpp0304233	24.07	14	910	100.2	63.53	2.377E7
Zw10	FBpp0070425	33.98	17	721	82.2	80.11	2.349E7
Klc	FBpp0303946	30.97	12	507	57.9	49.14	2.250E7
Cam*	FBpp0087109	41.61	6	149	16.8	39.21	2.244E7
Idgf2	FBpp0080418	32.05	9	440	49.1	31.02	2.217E7
beta'COP	FBpp0080048	28.34	18	914	102.6	104.44	2.123E7
Nup107*	FBpp0079710	21.42	13	845	97.3	68.44	2.113E7
AP-1gamma	FBpp0071231	27.41	20	963	104.4	93.12	2.100E7
Hmgcl	FBpp0078979	40.25	7	323	34.2	39.49	2.070E7
rb	FBpp0070670	17.67	16	1160	127.1	71.06	2.062E7
jar	FBpp0084020	21.47	22	1253	143.2	74.57	2.060E7
Tnpo	FBpp0076708	29.68	20	893	101.5	95.21	2.053E7
Pp2B-14D	FBpp0074069	20.88	12	570	63.1	38.14	2.029E7
sgg	FBpp0089162	27.24	11	514	53.8	41.20	1.996E7
Vps35	FBpp0071686	22.91	15	803	91.1	69.75	1.890E7
GCS2beta	FBpp0080551	23.91	13	548	61.5	36.13	1.871E7
Rab7	FBpp0083891	54.59	9	207	23.3	48.83	1.751E7
Nup205	FBpp0074568	23.17	35	2067	232.6	158.48	1.732E7
CG9547	FBpp0078893	30.31	7	419	45.7	36.80	1.721E7
Nup154	FBpp0088820	25.35	24	1365	153.8	69.18	1.700E7
CG8036	FBpp0081372	32.07	12	580	63.0	48.93	1.693E7
CG9853	FBpp0078589	33.92	8	339	38.5	43.81	1.630E7
CG9577	FBpp0070006	34.29	7	312	33.8	35.91	1.613E7
ND-75	FBpp0071128	29.82	12	731	78.6	85.40	1.585E7
krz	FBpp0085236	34.89	10	470	51.2	42.53	1.499E7
SH3PX1	FBpp0076142	27.26	13	565	63.1	46.64	1.473E7
CPT2	FBpp0072848	27.59	14	667	75.1	63.52	1.428E7
Nadsyn	FBpp0073675	25.03	12	787	87.6	47.58	1.427E7
Snx1	FBpp0077206	39.52	14	458	52.2	66.80	1.391E7
Synd	FBpp0083373	21.46	9	494	55.9	39.43	1.373E7
Cdc16	FBpp0083769	28.41	15	718	81.7	49.96	1.346E9
alpha-Spec	FBpp0072672	22.53	38	2415	278.1	142.01	1.338E7
zip	FBpp0291731	22.86	33	1964	226.6	172.69	1.334E7
lok	FBpp0080861	33.33	11	459	52.3	50.32	1.316E7

To further understand the functional relationships between IKK-ε and its mitotic interactors, I took the 82 proteins and subjected them to GO enrichment analysis (Table 4.15). 8 functional cellular component terms were identified – the ER membrane insertion complex, the cell-cell contact zone, the myosin V complex, the nuclear pore inner ring, the COPI-coated vesicle, the AP-1 adaptor complex, the signal recognition particle and the retromer complex. To aid visualisation, the protein-protein interaction software package, Cytoscape was again used. The network constituted the IKK-ε interacting proteins within the GO-enriched cellular components terms, along with IKK-ε interacting proteins already identified as enriched EB1-GFP interacting proteins, where the size of the nodes (Figure 4.8) corresponds to the abundance of the protein identified in the IKK-ε IP. To visually compare my experiment with the known protein-protein interaction data, I added any interactions already present in the biological general repository for interation datasets TheBioGrid database (`https://thebiogrid.org`) (Figure 4.8).

Table 4.15: **IK2 GO Enrichment Analysis.** IKK-epsilon analysed via GO enrichment, which shows common isolated proteins as part of cell components.

GO cellular component complete	Reference List (13811)	IK2 IP	Expected	Fold Enrichment	P-value	FDR	Proteins
ER membrane insertion complex (GO:0072379)	3	2	0.02	>100	3.74E-04	9.47E-03	Sgt, CG9853
cell-cell contact zone (GO:0044291)	3	2	0.02	>100	3.74E-04	9.29E-03	Rho, Zip
myosin V complex (GO:0031475)	3	2	0.02	>100	3.74E-04	9.13E-03	Didum, CaM
nuclear pore inner ring (GO:0044611)	4	2	0.02	80.3	5.59E-04	1.27E-02	Nup205, Nup154
COPI-coated vesicle (GO:0030137)	8	4	0.05	80.3	6.52E-07	3.97E-05	alphaCOP, betaCOP, beta'COP, gammaCOP
AP-1 adaptor complex (GO:0030121)	5	2	0.03	64.24	7.79E-04	1.63E-02	AP-1gamma, AP-1mu
signal recognition particle (GO:0048500)	6	2	0.04	53.53	1.03E-03	2.01E-02	Srp68, Srp72
retromer complex (GO:0030904)	7	2	0.04	45.88	1.32E-03	2.34E-02	Snx1, Vps35
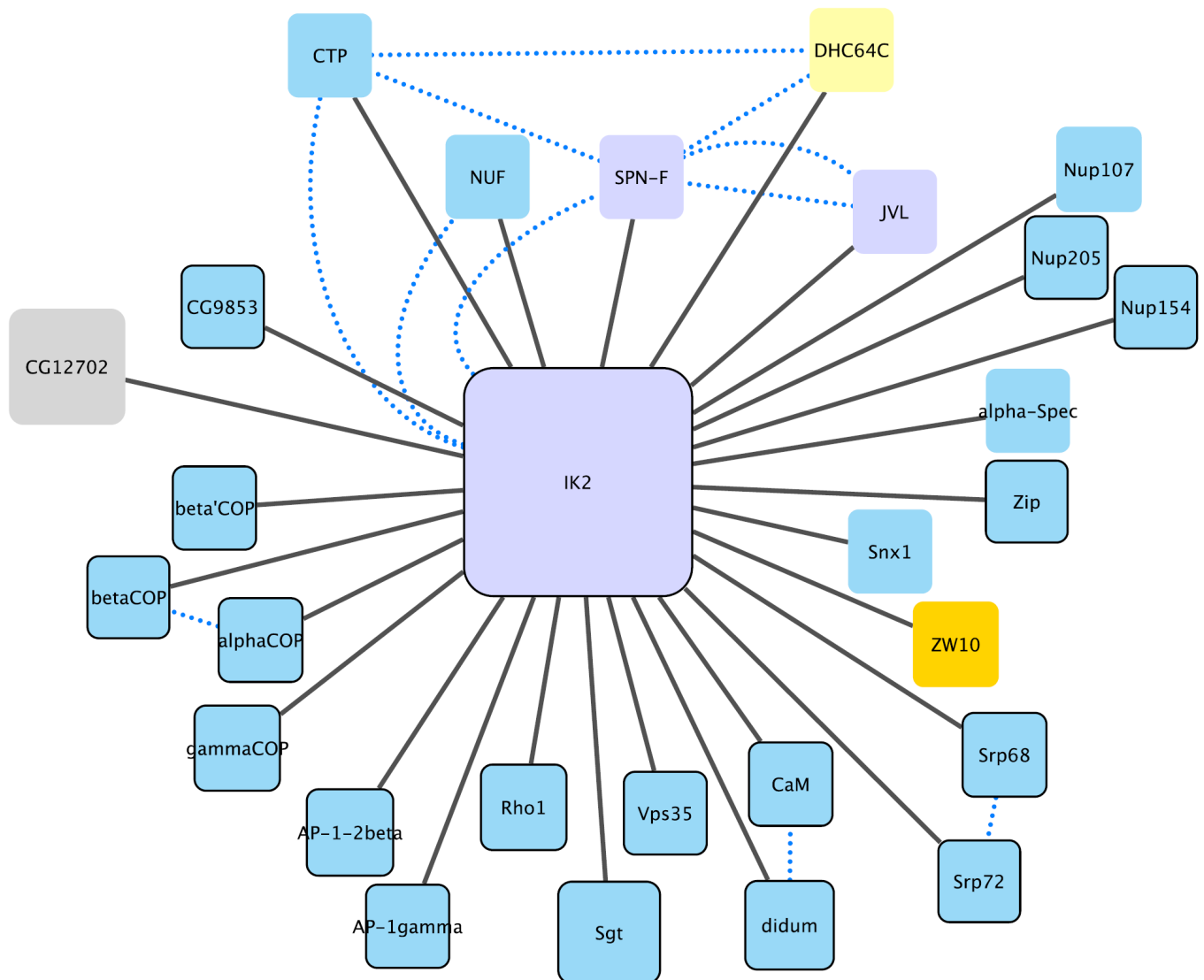
Figure 4.8: **IK2 interactors in metaphase.** IKK-epsilon interacts with several proteins in metaphase. Proteins identified in this experiment are connected by solid lines and those present in BioGrid database are indicated by dotted lines.

4.6.3 IKK-ε interacting proteins

To have the final IKK-ε interacting proteins in metaphase (Figure 4.8), in addition to IKK-ε binding proteins within GO-enriched cellular components terms (Table, 4.15), I manually chose IKK-ε interactors in metaphase from Table 4.14 that were already identified either as EB1 interacting proteins with a final cut-off of 1.2 fold increase in mitosis (Section 4.4 and Table 4.7) or EB1 interacting proteins within GO term enrichment cellular components (Table 4.2). This analysis demonstrates the presence of the full SPNF-JVL-IKK-epsilon complex in the IK2-GFP mitotic IP. The GO analysis identified complexes – the cell-cell contact zone, ER membrane insertion complex, retromer complex, Myosin V complex,

signal recognition particle, nuclear pore inner ring, COPI-coated vesicle and AP-1 adaptor complex. The IKK-ε IP identified the ZW10 subunit of RZZ. However, ROD and ZWILCH were not within 82 proteins. In addition, the IP also possessed CTP, which is the *Drosophila* dynein light chain (DLC8). DLC8 is present in the original EB1-GFP mitotic interactome, but was not within the Top 100 proteins; as such it appears in the Cytoscape network in Figure 4.8. Interestingly, EB1 was not identified as an enriched interactor of IKK-ε, despite it being the protein which identified Ikk-ε the original TMT analysis. (See Discussion 4.13 for a full explanation of why this might be).

4.6.4   General description of some IKK-ε binding proteins

Cell-cell contact zone

Rho and Zip: Cadherins are transmembrane proteins involved in cell-cell adhesion in calciun-dependent manner and in cytosol cadherin tails interact with actin cytoskeleton (Braga et al. 1997). Rhombooid (Rho) is the small GTPase involved in regulation of these biological processes, thereby regulating cell migration, cell polarity and cell cycle progression (Braga et al. 1997; Hodge and Ridley 2015). In *Drosophila*, the hexamer myosin II is composed of three pairs of proteins – the myosin II heavy chain which is encoded by *zipper (zip)*, the regulatory chain encoded by *spaghetti squash (sqh)* and the myosin II essential light is encoded by *Mlc-c)* (For review see Aldaz et al. 2013; L. Zhang and Ward 2011). Myosin II or non-muscle myosin II is involved in concentrating E-cadherin at cell-cell contact zones and is a key effector of Rho/Rho kinase signaling (Heuzé et al. 2019; Shewan et al. 2005).

ER membrane insertion complex

SGT and CG9853: Small glutamine-rich tetratricopeptide repeat-containing protein (SGT) as a co-chaperone (Chartron et al. 2011; Lin et al. 2021). This protein interacts with CG9853 (GET4) and GET5 which are subunits of transmembrane domain reconition complex (TRC) (Chartron et al. 2011), this complex plays various important functions in cells (See TRC, Page 115).

Retromer complex

VPS35 and SNX1: In mammals the retromer complex is composed of a vacuolar protein sorting-associated protein 26 (VPS26)-VPS29-VPS35 trimeric subcomplex and a dimer of membrane-associated sorting nexin (SNX) (Luo et al. 2018). The retromer complex is involved in endosomal trafficking and functions by recognising specific receptors within endosomal membranes containing specific recognition sequences, which targets them cargo to be transported to the appropriate destination (Luo et al. 2018; Seaman 2012; Suzuki et al. 2019). The dysfunction of this complex is linked to various neurodegenerative diseases, such as, Alzheimer's disease, Parkinson's disease and Down's syndrome (Luo et al. 2018).

Myosin V complex

CaM and Didum: Myosin V complex is a cargo transporter of organelles, secretory vesicles, membranous cargo, lipids, mRNA and protein vesicles using actin as tracks, in contrast of kinesin and dynein that use MTs as tracks, although they transport similar cargos (For review see Trybus 2008). Although this complex is also found at contractile rings of actin filaments, its function in the assembly and contraction of these rings is less known (Laplante et al. 2015). Calmodulin molecules bind to light chain-binding domain (LCBD) of the myosin V complex in Ca^{2+}-dependent manner to regulate its conformations and activities (For review see Shen et al. 2016), and the dilute class unconventional

myosin (Didum) is orthologous to the human Myosin V complex (Bonafé and Sellers, J.R. 1998; Larson 1996; MacIver et al. 1998).

Signal recognition particle

SRP68 and SRP72: Signal recognition particle (SRP68) is the heterodimer of SRP complex, which in mammals is composed of six proteins: SRP9, SRP14, SRP19, SRP54, SRP54, SRP68 and SRP72 (Gao et al. 2017). This complex is a ribonucleoprotein particle that functions as an adaptor between the synthesis of proteins and the translocation machinary in the membrane. Thus, the SRP plays crucial roles in the co-translational transport of secretory and membrane proteins into the ER (Gao et al. 2017; Wild et al. 2004).

Nuclear pore complexes

NUP154, NUP205 and NUP107: These subunits are components of nuclear pore complex (NUPCs), which comprises at least thirty two proteins (Guglielmi et al. 2020; Raices and D'Angelo 2012). The NPCs are localised to the nuclear envelope and mediate the exchange of large molecules between nucleoplasm and cytoplasm with involvement of the small GTPase Ran (Ran-GTP) in the nucleus and the Ran-GTPase activating protein 1 (RanGAP1) in the cytosol (For review see Grossman et al. 2012; Guglielmi et al. 2020). NUPs plays important role in mitotic progression and maintenance of genome integrity, thus avoid the accumulation of DNA damage (Loeillet et al. 2005; Nagai et al. 2008). During mitosis, NPC componets are located to kinetochores where regulate functions of these structures. NUPs regulate chromosome segregation, spindle assembly and trigger onset of anaphase (Chatel and Fahrenkrog 2011; Wozniak et al. 2010).

Table 4.16: **IKK-ε interacting proteins in metaphase.** The table summarises mitotic IKK-ε binding proteins (Figure 4.8).

Proteins and complexes	Known interactors and functions
Cell-cell contact zone proteins	These proteins which include Rho and Zip regulate cell-cell adhesion, cell migration, polarity and cell cycle progression (Braga et al. 1997; Hodge and Ridley 2015).
ER membrane insertion complex	SGT is a co-chaperone that interaacts with CG9853 (GET4) in TRC (Suloway et al. 2010), which plays different biological functions (Table 4.13)
Retromer complex	This complex in mammals is composed by VPS26, VPS29, VPS35 and SNX (Luo et al. 2018) and regulate cargo in endosomes to be transported to the appropriate destination (Luo et al. 2018; Seaman 2012; Suzuki et al. 2019).
Myosin V complex	Didum is the orthologue to the human Myosin V complex which is involved in transporting cargoes using actin filaments as tracks (Reviewed by Trybus 2008). Functions of this complex at contractile rings of acting are less known. CaM is a protein that regulates function of Didum (For review see Shen et al. 2016).
Signal recognition particle (SRP)	This complex is composed of various signal recognition particles (SRPs) (Gao et al. 2017) and plays important functions in secretory and membrane proteins into the ER (Gao et al. 2017; Wild et al. 2004).
Nuclear pore complex (NUPC)	The complex includes different components ($\approx$ 32 proteins) of the nuclear pore complexex (NUPCs) (Guglielmi et al. 2020; Raices and D'Angelo 2012) These complexes regulate the exchange of macromolecules between nucleoplasm and cytoplasm (Reviewed by Grossman et al. 2012; Guglielmi et al. 2020). In addition, nuclear pore proteins (NUPs) modulate maintenance of genome integrity, chromosome segregation, spindle assembly and the promotion of onset of the anaphase (Chatel and Fahrenkrog 2011; Loeillet et al. 2005; Nagai et al. 2008; Wozniak et al. 2010).

4.7 Dynamic localisation and protein-protein interaction network of mCh-JVL in the early embryo

To determine the localisation and identification of JVL binding proteins, I crossed female virgins of flies of genotype UASp-mCh-JVL to matαt-GAL4 males (Table 2.4) for early embryo collection and subsequently live imaging analysis. Previous studies using mCh-JVL have been conducted in *Drosophila* germline and bristles, these investigation illustrated that the JVL interacts with SPN-F and IK2 to organise MTs during oogenesis and bristle development (See SPNF-JVL-IK2 complex, Page 93). It has been shown that JVL is a MT-associated protein and physically interacts with EB1 *in vitro* (Baskar et al. 2019).

4.7.1 Mitotic Localisation of mCh-JVL

To investigate the dynamic localisation of mCh-JVL in early embryos, I imaged 1–2 hr old embryos laid by $\frac{L3mCh-JVL}{+};\frac{Pri}{mat\alpha t-GAL4}$ and $\frac{L3mCh-JVL}{+};\frac{mat\alpha t-GAL4}{TM6B}$ mothers using spinning disc confocal microscopy. Embryos were imaged every 5 seconds across 5 x 1 μm z planes. Image sets were analysed using ImageJ, as maximum intensity projections. 9 movies in total taken and analysed, showed similar JVL dynamic localisation in the early embryos. As illustrated in Figure 4.9, during late interphase and NEB, JVL is found concentrated at the centrosomes, between metaphase and early interphase it decreseases. During the entire cell cycle it was not seen in the region of the mitotic spindle, in contrast to the SPN-F and IK2 dynamic localisation.

(a) **Late interphase.** (b) **NEB.** (c) **Metaphase.** (d) **Met-Anaphase.**

(e) **Mid-Anaphase.** (f) **Telophase.** (g) **Early interphase.**
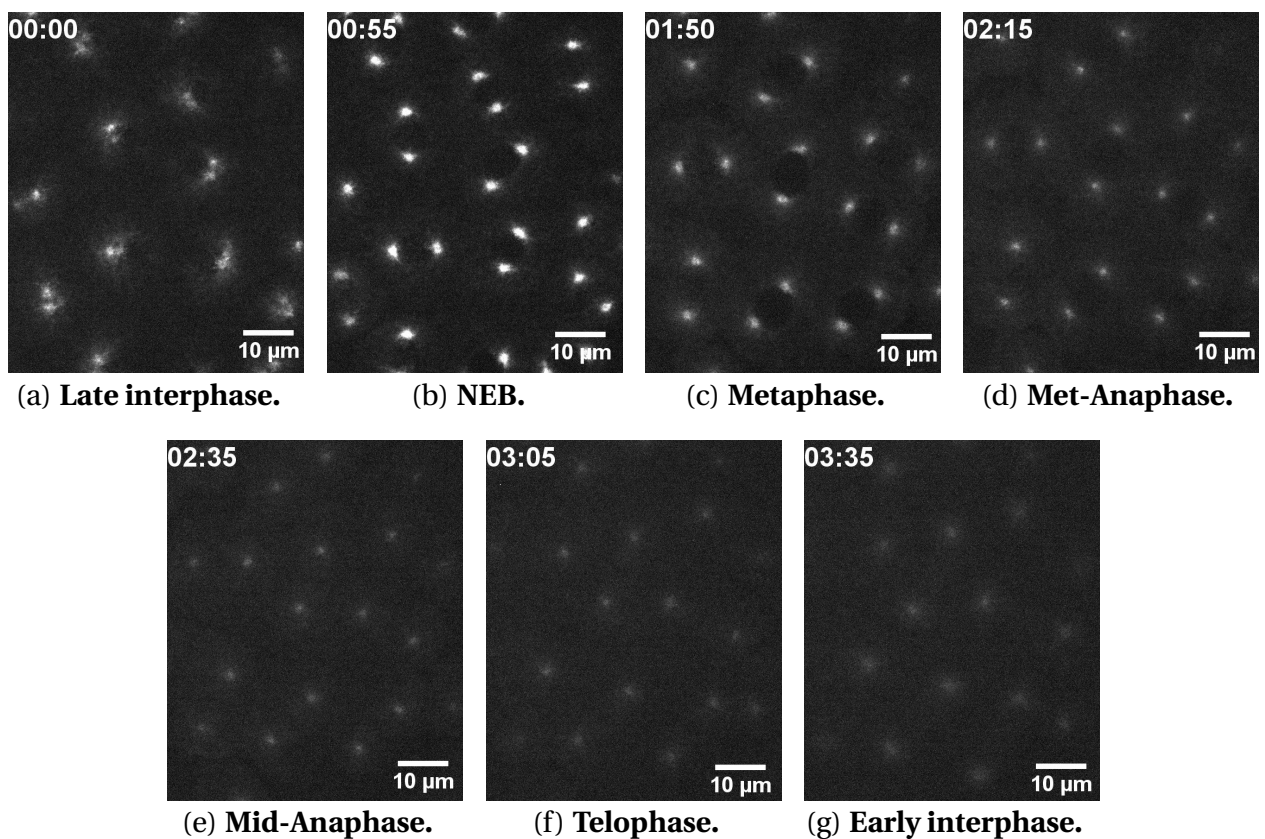
Figure 4.9: **Dynamic localisation of mCh-JVL in the early *Drosophila* embryo.** 9 movies were taken and analysed for dynamic localisation of JVL in the early embryo. The Figure shows that JVL gradually increases its localisation to the centrosomes between interphase and nuclear envelope breakdwon. Between metaphase and early interphase JVL retracts from centrosomes and during late interphase it starts relocalising to centrosomes to repeat the cycle. In contrast to IKK-epsilon and SPN-f, JVL is not localised in the region of the mitotic spindle throughout the cell cycle.

4.7.2 Identification of the JVL mitotic interactome

In order to characterise the JVL mitotic interactome, I undertook a RFP-TRAP-A purification, using ≈ 0.4 g of 0–3 hr MG-132 arrested mCh-JVL expressing embryos followed by LC-MS/MS analysis. The associated Western blot is shown in Figure 4.10, demonstrating the negativity of the assay in all samples – total extract, high speed supernatant, depleted and pellet. This may be due to the low expression of mCh-JVL in the embryos (area = 1.407E8). Despite the negative result, I therefore subjected the pellet to proteomics analysis.
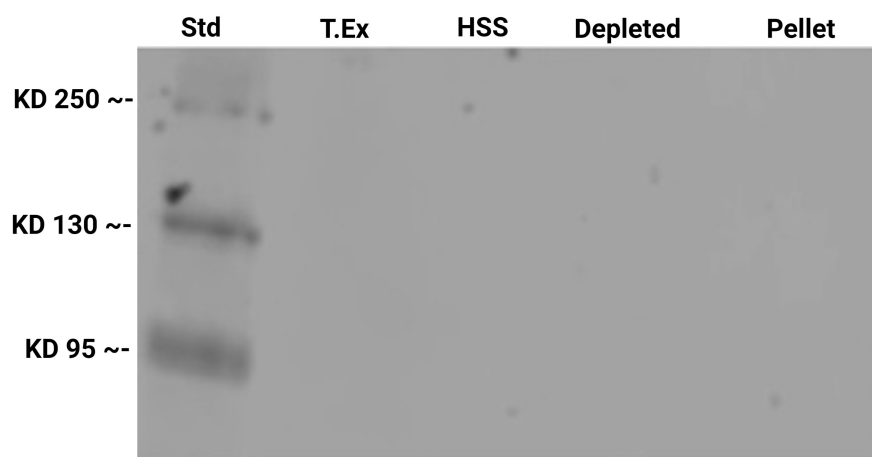
Figure 4.10: **Western blot of mCh-JVL.** The detaction of JVL using Western blot has failed and the reason may be correlated to low expression of the protein (Area = 1.407E8, Table 4.17), whereas the bioimage showed the expression of the mCh-JVL in the embryos (Figure 4.9). mCh-JVL MW ≈ 154 kD.

Following MS, the identified protein IDs were subjected to the Wakefield-Lab standard bioinformatics (Chapter 2). All remaining protein IDs were sorted by mean abundance and those proteins with an Area/Abundance of 1.3E7 and more were retained in the list. This bioinformatics pipeline resulted in the identification of 80 proteins (Table 4.17). 79 JVL binding proteins were identifed, although the JVL did not have the highest area as expected.

Table 4.17: **JVL interactors in metaphase.** The table illustates proteins that interact with JVL in metaphase.

Name	Accession	Coverage	# Unique Peptides	# AAs	MW [kDa]	Score	Area
betaTub60D	FBpp0072177	27.97	3	454	50.8	337.01	1.165E9
lrp-1B	FBpp0081736	78.87	44	899	98.5	892.94	6.624E8
TER94	FBpp0087479	78.28	56	801	88.8	757.36	6.330E8
alpha-Spec	FBpp0072672	72.55	174	2415	278.1	1775.97	5.031E8
Pp2A-29B	FBpp0099974	57.36	29	591	65.4	259.27	3.473E8
Zw10	FBpp0070425	69.07	33	721	82.2	489.68	3.355E8
kst	FBpp0089204	66.48	252	4207	483.4	2043.53	2.751E8
Ubi-p5E	FBpp0070894	72.10	6	534	60.0	34.47	1.999E8
Zwilch	FBpp0085138	61.62	36	641	72.4	351.67	1.997E8
Karybeta3	FBpp0078500	55.11	42	1105	123.5	356.17	1.777E8
Rod	FBpp0085156	52.99	95	2089	239.5	741.12	1.651E8
Jvl	FBpp0296974	20.24	5	1151	122.3	122.20	1.407E8
mts	FBpp0079148	61.17	13	309	35.4	161.84	1.367E8
Sar1	FBpp0083604	69.43	11	193	21.8	116.72	1.351E8
Fs(2)Ket	FBpp0294037	44.57	28	884	98.6	305.96	1.337E8
CG12702	FBpp0074578	59.31	38	870	97.1	224.08	1.303E8
CG5174	FBpp0085865	57.21	11	208	22.5	71.88	1.264E8
Nup107	FBpp0079710	45.09	29	845	97.3	162.60	6.966E7
Cp1	FBpp0086717	40.47	13	341	37.9	61.50	6.737E7
Rab1	FBpp0083503	55.12	6	205	22.7	50.38	5.909E7
Actn	FBpp0070330	68.94	50	895	103.7	319.95	5.889E7
pr	FBpp0088417	56.55	8	168	19.3	49.77	5.851E7
beta-Spec	FBpp0074228	45.22	82	2291	265.6	410.55	5.122E7
Khc	FBpp0086328	50.67	40	975	110.3	259.98	5.099E7
Prat	FBpp0081261	31.68	13	546	59.5	53.44	4.866E7
Klc	FBpp0303946	48.32	19	507	57.9	98.04	4.788E7
Rab5	FBpp0077475	51.14	7	219	23.9	45.26	4.624E7
HDAC6	FBpp0298373	32.49	24	1022	113.3	122.29	4.548E7
Chc	FBpp0073966	41.60	57	1678	191.1	270.73	4.521E7
ATPCL	FBpp0289823	44.42	33	1112	121.3	180.45	4.197E7
Uba1	FBpp0302038	44.64	33	1008	111.7	162.06	4.159E7
Nup75	FBpp0085954	43.26	22	668	76.8	127.55	4.079E7
zip	FBpp0099894	41.81	71	1971	226.8	428.00	4.077E7
Hook	FBpp0080722	39.91	22	679	76.6	115.19	4.016E7
CG41099	FBpp0112714	37.62	33	1111	123.0	145.12	3.818E7
alphaCOP	FBpp0072693	39.71	38	1234	139.2	165.21	3.807E7
Srp68	FBpp0076244	35.93	20	604	69.0	60.57	3.603E7
Nup98-96	FBpp0083851	11.58	18	1960	210.0	81.40	3.583E7
betaCOP	FBpp0074348	34.54	24	964	107.3	148.51	3.546E7
epsilonCOP	FBpp0078891	39.22	10	306	34.6	66.60	3.532E7
me31B	FBpp0079566	42.99	15	428	48.6	67.76	3.413E7
EndoB	FBpp0085743	21.16	6	378	42.3	38.65	3.342E7
Nup154	FBpp0088820	22.93	23	1365	153.8	98.07	3.236E7
sqh	FBpp0070842	52.30	7	174	19.9	63.03	3.166E7
IK2	FBpp0080919	39.24	22	711	81.0	102.48	3.124E7
CG10237	FBpp0080748	43.52	13	301	35.1	49.92	3.113E7
CG11899	FBpp0084759	37.09	11	364	39.5	32.84	3.057E7
CG6907	FBpp0078729	36.38	10	437	48.7	40.99	2.920E7
gammaCOP	FBpp0085154	37.54	1	879	97.2	122.28	2.817E7
Tnpo	FBpp0076708	31.80	21	893	101.5	105.43	2.712E7
CG8036	FBpp0081372	36.03	15	580	63.0	59.00	2.642E7
CG4572	FBpp0083269	23.44	7	482	54.4	35.67	2.436E7
Nup44A	FBpp0087936	47.46	12	354	39.5	55.18	2.357E7
HisRS	FBpp0074365	41.19	19	522	57.7	89.51	2.325E7
Snx1	FBpp0077206	31.66	12	458	52.2	67.17	2.303E7
Mtap	FBpp0086072	52.25	11	289	32.0	41.03	2.303E7
Nup43	FBpp0082998	28.21	8	358	40.1	36.97	2.249E7
beta'COP	FBpp0080048	30.09	19	914	102.6	106.57	2.219E7
Srp72	FBpp0083319	45.69	22	650	72.8	100.38	2.188E7
Nup160	FBpp0079788	28.56	28	1411	160.2	138.01	2.158E7
Nup205	FBpp0074568	21.43	32	2067	232.6	167.60	2.131E7
CG6617	FBpp0074386	34.67	7	225	26.0	37.00	2.079E7
Hmgcl	FBpp0078979	47.99	9	323	34.2	34.24	2.057E7
Nup37	FBpp0084187	37.50	9	320	35.3	34.14	2.040E7
Cam	FBpp0087109	35.57	6	149	16.8	30.39	2.021E7
CG3902	FBpp0074843	33.82	12	414	45.3	39.99	1.980E7
Nup93-1	FBpp0073659	26.25	16	823	93.8	65.46	1.868E7
shi	FBpp0110335	22.17	14	830	93.0	48.28	1.829E7
Rab7	FBpp0083891	44.93	8	207	23.3	35.52	1.782E7
Npl4	FBpp0084266	22.76	12	624	69.9	46.49	1.765E7
Nup133	FBpp0083695	25.17	23	1200	135.1	120.03	1.715E7
SPN-F	FBpp0085122	39.84	12	364	40.9	43.22	1.695E7
Mms19	FBpp0078425	32.43	24	959	107.0	81.87	1.663E7
RhoGAP68F	FBpp0075729	33.61	13	476	54.9	45.85	1.541E7
Ge-1	FBpp0079818	11.23	14	1354	149.2	48.18	1.540E7
sgg	FBpp0089162	21.21	9	514	53.8	34.84	1.521E7
Nup50	FBpp0087861	20.21	7	564	59.4	52.23	1.486E7
dgt6	FBpp0084783	32.42	15	654	72.8	69.78	1.435E7
Snx6	FBpp0079247	27.17	10	449	50.1	37.72	1.343E7
cnn	FBpp0086822	15.94	17	1148	129.8	55.22	1.307E7

To further understand the functional relationships between JVL and its mitotic interactors, I took the 80 proteins and subjected them to GO enrichment analysis (Table 4.18). 7 functional cellular component terms were identified – the RZZ complex, COPI-coated vesicle, signal recognition particle, retromer complex, nuclear pore, apicomedial cortex and spectrosome. To aid visualisation, the protein-protein interaction software package, Cytoscape was again used. The network constituted the JVL interacting proteins within the GO-enriched cellular components terms, along with JVL interacting proteins already identified as enriched EB1-GFP interacting proteins, where the size of the nodes (Figure 4.11) corresponds to the abundance of the protein identified in the JVL IP. To visually compare my experiment with the known protein-protein interaction data, I added any interactions already present in the biological general repository for interation datasets TheBioGrid database (`https://thebiogrid.org`) (Figure 4.11).

Table 4.18: **JVL GO Enrichment Analysis.** JVL interactors were analysed using GO Enrichment Analysis and the results show proteins of cell components.

GO cellular component complete	Reference List (13811)	JVL IP	Expected	Fold Enrichment	P-value	FDR	Proteins
RZZ complex (GO:1990423)	3	3	0.02	> 100	2.99E-06	9.34E-05	Rod, Zw10, Zwilch
COPI-coated vesicle (GO:0030137)	8	4	0.04	92.07	3.76E-07	1.68E-05	alphaCOP, betaCOP, gammaCOP, epsilonCOP
signal recognition particle (GO:0048500)	6	2	0.03	61.38	7.89E-04	1.51E-02	Srp68, Srp72
retromer complex (GO:0030904)	7	2	0.04	52.61	1.01E-03	1.81E-02	Snx1, Snx6
nuclear pore (GO:0005643)	46	12	0.25	48.04	1.80E-16	6.03E-14	Various Nups
apicomedial cortex (GO:0106037)	8	2	0.04	46.04	1.26E-03	2.20E-02	Sqh, Zip
spectrosome (GO:0045170)	8	2	0.04	46.04	1.26E-03	2.17E-02	alpha-Spec, beta-Spec
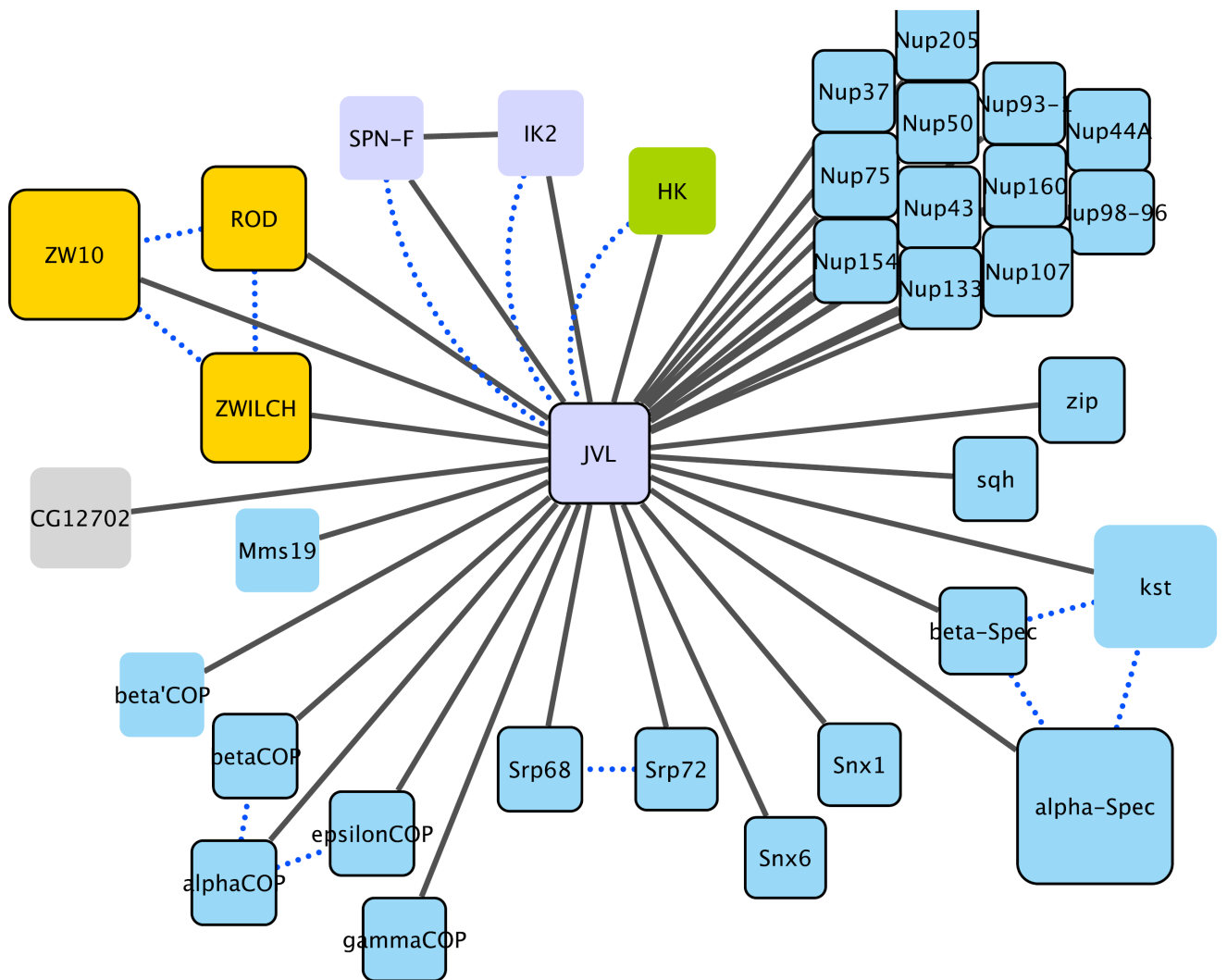
Figure 4.11: **JVL interactors in metaphase.** JVL interactors in metaphase after BioGrid Analysis for visualising interaction networks. Proteins isolated in this work are linked by solid lines and those in BioGrid database are shown with dotted lines.

4.7.3   JVL interacting proteins

To have the final JVL interacting proteins in metaphase (Figure 4.11), in addition to JVL binding proteins within GO-enriched cellular components terms (Table, 4.18), I manually chose JVL interactors in metaphase from Table 4.17 that were already identified either as EB1 interacting proteins with a final cut-off of 1.2 fold increase in mitosis (Section 4.4 and Table 4.7) or EB1 interacting proteins within GO term enrichment cellular components (Table 4.2). This analysis demonstrates the presence of the full SPNF-JVL-IKK-epsilon complex in the mCh-JVL mitotic IP. It also shows the presence of the full RZZ complex. The GO analysis also identified further complexes: COPI-coated vesicle, signal recognition particle, retromer complex, nuclear pore, apicomedial cortex and spectro-

some. Although HOOK protein was identified, CTP, DNApol-ε 58 and DNApol-ε 255 were not within the identified 80 proteins; as such they do not appear in the Cytoscape network in Figure 4.11. Furthermore, EB1 was not identified as an enriched interactor of JVL, despite it being the protein which identified JVL in the original TMT analysis (See Discussion 4.13 for a full explanation of why this might be).

4.7.4   General description of some JVL binding proteins

Mms19

Mms19: the Mms19 is the subunit of the cytosolic iron-sulfur protein assembly (CIA) complex which interacts with apoproteins and mediates the insertion of iron-sulfur cluster into these apoproteins implicated in methionine biosynthesis, DNA replication and rapair, as well as in telomere maintenace (Reviewed by Petronek et al. 2021; Stehling et al. 2012).

For description of the remaing JVL interacting proteins, see Sections 4.3, 4.5.4 and 4.6.4.

4.8   Dynamic localisation and protein-protein interaction network of PIGS in the early embryo

To investigate the localisation and identification of PIGS interacting proteins, I crossed female virgins of flies of genotype UASp-GFP-PIGS both to matαt-GAL4 males and HisRFP;matαt-GAL4 males (Table 2.5 and Table 2.6) for early embryo collection and subsequently live imaging analysis. The pickled eggs (PIGS) protein is reported to bind directly to both actin and MT cytoskeleton *in vitro* using cultured cells, however, *in vivo,* it is unclear if this is also the case (Pines et al. 2010). To date, no studies of interaction between PIGS and EB1 has been reported in any species, however, results of my EB1 IP suggest that PIGS is as an EB1 interactor which is supported by having two SxIP motifs at its C-terminus (Table 4.4).

4.8.1 Mitotic Localisation of PIGS

To determine the dynamic localisation of GFP-PIGS in early embryos, I imaged 1–2 hr old embryos laid by $w; \frac{HisRFP}{+}; \frac{GFP-PIGS}{mat\alpha t-GAL4}$ mothers using spinning disc confocal microscopy. Embryos were imaged every 5 seconds across 5 x 1 μm z planes. Image sets were analysed using ImageJ, as maximum intensity projections. 5 movies taken and analysed, showed similar dynamic localisation. As illustrated in Figure 4.12, between late interphase and metaphase , PIGS is found concentrated at the centrosomes and at the apical cortex, then it appears to decrease during anaphase and early interphase. These observations are in agreement with the roles of PIGS as actin-MT cross-linker and as +TIP protein, in accordance with studies reported by Girdler et al. (2016) and Pines et al. (2010). In contrast to this dynamic localisation, Yamamoto-Hino et al. (2018) and his colleagues, in their experiments using *Drosophila* S2 cells, state that the vast majority of PIGS is localised to the endoplasmic reticulum and only the minority is localised to the nuclear envelope.
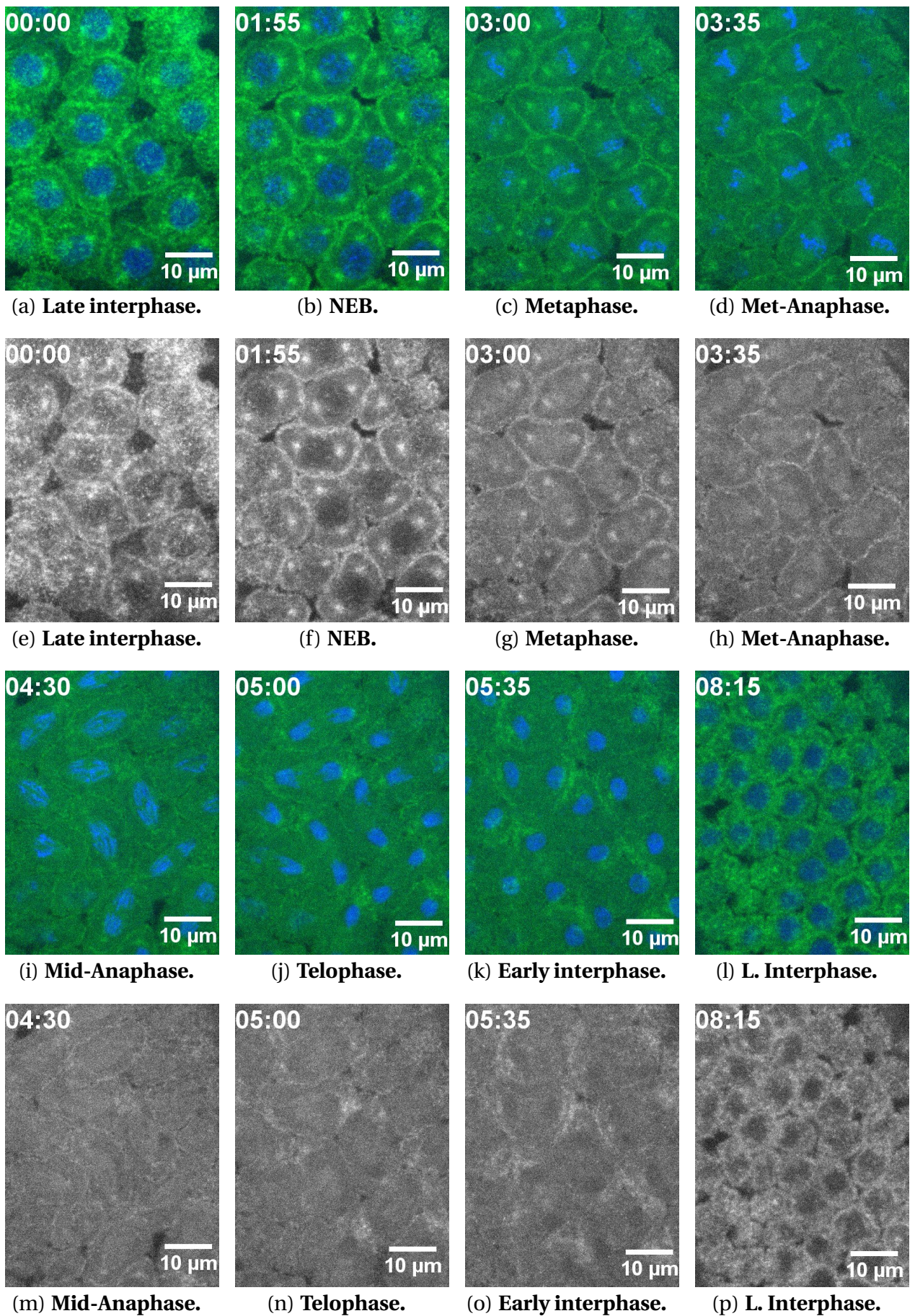
Figure 4.12: **Dynamic localisation of GFP-PIGS in the early *Drosophila* embryo.** 5 movies taken and analysed. As shown in the Figure, during late interphase and metaphase PIGS is highly concentrated at the centrosomes and at the apical cortex. Then the protein decreases between metaphase and early interphase. During late interphase, the protein localises again to the centrosomes and to the apical cortex for next cycle.

4.8.2 Identification of the PIGS mitotic interactome

In order to characterise the PIGS mitotic interactome, I undertook a GFP-TRAP-A purification, using ≈ 0.4 g of 0–3 hr MG-132 arrested GFP-PIGS expressing embryos followed by LC-MS/MS analysis. The associated Western blot is shown in Figure 4.13, demonstrating the negativity of the assay in all samples – total extract, high speed supernatant, depleted and pellet compared with EB1-GFP used as a control. Again, it is not clear why the anti-GFP Western failed to identify GFP-PIGS when the embryos showed expression via immunofluorescence. It is possible that the level of protein expression in these embryos is very low (Area = 2.918E8). Nonetheless, given the positive MS result from JVL and bioimage, I chose to continue to analyse the pellet using proteomics.
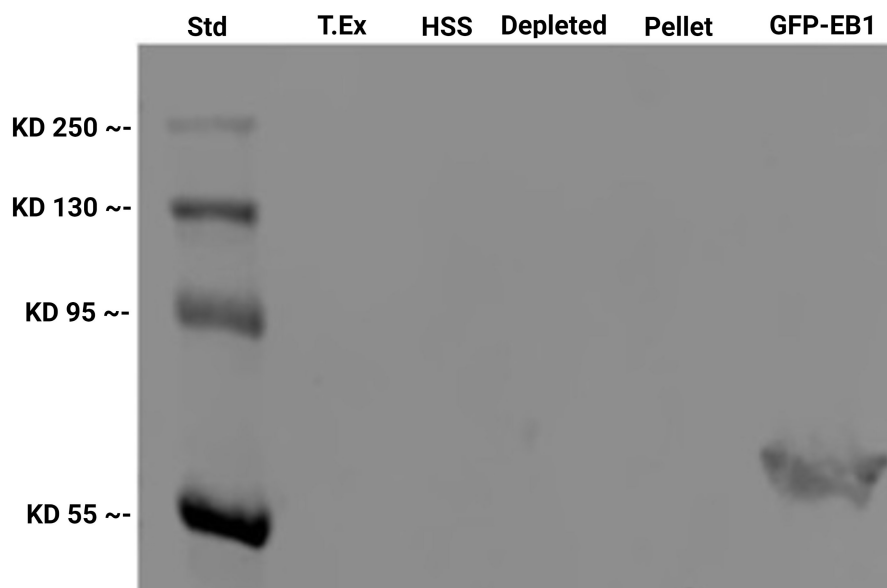
Figure 4.13: **Western blot of GFP-PIGS.** The Western blot has failed to reveal the GFP-PIGS. The bioimage (Figure 4.12) showed the expression of GFP-PIGS in the embryos, but it is not clear whether the reason of anti-GFP Western blot failing to identify GFP-PGS is due to the low expression of GFP-PIGS in the embryos (the area '2.918E8' of the protein was not the highest) or not. Whereas the EB1-GFP used as a control showed the respective band. GFP-PIGS MW ≈ 135 kD and EB1-GFP MW ≈ 59 kD.

Following MS, the identified protein IDs were subjected to the Wakefield-Lab standard bioinformatics (Chapter 2). All remaining protein IDs were sorted by mean abundance and those proteins with an Area/Abundance of 1.3E7 and more were retained in the list. This bioinformatics pipeline resulted in the identification of 75 proteins (Table 4.19). PIGS did not have the highest area (2.918 E8) as expected, however, it was the 3rd most abundant protein present. This suggests the MS results are valid, irrespective of the negative result from the associated Western blot, 74 PIGS interactors were identified.

To further understand the functional relationships between PIGS and its mitotic interactors, I took the 75 proteins and subjected them to GO enrichment analysis (Table 4.20). 3 functional cellular component terms were identified – the RZZ complex, the AP-3 adaptor complex and COPI-coated vesicle. To aid visualisation, the protein-protein interaction software package, Cytoscape was again used. The network constituted the PIGS interacting proteins within the GO-enriched cellular components terms, along with PIGS interacting proteins already identified as enriched EB1-GFP interacting proteins, where the size of the nodes (Figure 4.14) corresponds to the abundance of the protein identified in the PIGS IP. To visually compare my experiment with the known protein-protein interaction data, I added any interactions already present in the biological general repository for interation datasets TheBioGrid database (`https://thebiogrid.org`) (Figure 4.14).

Table 4.19: **PIGS interactors in metaphase.** The table shows proteins that interact with PIGS in metaphase in early *Drosophila* embryos.

Name	Accession	Coverage	# Unique Peptides	# AAs	MW [kDa]	Score	Area
alphaTub84D	FBpp0081062	82.89	14	450	49.9	691.81	9.520E8
26-29-p	FBpp0075508	59.20	29	549	62.1	773.73	6.613E8
pigs	FBpp0070909	17.20	17	977	104.4	219.05	2.918E8
alphaTub67C	FBpp0076122	72.08	25	462	51.1	427.30	2.838E8
ScsbetaA	FBpp0306436	59.42	24	451	49.0	238.53	2.392E8
CG5028	FBpp0084275	66.67	21	402	44.4	303.62	2.289E8
cathD	FBpp0087972	56.38	16	392	42.4	176.20	1.965E8
Drp1	FBpp0077424	54.56	32	735	82.5	232.33	1.361E8
sta	FBpp0070277	73.70	13	270	30.2	116.44	1.131E8
Uba5	FBpp0073354	70.30	16	404	44.1	187.31	9.965E7
CG9953	FBpp0076608	59.65	20	508	56.8	203.18	9.290E7
Cdk1	FBpp0079641	74.75	18	297	34.4	151.41	9.198E7
Mtpalpha	FBpp0079453	67.20	38	744	79.6	282.15	8.851E7
Mtpbeta	FBpp0072135	65.03	22	469	50.6	170.72	8.159E7
Nfs1	FBpp0079874	61.90	25	462	51.0	223.36	6.319E7
wmd	FBpp0072023	60.37	16	328	36.1	107.23	5.999E7
CG11241	FBpp0078188	63.19	24	508	55.8	178.40	5.706E7
B52	FBpp0082270	25.84	10	329	37.5	48.58	5.281E7
r	FBpp0088675	54.41	83	2224	246.5	494.17	5.159E7
me31B	FBpp0079566	68.69	30	428	48.6	170.18	5.159E7
Pdhb	FBpp0084735	67.40	19	365	39.3	135.99	4.676E7
fit	FBpp0083551	20.66	3	121	13.9	43.54	4.564E7
DNApol-epsilon58	FBpp0076789	65.90	27	525	58.7	213.47	4.320E7
Not1	FBpp0111586	21.94	37	2220	249.6	160.07	4.004E7
DNApol-delta	FBpp0075277	48.17	41	1092	124.8	176.46	3.779E7
CG7461	FBpp0289511	57.74	27	627	68.3	192.05	3.663E7
Rab1	FBpp0083503	63.90	7	205	22.7	59.87	3.508E7
eIF2beta	FBpp0075700	25.96	6	312	35.2	31.76	3.438E7
Apl	FBpp0303948	40.70	30	1059	118.8	190.05	3.065E7
coro	FBpp0085526	44.89	14	528	57.2	151.41	3.049E7
Rab4	FBpp0086008	51.64	8	213	23.6	32.63	2.904E7
HDAC6	FBpp0290988	42.02	24	883	98.2	147.84	2.868E7
Hmgcl	FBpp0078979	60.68	12	323	34.2	74.81	2.820E7
beta'COP	FBpp0080048	42.01	27	914	102.6	159.18	2.772E7
alphaCOP	FBpp0072693	47.97	47	1234	139.2	226.68	2.613E7
14-3-3epsilon	FBpp0082987	61.07	13	262	29.8	63.05	2.607E7
Drice	FBpp0084848	39.23	9	339	37.3	47.30	2.558E7
Fs(2)Ket	FBpp0294037	55.20	31	884	98.6	253.06	2.350E7
HDAC1	FBpp0073173	41.46	15	521	58.3	105.07	2.270E7
Torsin	FBpp0070658	44.71	12	340	38.1	65.93	2.267E7
Cp1	FBpp0086717	44.57	13	341	37.9	64.64	2.194E7
Dcp-1	FBpp0071971	44.89	10	323	35.9	53.82	2.185E7
CG4858	FBpp0077868	38.46	7	260	28.2	58.37	2.171E7
eff	FBpp0082477	48.98	6	147	16.7	32.57	2.063E7
smid	FBpp0304233	22.09	13	910	100.2	61.25	2.039E7
pic	FBpp0082177	46.14	35	1140	126.0	169.92	2.006E7
Lst8	FBpp0071303	46.96	11	313	35.3	54.10	2.005E7
betaCOP	FBpp0074348	33.71	24	964	107.3	132.48	1.979E7
Nup205	FBpp0074568	37.49	55	2067	232.6	279.05	1.904E7
UQCR-C2	FBpp0075069	71.36	20	440	45.4	106.78	1.892E7
lds	FBpp0081255	29.12	28	1061	118.3	108.55	1.863E7
rig	FBpp0085564	25.43	26	1235	137.7	96.20	1.860E7
Rab2	FBpp0085458	63.38	11	213	23.5	49.83	1.810E7
ben	FBpp0073686	52.32	7	151	17.2	51.59	1.791E7
CG8778	FBpp0086993	34.78	8	299	31.9	30.69	1.755E7
Chc	FBpp0073966	37.78	46	1678	191.1	231.62	1.751E7
Ranbp9	FBpp0081862	52.06	35	1018	114.3	193.31	1.680E7
eIF6	FBpp0072144	44.08	6	245	26.5	45.62	1.596E7
Rab5	FBpp0077475	41.55	7	219	23.9	35.59	1.580E7
RpII140	FBpp0082353	40.05	37	1176	134.0	172.17	1.540E7
Zw10	FBpp0070425	37.31	18	721	82.2	91.18	1.538E7
larp	FBpp0088624	13.99	10	965	106.2	54.60	1.505E7
yl	FBpp0073714	14.04	17	1937	214.8	129.93	1.456E7
hpo	FBpp0085688	20.33	11	669	75.1	44.86	1.448E7
CG5026	FBpp0076242	34.03	14	620	68.5	48.88	1.437E7
eIF3m	FBpp0086705	44.19	12	387	44.1	72.03	1.425E7
GCC185	FBpp0112136	26.70	26	1135	130.0	101.05	1.422E7
cm	FBpp0070992	51.08	14	415	46.8	53.21	1.418E7
NAT1	FBpp0086900	15.36	14	918	104.4	47.20	1.402E7
Uba1	FBpp0302038	50.10	32	1008	111.7	176.62	1.387E7
g	FBpp0073673	24.95	17	1034	114.7	80.24	1.370E7
Cbp80	FBpp0070651	34.50	20	800	93.2	91.20	1.361E7
Cam	FBpp0087109	56.38	6	149	16.8	36.44	1.330E7
rod	FBpp0085156	34.27	51	2089	239.5	263.55	1.317E7
Smyd4-4	FBpp0087091	37.87	15	573	66.5	58.66	1.309E7

Table 4.20: **PIGS GO Enrichment Analysis.** The table shows PIGS interactors as cell components after GO Enrichment Analysis.

GO cellular component complete	Reference List (13811)	PIGS IP	Expected	Fold Enrichment	P-value	FDR	Proteins
RZZ complex (GO:1990423)	3	2	0.02	> 100	2.85E-04	1.27E-02	Rod, Zw10
AP-3 adaptor complex (GO:0030123)	4	2	0.02	92.07	4.26E-04	1.59E-02	G, Cm
COPI-coated vesicle (GO:0030137)	8	3	0.04	69.05	2.42E-05	2.03E-03	alphaCOP, betaCOP, beta'COP
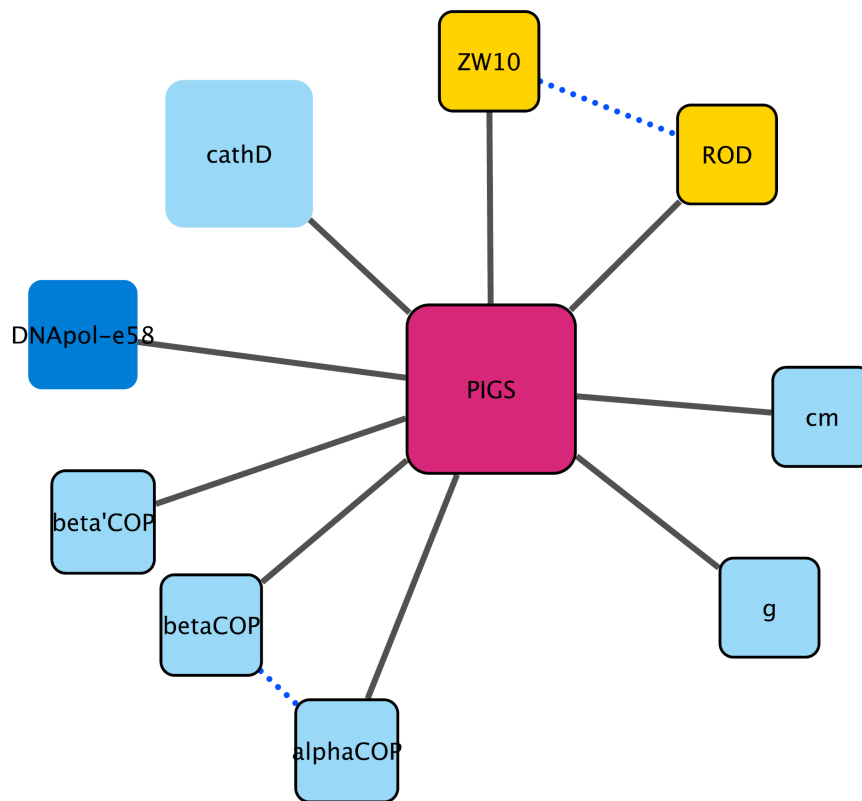
Figure 4.14: **PIGS interactors in metaphase.** The figures shows PIGS binding proteins after BioGrid Analysis for visualising interaction networks. Interactions identified in this experiment are indicated by solid lines and interactions from BioGrid database are shown with dotted lines.

4.8.3 PIGS interacting proteins

To have the final PIGS interacting proteins in metaphase (Figure 4.14), in addition to PIGS binding proteins within GO-enriched cellular components terms (Table, 4.20), I manually chose PIGS binding proteins in metaphase from Table 4.19 that were already identified either as EB1 interacting proteins with a final cut-off of 1.2 fold increase in mitosis (Section 4.4 and Table 4.7) or EB1 interacting proteins within GO term enrichment cellular components (Table 4.2). This analysis indicates the presence of two subunits of the full RZZ complex: ROD and ZW10. The GO analysis also identified further subunits of AP adaptor complex – G and Cnn, as well as the DNAPol epsilon complex component DNAPol-ε 58. However, EB1 was not identified as an enriched interactor of PIGS, despite it being the protein which identified PIGS in the orignial TMT analysis (See Discussion 4.13 for a full explanation of why this might be). For description of PIGS interacting proteins, see Sections 4.3, 4.5.4 and 4.6.4.

4.9 Dynamic localisation and protein-protein interaction network of HOOK in the early *Drosophila* embryo

To determine the localisation and identification of HOOK binding proteins, I crossed female virgins of flies of genotype UASp-HOOK-GFP to matαt-GAL4 males (Table 2.7) for early embryo collection and subsequently live imaging analysis. HOOK is reported to interact with dynein and SPNF-JVL-IK2 complex, However, there are no reports of direct interactions with MTs or with EB1 (See HOOK, Page 95).

4.9.1 Mitotic Localisation of HOOK-GFP

To investigate the dynamic localisation of HOOK-GFP in early embryos, I imaged 1–2 hr old embryos laid by $w; \frac{HOOK-GFP}{+}; \frac{+}{mat\alpha t-GAL4}$ mothers using spinning disc confocal microscopy. Embryos were imaged every 5 seconds across 5 x 1 μm z planes. Image sets were analysed using ImageJ, as maximum intensity projections. 6 movies were taken and analysed to determine the HOOK localisation in the early embryos. As illustrated in Figure 4.15, during nuclear envelope breakdown (NEB), HOOK is concentrated at the centrosomes and also in high-intensity spots throughout the embryo (these spots appear randomly positioned and quite immobile over the course of a movie and likely reflect insoluble, non-functional HOOK-GFP aggregates). Upon nuclear envelope breakdown, HOOK becomes less intense on centrosomes, concentrating in the region of the mitotic spindle. During anaphase HOOK visibly decreases on the centrosomes and in the region of the mitotic spindle. During post-telophase, as nuclei reform HOOK intensity increases at the centrosomes. currently, HOOK is not reported as MT associated protein (Olenick et al. 2016), instead is an adaptor protein that interacts with cytoplasmic dynein motor proteins and JVL-IK2-SPNF complex to regulate vesicle trafficking (Bitan et al. 2010; Krämer and Phistry 1999; J. Liu 2017). The dynamic localisation of HOOK (Figure 4.15) does not

differ much to that of SPN-F (Figure 4.3) and IK2 (Figure 4.6), suggesting its interactions with this complex.

(a) **NEB.**　　(b) **Metaphase.**　　(c) **Met-Anaphase.**　　(d) **Mi-Anaphase.**

(e) **Telophase.**　　(f) **Early interphase.**　　(g) **L. Interphase.**　　(h) **NEB.**
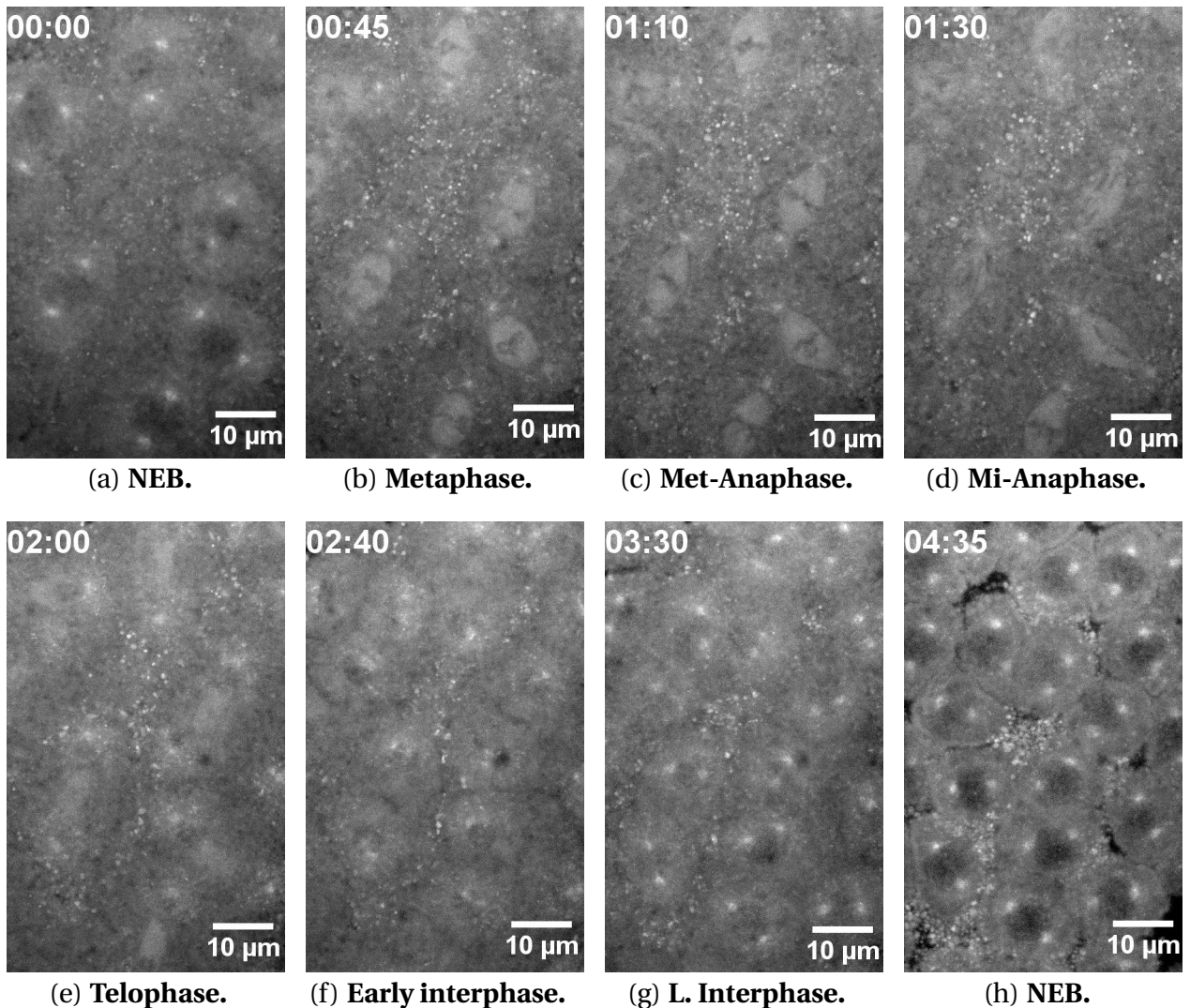
Figure 4.15: **Dynamic localisation of HOOK-GFP in the early *Drosophila* embryo.** To determine HOOK localisation in the early embryo, 6 movies were taken and analysed. As shown in the Figure, during nuclear envelope breakdown (NEB) HOOK is concentrated at the centrosomes. In metaphase HOOK is also localised in the region of the mitotic spindle, in addition to the centrosomes. Beetween metaphase-anapase transition and early interphase, the protein becomes less intense both on centrosomes and mitotic spindle region. During post-telophase, as nuclei reform, this intensity increases at the centrosomes for a new cell cycle.

4.9.2 Identification of the HOOK mitotic interactome

To characterise the HOOK mitotic interactome, I undertook a GFP-TRAP-A purification, using ≈ 0.4 g of 0–3 hr MG-132 arrested GFP-SPN-F expressing embryos followed by LC-MS/MS analysis. The associated Western blot is shown in Figure 4.16, demonstrating the presence of a GFP-positive band at the expected molecular weight, its presence in the GFP-TRAP-A pellet and its complete depletion in the extracts.
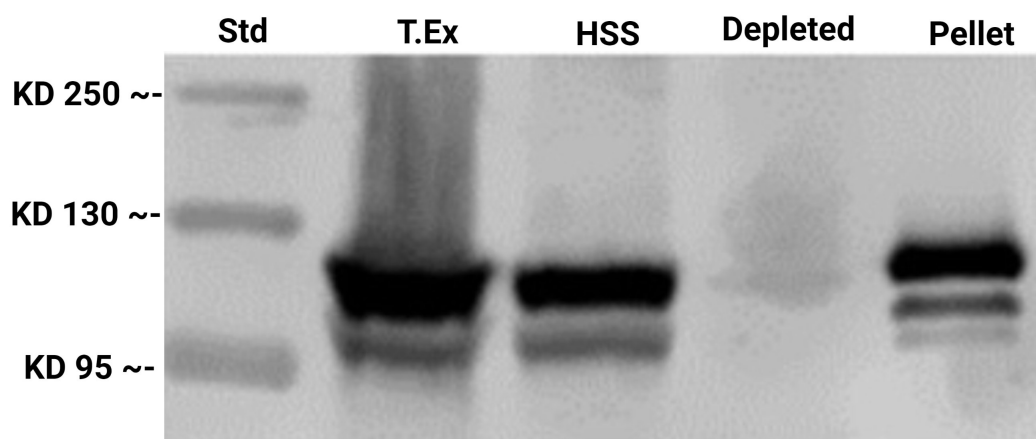
Figure 4.16: **Western blot.** The Western blot indicates the prensece of a GFP-positive band at the expected molecular weight (MW). HOOK-GFP MW ≈ 102 kD.

Following MS, the identified protein IDs were subjected to the Wakefield-Lab standard bioinformatics (Chapter 2). All remaining protein IDs were sorted by mean abundance and those proteins with an Area/Abundance of 1.3E7 and more were retained in the list. This bioinformatics pipeline resulted in the identification of 42 proteins (Table 4.21). HOOK has the highest area (1.78 E10), as expected, confirming the Western blot.

Table 4.21: HOOK interactors in metaphase The table illustrates HOOK interacting proteins in metaphase.

Name	Accession	Coverage	# Unique Peptides	# AAs	MW [kDa]	Score	Area
Hook	FBpp0080722	81.74	66	679	76.6	3978.61	3.792E9
Nurf-38	FBpp0271761	80.00	17	290	32.6	342.27	2.033E8
cbx	FBpp0087538	78.28	17	244	28.1	229.35	1.925E8
Pxt	FBpp0082932	65.64	34	809	90.5	369.12	1.490E8
tsr	FBpp0072097	54.73	12	148	17.1	172.99	1.489E8
26-29-p	FBpp0075508	48.82	22	549	62.1	249.12	1.188E8
cathD	FBpp0087972	48.47	15	392	42.4	123.09	9.908E7
Ubi-p5E	FBpp0070894	77.34	8	534	60.0	81.76	7.068E7
Act88F	FBpp0082597	36.44	2	376	41.7	105.27	5.580E7
Arts	FBpp0075073	45.51	37	1079	120.7	247.28	5.415E7
CG5028	FBpp0084275	55.72	16	402	44.4	157.44	5.361E7
Drp1	FBpp0077424	57.69	35	735	82.5	299.72	4.756E7
Dhc64C	FBpp0073215	54.19	211	4639	529.9	1278.08	4.363E7
Ranbp9	FBpp0081862	48.72	40	1018	114.3	281.65	3.794E7
Got1	FBpp0086371	53.13	19	416	46.1	100.95	3.714E7
Dcp1	FBpp0086717	47.21	14	341	37.9	130.95	3.697E7
CG8036	FBpp0081372	64.14	24	580	63.0	170.95	3.642E7
Sod1	FBpp0075958	80.39	8	153	15.7	111.10	3.581E7
CG9953	FBpp0076608	51.57	19	508	56.8	158.71	3.461E7
Cand1	FBpp0079643	43.51	49	1248	139.3	295.28	3.459E7
Akr1B	FBpp0075870	65.82	19	316	35.9	139.52	3.229E7
GlyS	FBpp0082494	45.28	25	689	79.2	228.93	3.066E7
ArfGAP1	FBpp0075713	33.55	10	468	50.5	53.63	3.033E7
sesB	FBpp0073277	58.86	19	299	32.9	68.21	2.828E7
GCS2alpha	FBpp0070057	59.42	42	924	105.7	271.50	2.787E7
Pgm2a	FBpp0087711	54.25	27	623	69.9	129.94	2.642E7
PCB	FBpp0087539	49.79	45	1197	132.6	248.21	2.411E7
Dlc90F	FBpp0082996	74.77	6	111	12.5	67.25	2.329E7
Dlic	FBpp0073299	44.22	23	493	54.4	134.69	1.984E7
Ranbp16	FBpp0292662	34.45	30	1077	123.1	139.15	1.922E7
Gl	FBpp0075498	41.42	37	1265	141.1	194.80	1.737E7
Impbeta11	FBpp0086416	34.88	29	1075	122.0	144.17	1.678E7
Psa	FBpp0072581	37.18	30	866	99.3	131.27	1.608E7
Sw	FBpp0088420	45.14	17	627	69.5	94.90	1.595E7
Vps4	FBpp0074278	35.75	17	442	49.6	83.49	1.585E7
Nup93-1	FBpp0073659	34.87	24	823	93.8	151.55	1.583E7
Nup205	FBpp0074568	32.75	51	2067	232.6	263.37	1.562E7
DNApol-delta	FBpp0075277	24.18	23	1092	124.8	112.49	1.468E7
CG3558	FBpp0077330	29.18	23	1028	112.4	113.42	1.441E7
CG9485	FBpp0071525	43.84	45	1542	173.5	249.69	1.385E7
CG1598	FBpp0088029	28.57	8	336	37.6	60.88	1.331E7
betaCOP	FBpp0074348	40.77	29	964	107.3	163.34	1.329E7

To further understand the functional relationships between HOOK and its mitotic interactors, I took the 42 proteins and subjected them to GO enrichment analysis (Table 4.22). One functional cellular component term was identified – the cytoplasmic dynein complex. To aid visualisation, the protein-protein interaction software package, Cytoscape was again used. The network constituted the HOOK interacting proteins within the GO-enriched cellular components terms, along with HOOK interacting proteins already identified as enriched EB1-GFP interacting proteins, where the size of the nodes (Figure 4.17) corresponds to the abundance of the protein identified in the HOOK IP. To visually compare my experiment with the known protein-protein interaction data, I added any interactions already present in the biological general repository for interation datasets TheBioGrid database (`https://thebiogrid.org`) (Figure 4.17).

Table 4.22: **HOOK GO Enrichment Analysis.** HOOK interactors after GO Enrichment Analysis which shows subunits of the Dynein/Dynactin complex.

GO cellular component complete	Reference List (13811)	HOOK IP	Expected	Fold Enrichment	P-value	FDR	Proteins
cytoplasmic dynein complex (GO:0005868)	27	3	0.09	32.65	1.39E-04	1.70E-02	Dhc64C, Dlic, Dlc90F*
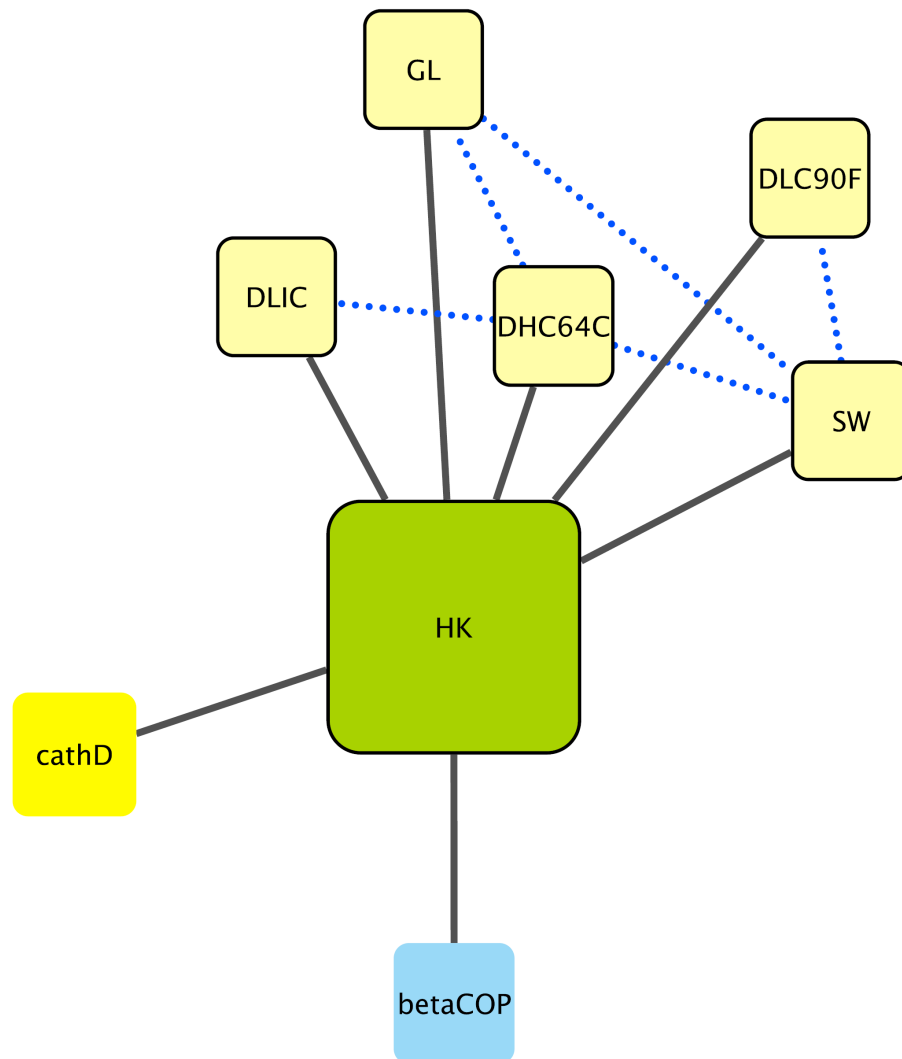
Figure 4.17: **HOOK interactors in metaphase.** The figure shows HOOK interactiong proteins after BioGrid database Analysis, which indicates that HOOK interactors mostly with subunits of the Dynein/Dynactin complex during metaphase. Interactions identified in this experiment are indicated by solid lines and interactions from BioGrid database are shown with dotted lines.

4.9.3 HOOK interacting proteins

To have the final HOOK interacting proteins in metaphase (Figure 4.17), in addition to HOOK binding proteins within GO-enriched cellular components terms (Table, 4.22), I manually chose HOOK interactors in metaphase from Table 4.21 that were already identified either as EB1 interacting proteins with a final cut-off of 1.2 fold increase in mitosis (Section 4.4 and Table 4.7) or EB1 interacting proteins within GO term enrichment cellular components (Table 4.2). As shown in the Figure 4.17, this analysis demonstrates the presence of different subunits, including DLIC, DHC64C, SW and DLC90F which are components of the dynein motor complex in the HOOK-GFP mitotic IP. The GO analysis also

identifed CATH-D which is present within the Top 100 proteins and betaCOP is not within Top 100 proteins although it was in the original EB1-GFP mitotic interactome. Therefore, they are shown in the Cytoscape network in Figure 4.17. However, EB1 was not identified as an enriched interactor of HOOK, despite it being the protein which identified HOOK in the original TMT analysis (See Discussion 4.13 for a full explanation of why this might be). For description of HOOK interacting proteins, see Sections 4.3, 4.5.4 and 4.6.4.

4.10 Dynamic localisation and protein-protein interaction network of SLAM in the early embryo

To determine the localisation, I crossed female virgins of flies of genotype UASp-SLAM-GFP to matαt-GAL4 males (Table 2.8) for early embryo collection and to HisRFP;matαt-GAL4 males (Table 2.9) for live imaging analysis. Studies involved SLM have been conducted in *Drosophila* embryos for its implication in invagination furrow process and regulation of vesicular transport (See NUF-SLAM complex, Page 100). To date, no physical interactions between SLAM and MTs or EB1 have been published.

4.10.1 Mitotic Localisation of SLAM-GFP

To investigate the dynamic localisation of SLAM-GFP in early embryos, I imaged 1–2 hr old embryos laid by $w; \frac{HisRFP}{Cyo}; \frac{SLAM-GFP}{mat\alpha t-GAL4}$ and $w; \frac{HisRFP}{SP}; \frac{SLAM-GFP}{mat\alpha t-GAL4}$ mothers using spinning disc confocal microscopy. Embryos were imaged every 5 seconds across 5 x 1 μm z planes. Image sets were analysed using ImageJ, as maximum intensity projections. 4 movies were taken and analysed for dynamic localisation of the protein. As shown in Figure 4.18, during mitosis, SLAM is concentrated at the metaphase furrows throughout the cell cycle, which prevents interactions between astral MTs from neighbouring mitotic spindles (Tram et al. 2002). This localisation is in perfect agreement with studies previously reported in literature (Acharya et al. 2014; Otani et al. 2011).

(a) **Early inter-phase.** (b) **L. Interphase.** (c) **NEB.** (d) **Metaphase.**

(e) **Early inter-phase.** (f) **L. Interphase.** (g) **NEB.** (h) **Metaphase.**

(i) **Met-Anaphase.** (j) **Mid-Anaphase.** (k) **Telophase.** (l) **Early inter-phase.**

(m) **Met-Anaphase.** (n) **Mid-Anaphase.** (o) **Telophase.** (p) **Early inter-phase.**
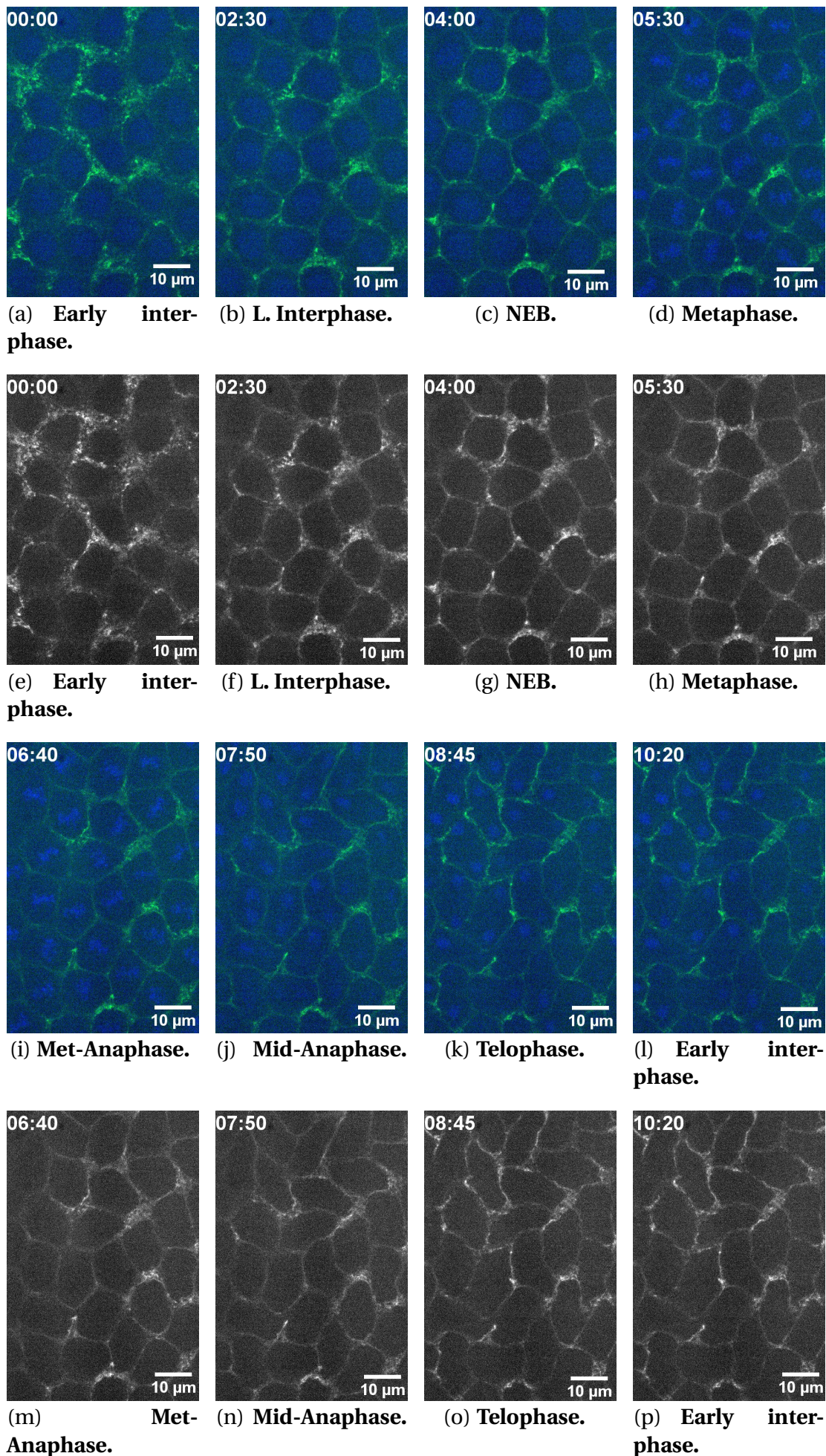
Figure 4.18: **Dynamic localisation of SLAM-GFP in the early *Drosophila* embryo.** For dynamic localisation, 4 SLAM movies were taken and analysed. As shown in the Figure, during mitosis, SLAM is concentrated to the metaphase furrows throughout the cell cycle, which is consistent with its functions during cell division (Acharya et al. 2014; Tram et al. 2002).

4.10.2 Identification of the SLAM mitotic interactome

In order to characterise the SLAM mitotic interactome, I undertook a GFP-TRAP-A purification, using ≈ 0.4 g of 0–3 hr MG-132 arrested SLAM-GFP expressing embryos followed by LC-MS/MS analysis. The associated Western blot is shown in Figure 4.19, demonstrating the absence of a GFP-positive band at the expected molecular weight. As with previous negative Western blot results, however, I decided to continue to subject the pellet to mass spectrometry.
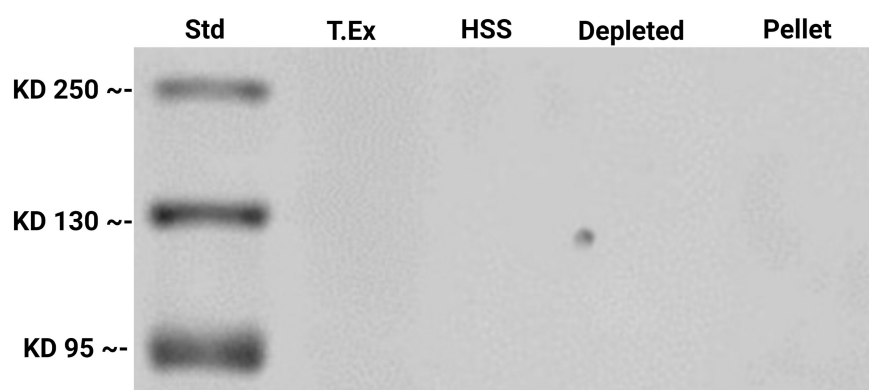
Figure 4.19: **Western blot.** The Western blot shows the absence of a GFP-positive band at the expected molecular weight. SLAM-GFP MW ≈ 156 kD.

Following MS, protein IDs were not identified, strongly suggesting that the IP did not successfully pull down either SLAM or SLAM interacting proteins, despite expressing the SLAM-GFP transgene.

4.11 Evaluating the EB1-GFP Protein-Protein interaction network using cytoscape

The final GO enrichment analysis of EB1-GFP binding protein-protein interaction network is shown in Figure 4.20. As illustrated in the Figure, the SPNF-JVL-IKK-ε complex is in the centre of this protein-protein interaction network. The complex interacts physically with cellular components – I) with all three subunits, the complex interacts with RZZ complex and COPI-coated vesicle, II) through IKK-ε and JVL, it interacts with nuclear pore complex, apical-medical cortex, signal recognition complex, retromer complex and spectrosome, III) via SPN-F and IKK-ε, the complex binds to cytoplasmic dynein complex and ER membrane insertion complex, IV) through SPN-F, the complex interacts with GID complex, V) through IKK-ε, the AP-1 adaptor and Myosin V complexes interact with the complex. In addition, the complex also interacts indirectly with some of these cellular components, for example – I) through NUF, the complex interacts with cytoplasmic dynein complex which is reported to be involved in vesicle trafficking, which is important for metaphase furrow formation (Figure 4.21). II) HOOK mediates the interaction between the JVL-IK2-SPNF complex and cytoplasmic dynein complex, and nuclear pore complex. III) through RZZ complex, the complex interacts with PIGS, which also connects AP-3 adaptor complex and COPI-coated vesicle.
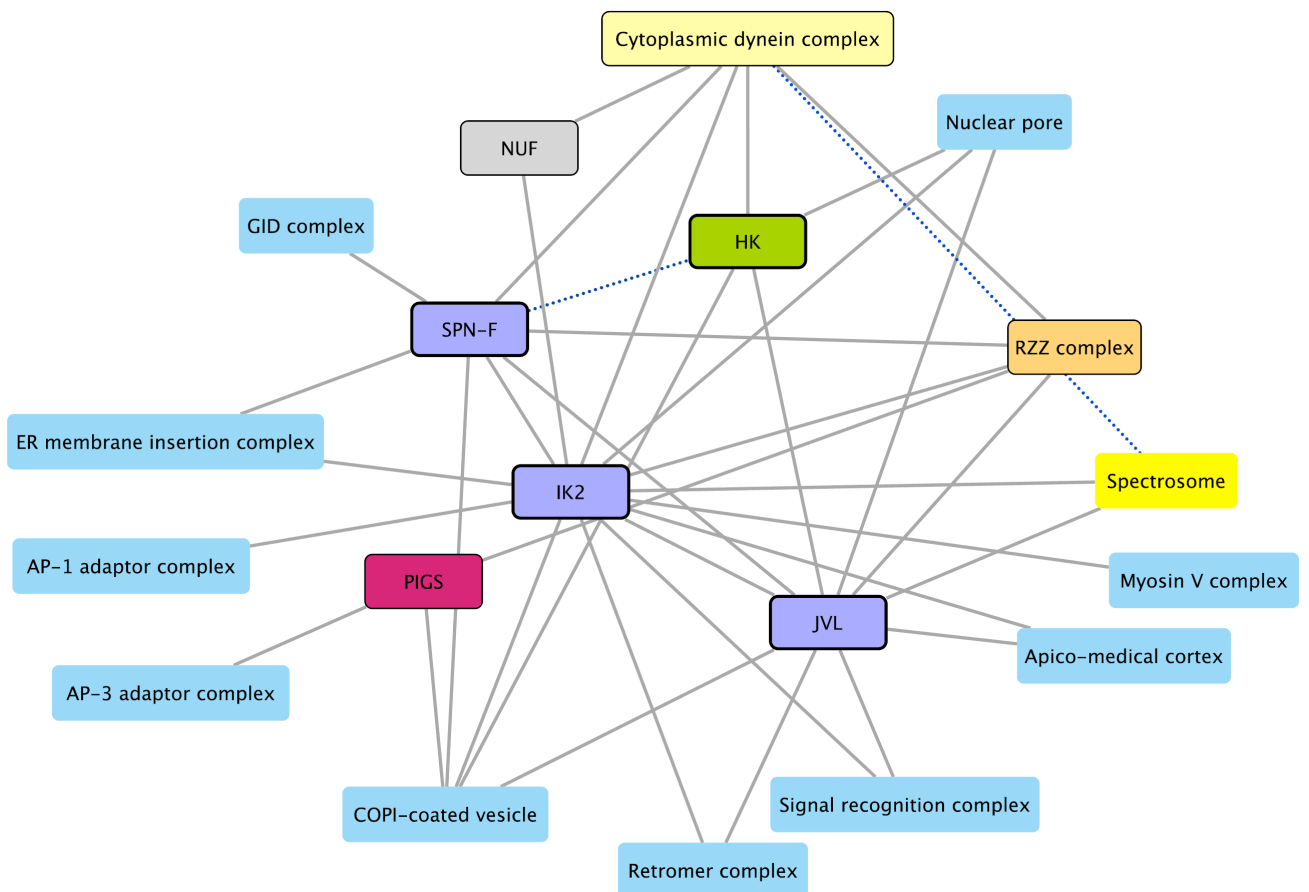
Figure 4.20: **SPNF-JVL-IKK-HK-PIGS complex.** The figure shows SPNF-JVL-IKK-espsilon complex interactions with cellular components identified in the AP-MS.

(a) Interphase

(b) Prophase

(c) Metaphase

(d) Anaphase

(e) Telophase
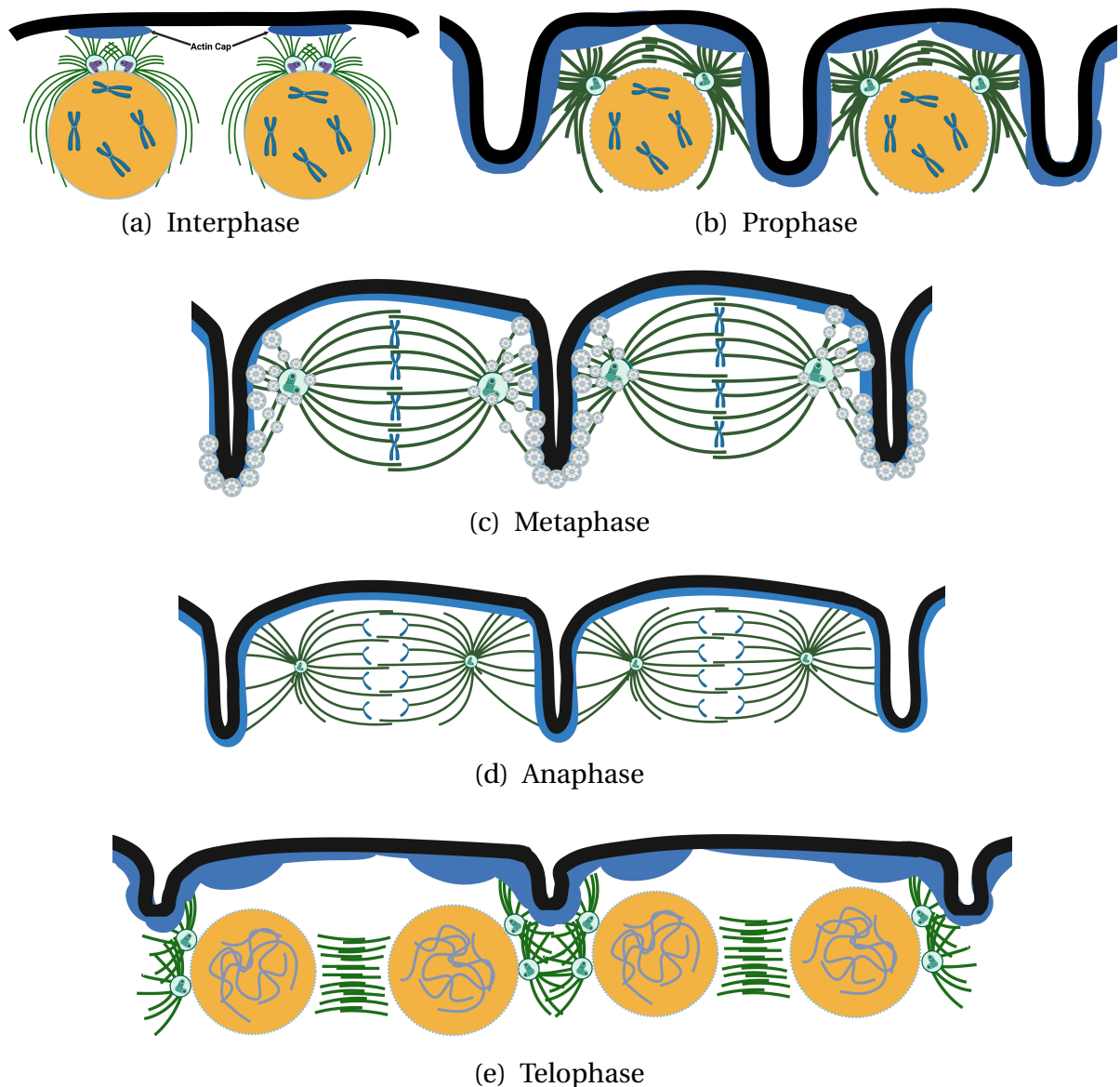
Figure 4.21: **Illustration of metaphase furrow formation during mitosis.** During interphase 4.21(a), the actin concentrates apically into actin caps above each nucleus and its pair of the centromosomes. During prophase progression 4.21(b), the centrosomes separate toward opposite poles and the actin caps redistribute and outiline each nucleus, along with its associated separated centrosome pair. At metaphase 4.21(c), the furrows invaginate to a depth of $\approx 10~\mu$m to form a shell that encompasses each mitotic spindle. These furrow structures have the same composition as cytokinesis furrows, these include actin, myosin II, spectrins, anillin, septins and formins. The furrow invagination is driven by fusion of vesicles that originate from the centrosome-associated recycling endosome and these vesicles provide a source of membrane, and components of the metaphase furrow structures, such as actin remodellers, spectrins, formins, anillin and myosin II. In my experiments, some EB1 interactors identified are known to play important role in this process of furrow invagination, such as Nuf, Dynein complex and Rab11. In addition, my investigations suggest also the involvement of other EB1 interactors, these include SPN-F, IKK-ε, JVL, HOOK and PIGS proteins (Figure 4.20). The chromosome segregation progresses into anaphase 4.21(d), at late anaphase and telophase 4.21(e), the metaphase forrows undergo a dramatic and rapid regression to reform an initial state of interphase 4.21(a).

4.12 Evaluating the degree of overlap between different datasets using Venn diagram.

Finally, I used a Venn diagram to further visualise relationships between various EB1 binding proteins (SPN-F, JVL, IK2, HOOK and PIGS). As shown in Figure 4.22 and Table 4.23, JVL ∩ IK2 shows the highest concentration of the overlapping cellular components, in which 10 components resulted overlapped (COPI-coated vsicle, SPN-F, JVL, IK2, RZZ complex, nuclear pore, signal recognition, apico-medical cortex, spectrosome and retromer complex) and the lowest degree is HOOK ∩ PIGS with 1 component overlapped (COPI-coated vesicle).

The degree of overlapping JVL ∩ SPN-F ∩ IK2 cellular components is 5 (COPI-coated vesicle, SPN-F, JVL, IK2 and RZZ complex), which strongly suggest to be a physical and functinal complex. In addition, HOOK shares also similarity with 5 components overlapped with each of subunits of JVL-SPNF-IK2 complex and with whole complex, suggesting that HOOK is functionally part of the whole complex. In contrast, PIGS with lowest degree of overlapping, 1 with HOOK (COPI-coated vesicle) and 2 with JVL-SPNF-IK2 complex (COPI-coated vesicle and RZZ complex) is less likely to be part of the entire complex.
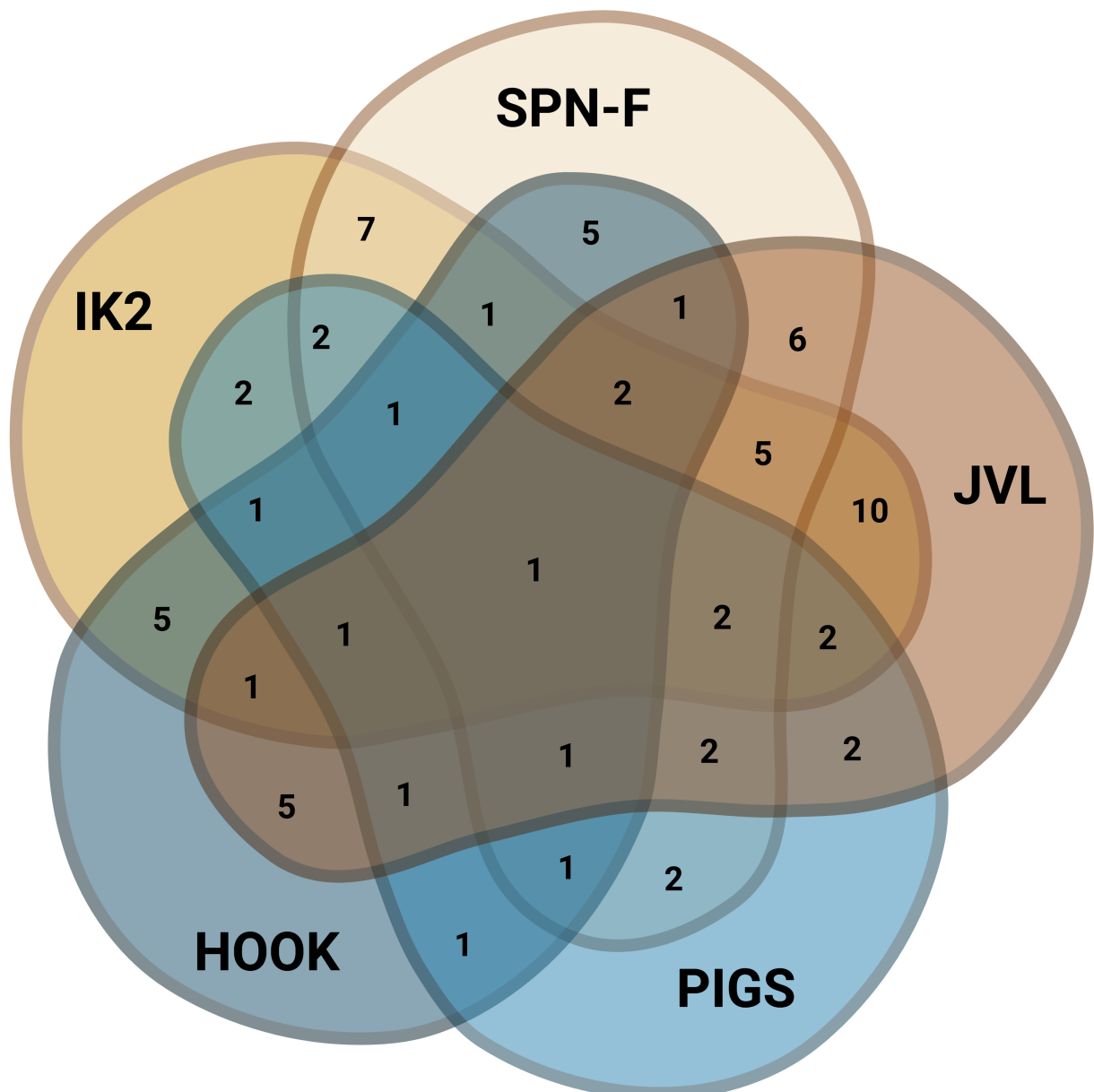
Figure 4.22: **Venn diagram of the overlapped EB1-GFP protein-protein interaction network.** The diagram shows the degree of overlap between different datasets. The degree of overlapping (10) of JVL ∩ IK2 is the highest (COPI-coated vesicle, SPN-F, JVL, IK2, RZZ complex, nuclear pore, signal recognition, apico-medical cortex, spectrosome and retromer complex). The degree of overlapping between HOOK, JVL, IK2 and SPN-F is 5 (Table 4.23) suggesting their functional link as a whole complex. However, the lowest degree of overlapping, 1 (COPI-coated vesicle) between PIGS and HOOK or 2 (COPI-coated vesicle and RZZ complex) between PIGS with PIGS and JVL-SPNF-IK2, suggest that PIGS is likely less to be part of the whole HOOK-SPNF-JVL.IK2 complex.

Table 4.23: **Illustrastion of different cellular components overlapped with various EB1 interactors in metaphase.** The table shows different cellular components, which resulted overlapped with EB1 binding proteins (SPN-F, JVL, IK2, HOOK and PIGS). SPN-F ∩ JVL ∩ IK2 ∩ HOOK ∩ PIGS = 1. SPN-F ∩ JVL ∩ IK2 ∩ HOOK = 2. SPN-F ∩ JVL ∩ IK2 ∩ PIGS = 2. SPN-F ∩ JVL ∩ HOOK = 1. SPN-F ∩ IK2 ∩ HOOK = 1. SPN-F ∩ IK2 = 7. SPN-F ∩ JVL ∩ IK2 = 5. JVL ∩ IK2 ∩ HOOK = 1. JVL ∩ IK2 = 10. SPN-F ∩ JVL = 6. IK2 ∩ PIGS = 2. JVL ∩ PIGS = 2. SPN-F ∩ PIGS = 2. SPN-F ∩ JVL ∩ PIGS = 2. HOOK ∩ PIGS = 1. JVL ∩ HOOK ∩ PIGS = 1. JVL ∩ HOOK = 5. SPN-F ∩ HOOK ∩ PIGS = 1. SPN-F ∩ HOOK = 5. JVL ∩ IK2 ∩ PIGS = 2. JVL ∩ IK2 ∩ HOOK ∩ PIGS = 1. IK2 ∩ HOOK ∩ PIGS = 1. IK2 ∩ HOOK = 5. SPN-F ∩ IK2 ∩ PIGS =2. SPN-F ∩ IK2 ∩ HOOK ∩ PIGS = 1.

SPN-F	JVL	IK2	HOOK	PIGS
COPI-coated vesicle	COPI-coated vesicle	COPI-coated vesicle	COPI-coated vesicle	COPI-coated vesicle
SPN-F	SPN-F	SPN-F	SPN-F	
JVL	JVL	JVL	JVL	
RZZ complex	RZZ complex	RZZ complex		RZZ complex
IK2	IK2	IK2		
HOOK	HOOK		HOOK	
Cytoplasmic dynein complex		Cytoplasmic dynein complex	Cytoplasmic dynein complex	
ER membrane insertion complex		ER membrane insertion complex		
	Nuclear pore	Nuclear pore	Nuclear pore	
	Signal recognition complex	Signal recognition complex		
	Apico-medical cortex	Apico-medical cortex		
	Spectrosome	Spectrosome		
	Retromer complex	Retromer complex		

4.13 Discussion

The EB1-GFP protein used as a bait, was purified from early *Drosophila* embryos at very high mean abundance during mitosis (Tables 4.1). This Table indicates that EB1 physically interacts with over 100 proteins during metaphase. Among these interactors, those of most interest are summarised in Table 4.7, in which EB1 binding proteins are grouped together by their functional and/or physical interactions. Dynein/Dynactin complex is a MT minus-end directed motor complex implicated in transporting different cargoes to the minus ends, and DHC64C, which constitutes the dynein heavy chain was the most abundant EB1 interactor. During metaphase, this complex is important to silence the spindle assembly checkpoint through interaction with RZZ complex, carrying subunits of the complex from kinetochores towards the MT minus ends present

at the spindle poles consequently triggering the onset of anaphase (Mosala-
ganti et al. 2017; Pereira et al. 2018). The Dynein/Dynactin complex is also
crucial in endosomal trafficking, which is essential for membrane invagination
during mitosis. Furthermore, the presence of immobilised Dynein/Dynactin at
the cell cortex during mitosis is used as a force generator, contributing centro-
some separation. To date, no studies have reported how the Dynein/Dynactin
complex localises to the MT plus ends or how it facilitates the interactions be-
tween EB1 and RZZ complex. However, my results suggest that in metaphase,
the Dynein/Dynactin complex may be transported to the MT plus ends by EB1.
Dynein/Dynactin complex is already known as EB1 interactor (Berrueta et al.
1999; Watson and Stephens 2006) and taking into account that Dynein/Dynacting
complex is a MT minus end directed and most of its subunits were pulled down
via EB1 with high abundance, for example within EB1 interactors in top 100
(Table 4.1), DHC64C was the most abundant subunit identified, suggesting its
strong interaction with EB1 in metaphase. Given the presence of an SxIP motif
at N-terminus of ROD (Table 4.4), EB1 may therefore directly mediates the bind-
ing of the Dynein/Dynactin complex to the RZZ complex. This hypothesis could
be tested through additional AP-MS studies, including ROD and DHC64C. These
studies can be complemented by gel filtration chromatography, cleavable affin-
ity purification (Cl-AP) and yeast two-hybrid system (Y2H) for comfirmation of
direct interaction.

Much of the work presented in the second part of this Chapter used Affin-
ity Purification Mass Spectrometry (AP-MS) from embryos expressing GFP (or
mCh) tagged versions of proteins identified as EB1 interactors (SPN-F, JVL, IKK,
PIGS and HOOK). The results suggest a physically and functionally linked net-
work and yet, in all cases, EB1 was not identified as a reciprocal interactor. This
protein functions as a dimer *in vivo* and one of its two calponin homology (CH)
domains binds non-covalently to the corner and interacts with four tubulins of

two adjacent protofilaments, whereas the other CH domain stays in the next corner of four tubulin dimers without participating in the interactions between EB1 dimer and MTs (Luo et al. 2014; Maurer et al. 2012; Zhang et al. 2015). These domains are large, about 130 residue amino acids (Figure 1.8) although all residues may not be involved in interactions with MTs. Furthermore, one CH domain interacting with four adjacent tubulin dimers may generate a large network of non-covalent interactions with MTs, resulting in strong interactions. While the end-binding homology domain of EB1 is much smaller, about 30 residue amino acids (Figure 1.8 and Table 1.4) which may generate fewer non-covalent interactions with EB1 binding proteins, consequently this creates weak interactions. This is obvious, EB1 must associate firmly with MTs as it recruits a plethora of its binding proteins during mitosis to regulate the dynamic instability. This is consistent with what was stated by Honnappa et al. (2009) that interactions between EB1 and its interacting proteins are weak. Then, the interactions between these proteins and EB1 may not be strong enough to pull down EB1 in AP-MS assay. Alternatively, these EB1 interactors were pull down indirctly with other proteins, such as Dynein/Dynactin complex, since reciprocal AP-MS identified subunits of this complex as their common interactors.

However, it is less likely that EB1 interacting proteins were pulled down indirectly with MTs, because the experiment was conducted at 4 °C which does not allow the MT formation, as confirmed by no enrichment of tubulin in results. In this experiment, more than 1/3 EB1 binding proteins have previously shown ralationships with EB1 and/or MT functions (Section 4.3). Therefore, considering all these together, the data strongly suggests that EB1 interactors were not pulled down indirectly, and it is a valid dataset which demonstrates the *in vivo* mitotic EB1 interactome.

Each of three subunits: SPN-F, JVL and IK2 IP, pulled down the other components of the SPNF-JVL-IK2 complex, which is consistent with their physical interactions within the complex. In addition, each component of the complex interacts with subunits of the dynein motor protein or with its adaptor, including CTP, Rab1, Rab5, and Rab7. The SPNF-JVL-IK2 complex further interacts with RZZ complex, with COPI-coated vesicles, and with CATH-D. These interactions support their role as a functional complex. Due to their involvement in invagination furrows and requirement of vesicular membranes by SPNF-JVL-IK2 complex during mitosis, my speculation is that these vesicles are carried by the Dynein/Dynactin complex and handed to SPNF-IK2-JVL complex in the transient membrane by interaction with CTP subunit and Rab adaptor proteins. This assumption is supported by the fact that HOOK, which physically interacts with SPNF-JVL-IK2 complex and PIGS which does not interact with the complex, have indicated COPI-coated vesicles as their respective interactors. Consequently, this suggests that SPN-F, JVL, IKK-ε, PIGS and HOOK act functionally as a whole complex. These observations are in agreement with studies conducted by Lu et al. (2020), who domonstrated that through SPN-F and CTP, HOOK physically interacts with SPNF-JVL-IK2 and Dynein/Dynactin complexes, respectively. PIGS, which is a Gas2-like protein is implicated in linking MTs to cytoskeletal network (Takács et al. 2017; Voelzmann et al. 2017; yue et al. 2017). Gel filtration chromatography could be used to investigate these components as part of a whole complex (Bai 2015).

In summary, immunoprecipitation followed by TMT-MS/MS is a sensitive, accurate and selective approach to identify and quantify proteins (Aebersikd and Mann 2016; Richards et al. 2015) used in my experiments. In agreement with these experiments, I found a robust enrichment of gene ontology terms (GO) among various EB1 interactors, pointing to good relationships among these interacting proteins (Ashburner et al. 2000) and these connections were also

confirmed through Venn diagram showing high degree of overlapping among proteins in analysis. Thus, this investigation, indicates that IK2-JVL-SPN-F and Dynein/Dynactin complexes, PIGS and HOOK proteins are EB1 interactors or can be considered as potential candidates for EB1 binding proteins in early *Drosophila* embryos during metaphase-anaphase transition.

However, numerous non-specific binding proteins or contaminants can be co-purified together with the protein of interest. To overcome this limitation, I subjected my TMT-MS/MS results to computational comparison with control experiments previously carried out by Wakefield lab members, which allowed me to exclude false interactors. Alternatively, the recently described cleavable Affinity Purification (Cl-AP) approach from our lab could be used. In this approach, a reagent comprising Protein A sepharose beads and GFP TRAP covalently linked by a short molecule, containing a reducible S-S moiety allows for purification of GFP-tagged protein complexes from embryos. Incubation with 50mM DTT reduces the S-S, specifically cleaving the purified protein complex from the beads for in vitro assays or Mass Spectrometry. As any contaminating or non-specific proteins are retained on the beads, this could verify the results obtained here. Alternatively, studies using gel filtration for fractionating extracts of embryos expressing these proteins fused with GFP tag, prior to AP-MS and complemented by Western blot, should be used to further confirm that these components are really part of the whole complex. Finally, binary protein-protein interactions could be investigated using yeast two-hybrid system (Brückner et al. 2009; Rajagopala 2015; Yugandhar et al. 2020).

Chapter 5: Investigating novel mitotic interactors of EB1 in the early *Drosophila* embryo

5.1 Introduction

In the previous Chapter, I identified CG12702, CORN and two subunits of the DNApol-ε complex as new EB1 associated proteins in metaphase, as determined by immunoprecipitation and TMT-MS/MS. A Bioinformatics analysis also demonstrated that the DNApol-ε complex possesses EB1 interacting domains (Table 4.4). However, this does not exclude that other proteins without EB1 motifs cannot interact with EB1, as the immunoprecipitation would have identified both direct and indirect EB1 interacting proteins and as more EB1 binding regions may yet exist.

So far, nothing is known about functions of these *Drosophila* proteins during mitosis. However, the human orthologue of CG12702, as determined by Flybase (`https://flybase.org/`) is termed cancerous inhibitor of protein phosphatase 2A (CIP2A) and is found in high concentration in cancer cells (Jeong et al. 2014; Kim et al. 2013). Moreover, CG12702 is reported to interact with Rab2 and Rab6, which are Dynein/Dynactin complex adaptors, and Cdc23, a component of the anaphase-promoting complex (APC/C); an E3 ubiquitin ligase important for the progression of cells from metaphase to anaphase (Bassermann et al. 2014; Bochis et al. 2015; Golsteyn et al. 1995).

CORN has been described as a MT binding protein, functioning in the regulation of exocytosis (Cramer 2000; Finan et al. 2011; Hasson 2003). It has been demonstrated to interact with Jaguar (jar), Inscuteable (insc) and β-Tub56D (Finan et al. 2011; Kraut et al. 1996). Jar works with CLIP-190 in regulating interactions between actin and MTs and may be implicated in vesicle transport, as well (Finan et al. 2011). Insc is essential for recruiting MT binding proteins to the apical cell cortex to promote apical-basal spindle orientation (Bulgheresi et al. 2001).

Finally, the DNApol-ε 58 is part of DNApol-ε complex, which include DNApol-ε 255, DNApol-ε subunit 3 (Chrac-14) and DNApol-ε subunit 4 (Mes4) (Burgess and Zhang, Z. 2010; Marygold et al. 2020). DNApol-ε 58 and 255 are catalytic subunits which are involved in DNA replication and repair (Oshige et al. 2000; Sahashi et al. 2013), whereas, Chrac-14 and Mes4 are involved in DNA replication-coupled nucleosome assembly (For review see Burgess and Zhang, Z. 2010; Marygold et al. 2020). However, the role of the DNApol-ε complex in metaphase is unknown.

Given the above evidence, but the lack of any data verifying a physical or functional link between these proteins and EB1 in metaphase, I decided to engineer transgenic flies to express GFP-fusions of CG12702, CORN and DNApol-ε 58 in the early *Drosophila* embryo. In this Chapter, I describe their localisation, interacting partners and investigate the consequences of inhibiting EB1and EB2 function via interfering antibody injection.

5.2 Generating new transgenic *Drosophila* to express GFP-fusions of novel EB1 interacting proteins: CG12702, CORN and DNApol-ε 58

To investigate novel mitotic EB1 interacting proteins, I designed DNA constructs that placed the cDNA sequences of *Drosophila* CG12702, CORN or DNApol-ε 58, fused with the cDNA sequence of GFP upstream. Following their synthesis and cloning into pPGW (DGRC; `https://dgrc.bio.indiana.edu//stock/1077`) a standard *Drosophila* vector that places the fluorescent transgene under the control of the germline optimised UASp promoter (Chapter 2, Section 2.3.8). The final constructs were validated and sent to BestGene for microinjection and random integration into w^{1118} embryos. Random integration was chosen, rather than attP platform insertion, in order to generate a series of lines whose expression might vary. In this way, the expression of the transgene can be tuned during the early syncytial cycles. Transgenic flies possessing mini-white (red eyes) were selected, crossed to w^{1118} male or virgin females and the chromosomal insertion determined. 4 such fly lines for CG12702 and 10 lines of CORN and DNApol-ε 58 were recovered.

For each gene, 2 lines with the darkest eye colour, likely corresponding to those which would deliver the highest expression were chosen for further characterization. Virgin females of these lines were crossed to homozygous flies that express GAL4 under the maternal-α-tubulin promoter (matαt-GAL4 flies). Then, 1–2 hour old embryos laid by the resultant flies were hand dechorionated and imaged using confocal spinning disc microscopy. In addition, batches of 0–3 hr old embryos were dechorionated using bleach for 1–2 minutes, treated with MG132 to arrest in metaphase and processed for immunoprecipitation, followed by TMT-MS/MS and Western blot, to identify their interactors in metaphase and verification of protein isolation.

5.3 Mitotic localisation and attempted IP of CG12702

To determine the dynamic localisation of CG12702, two independent sets of virgin females express ing GFP-CG12702 were crossed to homozygous flies that express GAL4 under maternal-α-tubulin promoter (Table 2.10). Then embryos with age 1–2 hours from offspring of this cross were dechorionated and imaged. Disappointingly, no specific localisation was observed at any stage of the cell cycle, or at any aged embryo for either fly line. Instead, discrete punctae of varying size and intensity were observed (Figure 5.1(a)). It is not clear whether these punctae correspond to autofluorescence of yolk granules or lipid droplets, or aggregates of GFP-CG12702. To assess whether GFP-CG12702 was being correctly expressed in embryos I performed a Western blot, probing with anti-GFP antibody (Figure 5.1(b)). This Westen blot indicates a protein of the correct predicted size ($\approx$ 125 kD) is expressed in these embryos. However, the embryos did not show any specific localisation when imaged using the spinning disc confocal microscope. Discrete dots of fluoresence, possibly corresponding to aggregates of CG12702-GFP were seen, that varied in size, shape and focal plane.

(a) **Dynamic localisation of CG12702.**   (b) **Western blot of CG12702.**
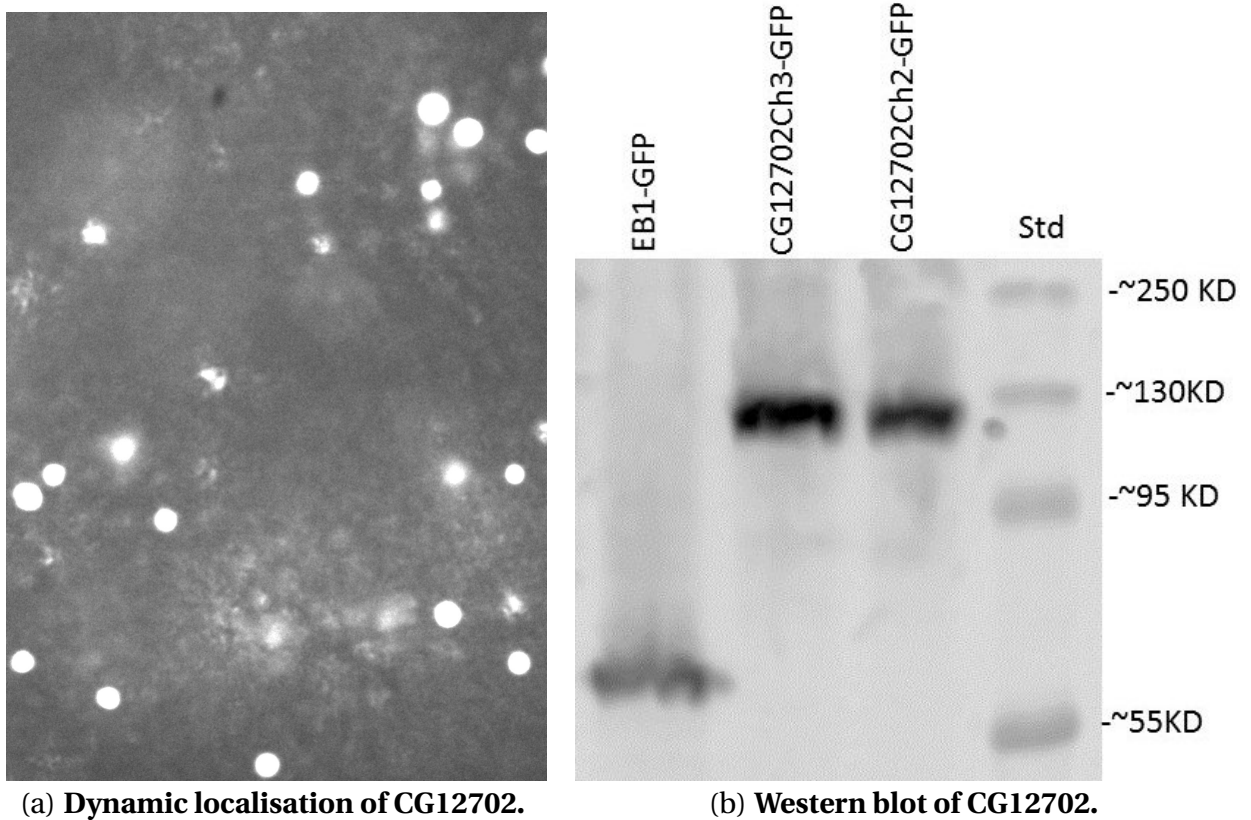
Figure 5.1: **Dynamic localisation and Western blot of CG12702 in the early embryo.** Time-lapse image 5.1(a) does not show a discrete localisation of CG12702 in the early *Drosophila* embryo. Instead, bright fluorescent punctae were observed. However, the Western blot 5.1(b) demonstrates CG12702 expression in syncytial *Drosophila* embryos. EB1-GFP was used as a control and two independent GFP-CG12702 lines, inserted into chromosomes 2 and 3 were tested for expression verification. EB1-GFP and GFP-CG12702 MW ≈ 59 kD and 123 kD, respectively. Probed with anti-GFP antibody (Roche).

Given the lack of localisation, I decided to focus instead on the two remaining transgenic lines and did not take investigations of GFP-CG12702 further.

5.4   Dynamic localisation and protein-protein interaction network of DNApol-ε 58

Two core subunits of the DNApol-ε complex, DNApol-ε 58 and DNApol-ε 255, were identified as being mitosis-specific EB1 interactors. Considering the weight of evidence for their presence as a complex, I decided to make only flies expressing GFP-DNApol-ε 58. Virgin females were crossed to homozygous males expressing GAL4 under maternal-α-tubulin promoter (Tables 2.11 and 2.12). Consequently, embryos aged 1–2 hours were prepared and bioimaged to ascertain the dynamic localisation of the protein (Figure 5.2). As embryos enter mitosis, from nuclear envelope breakdown (Figure5.2(a) and Figure 5.2(l)) GFP-DNApol-ε 58 accumulates in the region of the growing spindle. By metaphase (Figure 5.2(b)), it is clearly present throughout the spindle, but is also present at the centrosomes. Interestingly it is excluded from the mitotic chromosomes (showing as dark regions at the middle of the spindle shape). The spindle localisation is maintained into anaphase (Figure 5.2(d)), where the protein also appears at the anaphase asters. In telophase (Figure 5.2(i)), GFP-DNApol-ε 58 localises in the reforming nuclei but is also seen at the central spindle MTs, between the nuclei. During interphase (Figure 5.2(k)) DNApol-ε 58 is localised in nuclei, as expected for a DNA polymerase.
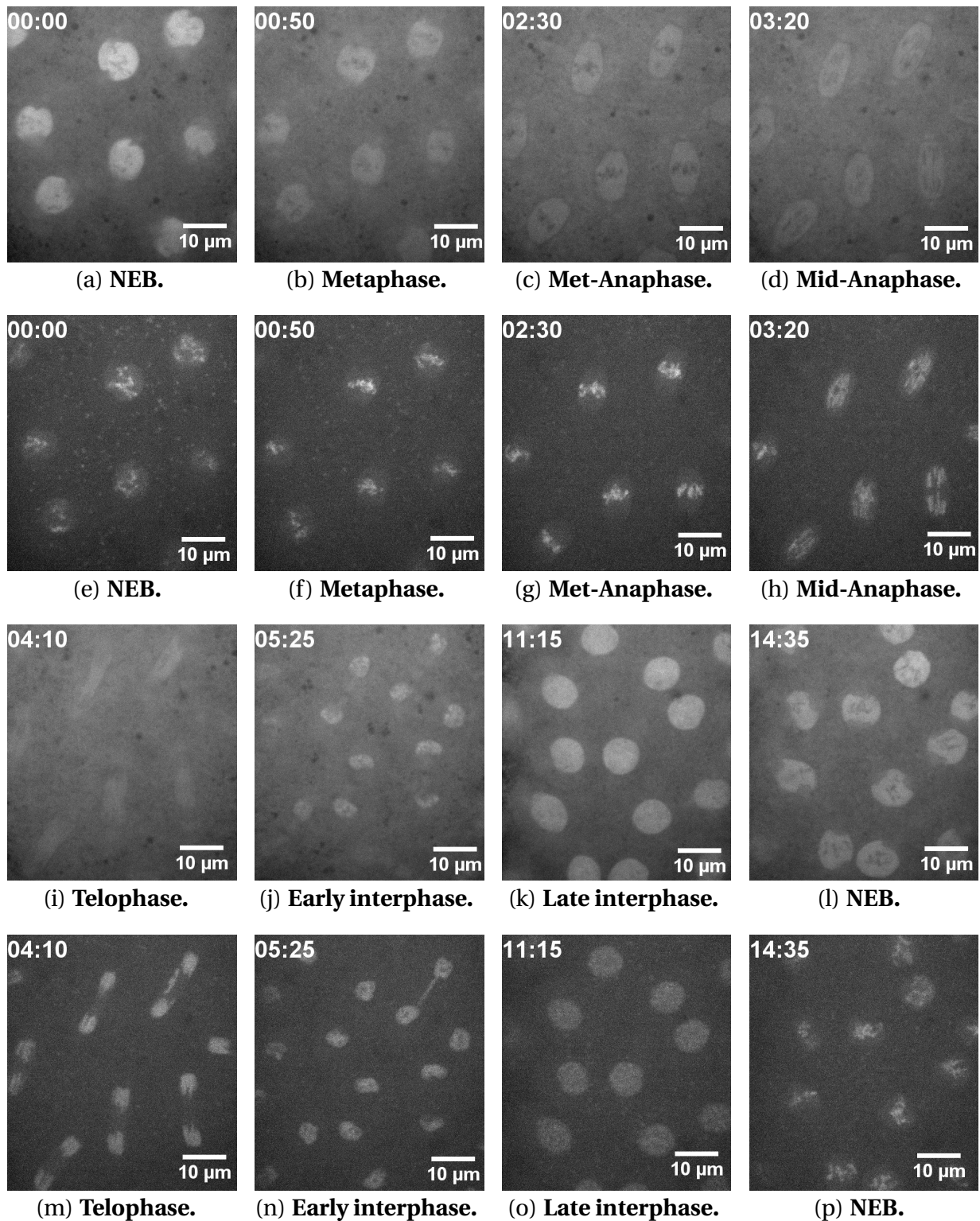
Figure 5.2: **Dynamic localisation of DNApol-epsilon 58 in different stages of mitosis.** To determine the localisation of DNApol-ε 58, 6 movies were taken and analysed. The Figure illustrates that during nuclear envelope breakdown (NEB) GFP-DNApol-ε 58 concentrates in the region of the mitotic spindle. In metaphase and anaphase, DNApol-ε 58 is found throughout the spindle and centrosomes. During interphase the protein localises in the reforming nuclei. 5.2(a) – 5.2(d) and 5.2(i) – 5.2(l) GFP-DNApol-ε 58 split. 5.2(e) – 5.2(h) and 5.2(m) – 5.2(p) HisRFP split.

Batches of 0–3 hr old GFP-DNApol-ε 58 embryos were collected, treated with MG132 and stored, prior to immunoprecipitation using GFP-TRAP-A. A Western blot of this experiment is shown in Figure 5.3. Encouragingly, a protein of $\approx$ 90 kD was isolated (corresponding to 58 kD + the $\approx$ 30 kD GFP tag). Samples were subjected to mass spectrometry to verify the presence of DNApol-ε 58 and to identify mitotic interacting partners (Table 5.1). DNApol-ε 58 was successfully isolated and was the most abundant protein. As expected, DNApol-ε 255 was also identified.
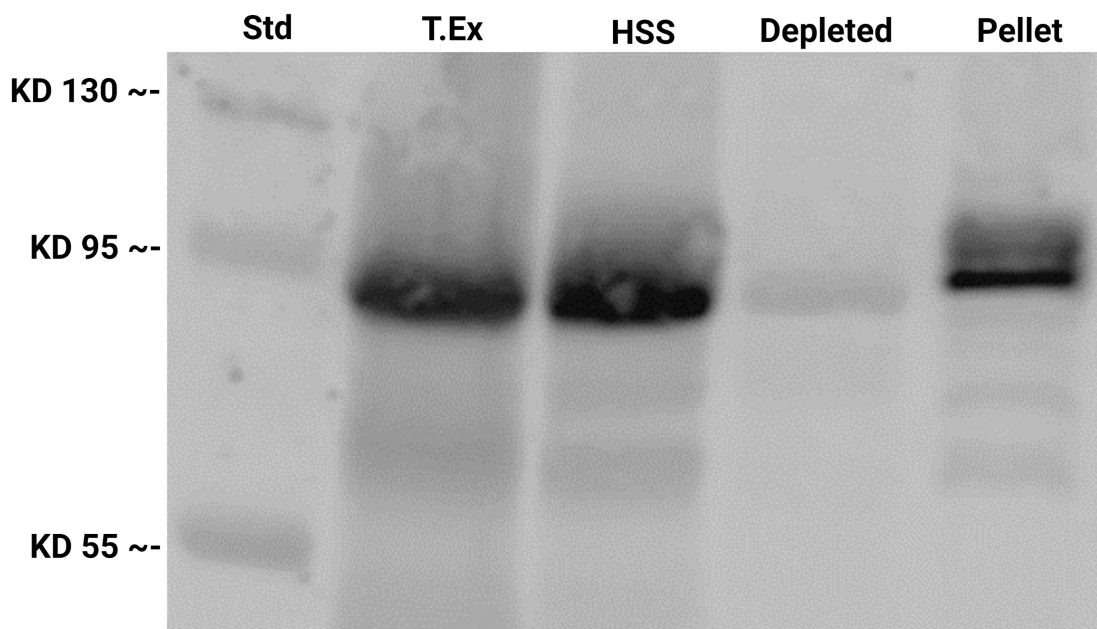
Figure 5.3: **Western blot of GFP-DNApol-ε 58.** Figure illustates the presence of a GFP positive band at the expected molecular weight, the presence of this band and its complete depletion in the respective GFP-TRAP-A pellet and extracts. DNApol-ε 58 MW $\approx$ 85 kD. Probed with anti-GFP antibody (Roche).

Table 5.1: **DNA-ε 58 IP in metaphase.** Isolated DNApol-ε 58 binding proteins in metaphase.

| Name	Accession	Coverage	# Unique Peptides	# AAs	MW [kDa]	Score	Area
DNApol-epsilon58	FBpp0076789	82.67	51	525	58.7	3882.20	8.599E9
Yp2	FBpp0071359	87.10	40	442	49.6	2933.11	8.033E9
alphaTub84D	FBpp0081062	82.89	13	450	49.9	683.16	1.278E9
ATPsynbeta	FBpp0088250	63.76	22	505	54.1	312.29	9.404E8
26-29-p	FBpp0075508	55.37	27	549	62.1	383.22	7.302E8
scu	FBpp0074285	80.39	18	255	26.9	343.20	6.872E8
Pen	FBpp0079527	82.38	34	522	57.8	546.50	4.751E8
Chrac-14	FBpp0099655	50.78	5	128	13.8	84.04	4.257E8
ScsbetaA	FBpp0306436	60.09	27	451	49.0	236.55	4.139E8
Echs1	FBpp0086770	72.88	18	295	31.6	273.71	4.002E8
Scsalpha1	FBpp0073010	49.09	14	328	34.4	219.38	3.031E8
Mes4	FBpp0071738	30.32	4	155	17.4	53.43	2.529E8
Droj2	FBpp0082219	69.23	26	403	45.2	263.32	2.513E8
Drp1	FBpp0077424	54.56	32	735	82.5	298.49	2.458E8
Sar1	FBpp0083604	69.95	13	193	21.8	128.25	2.022E8
DNApol-epsilon255	FBpp0083800	56.57	102	2236	256.5	675.47	1.698E8
sta	FBpp0070277	69.63	11	270	30.2	157.95	1.680E8
cathD	FBpp0087972	56.38	15	392	42.4	140.57	1.650E8
CG9953	FBpp0076608	54.92	21	508	56.8	174.22	1.626E8
CG5028	FBpp0084275	66.42	21	402	44.4	219.52	1.456E8
CG12702	FBpp0074578	55.98	36	870	97.1	279.93	1.368E8
Mtpbeta	FBpp0072135	57.57	20	469	50.6	159.92	1.084E8
Cdk1	FBpp0079641	70.37	17	297	34.4	116.34	1.059E8
Fs(2)Ket	FBpp0294037	54.41	34	884	98.6	282.11	1.039E8
fit	FBpp0083551	36.36	4	121	13.9	57.17	9.979E7
FeCH	FBpp0085208	74.48	21	384	43.6	97.77	9.168E7
CG18190	FBpp0271746	60.08	11	248	28.7	87.33	8.096E7
Vps4	FBpp0074278	48.87	22	442	49.6	132.62	7.651E7
Torsin	FBpp0070658	53.24	14	340	38.1	101.33	7.360E7
msps	FBpp0290695	21.35	36	2042	225.8	162.08	7.305E7
Sas-6	FBpp0084912	61.02	33	472	54.7	172.87	7.239E7
Uba5	FBpp0073354	45.54	10	404	44.1	99.51	7.201E7
GstT3	FBpp0077002	64.47	15	228	26.8	96.38	6.122E7
UQCR-C2	FBpp0075069	69.77	19	440	45.4	162.23	5.696E7
fax	FBpp0075170	44.98	17	418	47.1	81.92	5.612E7
Rab5	FBpp0077475	54.34	8	219	23.9	43.64	5.435E7
CG10237	FBpp0080748	48.17	14	301	35.1	65.19	5.173E7
Snx1	FBpp0077206	54.37	21	458	52.2	137.80	4.657E7
Rab8	FBpp0074690	33.82	3	207	23.7	31.10	4.328E7
Hsp23	FBpp0076181	73.66	10	186	20.6	65.27	4.200E7
Hmgcl	FBpp0078979	46.44	9	323	34.2	64.10	3.679E7
CG9281	FBpp0073872	29.13	16	611	69.5	65.39	3.604E7
Pdha	FBpp0070676	59.40	16	399	43.9	106.02	3.571E7
Tnpo	FBpp0076708	35.27	23	893	101.5	134.30	3.564E7
Not1	FBpp0111586	20.27	35	2220	249.6	147.60	3.523E7
CG4572	FBpp0083269	31.74	11	482	54.4	65.50	3.472E7
Prosalpha3	FBpp0071451	50.00	10	264	29.4	73.25	3.320E7
CG14309	FBpp0083001	23.50	18	966	110.5	65.14	3.268E7
Nfs1	FBpp0079874	51.95	18	462	51.0	132.05	3.241E7
smid	FBpp0089153	45.66	29	944	104.3	140.97	3.124E7
ben	FBpp0073686	57.62	8	151	17.2	33.16	3.018E7
AP-1-2beta	FBpp0074558	26.93	18	921	101.1	115.55	2.810E7
SdhB	FBpp0085489	60.27	15	297	33.7	61.67	2.744E7
wmd	FBpp0072023	48.17	12	328	36.1	60.43	2.714E7
Nup154	FBpp0088820	28.94	28	1365	153.8	107.95	2.639E7
sesB	FBpp0073277	43.14	14	299	32.9	32.16	2.549E7
gkt	FBpp0077263	26.21	8	580	64.2	56.83	2.514E7
GCS2beta	FBpp0080551	28.47	14	548	61.5	50.07	2.466E7
Coa7	FBpp0110448	61.28	15	266	29.6	58.37	2.424E7
Nup205	FBpp0074568	16.26	25	2067	232.6	107.72	2.308E7
CG11899	FBpp0084759	42.31	12	364	39.5	35.96	2.301E7
yl	FBpp0073714	10.22	13	1937	214.8	64.11	2.289E7
Rho1	FBpp0086354	57.81	8	192	21.7	32.22	2.192E7
Ids	FBpp0081255	29.12	26	1061	118.3	111.23	2.180E7
Rcd-1	FBpp0074512	33.55	8	304	34.2	42.86	2.130E7
Ctf4	FBpp0086732	23.02	15	895	96.6	62.79	2.108E7
GCC185	FBpp0112136	33.83	32	1135	130.0	101.70	2.062E7
Gorab	FBpp0074991	34.02	9	338	37.7	68.05	2.039E7
Dcp-1	FBpp0071971	33.13	7	323	35.9	33.20	2.033E7
GstZ1	FBpp0081522	65.04	11	246	27.9	58.12	2.023E7
CG9547	FBpp0078893	43.44	11	419	45.7	66.88	1.988E7
Ge-1	FBpp0079818	14.99	19	1354	149.2	71.60	1.976E7
Srp68	FBpp0076244	28.81	14	604	69.0	60.96	1.959E7
lok	FBpp0080861	38.13	14	459	52.3	62.17	1.880E7
AP-1mu	FBpp0081592	33.57	11	426	48.9	44.77	1.855E7
CG9853	FBpp0078589	51.33	12	339	38.5	39.11	1.848E7
GCS2alpha	FBpp0070057	37.01	23	924	105.7	75.77	1.781E7
CG2034	FBpp0072756	31.30	6	262	28.9	35.71	1.732E7
Vps35	FBpp0071686	26.77	19	803	91.1	72.89	1.701E7
CSN5	FBpp0082743	25.69	7	327	37.1	30.27	1.652E7
CG7546	FBpp0293610	24.11	18	1298	138.0	93.91	1.645E7
Mms19	FBpp0078425	29.72	20	959	107.0	69.74	1.635E7
CG12170	FBpp0078358	27.17	7	438	46.3	30.24	1.604E7
sgg	FBpp0089162	22.96	10	514	53.8	40.19	1.596E7
ND-75	FBpp0071128	30.37	16	731	78.6	59.22	1.580E7
krz	FBpp0085236	27.23	8	470	51.2	43.01	1.571E7
vimar	FBpp0089175	30.91	13	634	70.2	61.60	1.511E7
CG4538	FBpp0083264	23.33	15	673	71.2	62.60	1.470E7
Rassf	FBpp0083799	10.67	9	806	89.6	31.59	1.454E7

The GO Enrichment Analysis (Table 5.2) identified two other proteins, Mes4 and CHRAC-14 proteins, with the same ontology – DNA Polymerase epsilon complex, highlighting the robustness of the pull-down and verifying the presence of the entire DNA Polymerase epsilon complex. In addition, the GO analysis identified enrichment of three other complexes – the ER membrane insertion complex (CG7546 and CG9853), the nuclear pore inner ring (Nucleoporin 154 and 205, "Nup154 and 205"), and the succinate-CoA ligase complex (Succinyl-coenzyme A synthetase α subunit 1 and A "Scsalpha1 and A"); which couples the synthesis of ATP and GTP from hydrolysis of succinyl-CoA in the citric acid cycle (TCA). To compare my experiment with the known protein-protein interaction data, in Figure 5.4 I added any interactions already present in the biological general repository for interation datasets TheBioGrid database (`https://thebiogrid.org`).

DNApol-ε 58 interacts also with Rcd-l which belongs to the CCR4-NOT complex involved in gene regulation at DNA, RNA and protein level. This complex regulates decay of mRNA, transcription, translation and proteolytic process. Interestingly, the name Rcd1 stands for "reduction in centrosome dots 1", as it was identified in genome-wide RNAi screen in *Drosophila* S2 cells, for genes involved in centrosome duplication (Dobbelaere 2015). Ids is an lysosomal enzyme that belongs to the sulfatase family implicated in hydrolysis of sulfate esters and sulfamates. Although GFP-DNApol-ε 58 did not co-immunoprecipitate EB1, it did pull down CG18190 (EB2) with score 87.33 (Table 5.1), suggesting a physical interaction between the DNA polymerase epsilon complex and EB proteins in mitosis.

Table 5.2: **DNA-ε 58 GO Enrichment Analysis.** This analysis shows DNApol-ε partners as cellular components.

GO cellular component complete	Reference List (13811)	DNAPOLε58 IP	Expected	Fold Enrichment	P-value	FDR	Proteins
epsilon DNA polymerase complex (GO:0008622)	4	4	0.03	>100	1.29E-07	2.16E-05	DNAPolE255, DNAPolE58, Mes4, Chrac-14
ER membrane insertion complex (GO:0072379)	3	2	0.02	99	4.37E-04	2.34E-02	CG7546, CG9853
nuclear pore inner ring (GO:0044611)	4	2	0.03	74.25	6.52E-04	3.02E-02	Nup205, Nup154
succinate-CoA ligase complex (GO:0042709)	4	2	0.03	74.25	6.52E-04	2.92E-02	Scsalpha1, ScsbetaA
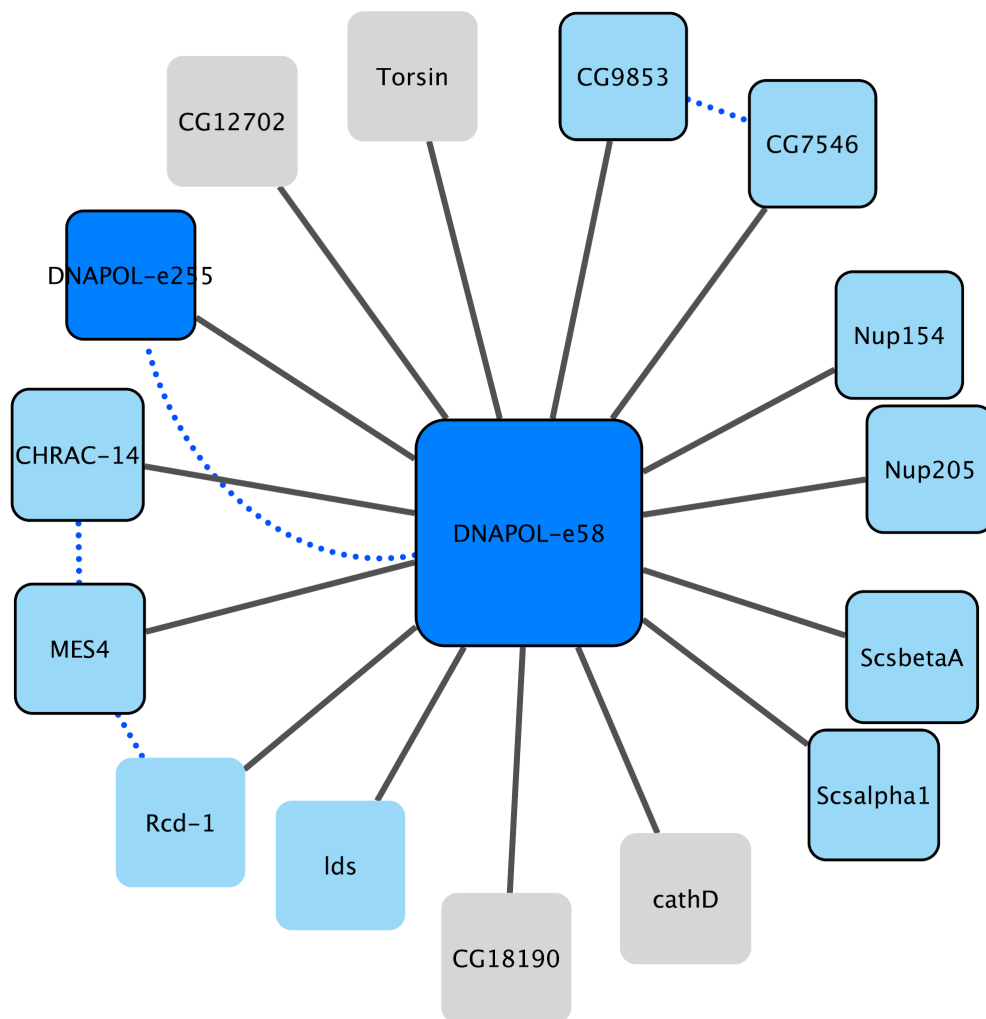
Figure 5.4: **DNApol-epsilon 58 interactors.** DNApol-ε 58 binding proteins in syncytial *Drosophila* embryos in metaphase were identified in this work and are connected by solid lines. Interactions from BioGrid database are shown by dotted lines.

5.4.1 DNApol-ε 58 interacting proteins

To have the final DNApol-ε 58 interacting proteins in metaphase (Figure 5.4), in addition to DNApol-ε 58 binding proteins within GO-enriched cellular components terms (Table, 5.2), I manually chose DNApol-ε 58 interactors in metaphase from Table 5.1 that were already identified either as EB1 interacting proteins with a final cut-off of 1.2 fold increase in mitosis (Section 4.4 and Table 4.7) or EB1 interacting proteins within GO term enrichment cellular components (Table 4.2). For description of DNApol-ε 58 binding proteins, see Sections 4.3, 4.5.4 and 4.6.4.

5.4.2 Injection of anti-EB1, anti-EB2 or the combination of anti-EB1 and anti-EB2 antibodies into GFP-DNApol-ε 58 embryos does not lead to mis-localisation of DNApol-ε 58

To investigate the relationship between EB1 and DNApol-ε 58, either anti-EB1, anti-EB2 or the combination of anti-EB1 and anti-EB2 antibodies were injected into embryos aged 1–2 hours from offspring of virgin flies expressing DNApol-ε 58 crossed to male expressing GAL4 under maternal-α-tubulin GAL4. Then, bioimaging was carried out using time-lapse confocal disc microscopy for phenotype observation.

In control embryos injected with microinjection buffer (Figures 5.5(a) – 5.5(c)), embryos expressing GFP-DNApol-ε 58 behaved normally – the GFP-fusion protein localised similarly to uninjected embryos (Figure 5.2) and the timing and distribution of nuclear cylces were unaffected. Injection of the anti-EB1 antibodies, purified in Chapter 3, resulted in defects in chromosome segregation consistent with disruption of EB1 function (Indicated by arrows, Figures 5.5(d) – 5.5(f)). However, no disruption was observed on DNApol-ε 58 dynamic localisation. To further investigate the relationship between DNApol-ε 58 and EB proteins, anti-EB2 antibodies, purified in Chapter 3, were injected into GFP-DNApol-ε expressing embryos. Similarly to EB1, chromosome separation and anaphase elongation phenotypes were observed (Indicated by arrows, Figures 5.6(d) and 5.6(f)) without a noticeable effect on the localisation of the GFP fusion protein. Finally, a mixture of both antibodies was used and the time-lapse image has shown similar effect to anti-EB1 or anti-EB2 antibodies injections (Shown by arrows, Figures 5.7(d) and 5.7(f)). As before, co-injection had no effect on GFP-DNApol-ε localisation (Figure 5.8), suggesting that this protein does not require EB proteins for its dynamic localisation to the mitotic spindle or MTs.

(a) **Telophase.** Embryo injected with microinjection buffer as a control. HisRFP in blue merged with GFP-DNApol-ε 58 in green.

(b) **Telophase.** Embryo injected with microinjection buffer as a control. GFP-DNApol-ε 58 split.

(c) **Telophase.** Embryo injected with microinjection buffer as a control. HisRFP split.

(d) **Telophase.** Embryo injected with anti-EB1 antibody. HisRFP in blue merged with GFP-DNApol-ε 58 in green.

(e) **Telophase.** Embryo injected with anti-EB1 antibody. HisRFP split.

(f) **Telophase.** Embryo injected with anti-EB1 antibody. GFP-DNApol-ε split.

Figure 5.5: **Anti-EB1 microinjection injected into 1–2 hr old embryos expressing HisRFP and GFP-DNApol-ε 58.** As a control (Figures 5.5(a) – 5.5(c)), microinjection buffer in a variable volume was injected into 5 embryos. However, after injection these embryos showed a normal progression through three consecutive cell cycles and the first telophase of the cycle is shown. The variable volume of anti-EB1 antibody was injected into 8 embryos, causing defects on chromosome segregation and anaphase elongation (Shown by arrows, Figures 5.5(d) and 5.5(f)) due to interference with EB1 functions.

(a) **Telophase.** Embryo injected with microinjection buffer. HisRFP in blue merged with GFP-DNApol-ε 58 in green.

(b) **Telophase.** Embryo injected with microinjection buffer. GFP-DNApol-ε 58 split.

(c) **Telophase.** Embryo injected with microinjection buffer. HisRFP split.

(d) **Telophase.** Embryo injected with anti-EB2 antibody. HisRFP in blue merged with GFP-DNApol-ε in green.

(e) **Telophase.** Embryo injected with anti-EB2 antibody. HisRFP split.

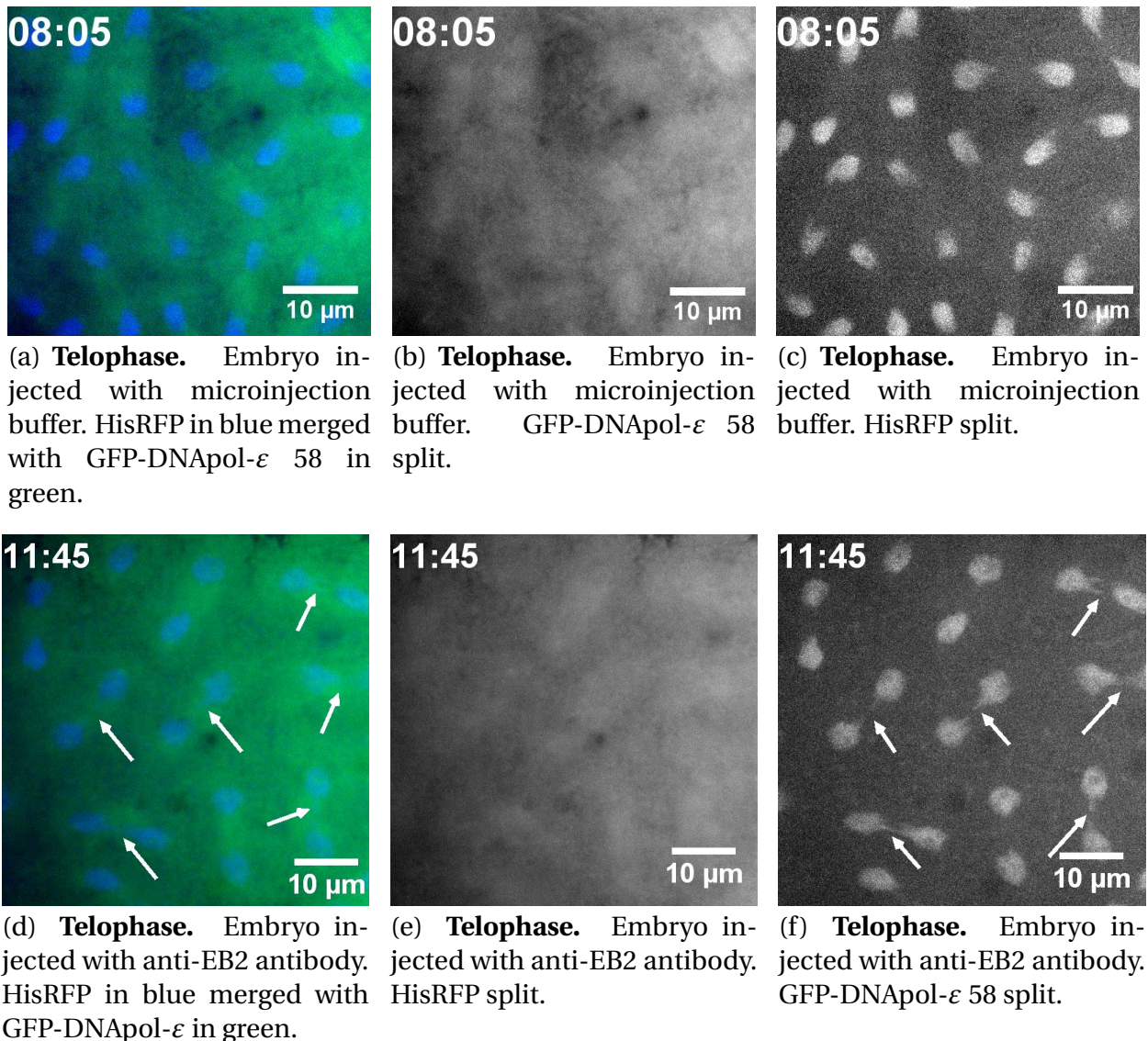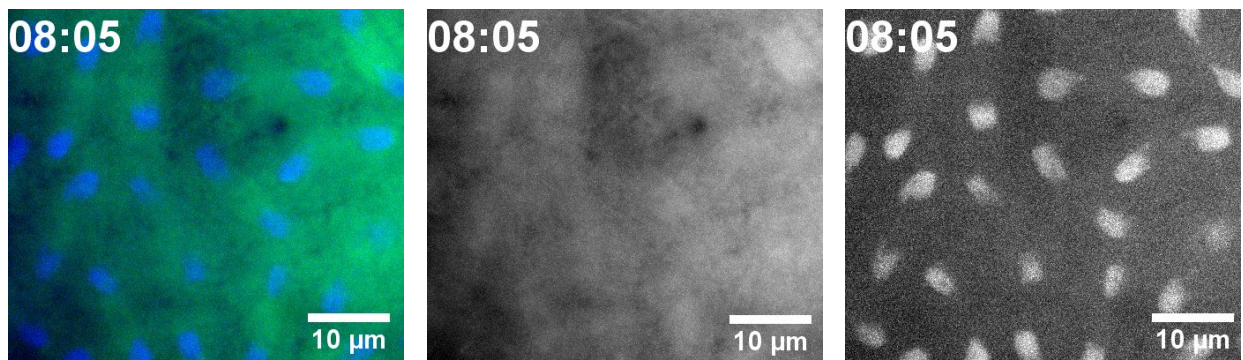(f) **Telophase.** Embryo injected with anti-EB2 antibody. GFP-DNApol-ε 58 split.

Figure 5.6: **Anti-EB2 microinjection into 1–2 hr old embryos expressing His-RFP and GFP-DNApol-ε 58.** Microinjection buffer was injected in a variable volume into 5 embryos as a control (Figures 5.6(a) – 5.6(c)). However, the injection of this buffer did not cause embryo phenotype. In contrast, when the variable volume of anti-EB2 antibody (2–4 mg/ml) was injected into 4 embryos, caused defects on chromosome segregation and anaphase elongations (Shown by arrowas, Figures 5.6(d) and 5.6(f)) as a consequence of interference with EB1 functions.
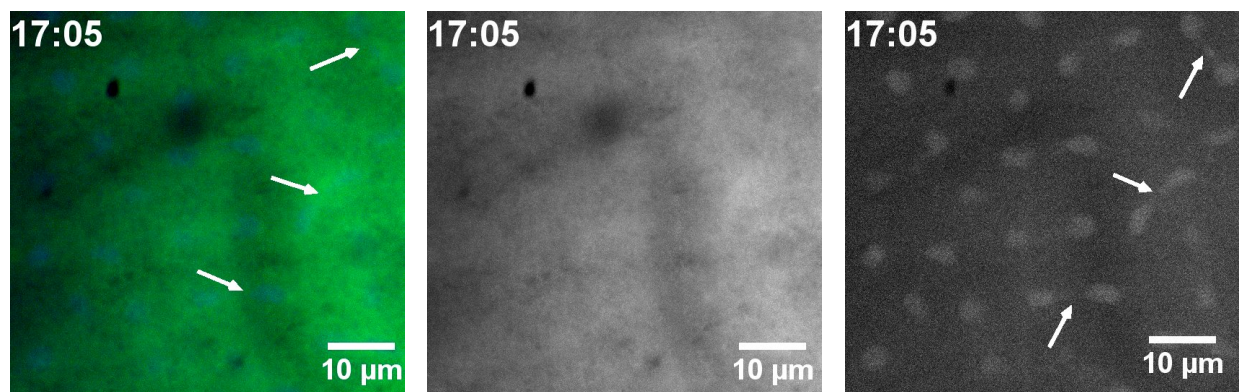
(a) **Telophase.** Embryo injected with microinjection buffer. HisRFP in blue merged with GFP-DNApol-ε 58 in green.

(b) **Telophase.** Embryo injected with microinjection buffer. GFP-DNApol-ε 58 split.

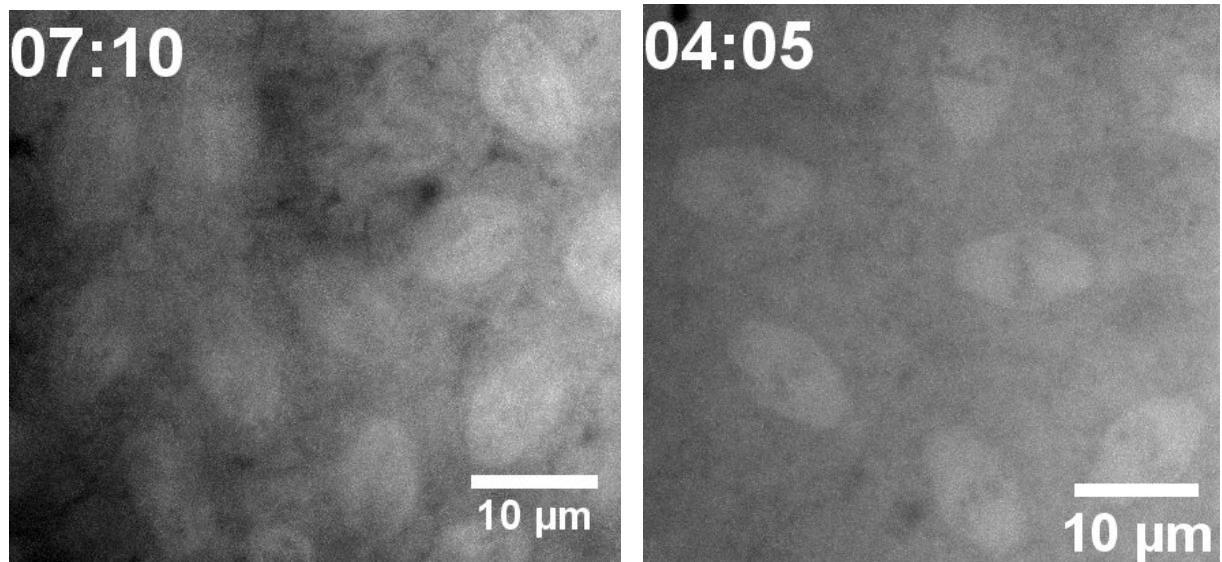(c) **Telophase.** Embryo injected with microinjection buffer. HisRFP split.

(d) **Telophase.** Embryo injected with the combination of anti-EB1 and anti-EB2 antibodies. HisRFP in blue merged with GFP-DNApol-ε 58 in green.

(e) **Telophase.** Embryo injected with the combination of anti-EB1 and anti-EB2 antibodies. GFP-DNApol-ε 58 split.

(f) **Telophase.** Embryo injected with the combination of anti-EB1 and anti-EB2 antibodies. HisRFP split.

Figure 5.7: **The combination of anti-EB1 and anti-EB2 antibody microinjection into 1–2 hr old embryos HisRFP and expressing GFP-DNApol-ε 58.** A variable volume of microinjection buffer was injected into 5 embryos as a control (Figures 5.7(a) and 5.7(c)). After buffer injection, embryos showed normal progression through three consecutive cell cycles and the first telophase of the cylce is shown. However, the combination of both anti-EB1 and anti-EB2 antibody (1:1, 2–4 mg/ml) when injected in a variable volume into 9 embryos, chromosome segregation and anaphase elongation were impaired as a result of interference with EB1 functions. (Indicated by arrows, Figures 5.7(d) and 5.7(f)).

(a) **Mid-Anaphase.** As a control, embryo was injected with microinjection buffer. GFP-DNApol-ε split.

(b) **Mid-Anaphase.** Embryo injected with anti-EB1 antibody. GFP-DNApol-ε split.
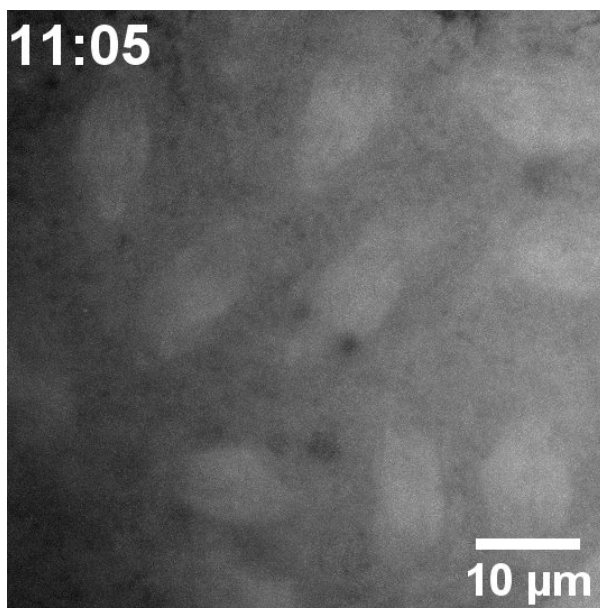
(c) **Mid-Anaphase.** Embryo injected with anti-EB2 antibody.
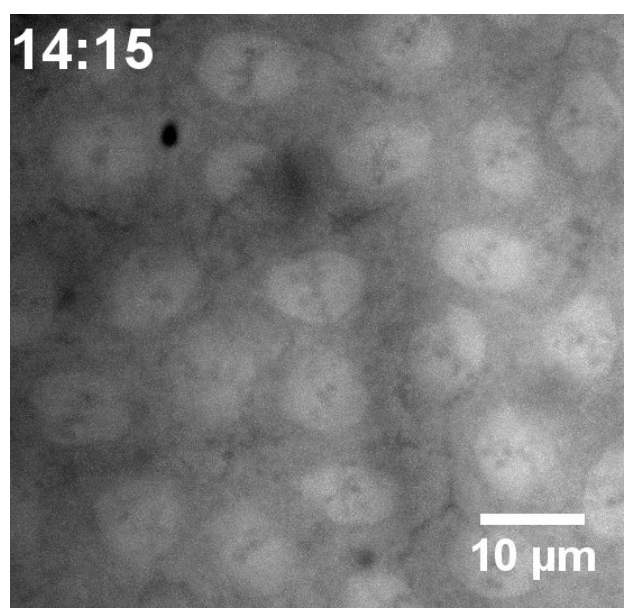
(d) **Mid-Anaphase.** Embryo injected with combination of anti-EB1 and anti-EB2 antibodies. GFP-DNApol-ε split.

Figure 5.8: **DNApol-ε 58 localisation is not displaced by antibody injections.** The same embryos as previous (Figures 5.5 – 5.7) were split in mid-anaphase and shown only the GFP-DNApol-ε 58 to visualise visualise the GFP-DNApol-ε 58 localisation. As shown in the Figure 5.8, DNApol-ε 58 was not displaced by the antibody injections, suggesting that EB1 is not nessecary for the localisation of DNApol-ε on the mitotic spindle.

5.5   Dynamic localisation and protein-protein interaction network of CORN

To determine the localisation of CORN in early *Drosophila* embryos, virgin female flies expressing GFP-CORN were crossed to homozygous males expressing GAL4 under maternal-α-tubulin promoter (Table 2.13) and resultant offspring embryos imaged via confocal spinning disc microscopy (Figure 5.9). GFP-CORN has a dynamic localisation throughout the cell cycle. Between mid-anaphase (Figures 5.9(a) and 5.9(i)) and early interphase GFP-CORN (Figure 5.9(c) and 5.9(k)) accumulates gradually at astral MTs. In late interphase (Figure 5.9(d) and 5.9(l)) and at nuclear envelope breakdown (Figures 5.9(m) and 5.9(u)), GFP-CORN is distributed in the cytoplasm with a slight enrichment in the area around centrosomes. As mitosis proceeds, the protein localises discretely but weakly to the area of the mitotic spindle, excluding centrosomes. In metaphase (Figures 5.9(n) and 5.9(v)) the protein concentrates on the mitotic spindle. However at the metaphase-anaphase transition (Figures 5.9(o) and 5.9(w)), there is a dramatic relocalisation. GFP-CORN accumulates rapidly at the astral MTs, increasing throughout through to early interphase. As interphase proceeds, fluorescence on the astral MTs decreases such that, by the following NEB the protein is almost exlusively cytoplasmic.
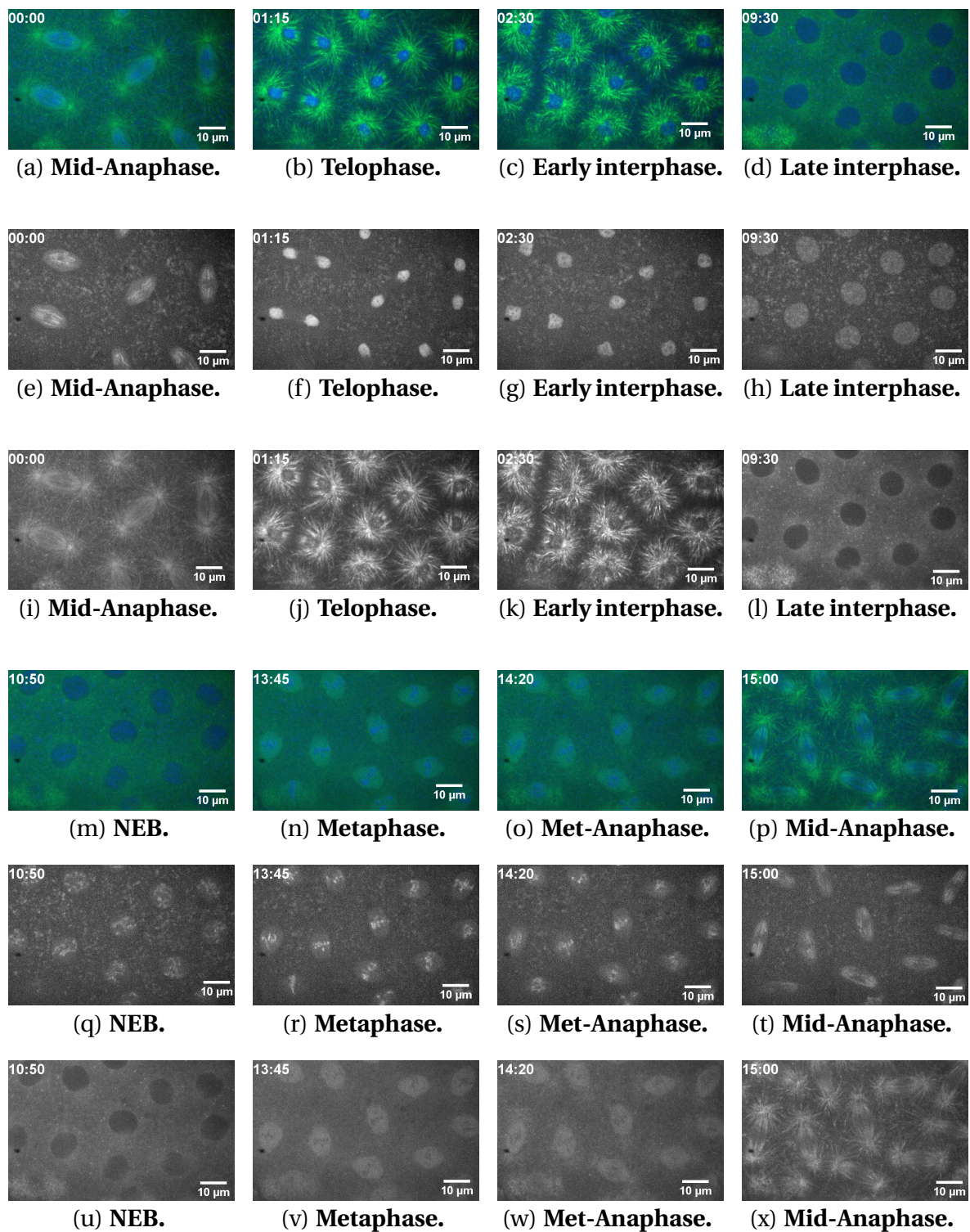
Figure 5.9: **Dynamic localisation of CORN in different stages of mitosis.** As shown in the Figure, between late interphase and nuclear envelope breakdown, the protein is ubiquitously localised in the cytoplasm with a slight enrichment in the area around the centrosomes. During metaphase, CORN localises weakly to the area of the mitotic spindle, excluding centrosomes. Between metaphase-anaphase transition and early interphase, the protein is accumlates at the astral MTs. 5.9(a) – 5.9(d) and 5.9(m) – 5.9(p) HisRFP in blue merged with GFP-CORN in green. 5.9(e) – 5.9(h) and 5.9(q) – 5.9(t) HisRFP split. 5.9(i) – 5.9(l) and 5.9(u) – 5.9(x) GFP-CORN split.

5.5.1 Injection of anti-EB1 and anti-EB2 antibodies into GFP-CORN embryos does not lead to reduction and mis-localisation of CORN at the apical MTs

Given the rapid and dramatic localisation of GFP-CORN to MTs upon entry to anaphase, and its specific co-immunoprecipitation with EB1 in MG132 arrested embryos, I hypothesized that EB1 is responsible for localising CORN. To test this hypothesis, virgin females of CORN were crossed to males of flies expressing GAL4 under maternal-α-tubulin GAL4 (Table 2.13), then embryos aged 1–2 hours of offspring from this cross were injected with either anti-EB1, anti-EB2 or the combination of anti-EB1 and anti-EB2 antibodies. Microinjection buffer was used as control, then followed by bioimaging using time-lapse confocal disc microscopy.

Injection of anti-EB1, anti-EB2 or a combination of both antibodies into early *Drosophila* embryos expressing GFP-CORN caused defects in chromosome segregation in anaphase and Figures 5.10 – 5.12 show telophases of each first cycle. This is consistent with the results from Chapter 3 and from injection into the GFP-DNApol-ε 58 embryos (Figures 5.5 – 5.7). However, there was no obvious relocalisation of the GFP-CORN under these conditions. Difference to control injected embryos were observed (Figures 5.10 – 5.12), but these could be correlated to defects in the MT cytoskeleton caused by disruption of EB1 function. So, for example, the organisation of GFP-CORN positive MTs during late anaphase and telophase were disrupted, seemingly shorter, more "speckled" and less expansive than in control injected embryos. However, the overall MT binding ability of GFP-CORN in anaphase was still present.
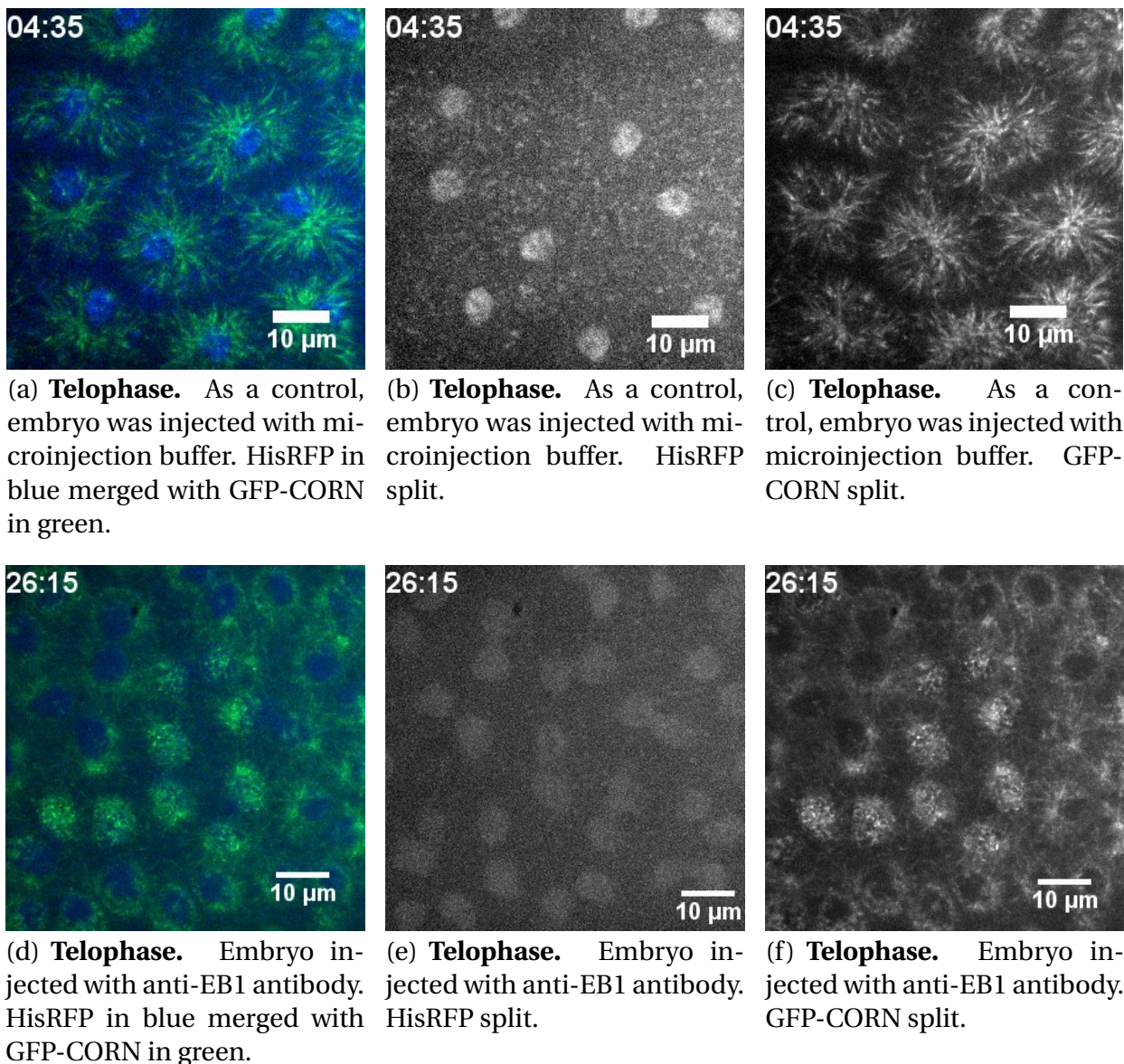
(a) **Telophase.** As a control, embryo was injected with microinjection buffer. HisRFP in blue merged with GFP-CORN in green.

(b) **Telophase.** As a control, embryo was injected with microinjection buffer. HisRFP split.

(c) **Telophase.** As a control, embryo was injected with microinjection buffer. GFP-CORN split.

(d) **Telophase.** Embryo injected with anti-EB1 antibody. HisRFP in blue merged with GFP-CORN in green.

(e) **Telophase.** Embryo injected with anti-EB1 antibody. HisRFP split.

(f) **Telophase.** Embryo injected with anti-EB1 antibody. GFP-CORN split.

Figure 5.10: **Anti-EB1 microinjection injected into 1–2 hr old embryos expressing HisRFP and GFP-CORN.** As a control (Figures 5.10(a) – 5.10(c)), microinjection buffer in a variable volume was injected into 16 early embryos. After injection, these embryos showed a normal progression through three consecutive cell cycles and the first telophase of the cycle is shown. The variable volume of anti-EB1 antibody (2–4 mg/ml) was injected into 13 early embryos. Movies taken and analysed showed defects on chromosome segregation and spindle elongation during anaphase and telophase (Figures 5.10(d) – 5.10(f)), although the relocalisation of the protein was not clear in this conditions. However, during anaphase and telophase, GFP-CORN on MTs was desplaced (Figures 5.10(d) and 5.10(f)), this may be as a consequence of the antibody interference with EB1 functions.

(a) **Telophase.** As a control, embryo was injected with microinjection buffer. HisRFP in blue merged with GFP-CORN in green.

(b) **Telophase.** As a control, embryo was injected with microinjection buffer. HisRFP split.

(c) **Telophase.** As a control, embryo was injected with microinjection buffer. GFP-CORN split.

(d) **Telophase.** Embryo injected with anti-EB2 antibody. HisRFP in blue merged with GFP-CORN

(e) **Telophase.** Embryo injected with anti-EB2 antibody. HisRFP split.

(f) **Telophase.** Embryo injected with anti-EB2 antibody. GFP-CORN split.

Figure 5.11: **Anti-EB2 microinjection injected into 1–2 hr old embryos expressing HisRFP and GFP-CORN.** A variable volume of microinjection was injected into 16 embryos as a control (Figures 5.11(a) – 5.11(c)) and this injection did not affect the embryo behavious. However, the injection of a variable volume of anti-EB2 antibody (2–4 mg/) into 11 embryos caused defects on chromosome segregation and spindle elongation during anaphase and telophase (Figures 5.11(d) – 5.11(f)), although the relocalisation of the protein was not clear in this conditions. However, during anaphase and telophase, GFP-CORN on MTs was desplaced (Figures 5.11(d) and 5.11(f)), this may be as a consequence of the antibody interference with EB1 functions.
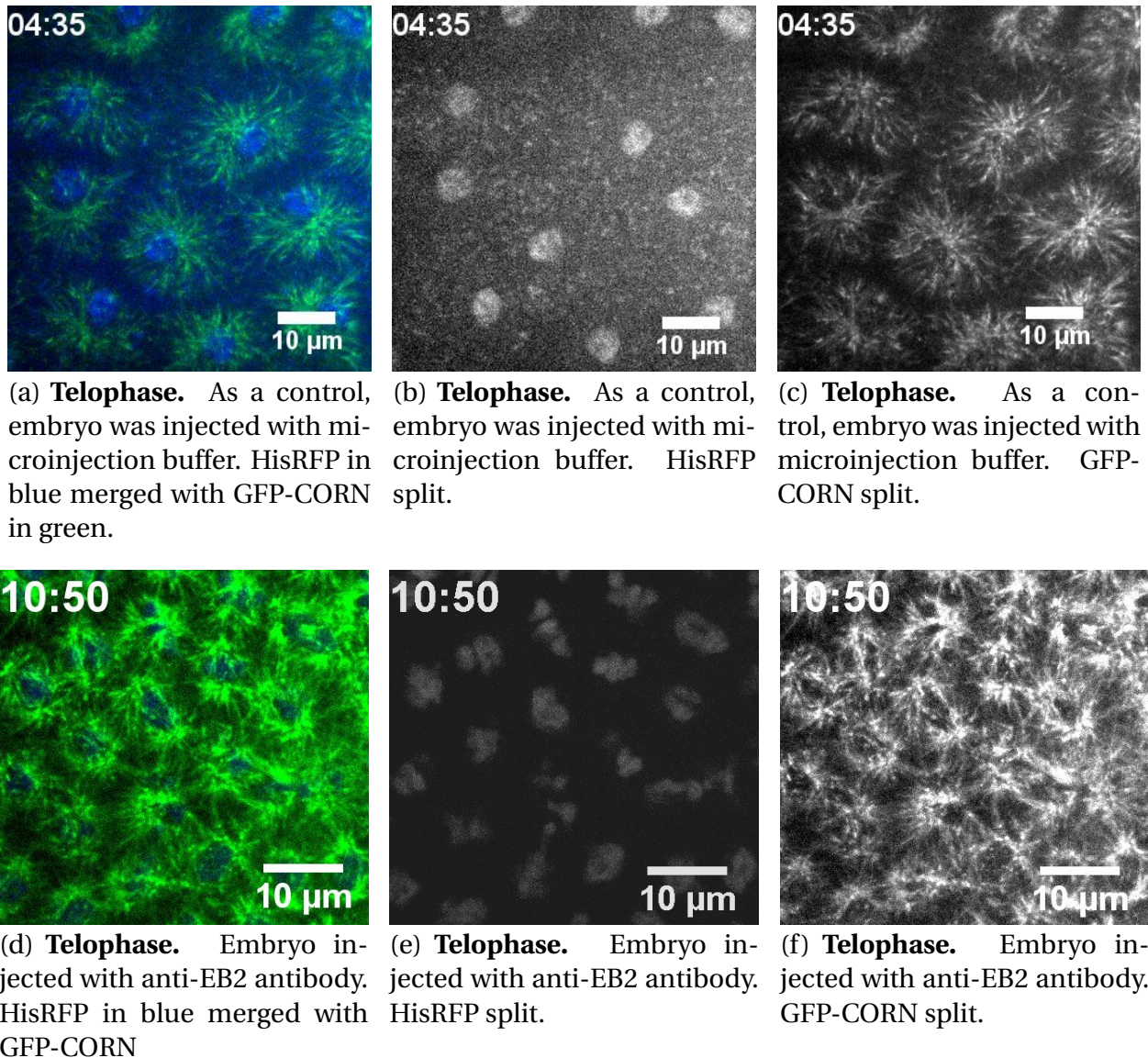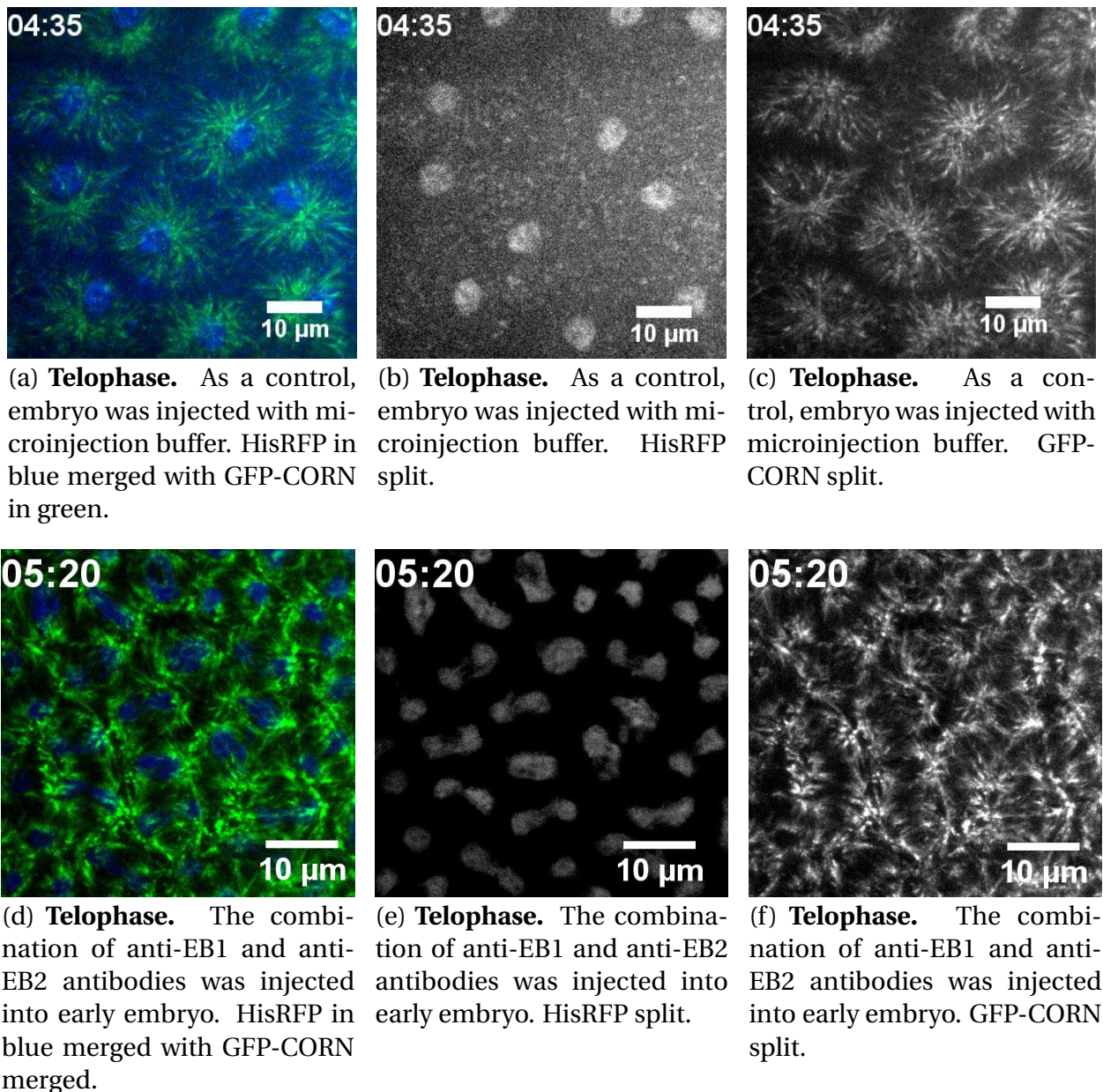
(a) **Telophase.** As a control, embryo was injected with microinjection buffer. HisRFP in blue merged with GFP-CORN in green.

(b) **Telophase.** As a control, embryo was injected with microinjection buffer. HisRFP split.

(c) **Telophase.** As a control, embryo was injected with microinjection buffer. GFP-CORN split.

(d) **Telophase.** The combination of anti-EB1 and anti-EB2 antibodies was injected into early embryo. HisRFP in blue merged with GFP-CORN merged.

(e) **Telophase.** The combination of anti-EB1 and anti-EB2 antibodies was injected into early embryo. HisRFP split.

(f) **Telophase.** The combination of anti-EB1 and anti-EB2 antibodies was injected into early embryo. GFP-CORN split.

Figure 5.12: **The combination of anti-EB1 and anti-EB2 microinjection buffer injected into 1–2 hr old embryos expressing HisRFP and GFP-CORN.** A variable volume of microinjection buffer was injected into 16 embryos as a control (Figures 5.12(a) – 5.12(c)). After buffer injections, these embryos showed normal progression through three consecutive cell cycles and the first interphase of the cycle is shown. However, the injection of the combination of anti-EB1 and anti-EB2 antibodies (2–4 mg/) with a variable volume into 9 embryos caused defects on chromosome segregation and spindle elongation during anaphase and telophase (The first telophase of the cycle is shown, Figures 5.11(d) – 5.11(f)), although the relocalisation of the protein was not clear in this conditions. However, during anaphase and telophase, GFP-CORN on MTs was disrupted (Figures 5.11(d) and 5.11(f)), this may be as a result of the antibody interference with EB1 functions.

5.6 Discussion

During this work, CG12702, CORN and DNApol-ε 58 and DNApol-ε 255 were identified as novel mitotic binding proteins of EB1 in syncytial *Drosophila* embryos. Transgenic flies expressing these novel proteins fused with GFP were generated and investigated to determine their localisation, their protein-protein interaction network and to test the hypothesis that EB1/2 are required for their dynamic localisation, using antibody injection interference.

There are some caveats associated with fusing GFP to proteins, these include the linker length as long linker can be cleaved by proteases, the insertion site should not disrupt the structure or function of the protein of interest and should not interact with other proteins. Moreover, GFP overexpression can cause cellular damage as a result of reactive oxgen specties (ROS) generation and immune mechanisms (Ansari et al. 2016; Gambotto et al. 2000; Liu et al. 1999).

Flies expressing GFP-CG12702 did not show the expected localisation. I identified CG12702 as a protein that physically interacts with EB1 significantly more in mitosis than in interphase. In humans, the closest homologue of CG12702, CIP2A is an inhibitor of protein phosphatase 2A (PP2A) and has been implicated in a variety of cancers (Jeong et al. 2014; Kim et al. 2013). Studies conducted by Jeong et al. (2014) and his colleagues show that depletion of CIP2A levels through anti-CIP2A antibody injection or through RNAi using HeLa cells causes defects in centrosome separation, mitotic spindle dynamics and SAC activation. These investigations are in agreement with previous studies conducted by Kim et al. (2013) using the same approach, including antibody against CIP2A and CIP2A RNAi in HeLa cells. I therefore hypothesized that it would localise to MTs. Instead, although Western blotting confirmed the presence of a protein of the correct size expressed in embryos, intense fluorescence puntae of various size and shape were observed that did not correlate to any cellular or subcellular

structure, One possibility is that the GFP-fusion tag, placed at the N-termiuns of CG12702, may interfere with the function and therefore localisation of the protein. As such, one way forwards would be to generate new transgenic flies, with the GFP tag at the C- rather than the N-terminus.

The finding that two subunits of the conserved DNApol-ε complex, DNApol-ε 58 and DNApol-ε 255, interact with EB1 in MG132 treated embryos led me to generate transgenic flies carrying a GFP-fusion of the smaller subunit. I found that, in the *Drosophila* early embryo, DNAPol-ε 58 is localised to the DNA during interphase but, after nuclear envelope breakdown and throughout mitosis, it is localised to the mitotic spindle and centrosomes. I also found that GFP-DNApol-ε 58 interacts with DNApol-ε 255, Mes4 and Chrac-14 – the other three conserved subunits of the conserved DNApol-ε complex. It is therefore likely that the entire complex localises to the mitotic spindle and centrosomes in the early embryo. However, any function of this complex related to MTs remains unconfirmed. The localisation of this protein was not disrupted by anti-EB1 or anti-EB2 antibody injections, or a combination of the two; neither did the GFP-fusion co-immunoprecipitate EB1 as an interacting protein. However, although it was not confirmed by other methods, such as Western blot or other pull down, DNApol-ε 58 did co-immunoprecipitate CG18190 (EB2), while both DNApol-ε 58 and 255 contain a S/TxIP motif (Table 4.4) – one of the classical EB1 binding motifs, leaving open the intriguing possibility that the DNApol-ε has a functional relationship with the mitotic spindle and EB proteins.

The dynamic localisation of DNApol-ε 58 (Figure 5.2) could reflect its role of stabilising and repairing DNA during mitosis. However, the reflection should be also the distribuition of some proteins onto DNA that may play important role during metaphase, such as lodestar identified in this experiment as a DNApol-ε 58 interactor in metaphase was previously suggested to be involved in promoting the onset of the anaphase during cell division (Szalontai et al. 2009) and

maintaining the genome integrity (Allard et al. 2004; Takada et al. 2003).

Cornetto (CORN) has been previous characterized as an apical MT binding protein in *Drosophila* oocytes (Bulgheresi et al. 2001) with functions relating to the regulation of exocytosis (Finan et al. 2011) . Although it does not have any known EB1 binding motifs (Table 4.4), as I identified it as a novel EB1 interactor in metaphase I expected it to localise similarly in the early embryo and that anti-EB1 antibody injection should interfere with localisation of CORN. The first hypothesis was correct – GFP-CORN showed a dramatic relocalisation to the astral MTs that interact with the embryonic cortex in anaphase and telophase. However, interference of EB1 or EB2 function did not result in a specific relocalisation of CORN. Instead, the changes in CORN localisation are most easily explained as a consequence of the changes in MT organisation brought about through disrupting EB function. Unfortunately, there was not time during these studies to undertake the affinity purification-mass spectrometry of GFP-CORN.

For all these proteins – CG12702, the DNApol-ε complex and CORN – further work will be required to understand their possible relationship with EB1 and MTs. Undoubtedly, all these proteins physically interact with overexpressed EB1 in the embryo; and at least DNApol-ε and CORN localise to MTs and the mitotic spindle. Future studies could concentrate on understanding the function of these proteins through traditional tools, such as mutants, *in vivo* RNAi depletion or micro-injection of interfering antibodies. This latter may well be appropriate for DNApol-ε complex. As a protein complex with a clear and conserved role in DNA replication, RNAi or mutational analysis would undoubtedly result in defects in S phase and so any effects on chromosome alignment and segregation or mitotic spindle morphology would be difficult to characterize. As interfering antibodies can be injected into embryos after NEB, in order to disrupt function (Bakal et al. 2005; Yew et al. 1994) this would be an experiment worth considering.

Chapter 6:   Discussion and Conclusion

6.1   Summary

EB1 is a +TIP that has been widely studied. Together with its binding partners, EB1 is involved in the regulation of MT dynamics, which is important for mitotic spindle orientation, chromosome alignment and segregation. However, the role of this protein in metaphase is unclear. *Drosophila melanogaster* has only two end binding proteins, EB1 and EB2. In this work I aimed to investigate the role of these proteins in mitotic early *Drosophila* embryos by generating tools to perturb their function, demonstrating efficacy of interfering antibody microinjection, and by determining and characterising the EB1 mitotic interactome.

To investigate the mitotic localisation of EB1 *in vivo*, I imaged 1–2 hr old embryos expressing EB1-GFP and as shown in Figure 3.2. EB1 interacts with MTs *in vivo* and during interphase the protein is localised at centrosomes and astral MTs, which can been seen as comets, corresponding to the growing MT plus ends. Shortly after nuclear envelope breakdown, EB1 decreases from astral MTs and concentrates at the mitotic spindle. During anaphase, the protein retracts from mitotic spindles and increases at the astral MTs. These results are in agreement with investigations conducted by Rogers et al. (2002). Having characterised the localisation of EB1, I assessed the capacity of EB1 and EB2 to bind to MTs by bacterially expressing and purifying MBP-EB1 and MBP-EB2 proteins, then undertaking MT cosedimentation. This confirmed that both proteins, directly associate with MTs *in vitro* (Figure 3.9). To attempt to disrupt EB function

in the early embryo I first attempted *in vivo* RNAi, driving the expression of a shRNAi construct during late oogenesis through the UAS-GAL4 system using maternal-α-tubulin promoter. This did not result in a phenotype; neither did driving the expression of a reported dominant negative version of EB1 in a similar way. Instead, I purified antibodies generated against EB1 or EB2 using the MBP-fusion proteins. I did not remove the MBP-tag, because the Factor Xa enzyme used (BioLabs, P8010S) cleaves the EB1 protein after arginine[130] residue in sequence Ala-Val-Arg[130], generating two respective fragments of 14 kD and 18 kD (Figure 3.6 and 3.7). However, although EB2 was not internally cleaved, the link between MBP and EB2 was partially cleaved after overnight incubation (Figure 3.7), precluding the MBP-tag removal; instead I used a dual column approach to remove anti-MBP antibodies and purify the specific antibodies. Injection of these antibodies into embryos expressing GFP-Tubulin and Histone-RFP resulted in defects in metaphase spindle length and chromosome segregation.

In Chapter 4, my hypothesis was that EB1 recruits proteins to the plus ends of MTs differentially between interphase and mitosis. To determine the complement of proteins that increase their interaction with EB1 specifically in metaphase, I used comparative quantitative proteomics – shown in Tables 4.1, 4.6 and 4.7. I found that EB1 associates with EB2 suggesting the presence of heterodimer to function as regulator of MT dynamics. During metaphase, components of the Dynein-Dynactin complex were abundantly identified as EB1 interacting partners, suggesting the entire Dynein/Dynactin complex increases its interaction with EB1 in a cell cycle dependent manner (Tables 4.1, 4.6 and 4.7).

As shown in Tables 4.1, 4.6 and 4.7, RZZ complex is a further mitotic EB1 interactor. Although RZZ is known to be removed from kinetochores on to MTs (via Dynein) during metaphase, to relieve the SAC (Mosalaganti et al. 2017; Pereira et al. 2018), a role for EB1 is not reported. Instead Dynein, through the protein Spindly, has been shown to be involved (Mosalaganti et al. 2017). My analysis suggests that EB1 could directly interact with RZZ complex.

A major focus of my work was to investigate the biochemical relationship between newly identified mitosis-specific EB1 interactors, JVL, SPN-F, IKK-ε, HOOK and PIGS (Tables 4.1, 4.6 and 4.7). I obtained flies carrying GFP or mCh-fusions to each protein, followed their dynamic localisation in early embryos and undertook affinity purification-mass spectrometry (AP-MS) to identify their interactomes. My work confirms that SPN-F, IKK-ε and JVL, which were previously shown to function together, form a complex (Tables 4.10, 4.14 and 4.17) (Baskar et al. 2019). As JVL contains 3 SxIP EB1 binding domains at its C terminus (Table 4.4), it may directly interact with EB1. My live imaging analysis shows that IKK-epsilon and SPN-F colocalise during mitosis confirming their relationships as subunits of the complex. In contrast, JVL is located only to centrosomes (Figure 4.9). During mitosis, IKK-epsilon and SPN-F appear at centrosomes at late interphase and nuclear envelope breakdown (Figure 4.3(a), 4.3(g) and 4.3(h) for SPN-F and 4.6(a), 4.6(g) and 4.6(h) for IKK-epsilon). During metaphase, these two proteins are localised also to the mitotic spindles as shown by respective SPN-F and IKK-epsilon Figures 4.3(b) and 4.6(b), then between metaphase-anaphase transition and early interphase, they decrease both from mitotic spindles and centrosomes (Figures 4.3(c) – 4.3(f) and 4.6(c) – 4.6(f)). However, although JVL is not localised to the mitotic spindles during mitosis, its dynamic localisation to centrosomes is similar to that observed with SPN-F and IK2. JVL increases its localisation at centrosomes between late interphase (Figure 4.9(a)) and reaches high concentration at nuclear envelope breakdown (Figure 4.9(b)), then it de-

creases between metaphase (Figure 4.9(c)) and early interphase (Figure 4.9(g)). Surprisingly, none of the three proteins co-immunoprecipitated with EB1 when individually used as bait and my suggestion is that this may be due to the transient interactions between these interactors and EB1 or indirect interactions with Dynein/Dynactin complex (See Discussion 4.13 in Chapter 4 and Section 6.4 in this Chapter for a full explanation of why this might be).

The EB1 immunoprecipitation results (Table 4.1) have identified PIGS as an EB1 binding protein which possesses two SxIP regions at its C-terminus (Table 4.4). This protein is implicated in modulating actin-MT cross-linking and vesicle trafficking. Table 4.19 illustrates that some of PIGS interactors are the same as JVL-SPNF-IK2 complex binding proteins, these include COP coated vesicles, subunits of RZZ complex, CATH-D and AP-3 adaptor complex. The mitotic localisation analysis of PIGS in Figure 4.12 indicates that the protein is localised to centrosomes and apical cortex between late interphase and metaphase from which it decreases between anaphase and early interphase. These results indicate that PIGS functions may be related to those HOOK and SPNF-JVL-IK complex.

In my experiments, SLAM was also identified as an EB1 interacting protein (Table 4.7). This protein interacts with NUF which is the dynein adaptor, to form a complex which is implicated in modulation of invagination furrows and recycling endosomes (Acharya et al. 2014; Kimpara et al. 2015). Figure 4.18 shows that SLAM is localised to the metaphase furrows during the cell cycle. This transient plasma membrane in the embryo is important to segregate adjacent mitotic spindles during mitosis. I was not able to identify its binding partners as, due to its localisation on the membranes, consequently the IP techniques failed to isolate it. However, the live analysis of the protein in Figure 4.18 suggests that SLAM may also be involved in the regulation of mitotic spindle orientation and elongation through interactions with EB1 and/or CORN localised at the apical

MTs, which leads to chromosome separation.

In my final Chapter I engineered flies to express GFP-fusion proteins to three previously uncharacterised proteins that I identified as mitotic EB1 interacting proteins, CG12702, DNApol-ε 58 and CORN. Despite that the Western blot shows CG12702 expression in embryos (Figure 5.1(b)), the dynamic localisation of this protein was not observed at any stage of the cell cycle. Instead, discrete punctae of varying size and intenstiy were observed (Figure 5.1(a)). It is unclear whether these punctae observed correspond to autofluorescnce of aggregates of GFP-CG12702 or yolk granulates or lipid droplets. Consequently, the AP-MS of this protein was not attempted.

So far, the relationship between DNApol-ε complex, EB1 and MTs during mitosi is not reported. However, I identified this complex as mitosis-specific EB1 interactor (Tables 4.1, 4.6 and 4.7). In addition, each subunit of the complex (DNApol-ε 58 and DNApol-ε 255) possesses one SxIP motif (Table 4.4). As a result, *Drosophila* DNApol-ε complex can be a potetial candidate for EB1 interactor during metaphase. Given the evidence that these two subunits form the complex, I decided to make only flies expressing GFP-DNApol-ε 58. As shown in the Figure 5.2, GFP-DNApol-ε 58 accumulates in the region of the growing spindle during nuclear envelope breakdown (Figures 5.2(a) and 5.2(l)). In metaphase, the protein localises to the mitotic spindle and centrosomes (Figure 5.2(b)), but does not localises to the mitotic chromosomes, shown as dark regions at the middle of the spindle shape. During anaphase (Figure 5.2(d)) the protein maintains the localisation on the mitotic spindle and centrosomes, but it also appears at the astral MTs. In telophase (Figure 5.2(i)) GFP-DNApol-ε 58 relocalises in the reforming nuclei and during interphase (Figure 5.2(k), the localisation of the protein is in nuclei.

CORN is characterised as an apical MT binding protein (Bulgheresi et al. 2001) and is not known as EB1 binding protein. The live imaging analysis (Figure 5.9) shows that between mid-anaphase (Figures 5.9(a) and 5.9(i)) and early interphase (Figure 5.9(c) and 5.9(k)) GFP-CORN gradually increases its intensity at astral MTs. In late interphase (Figure 5.9(d) and 5.9(l)) and during nuclear envelope breakdown (Figures 5.9(m) and 5.9(u)), GFP-CORN is uninformly distributed in the cytoplasm with a slight enrichment in the area around centrosomes. In metaphase (Figures 5.9(n) and 5.9(v)) the protein concentrates on the mitotic spindle. However at the metaphase-anaphase transition (Figures 5.9(o) and 5.9(w)), GFP-CORN accumulates rapidly at the astral MTs, increasing throughout through to early interphase.

Together, my work has generated a snap-shot of the complex mitotic EB1 interactome in the early *Drosophila* embryo. It suggests that many of the functions of EB1 in this system occur through the Dynein/Dynactin complex and its interacting partners, not only a kinetochores, via RZZ, but also at the embryonic cortex, where pseudocleavage/metaphase furrows must be co-ordinated. Finally, it points to a role for the DNApol-ε core complex during mitosis. The work in this thesis therefore opens up many new questions and areas of future research.

6.2 Interfering with EB function in the early embryo: Conclusions and future directions

In this part of the thesis, I microinjected antibodies into mitotic embryos expressing EB1-GFP to investigate the role of EB proteins. Initial attempts of EB1 depletion using EB1RNAi or EB1^{DN} did not show any phenotypes, suggesting either that these lines did not significantly affect EB1 levels, or possibly that they were not expressed as anticipated. A Western blot of embryos expressing the shRNA or the EB1DN, in comparison to wild type embryos, would have allowed

me to tell the difference. Unfortunately, at the time of the experiments, the Western blots did not work. Shortly afterwards, experimental work was halted due to the COVID-19 epidemic and I did not have the opportunity to repeat prior to thesis submission. Nonethless, I was able to interfere with EB function in the embryo, though purifying and injecting interfering antibodies against EB1 and EB2 into early embryos.

While the injection of buffer into embryos did not show any phenotypic difference in MT organisation, chromosome alignment and segregation, or mitotic progression, the injection of anti-EB1, anti-EB2 or the combination of anti-EB1 and anti-EB2 into the embryos expressing HisRFP and TubGFP caused a consistent, comparible and reproducible phenotype (Figures 3.14 – 3.16) and this is rescued by overexpression of EB1 (Tables 3.11 – 3.13). In these embryos, mitotic spindles in metaphase close to the site of injection appeared shorter than those further away, and also possessed smaller astral MTs. During anaphase, chromosome segregation was often inhibited during first cycle (8 embryos in 10 were inhibited in the first cell cycle and other two in the second cycle), resulting in "dumbbell-shaped" telophase chromosome complements and subsequent problems in the following mitoses. As shown in Figures 3.11 – 3.13, microinjection of anti-EB1, anti-EB2 or the combination of anti-EB1 and anti-EB2 antibodies into 1–2 hr old embryos expressing EB1-GFP did not appear to interfere with EB1-GFP localisation and the mitotic process appeared to progress through multiple cycles of mitosis with similar dynamics to embryos injected with buffer. This strongly suggests that the expression of exogenous GFP-tagged EB1, in addition to the endogenous EB1 and EB2 present in the embryo, sequesters the anti-EB1 and EB2 antibodies, such that functional EB1 and EB2 are still present, giving credence to the specificity of the phenotype observed when the same antibodies are injected into HisRFP and TubGFP embryos (Figures 3.14 – 3.16). I therefore conclude that the purified anti-EB1 and anti-EB2

antibodies have the ability to interfere with EB protein function in the early em-
bryo and this effect is rescued by overexpression of EB1-GFP. These antibodies
could be used in the future for important validation and experiments. The acute
disruption of protein function provides a unique tool with which to study nor-
mal protein function. Genetic disruption through null mutants or CRISPR com-
pletely remove function and so essential gene products required for normal cell
function result in non-viable cells. Partial removal, for example through RNAi or
expression of dominant negatives, work over the space of hours (or sometimes
days) meaning the cell has an opportunity to respond to depletion through the
upregulation of complementary pathways. Having an interfering antibody as
a tool therefore opens up new opportunities. I have shown this in principle by
analysing the localisation of two new EB1 interacting proteins, DNApol-ε 58 and
CORN, before and after antibody injection. Although the localisation of neither
protein changed following acute EB disruption, it does at least highlight where
future experiments might be taken.

6.3   Mitotic EB1-GFP PPI network: Conclusions and future directions

I have shown that in MG132 (metaphase) embryos, EB1 binds to subunits and
adaptors of the Dynein/Dynactin complex, these include – DHC64C, DCTN2-
P50, DIC,DLIC, LIS-1, ARP1,DCTN4-P62, ARP10, DCTN1-P150 AND CPA/MIRO,
but likely include all subunits of the complex. This 2MD complex is essential
to silence the SAC, to transport cargoes and to generate force at the cell cor-
tex to allow correct spindle opriention. The RZZ complex and Spindly were
also shown to be EB1 interactors in my experiment. The presence of EB1 bind-
ing motifs in this complex and my biochemical results suggest that the interac-
tions between EB1 and RZZ complex could help the Dynein/Dynactin complex
to bind to RZZ complex, resulting in promoting the onset of anaphase. This
could be followed up in a number of ways. Biochemically, similar approach

to the one I have taken in this thesis for other EB1 interactors – reciprocal IPs and AP-MS to identify the Rod, ZW10 or Zwilch interactome could help to define whether EB1 is a strong interactor of this complex. Functionally, Rod null mutant embryos (which are viable but have elevated levels of chromosome missegregation) (Buffin et al. 2005) could be injected with anti-EB1 and/or anti-EB2 antibodies to see how the phenotype changes and whether there is an effect on Rod-GFP localisation. Similar experiments could be carried out using DHC64C hypomorphs, which are female sterile and show mitotic defects in the early embryo (Gepner et al. 1996; Swan et al. 1999).

I have also shown that EB1 interacts also with IK2-JVL-SPNF complex, HOOK, PIGS, NUF, SLAM and CORN proteins, these proteins may be involved in modulating actin-MT organisation, endosome trafficking, invagination furrows, mitotic spindle orientation and anaphase progression. I describe the relevance of these interactions and future directions in Section 6.4.

EB1 interacts also with PLP which plays role in organising PCM. Between interphase and metaphase, DNApol-ε complex is localised to the DNA, and my results suggest that EB1 interacts with DNApol-ε complex to remove it from DNA, and transport it to MT minus ends via the Dynein/Dynactin complex. CG12702 is an EB1 interacting partner that may also be involved in modulating chromosome segregation and mitotic spindle functions during mitosis. Many other EB1 interactors have also been identified in my work, these include Torsin, CATH-D, CG4572 and CG9547. These proteins are implicated in removing membrane fragments from chromatin shortly after nuclear envelope breakdown and in regulating actin-MT cytoskeleton organisation and mitosis.

6.4 The relationship between EB1, the IK2-JVL-SPN-F complex, HOOK and PIGS during embryonic mitosis: Conclusions and future directions

I chose to focus my subsequent research on a functionally related group of proteins – SPN-F, JVL, IKK – and two others, PIGS and HOOK. All have published evidence of a functional and physical relationship to EB1 in interphase cells, but little else is known. Unexpectedly, although AP-MS of these GFP/mCh-tagged proteins identified physical relationships between them, the Dynein/Dynactin complex, membrane trafficking and the cell cortex, none of them immunoprecipitated EB1. This lack of reciprocal IP is difficult to explain. In my discussion (Section 4.13) in Chapter 4 I suggest that the transient nature of the way in which EB1 interacts with the proteins it targets may preclude EB1 from associating with them with high enough affinity to be identified by our stringent MS analysis; or that they interact with EB1 via Dynein/Dynactin and therefore the interaction is of low affinity. How is it, then, that I identified them as EB1 interactors to begin with? The answer may lie with the abundance of the proteins in the embryo. While the approximate abundance of EB1 and Dynein heavy chain subunits were all comparable (33217 and 36836 respectively), the abundance of SPN-F, JVL, IKK, PIGS and HOOK were > 10 fold lower. JVL and PIGS IPs were inefficient – the bait proteins were not the highest abundance proteins identified and the associated Western blots did not provide evidence of efficient pull down. Perhaps it is not surprising that a weak interactor, like EB1 was not identified above the threshold. Moreover, although HOOK IP identified Dynein components, they did so at ratios of < 1:100. Therefore, if EB1 were interacting with any of these proteins via Dynein/Dynactin, with low affinity, again this could why EB1 was not identified. One final possibility is that overexpression of EB1 drove an association with JVL, IKK-ε, SPN-F, HOOK and PIGS not normally present in the early embryo, given that the previously published work on

JVL-IKK-SPN-F and EB1 was undertaken in oocytes and hair follicle cells. In my investigation, componets of the SPNF-IK2-JVL complex were identified as EB1-binding proteins (Tables 4.1, 4.6 and 4.7) and I have co-immunoprecitated all three subunits that form SPNF-IK2-JVL complex as shown in Tables 4.10, 4.14 and 4.17.

The live imaging analysis shows the similar behavious of dynamic localisation between SPN-F and IKK-epsilon proteins during mitosis (Figure 4.3 and Figure 4.6, respectively). During mitosis, SPN-F and IKK-epsilon appear at centrosomes at late interphase and nuclear envelope breakdown (Figures 4.3(a), 4.3(g) and 4.3(h) for SPN-F and 4.6(a), 4.6(g) and 4.6(h) for IKK-epsilon). During metaphase, these two proteins are localised also to the mitotic spindles as shown by respective SPN-F and IKK-epsilon Figures 4.3(b) and 4.6(b), then between metaphase-anaphase transition and early interphase, they decrease both from mitotic spindles and centrosomes (Figures 4.3(c) – 4.3(f) and 4.6(c) – 4.6(f)). However, although JVL is not localised to the mitotic spindles during mitosis, its dynamic localisation to centrosomes is similar to that observed with SPN-F and IK2. JVL gradually concentrates at centrosomes between late interphase (Figure 4.9(a)) and nuclear envelope breakdown (Figure 4.9(b)), then it fades between metaphase (Figure 4.9(c)) and early interphase (Figure 4.9(g)).

As illustrated in Table 4.1, HOOK is an EB1 interacting protein and is involved in vesicle trafficking (Arst et al. 2014; Krämer and Phistry 1999; J. Liu 2017; Yao et al. 2014). The Table 4.21 shows that HOOK associates with dynein components and its adaptors, including DHC64C, DLIC, GL, DLC90F and SW, Rab5 and Rab11 – which are essential in transporting cargoes, such as vesicles required in modulation of invagination furrows. In addition, HOOK interacts with βCOP protein and CATH-D which are important in vesicle transport, protein degradation and regulation of actin structures in contractile rings involved in invagination furrows (Wang et al. 2021). The live imaging analysis in Figure

4.15 shows that the mitotic localisation of HOOK in early embryos is similar to that observed with SPN-F and IKK-ε subunits (Figures 4.3 and 4.6 respectively). Between late interphase and nuclear envelope breakdown, HOOK increases at centrosomes (Figure 4.15(a), 4.15(g) and 4.15(h)) and at metaphase in addition to centrosomes, HOOK is also found at the mitotic spindles (Figure 4.15(b)). Between metaphase-anaphase transition and early interphase, the protein decreases enormously both from mitotic spindles and centrosomes (Figures 4.15(c) – 4.15(f)). Given that most of HOOK interactors are the same as interactors of JVL-SPNF-IK2 complex, both JVL and SPN-F immunoprecitation identified HOOK as an interactor and the similarity between IKK-ε, SPN-F and HOOK in dynamic localisation during cell cycle, it is tempting to speculate that HOOK is functionally and structurally a subunit of the JVL-SPNF-IK2 complex (Figure 4.20).

PIGS is homologous to GAS2 in human. As mentioned in Chapter 4, Subection 4.3.3 (SHOT, Page, 94), in humans there are four members of GAS2-like proteins – GAS2, GAS2-like 1, GAS2-like 2 and GAS2-like 3 (Goriounov et al. 2003; Schneider et al. 1988; Stroud et al. 2014). While in *Drosophila* there is only one member of GAS2-like proteins, known as PIGS (Girdler et al. 2016; Pines et al. 2010; Stroud et al. 2014). In mammals GAS2-like proteins are involved in different cellular and physiological functions – GAS2-like 3 regulates mitosis (Gründl et al. 2017; Wolter et al. 2012), GAS2 modulates apoptosis (Brancolini et al. 1995; Schneider et al. 1988), and functions of of GAS2-like 1 and GAS2-like 2 are less known (Gamper et al. 2009). PIGS in *Drosophila* is also implicated in diverse cellular functions, such as regulation of mitosis and apoptosis, regulation of cell proliferation and differentiation via Notch pathwasy (Grotek et al. 2013; Kopan 2012). However, both GAS2-like proteins in human and PIGS in *Drosophila* have two motifs – CH domain and GAS2 domain. CH domain interacts with filaments of actin and GAS2 domain binds to MTs (Girdler et al. 2016; Stroud et al. 2014),

this actin-MT cross-liking plays important role in regulation of mitotic spindle orientation and elongation during mitosis. The localisation of these proteins at MT plus ends, requires the interactions with EB1 via SxIP motifs (Table 4.4) present at CH domains of GAS2-like and PIGS (Gründl et al. 2017; Stroud et al. 2014).

The structure-function analysis of PIGS undertaken in *Drosophila* S2 cells by Girdler et al. (2016) demonstrates specific truncations of PIGS that retain ability to bind to actin, MTs and the plus ends of MTs. One future avenue of research could be to make flies that express each of these truncations and undertake a similar functional and biochemical analysis as undertaken in this thesis. This may uncover those interacting proteins related to each of those functions. Null mutants for PIGS are female sterile, showing disrupted oogenesis and severe defects in follicle cell differentiation. This precludes a mutational analysis of PIGS during the syncytial mitoses. However, similar to the other proteins discussed, antibody injection, or in vivo shRNAi against PIGS might allow a deeper understanding of how this protein co-ordinates its activities on the spindle and the cell cortex.

When all the localisation and interactome data detailed in this thesis is combined with what is already known about JVL-IK2-SPNF complex, HOOK and Dynein/Dynactin function is taken into consideration, a plausible model of how they link to EB1 and MT plus ends during mitosis is revealed. Dynein/dynactin has at least three roles in the early embryo (and in many other cell types; in *Drosophila* and in humans). First, it is responsible for transporting RZZ from kinetochores to the spindle pole, facilitating the relief of the SAC (See Section 6.1). Second, it is thought to be immobilised at the cell cortex, where it can generate force on astral MTs, contributing to spindle position and orientation (Collins et al. 2012; di Pietro et al. 2016; Woodruff et al. 2009). Third, it transports early endosome protein Rab5 and recycling endosome protein Rab11, the

latter via interaction with Nuf (Figure 4.21). Nuf was another EB1 interacting protein as increasing its abundance with EB1 in metaphase/MG132 treated embryos. Nuf is part of a complex with SLAM (Table 4.7) – yet another protein I identified as a mitotic EB1interactor. I did not have time to perform Nuf-GFP AP-MS during the thesis, though this would be a high priority in the future.

The Nuf-Dynein-dependent movement of recycling endosomes to the cell cortex is also important in epithelial remodelling later in embryo development (Khanal et al. 2017; Le Droguen et al. 2015), where it sustains Shot, Patronin and Par-3 localisation at the apical cortex, maintaining epithelial cell polarity, a function that appears to be regulated by atypical Protein Kinase C (aPKC) (Calero-Cuenca et al. 2016). Recently, JVL-SPN-F has been shown to recruit Rab11-associated cargo to dynein and MTs in the *Drosophila* hair follicle cells, with IKK-ε phosphorylating Nuf to release the cargo from dynein (Baskar et al. 2019; Otani et al. 2011; Riggs et al. 2007), while in *Drosophila* oogenesis, Dynein-dependent transport has been demonstrated to bring PAR3 to the oocyte MT minus ends with Rab11 and Nuf positive recycling endosomal cargo (Jouette et al. 2019; Khanal et al. 2017; Riggs et al. 2007), and the PAR3 cargo released from the dynein through an IKK-ε-dependent process (Jouette et al. 2019). It would therefore be interesting to undertake FRAP (fluorescence recovery after photobleaching) of JVL, IKK and SPNF in the early embryo, to assess their dynamic relationship with the centrosome and spindle during mitosis. Also, to monitor their dynamics in the female sterile dynein mutant (Robinson et al. 1999).

One other interesting aspect of the biochemical network I have identified is the relationship between the RZZ complex and the JVL-SPNF-IKK-ε complex (Figure 4.20). This could suggest one of two things – either that the RZZ complex has a role in trafficking recycling endosomes at the astral MT plus ends; or that JVL-SPNF-IKK-ε has a role at the plus ends of kinetochore MTs. The localisations of the proteins do not reveal much about these possibilities – neither JVL, SPNF nor IKKε appear to localise to kinetochores or k-MTs; while RZZ does not appear to localise to the embryonic cortex. However, ZW10 has been shown to have a role later in mitosis, during cytokinesis in Golgi-ER retrograde (late endosome) transport, delivering membrane to the cytokinetic furrow (Wainman et al. 2012), suggesting a potential relationship between vesicles and the RZZ complex. Conversely, the human homologue of IKK-ε, Tank binding Kinase 1 (TBK1) has been shown to be a centrosomal kinase required for MT dynamics and mitosis (Pillai et al. 2015) and to be required for phosphorylating SAC proteins (Maan et al. 2021). To try to ascertain whether IKK-ε has a role in SAC in flies, the available pUAS-shRNAi line could be expressed using a maternal promoter and the early embryonic divisions monitored by spinning disc microscopy. This line has already been shown to be female semi-sterile when crossed to nanos-GAL4 (Jouette et al. 2019). Alternatively, similar to the other proteins discussed, antibodies against IKK-ε could be generated to attempt to acutely interfere with function during the syncytial divisions.

6.5 Investigating the functional relationships between EB and DNApol-e 58: Conclusions and future directions

During DNA replication, the DNApol-e complex interacts with Chr14-Mes4-Rcdl complex to reform nucleosomes immediately after the passage of the replication fork. This process is important to maintain the genome integrity during mitosis. The fact that I identified both core subunits of the DNApol-ε complex at "Top 100" interactors of EB1, and proteins whose association with EB1 is increased specifically in MG132 arrested (metaphase) embryos (Table 4.7), confirms my MS analysis which demonstrates the presence of a full DNApol-ε complex in embryos. Moreover, each component possesses one SxIP motif (Table 4.4). The localisation of DNApol-ε 58 to the area of the mitotic spindle, and weakly to centrosomes in metaphase (Figure 5.2), opens up the intriguing possibility that this protein and the DNApol-ε complex in general has a role in spindle formation. Similarly to other proteins studied in this thesis, DNApol-ε 58 IP did not co-precipitate EB1. It did, however, co-precipitate EB2 (CG18190). This result needs to be verified via Western blotting, and the purification of anti-EB1/EB2 antibodies provides the opportunity to take this forwards.

We do not know what the functional relationship between the DNApol-ε complex, EB1, the mitotic spindle or mitosis might be. To try to understand the functional relationships between EB1 and DNApol-ε 58, I injected anti-EB1, anti-EB2 or a recombination of anti-EB1 and anti-EB2 antibodies into 1–2 hr old embryos expressing HisRFPDNApol-ε58-GFP, monitoring the effect on mitosis. As shown in Figures 5.8, the injection of these antibodies did not cause the disruption of the DNApol-ε 58 localisation, but the chromosome segregation was affected as a consequence of EB1 and/or EB2 function interference (Figures 5.5 – 5.7). Thus, I conclude that EB1 or EB2 may not be required for DNApol-ε 58 localisation.

To take these studies further, it will be important to remove or inhibit DNApol-ε function in the early embryo. Mutational analysis, *in vivo* RNAi or CRISPR all pose the same problem – disruption of a core protein or complex required for DNA synthesis will cause defects in that process, leading to secondary consequences in chromosome movement, alignment and segregation during mitosis. Therefore, the best approach would be to follow the same method as for EB1 – – generating and purifying anti-DNAPol-ε 58 or 255 antibodies and injecting them into embryos that have entered mitosis. Such an approach has been used to unequivocally demonstrate a role for the conserved splicing factors, Sf3A2 and Prp31, in *Drosophila* mitosis (Pellacani et al. 2018).

6.6 Investigating the functional relationships between EB and CORN: Conclusions and future directions

CORN is an apical MT binding protein which was reported to interact with inscuteable and with filament of actin to regulate mitotic spindle orientation during mitosis in *Drosophila* neuroblasts and the molecular mechanisms of this regulation is unclear (Bulgheresi et al. 2001). Moreover, biochemical analysis conducted by Finan et al. (2011) demostrates that CORN interacts with Myosin VI to regulate protein secretion. I have identified CORN as a novel EB1 interactor in metaphase (Table 4.7) and shown that, between interphase (Figures 5.9(d) and 5.9(l)) and NEB (Figures 5.9(m) and 5.9(u)), GFP-CORN is ubiquitously localised in the cytosol and immediately after NEB, it rapidly colocalises to the mitotic spindles. During anaphase (Figures 5.9(a) and 5.9(i)) it is highly localised to the apical MTs. This investigation suggests that CORN might interact with EB1 to be transported to the apical MTs where its interacts with inscuteable and actin. These interactions could therefore be involved in regulating mitotic spindle orientation and anaphase progression. To investigate the functional relationships between EB and Corn, I injected anti-EB1, anti-EB2 or the combina-

tion of anti-EB1 and anti-EB2 antibodies into embryos expressing GFP-CORN. As shown in Figures 5.10 – 5.12, during anaphase, the injection of antibodies into these embryos caused shorter astral MTs and a reduction in their number, and their mis-orientation, consistent with inhibition of EB1 and EB2. As such, the morphology of GFP-CORN was altered, in repsect to control injected embryos. However, this change can be explained by the defects in MT organisation caused by EB1 disruption, rather than directly affecting CORN localisation. Thus, I conclude that EB1or EB2 are not required for CORN localisation.

Studies of CORN functions involving the use of CORN mutants, CORN depletion via RNAi and anti-CORN antibody injection were previously used by Bulgheresi et al. (2001). These authors did not detect phenotype in mitotic orientation during *Drosophila* neuroblast division in CORN mutants, neither in CORN RNAi, suggesting that other proteins invovled in regulation of mitotic spindle positioning could be recruited and compensate the functional loss of CORN. However, injecting anti-CORN antibody, they observed phenotype which led them to suggest the functional connection between CORN and the mitotic spindle functions. As these investigations were conducted in neuroblasts, future studies using early *Drosophila* embryos with similar approaches, might allow a deeper comprehension how this protein regulate the mitotic spindle orientation during mitosis. Furthermore, the future studies could concentrate on biochemical analysis invovlving reciprocal IP and AP-MS to identify CORN interactome and undertaking yeast two hybrid sytem, as well as anti-CORN antibody injection into embryos expressing EB1-GFP to verify interactions between EB1 and CORN. In addition, bacterial expression and purification of CORN, following by MT co-sedimentation assay could be also a tool to assess the capability of this protein to bind to MTs in future work.

6.7 Investigating the functional relationships between EB and CG12702: Conclusions and future directions

Although GFP-CG12702 failed to localise to discrete structures in early embryos (Chapter 5) there is scope for further work to try to better understand its relationship with EB1. CG12702 shows homology to cancerous inhibitor of protein phosphatase 2A (CIP2A). During G_2/M phase, CIP2A is reported to interact with NIMA (never in mitosis gene A)-related kinasis A (NEK2) to regulate centrosome segregation and mitotic spindle functions during mitosis (Jeong et al. 2014). However, in many types of human cancers, CIP2A is overexpressed in approximatly 39% – 90% in patient samples, thus it was proposed as biomarker for various human tumors (Khanna et al. 2013; Niemelä et al. 2012). In these tumors, the overxpression of CIP2A inhibits tumor suppressor protein – protein phosphatase 2A (PP2A), which results in activation of many oncogenic PP2A targets, such as MYC, E2F1 and Akt (Khanna et al. 2013). According to Soofiyani et al. (2017), depleting CIP2A by CIP2A siRNAi in prostate cancer cells (PC-3 cells) reduces the proliferation of these cancer cells. Similar studies conducted by Junttila et al. (2007) and Liu et al. (20017) demonstrate that CIP2A depletion by siRNA or via anti-CIP2A antibody injection significally impairs proliferation of HeLa cells and reduces tumor size in athymic mice, this effects could be rescued by CIP2A overexpression. First and foremost, given the possibility that GFP-CG12702 failed to localise due to the GFP moiety interfering with protein folding or function, it will be important to engineer flies that will express a fusion of CG12702 to GFP, at the C, rather than the N-terminus. Depending on this result, further future investigations could take place, similar to those described above.

Overall, the work in this thesis has provided a comprehensive mitotic EB1 interactome that is suggestive of a multi-functional role for this key +TIP in regulating MT end dynamics at the kinetochore and the cell cortex; through Dynein/Dynactin, JVL-SPNF-IKK-ε, HOOK, PIGS and CORN, with a potential novel mitotic role for the DNAPol-ε complex. This raises many more questions than it answers but paves the way for new and interesting findings relating MTs, chromosomes and membranes.

Bibliography

Abdu, U., Bar, D., and Schüpbach, (Apr. 2006). "spn-F encodes a novel protein that affects oocyte patterning and bristle morphology in *Drosophila*." In: *Development*. 133.8, pp. 1477–1484. ISSN: 0950-1991. DOI: `10.1242/dev.02319`. URL: `https://pubmed.ncbi.nlm.nih.gov/16540510/`.

Acharya, S., Laupsien, P., Wenzl, C., Yan, and S. Großhans, J. (Feb. 2014). "Function and dynamics of slam in furrow formation in early *Drosophila* embryo." In: *Dev Biol*. 386.2, pp. 371–384. ISSN: 1095-564X. DOI: `10.1016/j.ydbio.2013.12.022`. URL: `https://pubmed.ncbi.nlm.nih.gov/24368071/`.

Aebersikd, R. and M. Mann (Sept. 2016). "Mass-spectrometric exploration of proteome structure and function." In: *Nature*. 537.7620, pp. 347–355. ISSN: 1476-4687. DOI: `10.1038/nature19949`. URL: `https://www.nature.com/articles/nature19949`.

Akhmanova, A. and M.O. Steinmetz (Apr. 2008). "Tracking the ends: a dynamic protein network controls the fate of microtubule tips." In: *Nat. Rev. Mol. Cell Biol*. 9.4, pp. 309–322. DOI: `10.1038/nrm2369`. URL: `https://www.nature.com/articles/nrm2369`.

Albertson, R., Cao, J., Hsieh, T-S., and Sullivan, W. (June 2008). "Vesicles and actin are targeted to the cleavage furrow via furrow microtubules and the central spindle." In: *J Cell Biol*. 181.5, pp. 777–790. ISSN: 1540-8140. DOI: `10.1083/jcb.200803096`. URL: `https://pubmed.ncbi.nlm.nih.gov/18504302/`.

Aldaz, S., Escudero, L.M., and Freeman, M. (Aug. 2013). "Dual role of myosin II during *Drosophila* imaginal disc metamorphosis." In: *Nat Commun*. 4, p. 1761.

ISSN: 2041-1723. DOI: `10.1038/ncomms2763`. URL: `https://pubmed.ncbi.nlm.nih.gov/23612302/`.

Allard, S., Masson, J-Y, and Côté, J. (Mar. 2004). "*Drosophila* checkpoint kinase 2 couples centrosome function and spindle assembly to genomic integrity." In: *Biochim Biophys Acta.* 1677.1-3, pp. 158–164. DOI: `10.1016/j.bbaexp.2003.10.016`. URL: `https://pubmed.ncbi.nlm.nih.gov/15020056/`.

Almeida, T.B., Carnell, A.J., Barsukov, I.L., and Berry, N.G. (Nov. 2017). "Targeting SxIP-EB1 interaction: An integrated approach to the discovery of small molecule modulators of dynamic binding sites." In: *Sci Rep.* 7.1, p. 15533. DOI: `10.1038/s41598-017-15502-6`. URL: `https://pubmed.ncbi.nlm.nih.gov/29138501/`.

Alushin, G.M., Lander, G.C., Kellogg, E.H, Zhang, R., Baker, D., and Nogales, E. (May 2014). "High-resolution microtubule structures reveal the structural transitions in $\alpha\beta$-tubulin upon GTP hydrolysis." In: *Cell.* 157.5, pp. 1117–1129. ISSN: 1097-4172. DOI: `10.1016/j.cell.2014.03.053`. URL: `https://www.ncbi.nlm.nih.gov/pmc/articles/PMC4054694/`.

Amos, L.A. and D. Schlieper (2005). "Microtubules and maps." In: *Adv Protein Chem.* 72, pp. 257–298. ISSN: 0065-3233. DOI: `10.1016/S0065-3233(04)71007-4`. URL: `https://pubmed.ncbi.nlm.nih.gov/16230114/`.

Amsalem, S., Bakrhat, A., Otani, T., Hayashi, S., Goldstein, B., and Abdu, U. (Nov. 2013). "*Drosophila* Oocyte Polarity and Cytoskeleton Organization Require Regulation of Ik2 Activity by Spn-F and Javelin-Like." In: *Mol Cell Biol.* 33.22. American Society for Microbiology, pp. 4371–4380. DOI: `10.1128/MCB.00713-13`. URL: `https://www.ncbi.nlm.nih.gov/pmc/articles/PMC3838182/`.

Andreas, A. and K.E. Sawin (Apr. 2011). "Microtubule stabilization in vivo by nucleation-incompetent γ-tubulin complex". In: *J. Cell. Sci.* 124.8, pp. 1207–1213. ISSN: 1477-9137. DOI: `10.1242/jcs.083741`. URL: `https://pubmed.ncbi.nlm.nih.gov/21444751/`.

Ansari, A.M., Ahmed, A.K., Matsangos, A.E., Lay, F., Born, L.J., Marti, G., Harmon, J.W., and Sun, Z. (Oct. 2016). "Cellular GFP Toxicity and Immunogenicity: Potential Confounders in in Vivo Cell Tracking Experiments." In: *Stem Cell Rev Rep.* 12.5, pp. 553–559. DOI: 10.1007/s12015-016-9670-8. URL: https://pubmed.ncbi.nlm.nih.gov/27435468/.

Arden, S.D., Puri, C., Au, J.S-Y., Kendrick-Jnes, J., and Buss, F. (Dec. 2007). "Myosin VI Is Required for Targeted Membrane Transport during Cytokinesis." In: *Mol Biol Cell.* 18.12, pp. 4750–4761. ISSN: 1059-1524. DOI: 10.1091/mbc.E07-02-0127. URL: https://www.ncbi.nlm.nih.gov/pmc/articles/PMC2096599/.

Arst, H.N.J.R., Zhang, J., Qiu, R., Peñalva, M.A., and Xiang, X. (Mar. 2014). "HookA is a novel dynein-early endosome linker critical for cargo movement in vivo." In: *J Cell Biol.* 204.6, pp. 1009–1026. ISSN: 1540-8140. DOI: 10.1083/jcb.201308009. URL: https://pubmed.ncbi.nlm.nih.gov/24637327/.

Ashburner, M., Ball, C.A., Blake, J.A., Botstein, D., Butler, H., Cherry, J.M., Davis, A.P., Dolinski, K., Dwight andS.S., Eppig, J.T., Harris, M.A., Hill, D.P., Issel-Tarver, L., Kasarskis, A., Lewis, S., Matese, J.C., Richardson, J.E., Ringwald, M., Rubin, G.M., and Sherlock, G. (May 2000). "Gene ontology: tool for the unification of biology. The Gene Ontology Consortium." In: *Nat Genet.* 25.1, pp. 25–29. ISSN: 1061-4036. DOI: 10.1038/75556. URL: https://pubmed.ncbi.nlm.nih.gov/10802651/.

Askham, J.M., Vaughan, K.T., Goodson, H.V., and Morrison and E.E. (Feb. 2002). "Evidence that an interaction between EB1 and p150(Glued) is required for the formation and maintenance of a radial microtubule array anchored at the centrosome." In: *Mol Biol Cell.* 13.10, pp. 3627–3645. DOI: 10.1091/mbc.e02-01-0061. URL: https://www.ncbi.nlm.nih.gov/pmc/articles/PMC129971/.

Avides, doC.M and D.M. Gover (Mar. 1999). "Abnormal spindle protein, Asp, and the integrity of mitotic centrosomal microtubule organizing centers." In: *Science.* 283.5408, pp. 1733–1735. ISSN: 0036-8075. DOI: `10.1126/science.283.5408.1733`. URL: `https://pubmed.ncbi.nlm.nih.gov/10073938/`.

Bach, A-S., Derocq, D., Laurent-Matha, V., Montcourrier, P., Sebti, S., Orsetti, B., Theillet, C., Gongora, C., Pattingre, S., Ibing, E., Roger, P., Linares, L.K., Reinhckel, T., Meurice, G., Kaiser, F.J., Gespach, C., and Liaudet-Coopman, E. (Sept. 2015). "Nuclear cathepsin D enhances TRPS1 transcriptional repressor function to regulate cell cycle progression and transformation in human breast cancer cells." In: *Oncotarget.* 6.29, pp. 28084–28103. ISSN: 1949-2553. DOI: `10.18632/oncotarget.4394`. URL: `https://pubmed.ncbi.nlm.nih.gov/26183398/`.

Baek, J.H., Kim, M.J., Yun, H.S., Hong, E.H., Lee, S.J., Lee, C.W.and Yim, J.H., Kim, J.S., Park, J.K., Um, H.D., and Hwang, S.G. (Oct. 2013). "Depletion of end-binding protein 1 (EB1) promotes apoptosis of human non-small-cell lung cancer cells via reactive oxygen species and Bax-mediated mitochondrial dysfunction." In: *Cancer Lett.* 339 (1). DOI: `10.1016/j.canlet.2013.07.027`.

Bai, Y. (2015). "Detecting protein-protein interactions by gel filtration chromatography." In: *Methods Mol Biol.* 1278, pp. 223–232. DOI: `10.1007/978-1-4939-2425-7_13`. URL: `https://pubmed.ncbi.nlm.nih.gov/25859952/`.

Bakal, C.J., Finan, D., LaRose, J., Wells, C.D., Gish, G., Kulkarni, S., DeSepulveda, P., Wilde, and A. Rottapel, R. (July 2005). "The Rho GTP exchange factor Lfc promotes spindle assembly in early mitosis." In: *Proc Natl Acad Sci USA.* 102.27, pp. 9529–9534. ISSN: 0027-8424. DOI: `10.1073/pnas.0504190102`. URL: `https://pubmed.ncbi.nlm.nih.gov/15976019/`.

Barbosa, J., Martins, T., Bange, T., Tao, L., Conde, C., and Sunkel C. (Jan. 2020). "Polo regulates Spindly to prevent premature stabilization of kinetochore-

microtubule attachments." In: *EMBO J.* 39.2, pp. 1–22. DOI: `10.15252/embj.2018100789`. URL: `https://pubmed.ncbi.nlm.nih.gov/31849090/`.

Barve, M., Mohan, P.M.K, Chatterjee, A., and Hour, R.V. (Feb. 2006). "pH driven conformational dynamics and dimer-to-monomer transition in DLC8." In: *Protein Sci.* 15.2, pp. 335–342. DOI: `10.1110/ps.051854906`. URL: `https://www.ncbi.nlm.nih.gov/pmc/articles/PMC2242461/`.

Baskar, R., Bahkrat, A., Otani, T., Wada, H., Davidov, G., Pandey, H., Gheber, L., Zarivach, R., Hayashi, S., and Abdu, U. (Oct. 2019). "The plus-tip tracking and microtubule stabilizing activities of Javelin-like regulate microtubule organization and cell polarity." In: *FEBS J.* 286.19, pp. 3811–3830. ISSN: 0092-8674. DOI: `10.1111/febs.14944`. URL: `https://pubmed.ncbi.nlm.nih.gov/31152621/`.

Bassermann, F., Eichner, R., and Pagano, M. (Jan. 2014). "The ubiquitin proteasome system - implications for cell cycle control and the targeted treatment of cancer." In: *Biochim Biophys Acta.* 1843.1, pp. 150–162. ISSN: 0006-3002. DOI: `10.1016/j.bbamcr.2013.02.028`. URL: `https://pubmed.ncbi.nlm.nih.gov/23466868/`.

Baumann, K. (Oct. 2012). "Order in the pericentriolar material." In: *Nat Rev Mol cell Biol.* 13.12, pp. 749–749. ISSN: 1471-0080. DOI: `10.1038/ncb2597`. URL: `https://www.nature.com/articles/nrm3471`.

Bernards, R., Thijn R Brummelkamp, T.R., and Beijersbergen, R.L. (Aug. 2006). "shRNA libraries and their use in cancer genetics." In: *Nat Methods* 3.9, pp. 701–706. DOI: `10.1038/nmeth921`. URL: `https://pubmed.ncbi.nlm.nih.gov/16929315/`.

Berrueta, L., Kraeft, S.K., Tirnauer, J.S., Schuyelr, S.C., Chen, L.B., Hill, D.E., Pellman, D., and Bierer, B.E. (July 1998). "The adenomatous polyposis coli-binding protein EB1 is associated with cytoplasmic and spindle microtubules." In: *Proc Natl Acad Sci U S A.* 95, pp. 10596–10601. DOI: `10.1073/pnas.95.`

18.10596. URL: `https://www.ncbi.nlm.nih.gov/pmc/articles/PMC27940/`.

Berrueta, L., Tirnauer, J.S., Schuyler, S.C., Pellman, D., and Bierer, B.E. (Apr. 1999). "The APC-associated protein EB1 associates with components of the dynactin complex and cytoplasmic dynein intermediate chain." In: *Curr Biol.* 9.8, pp. 425–428. DOI: `10.1016/s0960-9822(99)80190-0`. URL: `https://pubmed.ncbi.nlm.nih.gov/10226031/`.

Bigman, L.S. and Y. Levy (Apr. 2020). "Tubulin tails and their modifications regulate protein diffusion on microtubules." In: *Proc Natl Acad Sci U S A.* 117, pp. 8876–8883. ISSN: 1091-6490. DOI: `10.1073/pnas.1914772117`. URL: `https://www.pnas.org/content/117/16/8876`.

Bitan, A., Guild, G.M., Bar-Dubin, D., and Abdu, U. (Jan. 2010). "Asymmetric microtubule function is an essential requirement for polarized organization of the *Drosophila* bristle." In: *Mol Cell Biol.* 30.2, pp. 496–507. ISSN: 1098-5549. DOI: `10.1128/MCB.00861-09`. URL: `https://pubmed.ncbi.nlm.nih.gov/19917727/`.

Bochis, O.V., Fetica, B., Vlad, C., Achimas-Cadariu, and P. Irimie, A. (Jan. 2015). "The Importance of Ubiquitin E3 Ligases, SCF and APC/C, in Human Cancers." In: *Clujul Med.* 88.1, pp. 9–14. ISSN: 1222-2119. DOI: `10.15386/cjmed-377`. URL: `https://www.ncbi.nlm.nih.gov/pmc/articles/PMC4508606/`.

Bodakuntla, S., Jijumon, A.S., Villablanca, C., Gonzalez-Billault, C., and Janke, C. (Oct. 2019). "Microtubule-Associated Proteins: Structuring the Cytoskeleton." In: *Trends in Cell Biology.* 29.10, pp. 804–819. ISSN: 1879-3088. DOI: `10.1016/j.tcb.2019.07.004`. URL: `https://pubmed.ncbi.nlm.nih.gov/31416684/`.

Böhler, A., Vermeulen, B.J.A, Martin Würtz, M., Zupa, E., Pfeffer, S., and Schiebel, E. (June 2021). "The gamma-tubulin ring complex: Deciphering the molecular organization and assembly mechanism of a major vertebrate microtubule

nucleator." In: *BioEssay.* 43.8, e2100114. ISSN: 1521-1878. DOI: `10.1002/bies.202100114`. URL: `https://onlinelibrary.wiley.com/doi/full/10.1002/bies.202100114`.

Bonaccorsi, S., Wakefield, J.G., and Gatt, M. (May 2001). "The *Drosophila* a protein asp is involved in microtubule organization during spindle formation and cytokinesis." In: *J Cell Biol.* 153.4, pp. 637–648. ISSN: 0021-9525. DOI: `10.1083/jcb.153.4.637`. URL: `https://pubmed.ncbi.nlm.nih.gov/11352927/`.

Bonafé, N. and Sellers, J.R. (Feb. 1998). "Molecular characterization of myosin V from *Drosophila melanogaster.*" In: *J Muscle Res Cell Motil.* 19.2, pp. 129–141. ISSN: 0142-4319. DOI: `10.1023/a:1005356511634`. URL: `https://pubmed.ncbi.nlm.nih.gov/9536440/`.

Bowman, S.K., Neumüller, R.A., Novatchkova, M., Du, Q., and Knoblich, J.A. (June 2006). "The *Drosophila* NuMA Homolog Mud regulates spindle orientation in asymmetric cell division." In: *Dev Cell.* 10.6, pp. 731–742. ISSN: 1534-5807. DOI: `10.1016/j.devcel.2006.05.005`. URL: `https://pubmed.ncbi.nlm.nih.gov/16740476/`.

Braga, V.M., Machesky, L.M., Hall, and A. Hotchin, N.A. (June 1997). "Regulating Rho GTPases and their regulators." In: *J Cell Biol.* 137.6, pp. 1421–1431. ISSN: 0021-9525. DOI: `10.1083/jcb.137.6.1421`. URL: `https://pubmed.ncbi.nlm.nih.gov/9182672/`.

Brancolini, C., Benedetti, M., and Schneider, C. (Nov. 1995). "Microfilament reorganization during apoptosis: the role of Gas2, a possible substrate for ICE-like proteases." In: *EMBO J.* 14.21, pp. 5179–5190. DOI: `10.1002/j.1460-2075.1995.tb00202.x`. URL: `https://pubmed.ncbi.nlm.nih.gov/7489707/`.

Brand, A.H. and N. Perrimon (June 1993). "Targeted gene expression as a means of altering cell fates and generating dominant phenotypes." In: *Development.*

118, pp. 401–415. ISSN: 0950-1991. URL: `https://pubmed.ncbi.nlm.nih.gov/8223268/`.

Broderick, M.J.F. and S.J. Winder (2005). "Spectrin, alpha-actinin, and dystrophin." In: *Adv Protein Chem.* 70, pp. 203–246. ISSN: 1557-7988. DOI: `10.1016/S0065-3233(05)70007-3`. URL: `https://pubmed.ncbi.nlm.nih.gov/15837517/`.

Brouhard, G.J. and L.M. Rice (July 2018). "Microtubule dynamics: an interplay of biochemistry and mechanics." In: *Nat Rev Mol Cell Biol* 19.7, pp. 451–463. ISSN: 1471-0080. DOI: `https://doi.org/10.1038/s41580-018-0009-y`. URL: `https://pubmed.ncbi.nlm.nih.gov/29674711/`.

Brückner, A., Polge, C., Lentze, N., Auerbach, D., and Schlattner, U. (June 2009). "Yeast two-hybrid, a powerful tool for systems biology." In: *Int J Mol Sci.* 10.6, pp. 2763–2788. ISSN: 1422-0067. DOI: `10.3390/ijms10062763`. URL: `https://pubmed.ncbi.nlm.nih.gov/19582228/`.

Brüning-Richardson, A., Langford, K.J., Ruane, P., Lee, T., Askham, J.M., and Morrison, E.E. (Dec. 2011). "EB1 is required for spindle symmetry in mammalian mitosis." In: *PLoS One.* 6.12, pp. 1–23. DOI: `10.1371/journal.pone.0028884`. URL: `https://www.ncbi.nlm.nih.gov/pmc/articles/PMC3244432/`.

Buffin, E., Lefebvre, C., Huang, J., Gagou, M.E., and Karess, R.E. (May 2005). "Recruitment of Mad2 to the Kinetochore Requires the *Rod/Zw10* Complex." In: *Current Biology* 15.9, pp. 856–861. ISSN: 0960-9822. DOI: `10.1016/j.cub.2005.03.052`. URL: `https://pubmed.ncbi.nlm.nih.gov/15886105/`.

Bulgakova, N.A., Grigoriev, I., Yap, A.S., Akhmanova, A., and Brown, N.H. (June 2013). "Dynamic microtubules produce an asymmetric E-cadherinâBazooka complex to maintain segment boundaries." In: *J Cell Biol.* 201.6, pp. 887–901. ISSN: 1540-8140. DOI: `10.1083/jcb.201211159`. URL: `https://pubmed.ncbi.nlm.nih.gov/23751496/`.

Bulgheresi, S., Kleiner, E., and Knoblich, J.A. (Oct. 2001). "Inscuteable-dependent apical localization of the microtubule-binding protein Cornetto suggests a

role in asymmetric cell division." In: *J Cell Sci.* 114.20, pp. 3655–3662. ISSN: 0021-9533. DOI: `10.1242/jcs.114.20.3655`. URL: `https://pubmed.ncbi.nlm.nih.gov/11707517/`.

Burgess, R.J. and Zhang, Z. (July 2010). "Histones, histone chaperones and nucleosome assembly." In: *Protein Cell.* 1.7, pp. 607–612. ISSN: 1674-8018. DOI: `10.1007/s13238-010-0086-y`. URL: `https://pubmed.ncbi.nlm.nih.gov/21203931/`.

Calero-Cuenca, F.J., Espinosa-Vázquez, J.M, Reina-Campos, M., Díaz-Meco, M.T., Moscat, J., and Sotillos, S. (Apr. 2016). "Nuclear fallout provides a new link between aPKC and polarized cell trafficking." In: *BMC Biol.* 14.32. ISSN: 1741-7001. DOI: `10.1186/s12915-016-0253-6`. URL: `https://pubmed.ncbi.nlm.nih.gov/27089924/`.

Cao, W.X., Kabelitz, S., Gupta, M., Yeung, E., Lin, S., Rammelt, C., Ihling, C., Pekovic, F., Low, T.C.H., Siddiqui, N.U., Cheng, M.H.K., Angers, S. Smibert, C.A., Wühr, M., Wahle, E., and Lipshitz, H.D. (June 2020). "Precise Temporal Regulation of Post-transcriptional Repressors Is Required for an Orderly *Drosophila* Maternal-to-Zygotic Transition." In: *Cell Reports.* 31.12, p. 107783. ISSN: 2211-1247. DOI: `10.1016/j.celrep.2020.107783`. URL: `https://www.sciencedirect.com/science/article/pii/S2211124720307634`.

Chaaban, S. and G.J. Brouhard (Nov. 2017). "A microtubule bestiary: structural diversity in tubulin polymers." In: *Mol Biol Cell.* 28.22, pp. 2924–2931. ISSN: 1939-4586. DOI: `10.1091/mbc.E16-05-0271`. URL: `https://pubmed.ncbi.nlm.nih.gov/29084910/`.

Chartron, J.W., Gonzalez, G.M., and Jr, W.M.C. (Sept. 2011). "A structural model of the Sgt2 protein and its interactions with chaperones and the Get4/Get5 complex." In: *J Biol Chem.* 286.39, pp. 34325–34334. ISSN: 1083-351X. DOI: `10.1074/jbc.M111.277798`. URL: `https://pubmed.ncbi.nlm.nih.gov/21832041/`.

Chase, A.R., Laudermilch, E., Wang, J., Shigematsu, H., Yokoyama, T., and Schlieker, C. (Oct. 2017). "Dynamic functional assembly of the Torsin AAA+ ATPase and its modulation by LAP1." In: *Mol Biol Cell.* 28.21, pp. 2765–2772. ISSN: 1939-4586. DOI: `10.1091/mbc.E17-05-0281`. URL: `https://pubmed.ncbi.nlm.nih.gov/28814508/`.

Chatel, G. and B. Fahrenkrog (Oct. 2011). "Nucleoporins: leaving the nuclear pore complex for a successful mitosis." In: *Cell Mol Life Sci* 23.10, pp. 1555–1562. DOI: `10.1016/j.cellsig.2011.05.023`. URL: `https://pubmed.ncbi.nlm.nih.gov/21683138/`.

Chen, Y. and W.O. Hancock (Oct. 2015). "Kinesin-5 is a microtubule polymerase." In: *Nat Commun.* 6, p. 8160. DOI: `10.1038/ncomms9160`. URL: `https://pubmed.ncbi.nlm.nih.gov/26437877/`.

Chircop, M. (June 2014). " Rho GTPases as regulators of mitosis and cytokinesis in mammalian cells." In: *Small GTPases.* 5.2, pp. 1–14. DOI: `10.4161/sgtp.29770`. URL: `https://www.ncbi.nlm.nih.gov/pmc/articles/PMC4160341/`.

Collins, E.S., Balchand, S.K., Faraci, J.L., Wadsworth, P., and Lee, W.L. (Sept. 2012). "Cell cycle-regulated cortical dynein/dynactin promotes symmetric cell division by differential pole motion in anaphase." In: *Mol Biol Cell.* 23.17, pp. 3380–3390. DOI: `10.1091/mbc.E12-02-0109`. URL: `https://pubmed.ncbi.nlm.nih.gov/22809624/`.

Conde, C., Osswald, M., Barbosa, J., Moutinho-Santos, T., Pinheiro, D., Guimarães, S., Matos, I., Maiato, H., and Sunkel, C.E. (June 2013). "*Drosophila* Polo regulates the spindle assembly checkpoint through Mps1-dependent BubR1 phosphorylation." In: *EMBO J.* 32.12, pp. 1761–1777. ISSN: 0261-4189. DOI: `10.1038/emboj.2013.109`. URL: `https://pubmed.ncbi.nlm.nih.gov/23685359/`.

Conduit, P.T., Hayward, D., and Wekafield, J.G. (2015). "Microinjection techniques for studying centrosome function in *Drosophila melanogaster* syncytial embryos." In: *Methods in Cell Biology.* 129, pp. 229–249. ISSN: 0091-679X. DOI: `https://doi.org/10.1016/bs.mcb.2015.03.007`. URL: `https://www.sciencedirect.com/science/article/abs/pii/S0091679X15000795`.

Corinne, A.T. and A.C. Paul (Dec. 2011). "Microtubule nucleation by γ-tubulin complexes and beyond." In: *Essay in Biochemistry.* 62.6, pp. 765–780. ISSN: 1744-1358. DOI: `10.1042/EBC20180028`. URL: `https://pubmed.ncbi.nlm.nih.gov/30315097/`.

Coulson, R.M., Brown, K.D., Yen, T.J., and Cleveland, D.W. (June 1994). "Cyclin-like accumulation and loss of the putative kinetochore motor CENP-E results from coupling continuous synthesis with specific degradation at the end of mitosis." In: *Cell Biol.* 125.6, pp. 1303–1312. ISSN: 0021-9525. DOI: `10.1083/jcb.125.6.1303`. URL: `https://pubmed.ncbi.nlm.nih.gov/8207059/`.

Cramer, L.P. (Sept. 2000). "Myosin VI: roles for a minus end-directed actin motor in cells." In: *J Cell Biol.* 150.6, F121–F126. ISSN: 0021-9525. DOI: `10.1083/jcb.150.6.f121`. URL: `https://pubmed.ncbi.nlm.nih.gov/10995456/`.

Davison, D. (July 1985). "Sequence similarity (Homology) searching for molecular biologists." In: *SpringerLink* 47, pp. 437–474. DOI: `10.1007/BF02460006`. URL: `https://link.springer.com/article/10.1007/BF02460006`.

Delgehyr, N., Rangone, H., Fu, J., Mao, G., Tom, B., Riparbelli, M.G., Callaini, G., and Glover, D.M. (Mar. 2012). "Klp10A, a microtubule-depolymerizing kinesin-13, cooperates with CP110 to control *Drosophila* centriole length. Curr Biol." In: *Curr Biol.* 22.6, pp. 502–509. DOI: `10.1016/j.cub.2012.01.046`. URL: `https://pubmed.ncbi.nlm.nih.gov/22365849/`.

Desai, A. and T.J. Mitchison (Nov. 1997). "Microtuble polymerization dynamics." In: *Annu. Rev. Cell Dev. Biol.* 13, pp. 83–117. ISSN: 081-0706. DOI: `10.1146/`

annurev.cellbio.13.1.83. URL: https://pubmed.ncbi.nlm.nih.gov/
9442869/.

di Pietro, F., Echard, A., and Morin, X. (Aug. 2016). "Regulation of mitotic spindle
orientation: an integrated view." In: *EMBO Rep.* 17.8, pp. 1106–1130. DOI: 10.
15252/embr.201642292. URL: https://www.ncbi.nlm.nih.gov/pmc/
articles/PMC4967962/.

Dobbelaere, J. (May 2015). "The ubiquitin proteasome system - implications for
cell cycle control and the targeted treatment of cancer." In: *Methods Cell Biol.*
129, pp. 279–300. ISSN: 0091-679X. DOI: 10.1016/bs.mcb.2015.03.011.
URL: https://pubmed.ncbi.nlm.nih.gov/26175444/.

Duan, R., Kim, J.H., Shilagardi, K., Schiffhauer, E., Lee, D.M., Son, S., Li, S., Thomas,
C., Luo, T., Fletcher, D.A., Robinson, D.N., and Che, E.H. (June 2018). "Spec-
trin is a mechanoresponsive protein shaping fusogenic synapse architecture
during myoblast fusion." In: *Nat Cell Biol.* 20.6, pp. 688–698. ISSN: 1476-4679.
DOI: 10.1038/s41556-018-0106-3. URL: https://pubmed.ncbi.nlm.
nih.gov/29802406/.

Dubin-Bar, D., Bitan, A., Bakhrat, A., Kaiden-Hasson, R., Etzion, S. Shaanann,
and Abdu, U. (Sept. 2008). "The *Drosophila* IKK-related kinase (Ik2) and Spindle-
F proteins are part of a complex that regulates cytoskeleton organization dur-
ing oogenesis." In: *BMC Cell Biol.* 9, p. 51. ISSN: 1471-2121. DOI: 10.1186/
1471-2121-9-51. URL: https://pubmed.ncbi.nlm.nih.gov/18796167/.

Edgar, B.A. and P.H. O'Farrell (Apr. 1989). "Genetic control of cell division pat-
terns in the *Drosophila* embryo." In: *Cell.* 57.1, pp. 177–187. DOI: 10.1016/
0092-8674(89)90183-9. URL: https://www.ncbi.nlm.nih.gov/pmc/
articles/PMC2755076/.

Elliott, S.L., Cullen, C.F., Wrobel, N., Kernan, M.J, and Ohkura, H. (Feb. 2005).
"EB1 Is Essential during *Drosophila* Development and Plays a Crucial Role in
the Integrity of Chordotonal Mechanosensory Organs." In: *Mol Biol Cell.* 16.2,

pp. 891–901. DOI: `10.1091/mbc.E04-07-0633`. URL: `https://www.ncbi.nlm.nih.gov/pmc/articles/PMC545920/`.

Evans, T., Rosenthal, E.T, Youngblom, J., Distel, D., and Hunt, T. (June 1983). "Cyclin: A protein specified by maternal mRNA in sea urchin eggs that is destroyed at each cleavage division." In: *Cell* 33.2, pp. 389–396. ISSN: 0092-8674. DOI: `10.1016/0092-8674(83)90420-8`. URL: `https://www.sciencedirect.com/science/article/pii/0092867483904208`.

Fabian, D.K., Lack, J.B., Mathur, V., Schlötterer, C., Schmidt, P.S., Pool, J.E., and Flatt, T. (Apr. 2015). "Spatially varying selection shapes life history clines among populations of *Drosophila melanogaster* from sub-Saharan Africa." In: *J Evol Biol.* 28.4, pp. 826–840. DOI: `10.1111/jeb.12607`. URL: `https://www.ncbi.nlm.nih.gov/pmc/articles/PMC4405473/`.

Farache, D., Emorine, L., Haren, L., and Merdes, A. (Mar. 2018). "Assembly and regulation of γ-tubulin complexes". In: *Open Biol.* 8.3. ISSN: 2046-2441. DOI: `10.1098/rsob.170266`. URL: `https://royalsocietypublishing.org/doi/10.1098/rsob.170266`.

Ferenz, N.P., Gable, A., and Wadsworth, P. (Jan. 2010). "Mitotic functions of kinesin-5." In: *Semin Cell Dev Biol.* 21.3, pp. 255–259. DOI: `10.1016/j.semcdb.2010.01.019`. URL: `https://www.ncbi.nlm.nih.gov/pmc/articles/PMC2844466/`.

Finan, D., Hartman, M.A., and Spudich, J.A. (Apr. 2011). "Proteomics approach to study the functions of *Drosophila* myosin VI through identification of multiple cargo-binding proteins." In: *Proc Natl Acad Sci USA.* 108.14, pp. 5566–5571. ISSN: 1091-6490. DOI: `10.1073/pnas.1101415108`. URL: `https://www.ncbi.nlm.nih.gov/pmc/articles/PMC3078346/`.

Fire, A., Xu, S., Montgomery, M.K., Kostas, S.A., Driver, S.E., and Mello, C.C. (Feb. 1998). "Potent and specific genetic interference by double-stranded RNA in

Caenorhabditis elegans." In: *Nature.* 391, pp. 806–811. DOI: `10.1038/35888`. URL: `https://pubmed.ncbi.nlm.nih.gov/9486653/`.

Flatt, T. (Jan. 2020). "Life-History Evolution and the Genetics of Fitness Components in *Drosophila melanogaster.*" In: *Genetics.* 214.1, pp. 3–48. DOI: `10.1534/genetics.119.300160`. URL: `https://www.ncbi.nlm.nih.gov/pmc/articles/PMC6944413/`.

Fletcher, G.C., Elbedwy, A., Khanal, I., Ribeiro, P.S., Tapon, N., and Thompson and B.J. (Apr. 2015). "The Spectrin cytoskeleton regulates the Hippo signalling pathway." In: *EMBO J.* 34.7, pp. 940–954. ISSN: 1460-2075. DOI: `10.15252/embj.201489642`. URL: `https://pubmed.ncbi.nlm.nih.gov/25712476/`.

Gama, J.B., Pereira, C., Simões, P.A., Celestino, R., Reis, R.M., Barbosa, D.J., Pires, H.R., Carvalho, C., Amorim, J., Carvalho, A.X., Cheerambathur, D.K., and Gassmann, R. (Apr. 2017). "Molecular mechanism of dynein recruitment to kinetochores by the Rod-Zw10-Zwilch complex and Spindly." In: *J Cell Biol.* 216.4, pp. 943–960. DOI: `10.1083/jcb.201610108`. URL: `https://pubmed.ncbi.nlm.nih.gov/28320824/`.

Gambotto, A., Dworacki, G., Cicinnati, V., Kenniston, T., Steitz, J., Tüting, T., Robbins, P.D., and DeLeo, A.B. (Dec. 2000). "Immunogenicity of enhanced green fluorescent protein (EGFP) in BALB/c mice: identification of an H2-Kd-restricted CTL epitope." In: *Gene Ther.* 7.23, pp. 2036–2040. DOI: `10.1038/sj.gt.3301335`. URL: `https://pubmed.ncbi.nlm.nih.gov/11175316/`.

Gamper, I., Koh, K.R, Ruau, D., Ullrich, K, Bartunkova, J., Piroth, D., Hacker, C., Bartunek, P., and Zenke, M. (May 2009). "GAR22: a novel target gene of thyroid hormone receptor causes growth inhibition in human erythroid cells." In: *Exp Hematol.* 37.5, pp. 539–548. DOI: `10.1016/j.exphem.2009.02.002`. URL: `https://pubmed.ncbi.nlm.nih.gov/19375645/`.

Gao, Y., Zhang, Q., Lang, Y., Liu, Y., Dong X., Chen, Z., Tian, W., Tang, J., Wu, W., Tong, Y., and Chen, Z. (June 2017). "Human apo-SRP72 and SRP68/72 com-

plex structures reveal the molecular basis of protein translocation." In: *J Mol Cell Biol.* 9.3, pp. 220–230. ISSN: 1759-4685. DOI: `10.1093/jmcb/mjx010`. URL: `https://pubmed.ncbi.nlm.nih.gov/28369529/`.

Garcia, K., Duncan, T., and Su, T.T. (Feb. 2007). "Analysis of the cell division cycle in *Drosophila.*" In: *Methods.* 41.2, pp. 198–205. DOI: `10.1016/j.ymeth.2006.08.013`. URL: `https://pubmed.ncbi.nlm.nih.gov/17189862/`.

Gepner, J., Li, M., Ludmann, S., Kortas, C., Boylan, K., Iyadurai, S.J., McGrail, M., and Hays, T.S. (Mar. 1996). "Cytoplasmic Dynein Function Is Essential in *Drosophila Melanogaster.*" In: *Genetics.* 142.3, pp. 865–878. DOI: `10.1093/genetics/142.3.865`. URL: `https://www.ncbi.nlm.nih.gov/pmc/articles/PMC1207024/`.

Gergely, F., Lee, M.J., Jeffers, K., Peak-Chew, S.Y., and Raff, J.W. (June 2001). "Msps/XMAP21 interacts with the centrosomal protein D-TACC to regulate microtubule behaviour." In: *Nat Cell Biol.* 3, pp. 643–649. ISSN: 2046-6390. DOI: `10.1038/35083033`. URL: `https://www.nature.com/articles/ncb0701_643`.

Girdler, G.C., Applewhite, D.A., Perry, W.M.G., Rogers, S.L., and Röper, K. (Jan. 2016). "The Gas2 family protein Pigs is a microtubule +TIP that affects cytoskeleton organisation." In: *J Cell Sci.* 129.1, pp. 121–134. ISSN: 1477-9137. DOI: `10.1242/jcs.176230`. URL: `https://pubmed.ncbi.nlm.nih.gov/26585311/`.

Golsteyn, R.M., Mundt, K.E., Fry, A.M., and Nigg, E.A. (June 1995). "Cell cycle regulation of the activity and subcellular localization of Plk1, a human protein kinase implicated in mitotic spindle function." In: *J Cell Biol.* 129.6, pp. 1617–1628. ISSN: 0021-9525. DOI: `10.1083/jcb.129.6.1617`. URL: `https://pubmed.ncbi.nlm.nih.gov/7790358/`.

González, J. and D.A. Petrov (Dec. 2009). "The adaptive role of transposable elements in the *Drosophila* genome." In: *Gene.* 448.2, pp. 124–133. ISSN: 0027-

8424. DOI: `10.1016/j.gene.2009.06.008`. URL: `https://pubmed.ncbi.nlm.nih.gov/19555747/`.

Goriounov, D., Leung, C.L., and Liem, R.K. (Mar. 2003). "Protein products of human Gas2-related genes on chromosomes 17 and 22 (hGAR17 and hGAR22) associate with both microfilaments and microtubules." In: *J Cell Sci.* 116.Pt 6, pp. 1045–1058. ISSN: 0021-9533. DOI: `10.1242/jcs.00272`. URL: `https://pubmed.ncbi.nlm.nih.gov/12584248/`.

Goshima, G. and R.D. Vale (Sept. 2003). "The roles of microtubule-based motor proteins in mitosis: comprehensive RNAi analysis in the *Drosophila* S2 cell line." In: *J Cell Biol.* 162.6, pp. 1003–1016. ISSN: 0021-9525. DOI: `10.1083/jcb.200303022`. URL: `https://pubmed.ncbi.nlm.nih.gov/12975346/`.

– (Aug. 2005). "Cell cycle-dependent dynamics and regulation of mitotic kinesins in *Drosophila* S2 cells." In: *Mol Biol Cell.* 16.8, pp. 3896–3907. DOI: `10.1091/mbc.e05-02-0118`. URL: `https://pubmed.ncbi.nlm.nih.gov/15958489/`.

Gratz, S.J., Ukken, F.P., Rubinstein, C.D., Thiede, G., Donohue, L.K., Cummings, A.M., and O'Connor-Giles, K.M. (Apr. 2014). "Highly specific and efficient CRISPR/Cas9-catalyzed homology-directed repair in *Drosophila.*" In: *Genetics.* 196.4, pp. 961–971. ISSN: 1943-2631. DOI: `10.1534/genetics.113.160713`. URL: `https://www.ncbi.nlm.nih.gov/pmc/articles/PMC3982687/`.

Green, R.A., Wollman, R., and Kaplan, K.B. (Oct. 2005). "APC and EB1 function together in mitosis to regulate spindle dynamics and chromosome alignment." In: *Mol Biol Cell.* 16.10, pp. 4609–4622. DOI: `10.1091/mbc.e05-03-0259`. URL: `https://pubmed.ncbi.nlm.nih.gov/16030254/`.

Grossman, E., Medalia, O., and Zwerger, M. (2012). "Functional architecture of the nuclear pore complex." In: *Annu Rev Biophys.* 41, pp. 557–584. ISSN: 1936-1238. DOI: `10.1146/annurev-biophys-050511-102328`. URL: `https://pubmed.ncbi.nlm.nih.gov/22577827/`.

Grotek, B., Wehner, D., and Weidinger, G. (Apr. 2013). "Notch signaling coordi- nates cellular proliferation with differentiation during zebrafish fin regenera- tion". In: *Development.* 140.7, pp. 1412–1423. ISSN: 1477-9129. DOI: `10.1242/ dev.087452`. URL: `https://pubmed.ncbi.nlm.nih.gov/23462472/`.

Gründl, M., Engel, F.B., and Gaubatz, S. (Oct. 2017). "GAS2L3: Coordinator of cardiomyocyte cytokinesis?" In: *Cell Cycle.* 16.20, pp. 1853–1854. ISSN: 1551- 4005. DOI: `10.1080/15384101.2017.1372546`. URL: `https://pubmed. ncbi.nlm.nih.gov/28937871/`.

Gudimchuk, N.B., Ulyanov, E.V., ÓToole, E.and Page, C.L., Vinogradov, D.S. Mor- gan, M., Li, Gabriella, Moore, J.K., Szczesna, E., Roll-Meck, A., Ataullakhanov, F.I., and McIntosh, R. (July 2020). "Mechanisms of microtubule dynamics and force generation examined with computational modeling and electron cry- otomography." In: *Nat Commun.* 11.1, p. 3765. ISSN: 2041-1723. DOI: `10.1038/ s41467-020-17553-2`. URL: `https://pubmed.ncbi.nlm.nih.gov/ 32724196/`.

Guglielmi, V., Sakuma, S., and D'Angelo M.A. (Dec. 2020). "Nuclear pore com- plexes in development and tissue homeostasis." In: *Development.* 147.23, dev183442. ISSN: 1477-9129. DOI: `10.1242/dev.183442`. URL: `https://pubmed.ncbi. nlm.nih.gov/33323374/`.

Gutiérrez-Cabalerro, C., Burgess, S.G., Bayliiss, R., and Royle, S.J. (Jan. 2015). "TACC3âch-TOG track the growing tips of microtubules independently of clathrin and Aurora-A phosphorylation." In: *Biol Open.* 4, pp. 170–179. ISSN: 2046- 6390. DOI: `10.1242/bio.201410843`. URL: `https://pubmed.ncbi.nlm. nih.gov/25596274/`.

Hahn, I., Ronshaugen, M., Sánchez-Soriano, N., and Prokop, A. (2016). "*Drosophila* oocyte polarity and cytoskeleton organization require regulation of Ik2 activ- ity by Spn-F and Javelin-like." In: *Methods Enzymol.* 569, pp. 373–405. ISSN:

1557-7988. DOI: `10.1016/bs.mie.2015.06.022`. URL: `https://pubmed.ncbi.nlm.nih.gov/26778568/`.

Harnish, J.M., Link, N., and Yamamoto, S. (Mar. 2021). " *Drosophila* as a Model for Infectious Diseases." In: *Int J Mol Sci.* 22.5, p. 2724. DOI: `10.3390/ijms22052724`. URL: `https://www.ncbi.nlm.nih.gov/pmc/articles/PMC7962867/`.

Harris, J., Schwinn, N., Mahoney, J.A., Lin, H-H., Shaw, M., Howard, C.J: da Silva, R.P., and Gordon, S. (Feb. 2006). "A vitellogenic-like carboxypeptidase expressed by human macrophages is localized in endoplasmic reticulum and membrane ruffles." In: *Int J Exp Pathol.* 87.1, pp. 29–39. ISSN: 0959-9673. DOI: `10.1111/j.0959-9673.2006.00450.x`. URL: `https://www.ncbi.nlm.nih.gov/pmc/articles/PMC2517344/`.

Hasson, T. (Sept. 2003). "Myosin VI: two distinct roles in endocytosis." In: *J Cell Sci.* 116.Pt 17, pp. 3453–3461. ISSN: 0021-9533. DOI: `10.1242/jcs.00669`. URL: `https://pubmed.ncbi.nlm.nih.gov/12893809/`.

Hayashi, I., Wilde, A., Mal, T.K., and Ikura, M. (Aug. 2005). "Structural basis for the activation of microtubule assembly by the EB1 and p150Glued complex." In: *Mol. Cell.* 19.4, pp. 449–460. ISSN: 1097-2765. DOI: `10.1016/j.molcel.2005.06.034`. URL: `https://pubmed.ncbi.nlm.nih.gov/16109370/`.

Haykal, M.M., Rodrigues-Ferreira, S., and Nahmias, C. (May 2021). "Microtubule-Associated Protein ATIP3, an Emerging Target for Personalized Medicine in Breast Cancer." In: *Cells.* 10.5, pp. 1–12. DOI: `10.3390/cells10051080`. URL: `https://www.mdpi.com/2073-4409/10/5/1080`.

Hayward, D., Metz, J., Pellacani, C., and Wakefield, J.G. (Jan. 2014). "Synergy between multiple microtubule-generating pathways confers robustness to centrosome driven mitotic spindle formation." In: *Dev Cell.* 28, pp. 81–93. DOI: `10.1016/j.devcel.2013.12.001`. URL: `https://pubmed.ncbi.nlm.nih.gov/24389063/`.

Heigwer, F., Port, F., and Boutros, M. (Mar. 2018). "RNA Interference (RNAi) Screening in *Drosophila*". In: *Genetics* 208.3, pp. 853–874. DOI: `10.1534/genetics.117.300077`. URL: `https://www.genetics.org/content/208/3/853`.

Hetzer, M.W. (Mar. 2010). "The Nuclear Envelope." In: *Cold Spring Harb Perspect Biol.* 2.3, e00539. ISSN: 1943-0264. DOI: `10.1101/cshperspect.a000539`. URL: `https://www.ncbi.nlm.nih.gov/pmc/articles/PMC2829960/`.

Heuzé, M.L., Narayana, G.H.N.S., D'Alessandro J., Cellerin, V., Dang, T., Williams, D.S., Hest, J.C.V., Marcq, P., Mège, R-M., and Ladoux, B. (Sept. 2019). "Myosin II isoforms play distinct roles in adherens junction biogenesis." In: *Elife.* 8, e46599. ISSN: 2050-084X. DOI: `10.7554/eLife.46599`. URL: `https://pubmed.ncbi.nlm.nih.gov/31486768/`.

Hevia, L.G. and M.L. Fanarraga (Dec. 2020). "Microtubule cytoskeleton-disrupting activity of MWCNTs: applications in cancer treatment." In: *J Nanobiotechnol.* 18.1, p. 181. ISSN: 1477-3155. DOI: `10.1186/s12951-020-00742-y`. URL: `https://pubmed.ncbi.nlm.nih.gov/33317574/`.

Hirokawa, N. (Apr. 1996). "Organelle transport along microtubules - the role of KIFs." In: *Trends Cell Biol.* 6.4, pp. 135–141. DOI: `10.1016/0962-8924(96)10003-9`. URL: `https://pubmed.ncbi.nlm.nih.gov/15157476/`.

Hirokawa, N., Takemura, R., and Hisanaga, S. (Nov. 1985). "Cytoskeletal architecture of isolated mitotic spindle with special reference to microtubule associated proteins and cytoplasmic dynein." In: *J Cell Biol.* 101.5 Pt 1, pp. 1858–1870. ISSN: 0021-9525. DOI: `10.1083/jcb.101.5.1858`. URL: `https://pubmed.ncbi.nlm.nih.gov/2932452/`.

Hodge, R.G. and A.J. Ridley (Aug. 2015). "Regulating Rho GTPases and their regulators." In: *Nat Rev Mol Cell Biol.* 17.8, pp. 496–510. ISSN: 1471-0080. DOI: `10.1038/nrm.2016.67`. URL: `https://pubmed.ncbi.nlm.nih.gov/27301673/`.

Holland, A.J. and D.W. Cleveland (June 2012). "Losing balance: the origin and impact of aneuploidy in cancer." In: *EMBO Rep.* 13.6, pp. 501–514. DOI: `10.1038/embor.2012.55`. URL: `https://pubmed.ncbi.nlm.nih.gov/22565320/`.

Honnappa, S., Gouveia, S, M., Weisbrich, A., Damberger, F.F., Bhavesh, N.S., Jawhari, H., Grigoriev, I., van Rijssel, F.J., Buey, R.M., Lawera, A., Jelesarov, I., Winkler, F.K., Wüthrich, K., Akhmanova, A., and Steinmetz, M.O. (July 2009). "An EB1-binding motif acts as a microtubule tip localization signal." In: *Cell.* 138.2, pp. 366–376. DOI: `10.1016/j.cell.2009.04.065`. URL: `https://pubmed.ncbi.nlm.nih.gov/19632184/`.

Hornig, N.C.D., Knowles, P.P., McDonald, N.Q., and Frank, U. (June 2002). "The dual mechanism of separase regulation by securin." In: *Curr Biol.* 12.12, pp. 973–982. DOI: `10.1016/s0960-9822(02)00847-3`. URL: `https://pubmed.ncbi.nlm.nih.gov/12123570/`.

Howard, J. and A. Hyman (Apr. 2003). "Dynamics and mechanics of the microtubule plus end." In: *Nature* 422, pp. 753–758. ISSN: 0028-0836. DOI: `10.1038/nature01600`. URL: `https://pubmed.ncbi.nlm.nih.gov/12700769/`.

Hu, L., Xiao, Y., Xiong, Z., Zhao, F., Yin, C., Zhang, Y., Su, P., Li, D., Chen, Z., Ma, X., Zhang, G., and Qian, A. (Sept. 2017). "MACF1, versatility in tissue-specific function and in human disease." In: *Semin Cell Dev Biol.* 69, pp. 3–8. ISSN: 1096-3634. DOI: `10.1016/j.semcdb.2017.05.017`. URL: `https://pubmed.ncbi.nlm.nih.gov/28577926/`.

Hughes, J.R., Meireles, A.M., Fisher, K.H., Garcia, A., Antrobus, P.R., Wainman, A., Zitzmann, N., Deane, C., Ohkura, H., and Wakefield, J.G. (Apr. 2008). "A Microtubule Interactome: Complexes with Roles in Cell Cycle and Mitosis." In: *PLoS Biol.* 6.4, e98. ISSN: 1544-9173. DOI: `10.1371/journal.pbio.0060098`. URL: `https://www.ncbi.nlm.nih.gov/pmc/articles/PMC2323305/`.

Inoue, Y.H., Avides M.doC., Shiraki, M., Yamaguchi, M., Nishimoto, Y., Matsuk-age, and Glover, D.M. (Apr. 2000). "Orbit, a novel microtubule-associated protein essential for mitosis in *Drosophila melanogaster.*" In: *J Cell Biol.* 139, pp. 153–166. ISSN: 0021-9525. DOI: `10.1083/jcb.149.1.153`. URL: `https://pubmed.ncbi.nlm.nih.gov/10747094/`.

Jain, I. and P.T. Tran (June 2017). "Multiple Motifs Compete for EB-Dependent Microtubule Plus End Binding." In: *Structure (London, England : 1993)* 25(6). https://doi.org/10.1016/j.str.2017.05.017, pp. 821–822. DOI: `10.1016/j.str.2017.05.017`.

Jauneau, A., Farache, D., Chemin, C., Chartrain, M., Rémy, M.H., Merdes, A, and Haren, L. (Oct. 2016). "Functional Analysis of γ-Tubulin Complex Proteins Indicates Specific Lateral Association via Their N-terminal Domains." In: *J. Biol. Chem.* 29.44, pp. 23112–23125. ISSN: 1083-351X. DOI: `10.1074/jbc.M116.744862`. URL: `https://www.ncbi.nlm.nih.gov/pmc/articles/PMC5087730/`.

Jeffers, K., Gergely, F., Kidd, D., Wakefield, J.G., and Raff, J.W. (Jan. 2020). "D-TACC: A novel centrosomal protein required for normal spindle function in the early *Drosophila* embryo." In: *EMBO J.* 19, pp. 241–252. ISSN: 0261-4189. DOI: `10.1093/emboj/19.2.241`. URL: `https://www.ncbi.nlm.nih.gov/pmc/articles/PMC305558/`.

Jeibmann, A. and W. Paulus (Feb. 2009). "*Drosophila melanogaster* as a model organism of brain diseases." In: *Int J Mol Sci.* 10.2, pp. 407–40. ISSN: 1750-1326. DOI: `10.3390/ijms10020407`. URL: `https://pubmed.ncbi.nlm.nih.gov/19333415/`.

Jeong, A.L., Lee, S., Park, J-S., Han, S., Jang, C-J, Lim, J-S., Lee, M.S., and Yang, Y. (Jan. 2014). "Cancerous inhibitor of protein phosphatase 2A (CIP2A) protein is involved in centrosome separation through the regulation of NIMA (never in mitosis gene A)-related kinase 2 (NEK2) protein activity." In: *J Biol Chem.*

289.1, pp. 28–40. ISSN: 1083-351X. DOI: `10.1074/jbc.M113.507954`. URL: `https://pubmed.ncbi.nlm.nih.gov/24214971/`.

Jones, L., Richardson, H., and Saint, R. (Nov. 2000). "Tissue-specific regulation of cyclin E transcription during *Drosophila melanogaster* embryogenesis." In: *Development.* 127.21, pp. 4619–4630. DOI: `10.1016/j.ymeth.2006.08.013`. URL: `https://pubmed.ncbi.nlm.nih.gov/11023865/`.

Jouette, J., Guichet, A., and Claret, S.B. (Jan. 2019). "Dynein-mediated transport and membrane trafficking control PAR3 polarised distribution." In: *eLife.* 8, e40212. DOI: `10.7554/eLife.40212`. URL: `https://www.ncbi.nlm.nih.gov/pmc/articles/PMC6358217/`.

Junttila, M.R., Puustinen, P., Niemelä, M., Ahola, R, Arnold, H., Böttzauw, T., Ala-aho, R. a nd Nielsen, C., Ivaska, J., Taya, Y., Lu, S.L., Lin, S., Chan, E.K., Wang, X.J., Grènman, R., Kast, J., Kallunki, T., Sears, R., Kähäri, V.M., and Westermarck, J. (July 2007). "CIP2A inhibits PP2A in human malignancies." In: *Cell.* 130.1, pp. 51–62. DOI: `10.1016/j.cell.2007.04.044`. URL: `https://pubmed.ncbi.nlm.nih.gov/17632056/`.

Khanal, I., Elbediwy, A., Diaz de la Loza, M., Fletcher, G.C., and Thompson, B.J. (July 2017). "Shot and Patronin polarise microtubules to direct membrane traffic and biogenesis of microvilli in epithelia." In: *J Cell Sci.* 130.13, p. 2221. DOI: `10.1242/jcs.206912`. URL: `https://www.ncbi.nlm.nih.gov/pmc/articles/PMC5536889/`.

Khanna, A., Pimanda, J.E., and Westermarck, J. (Nov. 2013). "Cancerous inhibitor of protein phosphatase 2A, an emerging human oncoprotein and a potential cancer therapy target." In: *Cancer Res.* 73.22, pp. 6548–6553. DOI: `10.1158/0008-5472.CAN-13-1994`. URL: `https://pubmed.ncbi.nlm.nih.gov/24204027/`.

Khodjakov, A. and C.L. Rieder (Apr. 2001). " Centrosomes enhance the fidelity of cytokinesis in vertebrates and are required for cell cycle progression." In: *J*

Cell Biol. 153.1, pp. 237–242. DOI: `10.1083/jcb.153.1.237`. URL: `https://pubmed.ncbi.nlm.nih.gov/11285289/`.

Kim, J-S., Kim, E.J., Oh, J.S., Park, I-C., and Hwang, S-G. (Nov. 2013). "CIP2A modulates cell-cycle progression in human cancer cells by regulating the stability and activity of Plk1." In: *Cancer Res.* 73.22, pp. 6667–6678. ISSN: 1538-7445. DOI: `10.1158/0008-5472.CAN-13-0888`. URL: `https://pubmed.ncbi.nlm.nih.gov/23983103/`.

Kimpara, A., Otani, T., Oshima, K., Takeda, M., Abdu, U., and Hayasgi, S. (Oct. 2015). "A transport and retention mechanism for the sustained distal localization of Spn-F-IKKε during *Drosophila* bristle elongation." In: *Development* 142.20, pp. 2338–2351. DOI: `10.1242/dev.130674`. URL: `https://journals.biologists.com/dev/article/142/20/3612/46998/A-transport-and-retention-mechanism-for-the`.

Kline-Smith, S.L. and C.E. Walczak (Aug. 2004). "Mitotic Spindle Assembly and Chromosome Segregation: Refocusing on Microtubule Dynamics." In: *Molecular Cell* 15.3, pp. 317–327. ISSN: 1097-2765. DOI: `10.1016/j.molcel.2004.07.012`. URL: `https://www.sciencedirect.com/science/article/pii/S1097276504004186`.

Kollman, J.M., Polka, J.K., Zelter, A., Davis, T.N., and Agard, DA. (Aug. 2010). "Microtubule nucleating gamma-TuSC assembles structures with 13-fold microtubule like symmetry." In: *Nature.* 466.7308, pp. 879–883. DOI: `10.1038/nature09207.`. URL: `https://www.nature.com/articles/nature09207`.

Komarova, Y., De Groot, C.O., Grigoriev, I., Gouveia, S.M., Munteanu, E.L. Schober, J.M., Honnappa, S., Buey, R.M., Hoogenraad, C.C, Dogterom, M., Borisy, G.G., Steinmetz, M.O., and Akhmanova, A. (Mar. 2009). "Mammalian end binding proteins control persistent microtubule growth." In: *J Cell Biol.* 184.5, pp. 691–706. DOI: `10.1083/jcb.200807179`. URL: `https://rupress.org/jcb/`

`article/184/5/691/35290/Mammalian‑end‑binding‑proteins‑` `control-persistent`.

Komiya, Y. and R. Habasi (Apr. 2008). "Wnt signal transduction pathways." In: *Organogenesis*. 4.2, pp. 68–75. DOI: `10.4161/org.4.2.5851`. URL: `https://www.ncbi.nlm.nih.gov/pmc/articles/PMC2634250/`.

Kononova, O., Kholodov, Y., Theisen, K.E., Marx, K.A., Dima, R.I., Ataullakhanov, F.I., Grishchuk, E.L., and Barsegov, V. (Dec. 2014). "Tubulin bond energies and microtubule biomechanics determined from nanoindentation in silico." In: *J Am Chem Soc*. 136.49, pp. 17036–17045. DOI: `10.1021/ja506385p`. URL: `https://pubmed.ncbi.nlm.nih.gov/25389565/`.

Kopan, R. (Oct. 2012). "Notch Signaling." In: *Cold Spring Harb Perspect Biol*. 4.10, a011213. ISSN: 1943-0264. DOI: `10.1101/cshperspect.a011213`. URL: `https://www.ncbi.nlm.nih.gov/pmc/articles/PMC3475170/`.

Krämer, H. and M. Phistry (Feb. 1999). "Genetic analysis of hook, a gene required for endocytic trafficking in *drosophila*." In: *Genetics*. 152.2, pp. 675–684. ISSN: 0015-6731. DOI: `1093/genetics/151.2.675`. URL: `https://pubmed.ncbi.nlm.nih.gov/9927460/`.

Kraut, R., Chia, W., Jan, L.Y., Jan, Y.N., and Knoblich, J.A. (Sept. 1996). "Role of inscuteable in orienting asymmetric cell divisions in *Drosophila*." In: *Nature*. 383.6595, pp. 50–55. ISSN: 0021-9533. DOI: `10.1038/383050a0`. URL: `https://doi.org/10.1038/383050a0`.

Kreis, T.E., Lowe, M., and Pepperkok, R. (1995). "COPs regulating membrane traffic." In: *Annu Rev Cell Dev Biol*. 11, pp. 677–706. ISSN: 1081-0706. DOI: `10.1146/annurev.cb.11.110195.003333`. URL: `https://pubmed.ncbi.nlm.nih.gov/8689572/`.

Krenciute, G., Liu, S., Yucer, N., Shi, Y., Ortiz, P., Liu, Q., Kim, B-J., Odejimi, A.O., Leng, M., Qin, J., and Wang, Y. (July 2013). "Nuclear BAG6-UBL4A-GET4 complex mediates DNA damage signaling and cell death." In: *J Biol Chem*. 288.28,

pp. 20547–20557. ISSN: 1083-351X. DOI: `10.1074/jbc.M112.443416`. URL: `https://pubmed.ncbi.nlm.nih.gov/23723067/`.

Krueger, D., Izquierdo, E., Viswanathan, R., Hartmann, J., Cartes, C.P., and Renzis, S.D. (Oct. 2019). "Principles and applications of optogenetics in developmental biology." In: *Development*. 146.20, dev175067. ISSN: 0950-1991. DOI: `10.1242/dev.175067`. URL: `https://pubmed.ncbi.nlm.nih.gov/31641044/`.

Kuge, O., Hara-Kuge, S., Orci, L., Ravazzola, M., Amherdt, M., Tanigawa, G., Wieland, F.T., and Rothman and J.E. (Dec. 1993). "zeta-COP, a subunit of coatomer, is required for COP-coated vesicle assembly." In: *J Cell Biol*. 123.6 Pt 2, pp. 1727–1734. ISSN: 0021-9525. DOI: `10.1083/jcb.123.6.1727`. URL: `https://pubmed.ncbi.nlm.nih.gov/8276893/`.

Külkens, S., Harting, I., Sauer, S., Zschocke andJ., Hoffmann, G.F., Gruber, S., Bodamer, O.A., and Kölker, S. (June 2005). "Late-onset neurologic disease in glutaryl-CoA dehydrogenase deficiency." In: *Neurology* 64.12, pp. 2142–2144. ISSN: 1526-632X. DOI: `10.1212/01.WNL.0000167428.12417.B2`. URL: `https://pubmed.ncbi.nlm.nih.gov/15985591/`.

Kumar, A., Manatschal, C., Rai, A., Grigoriev, I., Degen, M.S., Jaussi, R., Kretzschmar, I., Prota, A.E., Volkmer, R., Kammerer, R.A., Akhmanova, A., and Steinmetz, M.O. (June 2017). "Tracking the ends: a dynamic protein network controls the fate of microtubule tips." In: *ScienceDirect* 25(6), pp. 924–932. DOI: `10.1016/j.str.2017.04.010`.

Kwiatkowska, M., Poplonska, K., Stepinski, D., and Hejnowicz, Z. (June 2006). "Microtubules with different diameter, protofilament number and protofilament spacing in *Ornithogalum umbellatum* ovary epidermis cells". In: *Folia Histochemica et Cytobiologica*. 44.2, pp. 133–138. ISSN: 0239-8508. URL: `https://journals.viamedica.pl/folia_histochemica_cytobiologica/article/view/4580`.

Laplante, C., Berro, J. Karatekin, E., Hermandez-Leyva, A., Lee, R., and Pollard, T.D. (Aug. 2015). "Three myosins contribute uniquely to the assembly and constriction of the fission yeast cytokinetic contractile ring." In: *Curr Biol.* 25.15, pp. 1955–1965. ISSN: 1879-0445. DOI: 10.1016/j.cub.2015.06.018. URL: https://pubmed.ncbi.nlm.nih.gov/26144970/.

Larson, R.E. (Mar. 1996). "Myosin-V: a class of unconventional molecular motors." In: *Braz J Med Biol Res.* 29.3, pp. 309–318. ISSN: 0100-879X. URL: https://pubmed.ncbi.nlm.nih.gov/8736123/.

Laudermilch, E. and C. Schlieker (Jan. 2016). "Torsin ATPases: Structural insights and functional perspectives." In: *Curr Opin Cell Biol.* 40, pp. 1–7. ISSN: 0955-0674. DOI: 10.1016/j.ceb.2016.01.001. URL: https://www.ncbi.nlm.nih.gov/pmc/articles/PMC4887320/.

Le Droguen, P.M., Claret, S., Guichet, A., and Brodu, V. (Jan. 2015). "Microtubule-dependent apical restriction of recycling endosomes sustains adherens junctions during morphogenesis of the *Drosophila* tracheal system." In: *Development.* 142.2, pp. 363–374. DOI: 10.1242/dev.113472. URL: https://pubmed.ncbi.nlm.nih.gov/25564624/.

Leite, J., Osorio, D.S., Sobral, A.F., Silva aand A.M, and Carvalho, A.X. (May 2019). " Network Contractility During Cytokinesis-from Molecular to Global Views." In: *Biomolecules* 9.5, pp. 1–28. DOI: 10.3390/biom9050194. URL: https://www.ncbi.nlm.nih.gov/pmc/articles/PMC6572417/.

Lemos, C.L., Sampaio, P., Maiato, H., Costa, M., Omel'yanchuk, L.V., Liberal, V., and Sunkel, C.E. (July 2000). "Mast, a conserved microtubule-associated protein required for bipolar mitotic spindle organization." In: *EMBO J.* 19, pp. 3668–3682. ISSN: 0261-4189. DOI: 10.1093/emboj/19.14.3668. URL: https://www.ncbi.nlm.nih.gov/pmc/articles/PMC313969/.

Leśniewska, K., Warbrick, E., and Ohkura, H. (Apr. 2014). "Peptide aptamers define distinct EB1- and EB3-binding motifs and interfere with microtubule dy-

namics". In: *Mol Biol Cell.* 7.25, pp. 1025–1036. DOI: `10.1091/mbc.e13-08-0504`.

Levi, T., Sloutskin, A., Kalifa, R., Juven-Gershon, T., and Gerlitz, O. (July 2020). "Efficient *In Vivo* Introduction of Point Mutations Using ssODN and a Co-CRISPR Approach." In: *Biol Proced Online.* 22, p. 14. ISSN: 1480-9222. DOI: `10.1186/s12575-020-00123-7`. URL: `https://pubmed.ncbi.nlm.nih.gov/32684853/`.

Liang, Z-Y., Hallen, M.A., and Endow, S.A. (Jan. 2009). "Mature *Drosophila* meiosis I spindles comprise microtubules of mixed polarity." In: *Curr Biol.* 19.2, pp. 163–168. ISSN: 0960-9822. DOI: `10.1016/j.cub.2008.12.017`. URL: `https://pubmed.ncbi.nlm.nih.gov/19167226/`.

Lin, K-F., Fry, M.Y., Salad, S.M., and Jr, W.M.C. (June 2021). "Molecular basis of tail-anchored integral membrane protein recognition by the cochaperone Sgt2." In: *J Biol Chem.* 296, p. 100441. ISSN: 1083-351X. DOI: `10.1016/j.jbc.2021.100441`. URL: `https://pubmed.ncbi.nlm.nih.gov/33610544/`.

Liu, H.S., Jan, M.M., Chou, C.K., Chen, P.H., and Ke, N.J. (July 1999). "Is green fluorescent protein toxic to the living cells?" In: *Biochem Biophys Res Commun.* 260.3, pp. 712–717. DOI: `10.1006/bbrc.1999.0954`. URL: `https://pubmed.ncbi.nlm.nih.gov/10403831/`.

Liu, J.J. (June 2017). "Regulation of dynein-dynactin-driven vesicular transport." In: *Traffic.* 18, pp. 336–347. ISSN: 2296-634X. DOI: `10.1111/tra.12475`. URL: `https://pubmed.ncbi.nlm.nih.gov/28248450/`.

Liu, X., Cao, W., Qin, S., Zhang, T., Zheng, J., Dong, Y., Ming, P., Cheng, Q., Lu, Z., Guo, Y., Zhang, B., and Liu, Y. (May 20017). "Overexpression of CIP2A is associated with poor prognosis in multiple myeloma." In: *Signal transduction and targeted therapy.* 2.17013. DOI: `10.1038/sigtrans.2017.13`. URL: `https://www.nature.com/articles/sigtrans201713`.

Loeillet, S., Palancade, B., Cartron, M. Thierry, A., Richard, G-F., Dujon, B., Doye, and V. andNicolas, A. (Apr. 2005). "Genetic network interactions among replication, repair and nuclear pore deficiencies in yeast." In: *DNA Repair (Amst)* 4.4, pp. 459–469. DOI: `10.1016/j.dnarep.2004.11.010`. URL: `https://pubmed.ncbi.nlm.nih.gov/15725626/`.

Lu, L., Xu, L., Li, J, Liu, L., Gao, J., and Li, X. (Feb. 2007). "Construction of equalized short hairpin RNA library from human brain cDNA." In: *J Biotechnol.* 128.3, pp. 477–485. DOI: `10.1016/j.jbiotec.2006.11.013`. URL: `https://pubmed.ncbi.nlm.nih.gov/17187888/`.

Lu, Y., West, R.J.H., Pons, M., Sweeney, S.T., and Gao, F-B. (Aug. 2020). "Ik2/TBK1 and Hook/Dynein, an adaptor complex for early endosome transport, are genetic modifiers of FTD-associated mutant CHMP2B toxicity in *Drosophila.*" In: *Nature.* 10.1, p. 14221. ISSN: 2045-2322. DOI: `10.1038/s41598-020-71097-5`. URL: `https://www.nature.com/articles/s41598-020-71097-5`.

Luithle, N., uit de Bos, J., Hovius, R., Maslennikova, D., Lewis, R.T.M., Ungricht, R., Fierz, B., and Kutay, U. (Dec. 2020). "Torsin ATPases influence chromatin interaction of the Torsin regulator LAP1." In: *eLife.* 9, e63614. ISSN: 2050-084X. DOI: `10.7554/eLife.63614`. URL: `https://www.ncbi.nlm.nih.gov/pmc/articles/PMC7773337/`.

Luo, H., Zhang, H., Huang, T., Hong, Y., Yang, W., Zhang, X., Xu, H., and Wang, X. (Mar. 2018). "The Retromer Complex and Sorting Nexins in Neurodegenerative Diseases." In: *Front Aging Neurosci.* 10, p. 79. ISSN: 1663-4365. DOI: `10.3389/fnagi.2018.00079`. URL: `https://pubmed.ncbi.nlm.nih.gov/29632483/`.

Luo, Y., Chen, J. Li, L., Ran, J., Wang, X., Gao, S., Liu, M., Li., D., Shui, W., and Zhou, J. (Oct. 2014). "Phosphoregulation of the dimerization and functions of end-binding protein 1." In: *Protein Cell.* 5.10, pp. 705–799. DOI: `10.1007/`

s13238-014-0081-9. URL: `https://www.ncbi.nlm.nih.gov/pmc/articles/PMC4180461/`.

Maan, M., Agrawal, N.J., Padmanabhan, J., Leitzinger, C.C., Rivera-Rivera, Y., Saavedra, H.I, and Chellappan, S.P. (Mar. 2021). "Tank Binding Kinase 1 modulates spindle assembly checkpoint components to regulate mitosis in breast and lung cancer cells." In: *Biochim Biophys Acta Mol Cell Res.* 1868.3, p. 118929. DOI: `10.1016/j.bbamcr.2020.118929`. URL: `https://pubmed.ncbi.nlm.nih.gov/33310066/`.

MacIver, B., McCormack, A. Slee, R., and Bownes, M. (Nov. 1998). "Identification of an essential gene encoding a class-V unconventional myosin in *Drosophila melanogaster.*" In: *Eur J Biochem.* 257.3, pp. 529–537. ISSN: 0014-2956. DOI: `10.1046/j.1432-1327.1998.2570529.x`. URL: `https://pubmed.ncbi.nlm.nih.gov/9839940/`.

Mahoney, J.A., Ntolosi, B., da Silva a nd R.P., Gordon, and S. McKnight, A.J. (Mar. 2001). "Cloning and characterization of CPVL, a novel serine carboxypeptidase, from human macrophages." In: *Genomics.* 72.3, pp. 243–251. ISSN: 0888-7543. DOI: `10.1006/geno.2000.6484`. URL: `https://pubmed.ncbi.nlm.nih.gov/11401439/`.

Malumbres, M. and M. Barbacid (Nov. 2005). "Mammalian cyclin-dependent kinases." In: *Trends Biochem Sci.* 30.11, pp. 630–641. DOI: `10.1016/j.tibs.2005.09.005`. URL: `https://pubmed.ncbi.nlm.nih.gov/16236519/`.

Marlowe, C.K., Sinha, U., Gunn, A.C., and Scarborough, R.M. (Jan. 2000). "Design, synthesis and structure-activity relationship of a series of arginine aldehyde factor Xa inhibitors. Part 1: structures based on the (D)-Arg-Gly-Arg tripeptide sequence." In: *Bioorg Med Chem Lett.* 10.1, pp. 13–16. ISSN: 0960-894X. DOI: `10.1016/s0960-894x(99)00582-x`. URL: `https://pubmed.ncbi.nlm.nih.gov/10636232/`.

Marygold, S.J., Attrill, H. Speretta, E., Warner, K., Magrane, M., Berloco, M., Cotterill, S., McVey, M., Rong, Y., and Yamaguchi, M. (Jan. 2020). "The DNA polymerases of *Drosophila melanogaster*." In: *Fly (Austin)*. 14.1-4, pp. 49–61. ISSN: 1933-6934. DOI: `10.1080/19336934.2019.1710076`. URL: `https://www.ncbi.nlm.nih.gov/pmc/articles/PMC7714529/`.

Masson, O., Bach, A-S., Derocq, D., Prébois, C., Laurent-Matha, V., Pattingre, S., and Liaudet-Coopman, E. (Nov. 2010). "Pathophysiological functions of cathepsin D: Targeting its catalytic activity versus its protein binding activity?" In: *Biochimie*. 92.11, pp. 1635–1643. ISSN: 1638-6183. DOI: `10.1016/j.biochi.2010.05.009`. URL: `https://pubmed.ncbi.nlm.nih.gov/20493920/`.

Maurer, S.P., Fourniol, F.J., Bohner, G., Moores, C.A, and Surrey, T. (Apr. 2012). "EBs recognize a nucleotide-dependent structural cap at growing microtubule ends." In: *Cell*. 143.2, pp. 371–382. ISSN: 1097-4172. DOI: `10.1016/j.cell.2012.02.049`. URL: `https://pubmed.ncbi.nlm.nih.gov/22500803/`.

McClelland, V.M., Gissen, P., Hendriksz, C., and Chakrapani, A. (Jan. 2007). "Glutaryl-CoA dehydrogenase deficiency." In: *Pediatr Res*. 61.1, p. 134. ISSN: 0031-3998. DOI: `10.1203/01.pdr.0b013e31802d9ab4`. URL: `https://pubmed.ncbi.nlm.nih.gov/17211155/`.

McEwn, B.F., Chan, G.K., Zubrowski, B., Sovoian, M.S., Sauer, M.T., and Yen, T.J. (Sept. 2001). "CENP-E is essential for reliable bioriented spindle attachment, but chromosome alignment can be achieved via redundant mechanisms in mammalian cells." In: *Mol Biol Cell*. 12.9, pp. 2776–2789. DOI: `10.1091/mbc.12.9.2776`. URL: `https://pubmed.ncbi.nlm.nih.gov/11553716/`.

McIntosh, J.R. (Sept. 2016). "Mitosis." In: *Cold Spring Harb Perspect Biol*. 8.9, pp. 1–16. DOI: `10.1101/cshperspect.a023218`. URL: `https://www.ncbi.nlm.nih.gov/pmc/articles/PMC5008068/`.

McKean, P.G., Vaughan, S., and Gull, K. (Aug. 2001). "The extended tubulin superfamily." In: *J Cell Sci.* 114, pp. 2723–2733. URL: `https://pubmed.ncbi.nlm.nih.gov/11683407/`.

McRae, B.J., Kurachi, K., Heimark, R.L., Fujikawa, K., Davie, E.W., and Powers, J.C. (Dec. 1981). "Mapping the active sites of bovine thrombin, factor IXa, factor Xa, factor XIa, factor XIIa, plasma kallikrein, and trypsin with amino acid and peptide thioesters: development of new sensitive substrates." In: *Biochemistry.* 20.25, pp. 196–206. ISSN: 0006-2960. DOI: `10.1021/bi00528a022`. URL: `https://pubmed.ncbi.nlm.nih.gov/6976185/`.

Meltzer, H., Marom, E., Alyagor, I., Mayseless, O., Berkun, V., Segal-Gilboa, N., Unger, T., Luginbuhl, and D. abd Schuldiner, O. (May 2019). "Tissue-specific (ts)CRISPR as an efficient strategy for in vivo screening in *Drosophila.*" In: *Nature communications.* 10.2113, pp. 1–9. DOI: `10.1038/s41467-019-10140-0`. URL: `https://www.nature.com/articles/s41467-019-10140-0`.

Mennella, V., Keszthelyi, B., McDonald, K.L., Chhun, B., Kan, F., Rogers, G.C., Huang, B., and Agard, D.A. (Nov. 2012). "Subdiffraction-resolution fluorescence microscopy reveals a domain of the centrosome critical for pericentriolar material organization." In: *Nat Cell Biol.* 14.11, pp. 1159–1168. ISSN: 1476-4679. DOI: `10.1038/ncb2597`. URL: `https://pubmed.ncbi.nlm.nih.gov/23086239/`.

Menssen, R., Schweiggert, J., Schreiner, J., Kusevic, D., Reuther, J., Braun, B., and Wolf, D.H. (July 2012). "Exploring the topology of the Gid complex, the E3 ubiquitin ligase involved in catabolite-induced degradation of gluconeogenic enzymes." In: *J Biol Chem.* 287.30, pp. 25602–25614. ISSN: 1083-351X. DOI: `10.1074/jbc.M112.363762`. URL: `https://pubmed.ncbi.nlm.nih.gov/22645139/`.

Merdes, A., Kollman, J.M., Mourey, L., and Agar, D.A. (Oct. 2011). "Microtubule nucleation by γ-tubulin complexes." In: *Nat Rev Mol Cell Biol.* 12.11, pp. 709–

721. ISSN: 1471-0080. DOI: `10.1038/nrm3209`. URL: `https://www.nature.com/articles/nrm3209`.

Mirzoyan, Z., Sollazzo, M., Allocca, M., Valenza, A.M., Grifoni, D., and Bellosta, P. (Mar. 2019). "*Drosophila melanogaster:* A Model Organism to Study Cancer." In: *Front. Genet.* 10.51, pp. 1–16. DOI: `10.3389/fgene.2019.00051`. URL: `https://www.frontiersin.org/articles/10.3389/fgene.2019.00051/full%5C#B187`.

Mitchson, T. and M. Kirschner (Nov. 1984). "Dynamic instability of microtubule growth." In: *Nature.* 312.5991, pp. 237–242. DOI: `10.1038/312237a0`. URL: `https://pubmed.ncbi.nlm.nih.gov/6504138/`.

Mohan, P.M.K. and R.V. Hosur (June 2008). "NMR characterization of structural and dynamics perturbations due to a single point mutation in *Drosophila* DLC8 dimer: functional implications." In: *Biochemistry.* 47.23, pp. 6251–6259. DOI: `10.1021/bi800531g`. URL: `https://pubmed.ncbi.nlm.nih.gov/18465876/`.

Moriwaki, T. and G. Goshima (Oct. 2016). "Five factors can reconstitute all three phases of microtubule polymerization dynamics." In: *J Cell Biol.* 215, pp. 357–368. DOI: `10.1083/jcb.201604118`. URL: `https://rupress.org/jcb/article/215/3/357/38783/Five-factors-can-reconstitute-all-three-phases-of`.

Mosalaganti, S., Keller, J., Altenfeld, A., Winzker, M., Rombaut, P., Saur, M.and Petrovic, A.and Wehenkel, A.and Wohlgemuth, S., Müller, F., Maffini, S., Bange, T., Herzog, F., Waldmann, H., Raunser, S., and Musacchio, A. (Apr. 2017). "Structure of the RZZ complex and molecular basis of its interaction with Spindly." In: *J. Cell Biol.* 216.4, pp. 961–981. ISSN: 0021-9525. DOI: `10.1083/jcb.201611060`. URL: `https://www.ncbi.nlm.nih.gov/pmc/articles/PMC5379955/`.

Nagai, K. and H.C. Thiϕgerson (June 1984). "Generation of beta-globin by sequence specific proteolysis of a hybrid protein produced in *Escherichia coli*." In: *Nature.* 309, pp. 810–812. DOI: `10.1038/309810a0`. URL: `https://pubmed.ncbi.nlm.nih.gov/6330564/`.

– (1987). "Synthesis and sequence-specific proteolysis of hybrid proteins produced in Escherichia coli." In: *Methods Enzymol.* 153, pp. 461–481. ISSN: 0076-6879. DOI: `10.1016/0076-6879(87)53072-5`. URL: `https://pubmed.ncbi.nlm.nih.gov/3323806/`.

Nagai, S., Dubrana, K., Tsai-Pflugfelder, M., Davidson, M.B., Roberts, T.M., Brown, G.W., Varela, V., Hediger, E., Gasser, S.M., and Krogan, N.J. (Oct. 2008). "Functional targeting of DNA damage to a nuclear pore-associated SUMO-dependent ubiquitin ligase." In: *Science* 322.5901, pp. 597–602. DOI: `10.1126/science.1162790`. URL: `https://pubmed.ncbi.nlm.nih.gov/18948542/`.

Nakagawa, T., Setou, M., Seog, D., Ogasawara, K., Dohmae, N., Takio, K., and Hirokawa, N. (Nov. 2000). "A novel motor, KIF13A, transports mannose-6-phosphate receptor to plasma membrane through direct interaction with AP-1 complex." In: *Cell.* 103.4, pp. 569–581. DOI: `10.1016/s0092-8674(00) 00161-6`. URL: `https://pubmed.ncbi.nlm.nih.gov/11106728/`.

Nakamura, S., Grigoriev, I., Nogi, T., Hamaji, T., Cassimeris, L., and Mimori-Kiyosue, Y. (Dec. 2012). "Dissecting the Nanoscale Distributions and Functions of Microtubule End Binding Proteins EB1 and ch-TOG in Interphase HeLa Cells." In: *PLoS One.* 7.12, pp. 1–20. DOI: `10.1371/journal.pone.0051442`. URL: `https://www.ncbi.nlm.nih.gov/pmc/articles/PMC3520847/`.

Nakatsu, F. and H. Ohno (Oct. 2003). "Adaptor protein complexes as the key regulators of protein sorting in the post-Golgi network." In: *Cell Struct Funct.* 28.5, pp. 419–429. ISSN: 0386-7196. DOI: `10.1247/csf.28.419`. URL: `https://pubmed.ncbi.nlm.nih.gov/14745134/`.

Nazgiewicz, A., Atherton, P., and Ballestrem, C. (Apr. 2019). "GAS2-like 1 coordinates cell division through its association with end-binding proteins." In: *Sci Rep.* 9.1, p. 5805. ISSN: 2045-2322. DOI: `10.1038/s41598-019-42242-6`. URL: `https://pubmed.ncbi.nlm.nih.gov/30967572/`.

Nehlig, A., Molina, A., Rodrigues-Ferreira, S., Honoré, S., and Nahmias, C. (Feb. 2017). "Regulation of end-binding protein EB1 in the control of microtubule dynamics." In: *Cell. Mol. Life Sci.* 74. DOI: `10.1007/s00018-017-2476-2`.

Neuner, A., Liu, P., Zupa, E., Böhler, A., Loerke, J., Flemming, D., Ruppert, T., Rudack, T., Peter, C., Spahn, C., Gruss, O.J., Pfeffer, S., and Schiebel, E. (Feb. 2020). "Insights into the assembly and activation of the microtubule nucleator γ-TuRC." In: *Nature.* 578.7796, pp. 467–571. ISSN: 1476-4687. DOI: `10.1038/s41586-019-1896-6`. URL: `https://pubmed.ncbi.nlm.nih.gov/31856152/`.

Ni, J-Q., Zhou, R., Czech, B., Liu, L-P., Holderbaum, L., Yang-Zhou, D. Shim, H-S. a nd Tao, R., Handler, D., Karpowicz, P., Binari, R., Booker, M., Brennecke, J., Perkins, L.A., Hannon, G.J., and Perrimon, N. (Apr. 2011). "A genome-scale shRNA resource for transgenic RNAi in *Drosophila.*" In: *Nature.* 8.5, pp. 405–407. ISSN: 1548-7105. DOI: `10.1038/nmeth.1592`. URL: `https://www.nature.com/articles/nmeth.1592`.

Niemelä, M., Kauko, O., Sihto, H., Mpindi, J.P., Nicorici, D., Pernilä, P., Kallioniemi, O.P., Joensuu, H., Hautaniemi, S., and Westermarck, J. (Sept. 2012). "CIP2A signature reveals the MYC dependency of CIP2A-regulated phenotypes and its clinical association with breast cancer subtypes." In: *Oncogene.* 31.39, pp. 4266–4278. DOI: `10.1038/onc.2011.599`. URL: `https://pubmed.ncbi.nlm.nih.gov/22249265/`.

Nishikawa, Y. and T. Sugiyama (Nov. 2010). "A shRNA library constructed through the generation of loop-stem-loop DNA." In: *J Gene Med.* 12.11, pp. 927–933.

DOI: `10.1002/jgm.1513`. URL: `https://pubmed.ncbi.nlm.nih.gov/21105152/`.

Nogales, E., Wolf, SG., and Downing, KH. (Jan. 1998). "Structure of the $\alpha\beta$ tubulin dimer by electron crystallography." In: *Nature.* 391.6663, pp. 199–203. DOI: `10.1038/34465`. URL: `https://www.nature.com/articles/34465`.

Oakley, BR. (Dec. 2000). "An abundance of tubulins." In: *Trend Cell Biology.* 10.12, pp. 537–542. ISSN: 0962-8924. DOI: `10.1016/S0962-8924(00)01857-2`. URL: `https://pubmed.ncbi.nlm.nih.gov/31416684/`.

Olenick, M.A., Tokito, M., Boczkowska, M., Dominguez, R., and Holzbaur, E.L.F. (Aug. 2016). "Hook Adaptors Induce Unidirectional Processive Motility by Enhancing the Dynein-Dynactin Interaction." In: *J Biol Chem.* 291.35, pp. 18239–18251. ISSN: 1083-351X. DOI: `10.1074/jbc.M116.738211`. URL: `https://pubmed.ncbi.nlm.nih.gov/27365401/`.

Oshige, M., Yoshida, H. Hirose, F., Takata, K.I., Inoue, Y., Aoyagi, N., Yamaguchi, M., Koiwai, O., Matsukage, A., and Sakaguchi, K. (Oct. 2000). "Molecular cloning and expression during development of the *Drosophila* gene for the catalytic subunit of DNA polymerase epsilon." In: *Gene.* 256.1-2, pp. 93–100. ISSN: 0378-1119. DOI: `10.1016/s0378-1119(00)00370-x`. URL: `https://pubmed.ncbi.nlm.nih.gov/11054539/`.

Otani, T., Oshima, K., Oneshi, S., Takeda, M., Shinmyozu, K., Yonemura, S., and Hayashi, S. (Feb. 2011). "IKKε Regulates Cell Elongation through Recycling Endosome Shuttling." In: *Developmental Cell.* 20.2, pp. 219–232. ISSN: 1534-5807. DOI: `10.1016/j.devcel.2011.02.001`. URL: `https://www.science%20direct.com/science/article/pii/S1534580711000463`.

Palumbo, V., Borgal, L., Tariq, A., Metz, J., Brancaccio, M., Gatti, M., Wakefield, J.G., and Bonaccorsi, S. (Jan. 2020). "*Drosophila* Morgana is an Hsp90 – interacting protein with a direct role in microtubule polymerisation." In: *J Cell Sci.*

133.2, jcs236786. ISSN: 1477-9137. DOI: `10.1242/jcs.236786`. URL: `https://pubmed.ncbi.nlm.nih.gov/31907206/`.

Palumbo, V., Pellacani, C., Heesom, K.J., Rogala, K.B., Deane, C.M., Mottier-Pavie, V., Gatti, M., Bonaccorsi, and S. Wakefield, J.G. (June 2015). "Misato Controls Mitotic Microtubule Generation by Stabilizing the Tubulin Chaperone Protein-1 Complex." In: *Curr Biol.* 25.13, pp. 1777–1783. ISSN: 0960-9822. DOI: `10.1016/j.cub.2015.05.033`. URL: `https://www.ncbi.nlm.nih.gov/pmc/articles/PMC4510148/`.

Park, S.Y. and X. Guo (July 2014). "Adaptor protein complexes and intracellular transport." In: *Biosci Rep.* 34.4, e00123. ISSN: 0144-8463. DOI: `10.1042/BSR20140069`. URL: `https://www.ncbi.nlm.nih.gov/pmc/articles/PMC4114066/`.

Pearson, W.R. (June 2013). "An introduction to sequence similarity (homology) searching". In: *Curr Protoc Bioinformatics.* 3, pp. 1–9. DOI: `10.1002/0471250953.bi0301s42`. URL: `https://www.ncbi.nlm.nih.gov/pmc/articles/PMC3820096/`.

Pellacani, C., Bucciarelli, E., Renda, F., Hayward, D., Palena, A., Chen, J., Bonaccorsi, S., Wakefield, J.G., Gatti, M., and Somma, M.P. (Nov. 2018). "Splicing factors Sf3A2 and Prp31 have direct roles in mitotic chromosome segregation." In: *Elife.* 7, e40325. DOI: `10.7554/eLife.40325`. URL: `https://pubmed.ncbi.nlm.nih.gov/30475206/`.

Pereira, C., Reis, R.M., Gama, J.B., Celestino, R., Cheerambathur, D.K., Carvalho, A.X., and Gassmann, R. (Nov. 2018). "Self-Assembly of the RZZ Complex into Filaments Drives Kinetochore Expansion in the Absence of Microtubule Attachment." In: *Current Biology.* 28, pp. 3408–3421. ISSN: 0960-9822. DOI: `10.1016/j.cub.2018.08.056`. URL: `https://www.sciencedirect.com/science/article/pii/S0960982218311400`.

Peset, I. and I. Vernos (Aug. 2008). "The TACC proteins: TACC-ling microtubule dynamics and centrosome function." In: *Trends in Cell Biology.* 18, pp. 379–388. ISSN: 0962-8924. DOI: `10.1016/j.tcb.2008.06.005`. URL: `https://www.sciencedirect.com/science/article/pii/S0962892408001694`.

Peter, F., Plutner, H., Zhu, H., Kreis, T.E., and Balch, W.E. (Sept. 1993). "Beta-COP is essential for transport of protein from the endoplasmic reticulum to the Golgi *in vitro.*" In: *J Cell Biol.* 122.6, pp. 1155–1167. ISSN: 0021-9525. DOI: `10.1083/jcb.122.6.1155`. URL: `https://pubmed.ncbi.nlm.nih.gov/8376457/`.

Peters, J-M. (May 2002). "The Anaphase-Promoting Complex: Proteolysis in Mitosis and Beyond." In: *Molecular Cell* 9.5, pp. 931–943. ISSN: 1097-2765. DOI: `10.1016/S1097-2765(02)00540-3`. URL: `https://www.sciencedirect.com/science/article/pii/S1097276502005403`.

Petronek, M.S., Spitz, D.R., and Allen, B.G. (Sept. 2021). "Iron-Sulfur Cluster Biogenesis as a Critical Target in Cancer." In: *Antioxidants (Basel).* 10.9, p. 1458. ISSN: 2076-3921. DOI: `10.3390/antiox10091458`. URL: `https://pubmed.ncbi.nlm.nih.gov/34573089/`.

Pierson, G.B., Burton, P.R., and Himes, R.H. (Jan. 1978). "Alterations in number of protofilaments in microtubules assembled in vitro." In: *J Cell Biol.* 76.1, pp. 223–228. DOI: `10.1083/jcb.76.1.223`. URL: `https://www.ncbi.nlm.nih.gov/pmc/articles/PMC2109969/`.

Pillai, S., Nguyen, J., Johnson, J., Haura, E., Coppola, D., and Chellappan, S. (Dec. 2015). "Tank binding kinase 1 is a centrosome-associated kinase necessary for microtubule dynamics and mitosis." In: *Nat Commun.* 6, p. 10072. ISSN: 2041. DOI: `10.1038/ncomms10072`. URL: `https://pubmed.ncbi.nlm.nih.gov/26656453/`.

Pines, M.K., Houseden, B.E., Bernard, F., Bray, S.J., and Röper, K. (Mar. 2010). "The cytolinker Pigs is a direct target and a negative regulator of Notch sig-

nalling." In: *Development.* 137.6, pp. 913–922. ISSN: 1477-9129. DOI: `10.1242/dev.043224`. URL: `https://pubmed.ncbi.nlm.nih.gov/20150280/`.

Platet, N., Garcia, M., Liaudet, E., Laurent, V., Derocq, D., Brouillet, J.P., and Rochefort, H. (Nov. 1996). "Biological and clinical significance of cathepsin D in breast cancer metastasis." In: *Stem Cells.* 14.6, pp. 642–650. ISSN: 1066-5099. DOI: `10.1002/stem.140642`. URL: `https://pubmed.ncbi.nlm.nih.gov/8948022/`.

Plochocka, A.Z., Moreno, M.R., Davie, A.M., Bulgakova, N.A., and Chumakova, L. (Feb. 2021). "Robustness of the microtubule network self-organization in epithelia". In: *Elife.* 10, e59529. DOI: `10.7554/eLife.59529`. URL: `https://pubmed.ncbi.nlm.nih.gov/33522481/`.

Port, F., Strein, C., Stricker, M., Rauscher, B., Heigwer, F., Zhou, J., Beyersdörffer, C., Frei, J., Hess, J., Kern, K., Lange, L., Langner, N., Malamud, R., Povlović, B., Rädecke, K., Schmitt, L., Voos, L., Valentini, E., and Boutros, M. (Feb. 2020). "A large-scale resource for tissue-specific CRISPR mutagenesis in *Drosophila.*" In: *Elife.* 9, e53865. DOI: `10.7554/eLife.53865`. URL: `https://elifesciences.org/articles/53865`.

Prü*β*ing, K., Voigt, A., and Schulz, J.B. (Nov. 2013). "*Drosophila melanogaster* as a model organism for Alzheimer's disease." In: *Mol Neurodegener.* 8.35. ISSN: 1750-1326. DOI: `10.1186/1750-1326-8-35`. URL: `https://pubmed.ncbi.nlm.nih.gov/24267573/`.

Prumbaum, D., Thakur, H.C., Singh, M., Nagel-Steger, L., Fansa, E.K., Gremer, L., Ezzahoini, H., Abts, A. snf Schmitt, L., Raunser, S., Ahmadian, M.R., and Piekorz, R.P. (June 2013). "Role of centrosomal adaptor proteins of the TACC family in the regulation of microtubule dynamics during mitotic cell division." In: *J. Biol. Chem.* 394, pp. 1411–1423. ISSN: 1437-4315. DOI: `10.1515/hsz-2013-0184`. URL: `https://www.degruyter.com/document/doi/10.1515/hsz-2013-0184/html2`.

Prykhozhij, S.V., Fuller, C., Steele, S.L., Veinotte, C.J., Razaghi, B., Robitaille, J.M., McMaster, C.R., Shlien, A., Malkin, D., and Berman, J.N. (Sept. 2018). "Optimized knock-in of point mutations in zebrafish using CRISPR/Cas9." In: *Nucleic Acids Res.* 46.17, e102. ISSN: 1362-4962. DOI: `10.1093/nar/gky512`. URL: `https://pubmed.ncbi.nlm.nih.gov/29905858/`.

Putkey, F.R., Cramer, T., Morphew, M.K., Silk, A.D., Johnson, R.S., McIntosh, J.R., and Cleveland, D.W. (Sept. 2002). "Unstable kinetochore-microtubule capture and chromosomal instability following deletion of CENP-E." In: *Dev Cell.* 2.3, pp. 351–365. ISSN: 1534-5807. DOI: `10.1016/s1534-5807(02)00255-1`. URL: `https://pubmed.ncbi.nlm.nih.gov/12361599/`.

Raices, M. and M.A. D'Angelo (Nov. 2012). "Nuclear pore complex composition: a new regulator of tissue-specific and developmental functions." In: *Nat Rev Mol Cell Biol.* 13.11, pp. 687–699. ISSN: 1471-0080. DOI: `10.1038/nrm3461`. URL: `https://pubmed.ncbi.nlm.nih.gov/23090414/`.

Rajagopala, S.V. (2015). "Mapping the Protein-Protein Interactome Networks Using Yeast Two-Hybrid Screens." In: *Adv Exp Med Biol.* 883, pp. 187–214. ISSN: 1422-0067. DOI: `10.1007/978-3-319-23603-2_11`. URL: `https://pubmed.ncbi.nlm.nih.gov/26621469/`.

Ran, F.A., Hsu, P.D., Wright, J., Agarwala, V., Scott, D.A., and Zhang, F. (Oct. 2013). "Genome engineering using the CRISPR-Cas9 system." In: *Nature Protocols.* 8.11, pp. 2281–2308. ISSN: 1750-2799. DOI: `10.1038/nprot.2013.143`. URL: `https://www.nature.com/articles/nprot.2013.143`.

Richards, A.L., Merrill, A.E., and Coon, J.J. (Feb. 2015). "Proteome sequencing goes deep." In: *Curr Opin Chem Biol.* 24, pp. 11–17. ISSN: 1367-5931. DOI: `10.1016/j.cbpa.2014.10.017`. URL: `https://pubmed.ncbi.nlm.nih.gov/25461719/`.

Richens, J.H., Barros, T.P., Lucas, E.P., Peel, N., Pinto, D.M.S., Wainman, A., and Raff, J.W. (July 2015). "The *Drosophila* Pericentrin-like-protein (PLP) cooper-

ates with Cnn to maintain the integrity of the outer PCM." In: *Biology Open.* 4.8, pp. 1052–1061. ISSN: 2046-6390. DOI: `10.1242/bio.012914`. URL: `https://pubmed.ncbi.nlm.nih.gov/26157019/`.

Riggs, B., Fasulo, B., Royou, A., Mische, S., Cao, J., Hays, T.S., and Sullivan, W. (Sept. 2007). "The concentration of Nuf, a Rab11 effector, at the microtubule-organizing center is cell cycle regulated, dynein-dependent, and coincides with furrow formation." In: *Mol Biol Cell.* 18.9. ISSN: 1741-7001. DOI: `10.1091/mbc.e07-02-0146`. URL: `https://pubmed.ncbi.nlm.nih.gov/17581858/`.

Robinson, J.T., Wojcik, E.J., Sanders, M.A., McGrail, M., and Hays, T.S. (Aug. 1999). "Cytoplasmic Dynein Is Required for the Nuclear Attachment and Migration of Centrosomes during Mitosis in *Drosophila.*" In: *J Cell Biol.* 146.3, pp. 597–608. DOI: `10.1083/jcb.146.3.597`. URL: `https://www.ncbi.nlm.nih.gov/pmc/articles/PMC2150560/`.

Rogala, K.B., Chen, J.W.C., Chen, Z.A., Metz, J., Deane, C.M.a nd Rappsilber, J., and Wakefield1, J.G. (May 2017). "Cross-linking mass spectrometry identifies new interfaces of Augmin required to localise the γ-tubulin ring complex to the mitotic spindle." In: *Biol Open.* 6.5, pp. 654–663. ISSN: 2056-6390. DOI: `10.1242/bio.022905`. URL: `https://www.ncbi.nlm.nih.gov/pmc/articles/PMC5450317/`.

Rogers, S.L., Rogers, G.C, Sharp, D.J., and Vale, R.D. (Sept. 2002). "*Drosophila* EB1 is important for proper assembly, dynamics, and positioning of the mitotic spindle." In: *J Cell Biol.* 158.5, pp. 873–884. DOI: `10.1083/jcb.200202032`. URL: `https://www.ncbi.nlm.nih.gov/pmc/articles/PMC2173155/`.

Roncaglia, P., Martone, M.E., Hill, D.P., Berardini, T.Z., Foulger, R.E., Imam, F., Drabkin, H., Mungall, C.J., and Lomax, J. (Oct. 2013). "The Gene Ontology (GO) Cellular Component Ontology: integration with SAO (Subcellular Anatomy Ontology) and other recent developments." In: *J Biomed Semantics.* 4.20, pp. 1–

11. ISSN: 2041-1480. DOI: `10.1186/2041-1480-4-20`. URL: `https://www.ncbi.nlm.nih.gov/pmc/articles/PMC3852282/`.

Roque, H., Saurya, S., Pratt, M.B., Johnson, E., and Raff, J.W. (Feb. 2018). "*Drosophila* PLP assembles pericentriolar clouds that promote centriole stability, cohesion and MT nucleation." In: *PLOS Genetics.* 14.2, e1007198. ISSN: 1553-7404. DOI: `10.1371/journal.pgen.1007198`. URL: `https://pubmed.ncbi.nlm.nih.gov/29425198/`.

Sahashi, R., Matsuda, R., Suyari, O., Kawai, M., Yoshida, H., Cotterill, S., and Masamitsu, M. (Nov. 2013). "Functional analysis of *Drosophila* DNA polymerase ε p58 subunit." In: *Am J Cancer Res.* 3.5, pp. 478–489. ISSN: 2156-6976. URL: `https://www.ncbi.nlm.nih.gov/pmc/articles/PMC3816967/`.

Salemi, L.M., Maitland, M.E.R., McTavish, C.J., and Schild-Poulter, C. (June 2017). "Cell signalling pathway regulation by RanBPM: molecular insights and disease implications." In: *Open Biol.* 7.6, p. 170081. ISSN: 2046-2441. DOI: `10.1098/rsob.170081`. URL: `https://pubmed.ncbi.nlm.nih.gov/28659384/`.

Salmon, E.D., Walker, R.A., and Endow, S.A. (Oct. 1990). "The *Drosophila* claret segregation protein is a minus-end directed motor molecule." In: *Nature.* 347.6295, pp. 780–782. ISSN: 1476-4687. DOI: `10.1038/347780a0`. URL: `https://www.nature.com/articles/347780a0`.

Santt, O., Pfirmann, T., Braun, B., Juretschke, J., Kimmig, P., Scheel, H., Hofmann, K., Thumm, M., and Wolf, D.H. (Aug. 2008). "The Yeast GID Complex, a Novel Ubiquitin Ligase (E3) Involved in the Regulation of Carbohydrate Metabolism." In: *Mol Biol Cell* 19.8, pp. 3323–3333. ISSN: 1059-1524. DOI: `10.1091/mbc.E08-03-0328`. URL: `https://www.ncbi.nlm.nih.gov/pmc/articles/PMC2488282/`.

Satyanarayana, A. and P. Kaldis (Aug. 2009). " Mammalian cell-cycle regulation: several Cdks, numerous cyclins and diverse compensatory mechanisms." In:

Oncogene. 28.33, pp. 2925–2939. DOI: `10.1038/onc.2009.170`. URL: `https://pubmed.ncbi.nlm.nih.gov/19561645/`.

Saunders, R.D., Avides, M.C., Howard, T., Gonzalez, C., and Glover, D.M. (May 1997). "The *Drosophila* gene abnormal spindle encodes a novel microtubule-associated protein that associates with the polar regions of the mitotic spindle." In: *J Cell Biol.* 137.4, pp. 881–890. ISSN: 0021-9525. DOI: `10.1083/jcb.137.4.881`. URL: `https://www.ncbi.nlm.nih.gov/pmc/articles/PMC2139842/`.

Schaar, B.T., Chan, G.K., Maddox, P., Salmon, E.D, and Yen, T.J. (Dec. 1997). "CENP-E function at kinetochores is essential for chromosome alignment." In: *Cell Biol.* 139.6, pp. 1373–1382. ISSN: 0021-9525. DOI: `10.1083/jcb.139.6.1373`. URL: `https://pubmed.ncbi.nlm.nih.gov/9396744/`.

Schafer, K.A. (Nov. 1998). "The cell cycle: a review." In: *Vet Pathol.* 35.6, pp. 461–476. DOI: `10.1177/030098589803500601`. URL: `https://pubmed.ncbi.nlm.nih.gov/9823588/#affiliation-1`.

Schneider, C., King, R.M., and Philipson, L. (Sept. 1988). "Genes specifically expressed at growth arrest of mammalian cells." In: *Cell.* 54.6, pp. 787–793. ISSN: 0092-8674. DOI: `10.1016/s0092-8674(88)91065-3`. URL: `https://pubmed.ncbi.nlm.nih.gov/3409319/`.

Schwimmer, T.A., Rogers, G.C., Rogers, S.L., Ems-McClung, S.C., Walczak, C.E., Vale, R.D, Scholey, J.M., and Sharp, D.J. (Jan. 2004). "Two mitotic kinesins cooperate to drive sister chromatid separation during anaphase." In: *Nature.* 427.6972, pp. 364–370. DOI: `10.1038/nature02256`. URL: `https://pubmed.ncbi.nlm.nih.gov/14681690/`.

Seaman, M.N.J. (Oct. 2012). "The retromer complex – endosomal protein recycling and beyond." In: *J Cell Sci.* 125.20, pp. 4693–4702. ISSN: 1477-9137. DOI: `10.1242/jcs.103440`. URL: `https://pubmed.ncbi.nlm.nih.gov/23148298/`.

She, Z-Y. and W-X. Yang (July 2017). "Molecular mechanisms of kinesin-14 motors in spindle assembly and chromosome segregation." In: *J Cell Biol.* 130.13, pp. 2097–2110. ISSN: 1477-9137. DOI: `10.1242/jcs.200261`. URL: `https://pubmed.ncbi.nlm.nih.gov/28668932/`.

Shen, M., Zhang, N., Zheng, S., Zhang, W-B., Zhang, H-M., Lu, Z., Su, Q.P., Sun, Y., Ye, K., and Li, X-D. (Oct. 2016). "Three myosins contribute uniquely to the assembly and constriction of the fission yeast cytokinetic contractile ring." In: *Proc Natl Acad Sci USA.* 113.40, E5812–E5820. ISSN: 1091-6490. DOI: `10.1073/pnas.1607702113`. URL: `https://pubmed.ncbi.nlm.nih.gov/27647889/`.

Shewan, A.M., Maddugoda, M., Kraemer, A., Stehbens, S.J., Verma, S., Kovacs, E.M., and Yap, A.S. (Oct. 2005). "Myosin 2 is a key Rho kinase target necessary for the local concentration of E-cadherin at cell-cell contacts." In: *Mol Biol Cell.* 16.10, pp. 4531–4531. ISSN: 1059-1524. DOI: `10.1091/mbc.e05-04-0330`. URL: `https://pubmed.ncbi.nlm.nih.gov/16030252/`.

Shirane, D., Sugao, K., Namiki, S., Tanabe, M., Iino, M., and Hirose, K. (Feb. 2004). "Enzymatic production of RNAi libraries from cDNAs." In: *Nat Genet.* 36.3, pp. 190–196. DOI: `10.1038/ng1290`. URL: `https://pubmed.ncbi.nlm.nih.gov/14704669/`.

Simpson, P.J., Schwappach, B., Dohlman, H.G., and Isaacson, R.L. (Aug. 2010). "Structures of Get3, Get4, and Get5 Provide New Models for TA Membrane Protein Targeting." In: *Structure.* 18.8, pp. 897–902. ISSN: 0969-2126. DOI: `10.1016/j.str.2010.07.003`. URL: `https://www.ncbi.nlm.nih.gov/pmc/articles/PMC3557799/`.

Skidgel, R.A. and E.G. Erdös (Feb. 1998). "Cellular carboxypeptidases." In: *Immunol Rev.* 161, pp. 129–141. ISSN: 0105-2896. DOI: `10.1111/j.1600-065x.1998.tb01577.x`. URL: `https://pubmed.ncbi.nlm.nih.gov/9553770/`.

Slep, K.C. and D.V. Ronald (Sept. 2007). "Structural basis of microtubule plus end tracking by XMAP215, CLIP-170, and EB1." In: *Molecular Cell.* 27.6, pp. 976–991. ISSN: 1097-2765. DOI: `10.1016/j.molcel.2007.07.023`. URL: `https://pubmed.ncbi.nlm.nih.gov/17889670/`.

Sobral, A.F., Chan, F-Y., Norman, M.J., Osório D.S., Dias, A.B., Ferreira, V., Barbosa, D., Cheerambathur, D., Gassmann, R., Belmonte, J.M., and Carvalho, A.X. (Dec. 2021). "Plastin and spectrin cooperate to stabilize the actomyosin cortex during cytokinesis." In: *Current Biology.* 31.24, 5415–5428.e10. ISSN: 0960-9822. DOI: `10.1016/j.cub.2021.09.055`. URL: `https://www.sciencedirect.com/science/article/pii/S0960982221012951`.

Soofiyani, S.R., Hoseini, A.M., Mohammadi, A., Shahgoli, V.K., Baradaran, B., and Hejazi, M.S. (Dec. 2017). "siRNA-Mediated Silencing of CIP2A Enhances Docetaxel Activity Against PC-3 Prostate Cancer Cells." In: *Adv Pharm Bull.* 7.4, pp. 637–643. DOI: `10.15171/apb.2017.076`. URL: `https://www.ncbi.nlm.nih.gov/pmc/articles/PMC5788219/`.

Stehling, O., Vashisht, A.A., Mascarenhas, J., Jonsson, Z.O., Sharma, T., Netz, D.J.A., Pierik, A.J., Wohlschlegel, J.A., and Lill, R. (July 2012). "MMS19 assembles iron-sulfur proteins required for DNA metabolism and genomic integrity." In: *Science.* 337.6091, pp. 195–199. ISSN: 1095-9203. DOI: `10.1126/science.1219723`. URL: `https://pubmed.ncbi.nlm.nih.gov/22678362/`.

Stenbeck, G., Harter, C., Brecht, A., Hermann, D., Lottspeich, F. Orci, L., and Wirland, F.T. (July 1993). "beta'-COP, a novel subunit of coatomer." In: *EMBO J.* 12.7, pp. 2841–2845. ISSN: 0261-4189. URL: `https://www.ncbi.nlm.nih.gov/pmc/articles/PMC413534/`.

Stewart, R.J., McDonald, H.B., and Goldstein, L.S.B. (Dec. 1990). "The kinesin-like ncd protein of *Drosophila* is a minus end-directed microtubule motor." In: *Cell.* 63.6, pp. 1159–1165. ISSN: 0092-8674. DOI: `10.1016/0092-8674(90)90412-8`. URL: `https://pubmed.ncbi.nlm.nih.gov/2261638/`.

Still, I.H., Vettaikkorumakankauv, A.K., DiMatteo, and A. Liang, P. (Jan. 2004). "Structure-function evolution of the Transforming acidic coiled coil genes revealed by analysis of phylogenetically diverse organismsi." In: *BMC Evolutionary Biology.* 4, p. 16. ISSN: 1471-2148. DOI: `10.1186/1471-2148-4-16`. URL: `https://pubmed.ncbi.nlm.nih.gov/15207008/`.

Stopp, S., Gründl, M., Fackler, M., Malkmus, J., Leone, M., Naumann, R., Frantz, S., Wolf, E., vo Eyss, B., Engel, F.B., and Gaubatz, S. (July 2017). "Deletion of Gas2l3 in mice leads to specific defects in cardiomyocyte cytokinesis during development." In: *Proc Natl Acad Sci USA.* 114.30, pp. 8029–8034. ISSN: 1091-6490. DOI: `10.1073/pnas.1703406114`. URL: `https://pubmed.ncbi.nlm.nih.gov/28698371/`.

Stroud, M.J., Nazgiewicz, A., McKenzie, E.A., Wang, Y., Kammerer, R.A., and Ballestrem, C. (June 2014). "GAS2-like proteins mediate communication between microtubules and actin through interactions with end-binding proteins." In: *J Cell Sci.* 127.Pt 12, pp. 2672–2682. ISSN: 1477-9137. DOI: `10.1242/jcs.140558`. URL: `https://pubmed.ncbi.nlm.nih.gov/24706950/`.

Sulimenko, V., Hájková, Z., Klebanovych, A., and Dáber, P. (May 2017). "Regulation of microtubule nucleation mediated by γ-tubulin complexes." In: *Protoplasma.* 254.3, pp. 1187–1199. ISSN: 1615-6102. DOI: `10.1007/s00709-016-1070-z`. URL: `https://pubmed.ncbi.nlm.nih.gov/28074286/`.

Suloway, C.J.M., Chartron, J.W, Zaslaver, M., and Jr, W.M.C. (July 2010). "Structural characterization of the Get4/Get5 complex and its interaction with Get3." In: *Proc Natl Acad Sci USA.* 107.27, pp. 12127–12132. ISSN: 1091-6490. DOI: `10.1073/pnas.1006036107`. URL: `https://pubmed.ncbi.nlm.nih.gov/20554915/`.

Suzuki, S.W., Chuang, Y-S., Li, M., Seaman, M.N.J., and Emr, S.D. (Sept. 2019). "A bipartite sorting signal ensures specificity of retromer complex in membrane

protein recycling." In: *J Cell Biol.* 218, p. 9. ISSN: 1540-8140. DOI: `10.1083/jcb.201901019`. URL: `https://pubmed.ncbi.nlm.nih.gov/31337624/`.

Swan, A., Nguyen, T., and Suster, B. (Nov. 1999). "*Drosophila* Lissencephaly-1 functions with Bic-D and dynein in oocyte determination and nuclear positioning." In: *Nat Cell Biol.* 1.7, pp. 444–449. ISSN: 1465-7392. DOI: `10.1038/15680`. URL: `https://pubmed.ncbi.nlm.nih.gov/10559989/`.

Szalontai, T., Gaspar, I., Belecz, I., Kerekes, I., Erdelyi, M., Boros, I., and Szabad, J. (Feb. 2009). "HorkaD, a chromosome instability-causing mutation in *Drosophila,* is a dominant-negative allele of Lodestar." In: *Genetics.* 181.2, pp. 367–377. ISSN: 0016-6731. DOI: `10.1534/genetics.108.097345`. URL: `https://pubmed.ncbi.nlm.nih.gov/19047413/`.

Takács, Z., Jankovics, F., Vilmos, P., Lénárt, P., Röper, and K. Erdélyl, M. (Feb. 2017). "The spectraplakin Short stop is an essential microtubule regulator involved in epithelial closure in *Drosophila.*" In: *J Cell Sci.* 130.4, pp. 712–724. ISSN: 0021-9533. DOI: `10.1242/jcs.193003`. URL: `https://www.ncbi.nlm.nih.gov/pmc/articles/PMC5339884/`.

Takada, S., Kelkar, A., and Theurkauf, W.E. (Apr. 2003). "*Drosophila* checkpoint kinase 2 couples centrosome function and spindle assembly to genomic integrity." In: *Cell.* 113.1, pp. 87–99. DOI: `10.1016/s0092-8674(03)00202-2`. URL: `https://pubmed.ncbi.nlm.nih.gov/12679037/`.

Tambe, M.A., Ng, B.G., Shimada, S., Wolfe, L.A., Adams, D.R., Gahl, W.A., Bamshad, M.J., Nickerson, D.A., Malicdan, M.C.V., and Freez, H.H. (Sept. 2020). "Mutations in GET4 disrupt the transmembrane domain recognition complex pathway". In: *J Inherit Metab Dis.* 43.5, pp. 1037–1045. ISSN: 0141-8955. DOI: `10.1002/jimd.12249`. URL: `https://www.ncbi.nlm.nih.gov/pmc/articles/PMC7508799/`.

Tan, E., Duncan, F. E., and Slawson, C. (Apr. 2017). " The sweet side of the cell cycle." In: *Biochem Soc Trans.* 45.2, pp. 313–322. DOI: `10.1042/BST20160145`. URL: `https://www.ncbi.nlm.nih.gov/pmc/articles/PMC5515282/`.

Tan, R., Foster, P.J., Needleman, D.J., and McKenney, R.J. (Jan. 2018). "Cooperative Accumulation of Dynein-Dynactin at Microtubule Minus-Ends Drives Microtubule Network Reorganization." In: *Dev Cell.* 44.2, pp. 233–247. ISSN: 1878-1551. DOI: `10.1016/j.devcel.2017.12.023`. URL: `https://pubmed.ncbi.nlm.nih.gov/29401420/`.

Tang, Z. (2016). "Model Organisms for Studying the Cell Cycle." In: *Coutts A. and Weston L. (eds) Cell Cycle Oscillators. Methods in Molecular Biology.* 1342, pp. 21–57. DOI: `10.1007/978-1-4939-2957-3_2`. URL: `https://link.springer.com/protocol/10.1007%5C%2F978-1-4939-2957-3_2`.

Tariq, A., Green, L., Jeynes, J.C.G., Soeller, C., and Wakefield, J.G. (Jan. 2020). "In vitro reconstitution of branching microtubule nucleation." In: *eLife.* 9, e49769. ISSN: 2050-084X. DOI: `10.7554/eLife.49769`. URL: `https://pubmed.ncbi.nlm.nih.gov/31933481/`.

Teixidó-Travesa, N., Roig, J., and Lüders, J. (Nov. 2012). "The where, when and how of microtubule nucleation – one ring to rule them all." In: *J. Cell Sci.* 125.Pt 19, pp. 4445–4456. ISSN: 1477-9137. DOI: `10.1242/jcs.106971`. URL: `https://pubmed.ncbi.nlm.nih.gov/23132930/`.

Thakur, H.C., Singh, M., Nagel-Steger, L., Kremer, J., Prumbaum, D., Fansa, E.K., Ezzahoini, H., Nouri, K., Gremer, L., Abts, A., schmitt, L., Raunser, S., Ahmadian, M., and Piekorz, R.P. (Jan. 2014). "The centrosomal adaptor TACC3 and the microtubule polymerase chTOG interact via defined C-terminal subdomains in an Aurora-A kinase-independent manner." In: *J. Biol. Chem.* 289, pp. 74–88. ISSN: 1083-351X. DOI: `10.1074/jbc.M113.532333`. URL: `https://pubmed.ncbi.nlm.nih.gov/24273164/`.

Ti, S-C., Pamula, M.C., Howes, S.C., Duellberg, C., Cade, N.I., Kleiner, R.E., Forth, S., Surrey, T., Nogales, E., and Kapoor, T.M. (Apr. 2016). "Mutations in Human Tubulin Proximal to the Kinesin-Binding Site Alter Dynamic Instability at Microtubule Plus- and Minus-Ends." In: *Dev Cell.* 37.1, pp. 72–84. ISSN: 1534-5807. DOI: `10.1016/j.devcel.2016.03.003`. URL: `https://pubmed.ncbi.nlm.nih.gov/27046833/`.

Tipton, A.R., Ji, W., Sturt-Gillespie, B., Bekier 2nd, M.E., Wang, K., Taylor, W.R., and Liu, S-T. (Dec. 2013). "Monopolar spindle 1 (MPS1) kinase promotes production of closed MAD2 (C-MAD2) conformer and assembly of the mitotic checkpoint complex." In: *J Biol Chem.* 288.49, pp. 35149–35158. ISSN: 1083-351X. DOI: `10.1074/jbc.M113.522375`. URL: `https://pubmed.ncbi.nlm.nih.gov/24151075/`.

Tram, U., Riggs, B., and Sullivan, W. (Mar. 2002). "Cleavage and Gastrulation in *Drosophila* Embryos." In: *Wiley Online Library.*, pp. 1–7. DOI: `10.1038/npg.els.0001071`. URL: `https://onlinelibrary.wiley.com/doi/10.1038/npg.els.0001071`.

Trybus, K.M. (May 2008). "Myosin V from head to tail." In: *Cell Mol Life Sci.* 65.9, pp. 1378–1389. ISSN: 1420-682X. DOI: `10.1007/s00018-008-7507-6`. URL: `https://pubmed.ncbi.nlm.nih.gov/18239852/`.

Ugur, B., Chen, K., and Bellen, H.J. (Mar. 2016). "*Drosophila* tools and assays for the study of human diseases." In: *Dis. Model & Mech.* 9.3, pp. 235–244. DOI: `10.1242/dmm.023762`. URL: `https://journals.biologists.com/dmm/article/9/3/235/20105/Drosophila-tools-and-assays-for-the-study-of-human`.

van der Vaart, B., Manatschal, C., Grigoriev, I., Olieric, V., Gouveia, S.M, Bjelic, S., Demmers, J., Vorobjev, I., Hoogenraad, G.C, Steinmetz, M.O., and Akhmanova, A. (Feb. 2011). "SLAIN2 links microtubule plus end-tracking proteins and controls microtubule growth in interphase". In: *J Cell Biol.* 193.6, pp. 1083–1099.

DOI: `10.1083/jcb.201012179`. URL: `https://rupress.org/jcb/article/193/6/1083/36515/SLAIN2-links-microtubule-plus-end-tracking`.

Vermeulen, K., Van Bockstaele, D.R., and Berneman, Z.N. (June 2003). " The cell cycle: a review of regulation, deregulation and therapeutic targets in cancer." In: *Cell Prolif.* 36.3, pp. 131–149. DOI: `10.1046/j.1365-2184.2003.00266.x`. URL: `https://pubmed.ncbi.nlm.nih.gov/12814430/`.

Vitre, B.D. and D.W. Cleveland (Dec. 2012). "Centrosomes, chromosome instability (CIN) and aneuploidy." In: *Curr Opin Cell Biol.* 24.6, pp. 111–158. DOI: `10.1016/j.ceb.2012.10.006`. URL: `https://pubmed.ncbi.nlm.nih.gov/23127609/`.

Voelzmann, A., Liew, Y-T., Qu, Y., Hahn, I., Melero, C. Sánchez-Soriano, N., and Prokop, A. (Sept. 2017). "The *Drosophila* Short stop as a paradigm for the role and regulation of spectraplakins." In: *Semin Cell Dev Biol.* 69, pp. 40–57. ISSN: 1096-3634. DOI: `10.1016/j.semcdb.2017.05.019`. URL: `https://pubmed.ncbi.nlm.nih.gov/28579450/`.

Wainman, A., Giansanti, M.G., Goldberg, M.L., and Gatti, M. (Sept. 2012). "The *Drosophila* RZZ complex - roles in membrane trafficking and cytokinesis." In: *J Cell Sci.* 125.Pt 17, pp. 4014–4025. DOI: `10.1242/jcs.099820`. URL: `https://pubmed.ncbi.nlm.nih.gov/22685323/`.

Wakabayashi-Ito, N., Doherty, O.M., Moriyama, H., Breakefield, X.O., Gusella, J.F., O'Donnell, J.M., and Ito, N. (Oct. 2011). "Dtorsin, the *Drosophila* ortholog of the early-onset dystonia TOR1A (DYT1), plays a novel role in dopamine metabolism." In: *PLoS One.* 6.10, e26183. ISSN: 1932-6203. DOI: `10.1371/journal.pone.0026183`. URL: `https://pubmed.ncbi.nlm.nih.gov/22022556/`.

Wakefield, J.G. and D. Hayward (Apr. 2014). "Chromatin-mediated microtubule nucleation in *Drosophila* syncytial embryos." In: *Commun Integr Biol.* 7, e28512.

ISSN: 1942-0889. DOI: `10.4161/cib.285122`. URL: `https://www.ncbi.nlm.nih.gov/pmc/articles/PMC4091100/`.

Walczak, C.E. and R. Heald (2008). "Mechanisms of mitotic spindle assembly and function." In: *Int Rev Cytol.* 265, pp. 111–158. DOI: `10.1016/S0074-7696(07)65003-7`. URL: `https://pubmed.ncbi.nlm.nih.gov/18275887/`.

Wang, X., Liu, Y-J., Zhang, T. Chen, S., Cheng, D., Wu, C., Duan, D., Zhu, L., Lou, H., Gong, Z., Wang, X-D., Ho, M.S., and Duan, S. (Jan. 2021). "The noncanonical role of the protease cathepsin D as a cofilin phosphatase." In: *Cell Res.* 31.7, pp. 801–813. ISSN: 1748-7838. DOI: `10.1038/s41422-020-00454-w`. URL: `https://www.nature.com/articles/s41422-020-00454-w`.

Watson, P. and D.J. Stephens (July 2006). "Microtubule plus-end loading of p150(Glued) is mediated by EB1 and CLIP-170 but is not required for intracellular membrane traffic in mammalian cells." In: *J Cell Sci.* 119.Pt 13, pp. 2758–2767. DOI: `10.1242/jcs.02999`. URL: `https://pubmed.ncbi.nlm.nih.gov/16772339/`.

Weaver, B.A.A., Bonday, Z.Q., Putkey, F. R., Kops, G.J.P.L., Silk, A.D., and Cleveland, D.w (Aug. 2003). "Centromere-associated protein-E is essential for the mammalian mitotic checkpoint to prevent aneuploidy due to single chromosome loss." In: *J Cell Biol.* 162.4, pp. 551–563. ISSN: 0021-9525. DOI: `10.1083/jcb.200303167`. URL: `https://pubmed.ncbi.nlm.nih.gov/12925705/`.

Wild, K., Rosendal, K.R., and Sinning, I. (July 2004). "A structural step into the SRP cycle." In: *Mol Microbiol.* 53.3, pp. 357–363. ISSN: 0950-382X. DOI: `10.1111/j.1365-2958.2004.04139.x`. URL: `https://pubmed.ncbi.nlm.nih.gov/15228518/`.

Wolf, M.J. and H.A. Rockman (Oct. 2008). "*Drosophila melanogaster* as a model system for genetics of postnatal cardiac function." In: *Drug Discov Today Dis Models.* 5.3, pp. 117–123. DOI: `10.1016/j.ddmod.2009.02.002`. URL: `https://pubmed.ncbi.nlm.nih.gov/19802348/`.

Wolter, P., Schmitt, K., Fackler, M., Kremling, H., Probst, L., Hauser, S., Gruss, O.J., and Gaubatz, S. (May 2012). "GAS2L3, a target gene of the DREAM complex, is required for proper cytokinesis and genomic stability." In: *J Cell Sci.* 125.Pt 10, pp. 2393–2406. ISSN: 1477-9137. DOI: `10.1242/jcs.097253`. URL: `https://pubmed.ncbi.nlm.nih.gov/22344256/`.

Woodruff, J.B., Drubin, D G., and Barnes, G. (July 2009). "Dynein-Driven Mitotic Spindle Positioning Restricted to Anaphase by She1p Inhibition of Dynactin Recruitment." In: *Mol Biol Cell.* 20.13, pp. 3003–3011. DOI: `10.1091/mbc.E09-03-0186`. URL: `https://www.ncbi.nlm.nih.gov/pmc/articles/PMC2704152/`.

Wozniak, R., Burke, B., and Doye, V. (July 2010). "Nuclear transport and the mitotic apparatus: an evolving relationship." In: *Cell Mol Life Sci* 67.13, pp. 2215–2230. DOI: `10.1007/s00018-010-0325-7`. URL: `https://pubmed.ncbi.nlm.nih.gov/20372967/`.

Xiang, X. and R. Qiu (Oct. 2020). "Cargo-Mediated Activation of Cytoplasmic Dynein in vivo." In: *Front Cell Dev Biol.* 8, p. 598952. ISSN: 2296-634X. DOI: `10.3389/fcell.2020.598952`. URL: `https://pubmed.ncbi.nlm.nih.gov/33195284/`.

Xu, Y., Liu, Y., Lee, J-g., and Ye, Y. (June 2013). "A ubiquitin-like domain recruits an oligomeric chaperone to a retrotranslocation complex in endoplasmic reticulum associated degradation." In: *J Biol Chem.* 288.25, pp. 18068–18076. ISSN: 1083-351X. DOI: `10.1074/jbc.M112.449199`. URL: `https://pubmed.ncbi.nlm.nih.gov/23665563/`.

Yamamoto-Hino, M., Katsumata, E., Suzuki, E., Maeda, Y., Knoshita, T., and Goto, S. (Oct. 2018). "Nuclear envelope localization of PIG-B is essential for GPI-anchor synthesis in *Drosophila.*" In: *J Cell Sci.* 131.20, jcs218029. ISSN: 0021-9533. DOI: `10.1242/jcs.218024`. URL: `https://pubmed.ncbi.nlm.nih.gov/30266758/`.

Yang, H., Liu, X., Zhu, X., Li, X., Jiang, L., Zhong, M., Zhang, M., Chen, T., Ma, M., Liang, X., and Lv, K. (Nov. 2021). "CPVL promotes glioma progression via STAT1 pathway inhibition through interactions with the BTK/p300 axis." In: *JCI Insight.*, e146362. ISSN: 2379-3708. DOI: `10.1172/jci.insight.146362`. URL: `https://pubmed.ncbi.nlm.nih.gov/34784299/`.

Yao, X., Wang, X., and Xiang, X. (July 2014). "FHIP and FTS proteins are critical for dynein-mediated transport of early endosomes in Aspergillus." In: *Mol Biol Cell.* 25.14, pp. 2181–2189. ISSN: 1939-4586. DOI: `10.1091/mbc.E14-04-0873`. URL: `https://pubmed.ncbi.nlm.nih.gov/24870033/`.

Yew, N., Wang, Y.M., Peloquin, J.G., Woude, G.F.V., and Borisy, G.G. (May 1994). "Mos oncogene product associates with kinetochores in mammalian somatic cells and disrupts mitotic progression." In: *Proc Natl Acad Sci USA.* 91.18, pp. 8329–8333. ISSN: 0027-8424. DOI: `10.1073/pnas.91.18.8329`. URL: `https://pubmed.ncbi.nlm.nih.gov/8078882/`.

Yu, K-W., Zhong, N., Xiao, Y., and She, Z-Y. (June 2019). "Mechanisms of kinesin-7 CENP-E in kinetochore-microtubule capture and chromosome alignment during cell division." In: *Cell Biol.* 111.6, pp. 143–160. ISSN: 1768-322X. DOI: `10.1111/boc.201800082`. URL: `https://pubmed.ncbi.nlm.nih.gov/30784092/`.

Yucel, J.K., Marszalek, J.D., McIntosh, J.R., Goldstein, L.S.B., Cleveland, and D.W. Philip, A.V. (July 2000). "*CENP-meta,* an Essential Kinetochore Kinesin Required for the Maintenance of Metaphase Chromosome Alignment in *Drosophila.*" In: *J Cell Biol.* 150.1, pp. 1–12. ISSN: 0021-9525. DOI: `10.1083/jcb.150.1.1`. URL: `https://www.ncbi.nlm.nih.gov/pmc/articles/PMC2185570/`.

yue, J., Zhang, J., and Wu, X. (Aug. 2017). "*Drosophila* oocyte polarity and cytoskeleton organization require regulation of Ik2 activity by Spn-F and Javelin-like." In: *J Cell Sci.* 130.15, pp. 2447–2457. ISSN: 1557-7988. DOI: `10.1242/`

jcs.196154. URL: `https://www.ncbi.nlm.nih.gov/pmc/articles/PMC5558266/`.

Yugandhar, K., Wang, T.Y., Wierbowski, S.D., Shayhidin, E.E., and Yu, H. (Oct. 2020). "Structure-based validation can drastically underestimate error rate in proteome-wide cross-linking mass spectrometry studies." In: *Nat Methods.* 17.10, pp. 985–988. DOI: `10.1038/s41592-020-0959-9`. URL: `https://pubmed.ncbi.nlm.nih.gov/32994567/`.

Zavortink, M., Rutt, L.N., Dzitoyeva, S., Henrikesen, J.C., Barrington, C., Bilodeau, D.Y., Wang, M., Chen, X.X.L., and Rissland, O.S. (June 2020). "The E2 Marie Kondo and the CTLH E3 ligase clear deposited RNA binding proteins during the maternal-to-zygotic transition." In: *eLife.* 9, e53889. ISSN: 2050-084X. DOI: `10.7554/eLife.53889`. URL: `https://www.ncbi.nlm.nih.gov/pmc/articles/PMC7384856/`.

Zhang, L., Shao, H., Zhu, T., Xia, P., Wang, Z., Liu, L., Yan, M., Hill, D.L., Fang, G., Chen, Z., Wang, D., and Yao, X. (2013). "DDA3 associates with microtubule plus ends and orchestrates microtubule dynamics and directional cell migration." In: *Sci Rep.* 3, p. 1681. DOI: `10.1038/srep01681`. URL: `https://pubmed.ncbi.nlm.nih.gov/23652583/`.

Zhang, L. and R.E. Ward (Feb. 2011). "Distinct tissue distributions and subcellular localizations of differently phosphorylated forms of the myosin regulatory light chain in *Drosophila.*" In: *Gene Expr Patterns.* 11.1-2, pp. 93–104. ISSN: 1872-7298. DOI: `10.1016/j.gep.2010.09.008`. URL: `https://pubmed.ncbi.nlm.nih.gov/20920606/`.

Zhang, R., Alushin, G.M, Brown, A., and Nogales, E. (Aug. 2015). "Mechanistic Origin of Microtubule Dynamic Instability and Its Modulation by EB Proteins." In: *Cell.* 162.4, pp. 849–859. ISSN: 1097-4172. DOI: `10.1016/j.cell.2015.07.012`. URL: `https://pubmed.ncbi.nlm.nih.gov/26234155/`.

Zhang, Y., Luo, Y., Lyu, R., Chen, J., Liu, R., Li, D., Liu, M, and Zhou, J. (Sept. 2016).
"Proto-Oncogenic Src Phosphorylates EB1 to Regulate the Microtubule-Focal
Adhesion Crosstalk and Stimulate Cell Migration." In: *Theranostics.* 6.12, pp. 2129–
2140. DOI: `10.7150/thno.16356`. URL: `https://www.ncbi.nlm.nih.gov/`
`pmc/articles/PMC5039685/`.

Zhao, Q., Zhang, R., Zhang, C.Y., and Li, DH. (Dec. 2013). "Spectrin: structure,
function and disease." In: *Sci China Life Sci.* 56.12, pp. 1076–1085. ISSN: 1869-
1889. DOI: `10.1007/s11427-013-4575-0`. URL: `https://pubmed.ncbi.`
`nlm.nih.gov/24302288/`.

Zhu, Z.C., Gupata, K.K, Slabbekoorn, A.R., Paulson, B.A., Folker, E.S., and Good-
son, H.V. (Nov. 2009). "Interactions between EB1 and microtubules: dramatic
effect of affinity tags and evidence for cooperative behavior." In: *Journal of Bi-
ological Chemistry.* 284.47, pp. 32651–32661. ISSN: 0021-9258. DOI: `10.1074/`
`jbc.M109.013466`. URL: `https://pubmed.ncbi.nlm.nih.gov/19778897/`.